CANADIAN THESES ON MICROFICHE

I.S.B.N.

THESES CANADIENNES SUR MICROFICHE

National Library of Canada
Collections Development Branch

Canadian Theses on
Microfiche Service

Ottawa, Canada
K1A 0N4

Bibliothèque nationale du Canada
Direction du développement des collections

Service des thèses canadiennes
sur microfiche

NOTICE

The quality of this microfiche is heavily dependent upon the quality of the original thesis submitted for microfilming. Every effort has been made to ensure the highest quality of reproduction possible.

If pages are missing, contact the university which granted the degree.

Some pages may have indistinct print especially if the original pages were typed with a poor typewriter ribbon or if the university sent us a poor photocopy.

Previously copyrighted materials (journal articles, published tests, etc.) are not filmed.

Reproduction in full or in part of this film is governed by the Canadian Copyright Act, R.S.C. 1970, c. C-30. Please read the authorization forms which accompany this thesis.

THIS DISSERTATION
HAS BEEN MICROFILMED
EXACTLY AS RECEIVED

AVIS

La qualité de cette microfiche dépend grandement de la qualité de la thèse soumise au microfilmage. Nous avons tout fait pour assurer une qualité supérieure de reproduction.

S'il manque des pages, veuillez communiquer avec l'université qui a conféré le grade.

La qualité d'impression de certaines pages peut laisser à désirer, surtout si les pages originales ont été dactylographiées à l'aide d'un ruban usé ou si l'université nous a fait parvenir une photocopie de mauvaise qualité.

Les documents qui font déjà l'objet d'un droit d'auteur (articles de revue, examens publiés, etc.) ne sont pas microfilmés.

La reproduction, même partielle, de ce microfilm est soumise à la Loi canadienne sur le droit d'auteur, SRC 1970, c. C-30. Veuillez prendre connaissance des formules d'autorisation qui accompagnent cette thèse.

LA THÈSE A ÉTÉ
MICROFILMÉE TELLE QUE
NOUS L'AVONS REÇUE

NL-339 (r. 82/08)

Canada

0-315-06051-4

National Library of Canada
Bibliothèque nationale du Canada

Canadian Theses Division
Division des thèses canadiennes

Ottawa, Canada
K1A 0N4

53971

PERMISSION TO MICROFILM — AUTORISATION DE MICROFILMER

- Please print or type — Écrire en lettres moulées ou dactylographier

Full Name of Author — Nom complet de l'auteur
RAYMOND WAI-SHING LEE

Date of Birth — Date de naissance NOV. 15 1954	Country of Birth — Lieu de naissance HONG KONG

Permanent Address — Résidence fixe
11816 - 57 St., EDMONTON, ALBERTA
CANADA T5W 3V4

Title of Thesis — Titre de la thèse
Behavior of Restrained Masonry Beams

University — Université
University of Alberta

Degree for which thesis was presented — Grade pour lequel cette thèse fut présentée
M.Sc.

Year this degree conferred — Année d'obtention de ce grade 1981	Name of Supervisor — Nom du directeur de thèse J. LONGWORTH & J. WARWARUK

Permission is hereby granted to the NATIONAL LIBRARY OF CANADA to microfilm this thesis and to lend or sell copies of the film.

The author reserves other publication rights, and neither the thesis nor extensive extracts from it may be printed or otherwise reproduced without the author's written permission.

L'autorisation est, par la présente, accordée à la BIBLIOTHÈQUE NATIONALE DU CANADA de microfilmer cette thèse et de prêter ou de vendre des exemplaires du film.

L'auteur se réserve les autres droits de publication; ni la thèse ni de longs extraits de celle-ci ne doivent être imprimés ou autrement reproduits sans l'autorisation écrite de l'auteur.

~~Oct. 16/81~~

Date Oct. 16/81	Signature Raymond

NL-91 (4/77)

THE UNIVERSITY OF ALBERTA

Behavior of Restrained Masonry Beams

by

© Raymond Wai-Shing Lee

A THESIS
SUBMITTED TO THE FACULTY OF GRADUATE STUDIES AND RESEARCH
IN PARTIAL FULFILMENT OF THE REQUIREMENTS FOR THE DEGREE
OF Master of Science
IN
Civil Engineering

Department of Civil Engineering

EDMONTON, ALBERTA
Fall 1981

THE UNIVERSITY OF ALBERTA

RELEASE FORM

NAME OF AUTHOR Raymond Wai-Shing Lee

TITLE OF THESIS Behavior of Restrained Masonry Beams

DEGREE FOR WHICH THESIS WAS PRESENTED Master of Science

YEAR THIS DEGREE GRANTED Fall 1981

Permission is hereby granted to THE UNIVERSITY OF ALBERTA LIBRARY to reproduce single copies of this thesis and to lend or sell such copies for private, scholarly or scientific research purposes only.

The author reserves other publication rights, and neither the thesis nor extensive extracts from it may be printed or otherwise reproduced without the author's written permission.

(SIGNED) ..Raymond Lee..

PERMANENT ADDRESS:

11816-57st.,

EDMONTON ALBERTA

CANADA T5W3V4

DATED ..October 15, ..1981

THE UNIVERSITY OF ALBERTA

FACULTY OF GRADUATE STUDIES AND RESEARCH

The undersigned certify that they have read, and recommend to the Faculty of Graduate Studies and Research, for acceptance, a thesis entitled Behavior of Restrained Masonry Beams submitted by Raymond Wai-Shing Lee in partial fulfilment of the requirements for the degree of Master of Science in Civil Engineering.

.....J Longworth.....
Supervisor

....

.....D J L Kennedy.....

Date.....October 15, 1981.....

Abstract

Reinforced masonry beams are frequently used to span over openings in masonry walls. Such beams are restrained from rotating freely at their ends thereby creating conditions which differ from those in simply supported beams. In order to analyse restrained beams the magnitude and location of the restraining forces must be evaluated.

The present study is concerned with the behavior of restrained reinforced concrete block beams. This behavior is related to the nonisotropic behavior of concrete masonry.

The experimental study consists of tests of fourteen full-scale reinforced concrete block beams and compressive tests of thirty-one grouted masonry prisms under two different orientations. Variables for the beam tests included type of support conditions, beam depth and use of web reinforcement. The end restraints were provided either by fixed abutments or short support masonry walls. The behavior of the beam specimens was monitored by measurements of load, strains in reinforcement and masonry, and vertical deflections.

Test results were analysed using basic principles and procedures developed for reinforced concrete. A three-hinged arch model was used for determining the ultimate strength of restrained beams and the amount of restraining force was estimated using approximate procedures.

It is concluded that the behavior of masonry beams can be predicted by analysis similar to that employed for reinforced concrete. Moreover, the ultimate loads for restrained masonry beams can be reasonably predicted on the basis of an idealized three-hinged arch model.

Acknowledgements

This investigation was made possible through funds from the Natural Sciences and Engineering Research Council of Canada and the Canadian Masonry Research Council. Testing facilities were provided by the Department of Civil Engineering at the University of Alberta.

This report was prepared as a Master of Science thesis under the joint supervision of Prof. J. Longworth and Prof. J. Warwaruk at The University of Alberta.

Table of Contents

Chapter Page

1. Introduction 1

1.1 General Remarks 1

1.2 Object and Scope 2

2. Review of Previous Research and Analysis Methods 3

2.1 Introduction 3

2.2 Review of Previous Investigations 3

2.2.1 Unrestrained Brick Masonry Beams 3

2.2.2 Unrestrained Concrete Block Beams 7

2.2.3 Restrained Masonry Members 9

2.3 Analysis of Masonry Beams 10

2.3.1 Cracking Moment 11

2.3.2 Location of Neutral Axis 11

2.3.3 Flexure of a Singly Reinforced Masonry Beam Section in the Service Load Range 11

2.3.4 Ultimate Strength of Masonry Beams 12

2.3.5 Effective Moment of Inertia 13

2.3.6 Shear Resistance 14

2.4 Three-Hinged Arch Failure Model 15

2.5 Prediction of End Restraint 17

3. Experimental Program 23

3.1 Materials 23

3.1.1 Concrete Block Units 23

3.1.2 Mortar 23

3.1.3 Grout 24

3.1.4 Reinforcement 25

3.2 Test Specimens 26

3.2.1 Prisms 26

3.2.2 Full Scale Beam Specimens 27

3.2.2.1 General 27

3.2.2.2 Reinforcement Details 28

3.2.2.3 Beam Fabrication 29

3.3 Instrumentation 32

3.3.1 Prisms 32

3.3.2 Full Scale Beam Specimens 33

3.4 Test Procedure 35

3.4.1 Prisms 35

3.4.2 Full Scale Beam Specimens 35

4. Material Tests and Prism Tests 56

4.1 Introduction 56

4.2 Properties of Mortar Cubes 56

4.3 Properties of Grout 57

4.4 Properties of Masonry Units 58

4.4.1 Compressive Strength 58

4.4.2 Modulus of Elasticity 59

4.5 Prism Investigation 61

4.5.1 General 61

4.5.2 Prism Failure Modes 62

4.5.3 Compressive Strength of Prism 63

4.5.4 Modulus of Elasticity of Prisms 66

5. Test Results 91

5.1 Introduction 91

5.2 General Behavior 91

5.3 Load-Deflection Relationships 99

5.4 Load-Strain Relationships 99

5.5 Load-Restraining Force and Load-Displacement Relationships 100

5.6 Crack Patterns 100

6. Discussion of Beam Test Results 186

6.1 Introduction 186

6.2 Failure Mode - General Remarks 187

6.3 Cracking Moments for Simply Supported Beams 190

6.4 Location of the Neutral Axis 191

6.5 Simply Supported Masonry Beams in the Service Load Range 192

6.6 Ultimate Strength of Simply Supported Beams 193

6.7 Deflection of Simply Supported Beams 195

6.8 Effect of End Restraint on the Load-Deflection Relationship for Masonry Beams 197

6.9 Effect of End Restraints on the Load-Tension Reinforcement Strain Relationships 198

6.10 Effect of Shear Reinforcement 200

6.11 Ultimate Capacity of Restrained Masonry Beams ...202

6.12 End Restraint 203

7. Summary and Conclusions 236

7.1 Summary 236

7.2 Observations and Conclusions 237

Bibliography 239

Appendix A 243

List of Tables

Table Page

3.1 Dimensions of Concrete Block Units 37

3.2 Grout Mix Design 37

3.3 Physical Properties of Reinforcing Steel 38

3.4 Properties of Prisms 39

4.1 Compressive Strength of 50x50x50 mm Mortar Cubes 70

4.2 Compressive Strength of Concrete Cylinders 71

4.3 Compressive Strength of 75x75x150 mm Concrete Prisms 72

4.4 Compressive Strength and Modulus of Elasticity of Masonry Units 73

4.5 Results of Prism Tests 74

5.1 Beam Classification 101

5.2 Test Results 102

6.1 Measured and Predicted Values 205

6.2 Ratio of Maximum Loads 206

6.3 Measured and Predicted Values 207

List of Figures

Figure Page

2.1 Stress and Strain Distributions in a Singly Reinforced Section 20

2.2 Distribution of Thrust in a Restrained Beam 21

2.3 Equilibrum Conditions for a Restrained Beam 22

3.1 Masonry Units 40

3.2 Stress-Strain Relations for Reinforcing Steel 41

3.3 Masonry Prisms 42

3.4 Type SB Beam Details 43

3.5 Type RB Beam Details 45

3.6 Type EB Beam Details 47

3.7 Location of Beam Instrumentation 50

3.8 Location of Strain Gauges on Tension Reinforcement at End of Type EB and RB Beams 51

4.1 Stress-Strain Relationship for Masonry Units 75

4.2 Comparison of Masonry Prism Strength and Mortar Cube Strength 76

4.3 Comparison of Prism and Cylinder Strengths for Grout 77

4.4 Comparison of Prism and Cylinder Strengths for Grout 78

4.5 Stress-Strain Relationships for Masonry Prisms 79

4.6 Stress-Strain Relationships for Masonry Prisms 80

4.7 Stress-Strain Relationships for Masonry Prisms 81

4.8 Stress-Strain Relationships for Masonry

Figure Page

Prisms 82

4.9 Stress-Strain Relationships for Masonry Prisms 83

4.10 Stress-Strain Relationships for Masonry Prisms 84

4.11 Modulus of Elasticity versus Compressive Strength for Masonry Prisms 85

4.12 Modulus of Elasticity versus Compressive Strength for Masonry Prisms 86

5.1 Load versus Vertical Deflection for Beam SB1 103

5.2 Load versus Vertical Deflection for Beam SB2 104

5.3 Load versus Vertical Deflection for Beam SB3 105

5.4 Load versus Vertical Deflection for Beam SB4 106

5.5 Load versus Vertical Deflection for Beam RB1 107

5.6 Load versus Vertical Deflection for Beam RB2 108

5.7 Load versus Vertical Deflection for Beam RB3 109

5.8 Load versus Vertical Deflection for Beam RB4 110

5.9 Load versus Vertical Deflection for Beam EB1 111

5.10 Load versus Vertical Deflection for Beam EB2 112

5.11 Load versus Vertical Deflection for Beam EB3 113

5.12 Load versus Vertical Deflection for Beam EB4 114

5.13 Load versus Vertical Deflection for Beam

Figure Page

EB5 115

5.14 Load versus Vertical Deflection for Beam EB6 116

5.15 Deflected Shape of Beam SB1 117

5.16 Deflected Shape of Beam SB2 118

5.17 Deflected Shape of Beam SB3 119

5.18 Deflected Shape of Beam SB4 120

5.19 Deflected Shape of Beam RB1 121

5.20 Deflected Shape of Beam RB2 122

5.21 Deflected Shape of Beam RB3 123

5.22 Deflected Shape of Beam RB4 124

5.23 Deflected Shape of Beam EB1 125

5.24 Deflected Shape of Beam EB2 126

5.25 Deflected Shape of Beam EB3 127

5.26 Deflected Shape of Beam EB4 128

5.27 Deflected Shape of Beam EB5 129

5.28 Deflected Shape of Beam EB6 130

5.29 Load versus Tension Reinforcement Strain at Midspan for Type SB Beams 131

5.30 Load versus Tension Reinforcement Strain at Midspan for Type RB Beams 132

5.31 Load versus Tension Reinforcement Strain at Midspan for Type EB Beams 133

5.32 Load versus Reinforcement Strain at the End of Beam RB1 135

5.33 Load versus Reinforcement Strain at the End of Beam RB2 136

5.34 Load versus Reinforcement Strain at the End of Beam RB3 138

Figure Page

5.35 Load versus Reinforcement Strain at the End of Beam RB4 139

5.36 Load versus Reinforcement Strain at the End of Beam EB1 140

5.37 Load versus Reinforcement Strain at the End of Beam EB3 141

5.38 Load versus Reinforcement Strain at the End of Beam EB4 142

5.39 Load versus Reinforcement Strain at the End of Beam EB5 143

5.40 Load versus Web Reinforcement Strain for Beam SB1 144

5.41 Load versus Web Reinforcement Strain for Beam SB2 145

5.42 Load versus Web Reinforcement Strain for Beam SB4 146

5.43 Load versus Web Reinforcement Strain for Beam RB1 147

5.44 Load versus Web Reinforcement Strain for Beam RB2 148

5.45 Load versus Web Reinforcement Strain for Beam RB4 149

5.46 Load versus Web Reinforcement Strain for Beam EB3 150

5.47 Load versus Web Reinforcement Strain for Beam EB6 151

5.48 Load versus Horizontal Surface Strain in the Constant Moment Region for Beam SB1 152

5.49 Load versus Horizontal Surface Strain in the Constant Moment Region for Beam SB2 153

5.50 Load versus Horizontal Surface Strain in the Constant Moment Region for Beam SB3 154

5.51 Load versus Horizontal Surface Strain in the Constant Moment Region for Beam SB4 155

Figure Page

5.52 Load versus Horizontal Surface Strain in the Constant Moment Region for Beam RB1 156

5.53 Load versus Horizontal Surface Strain in the Constant Moment Region for Beam RB2 157

5.54 Load versus Horizontal Surface Strain in the Constant Moment Region for Beam RB3 159

5.55 Load versus Horizontal Surface Strain in the Constant Moment Region for Beam RB4 160

5.56 Load versus Horizontal Surface Strain in the Constant Moment Region for Beam EB1 161

5.57 Load versus Horizontal Surface Strain in the Constant Moment Region for Beam EB2 162

5.58 Load versus Horizontal Surface Strain in the Constant Moment Region for Beam EB3 163

5.59 Load versus Horizontal Surface Strain in the Constant Moment Region for Beam EB4 164

5.60 Load versus Horizontal Surface Strain in the Constant Moment Region for Beam EB5 165

5.61 Load versus Horizontal Surface Strain in the Constant Moment Region for Beam EB6 166

5.62 Load versus Horizontal Restraining Force for Type EB Beams 167

5.63 Load versus Displacement for Type EB Beams 169

6.1 Cracking Moment versus Effective Depth of Simply Supported Beams 208

6.2 Neutral Axis Position in Type SB Beams 209

6.3 Neutral Axis Position in Type RB Beams 210

6.4 Neutral Axis Position in Type EB Beams 211

6.5 Load versus Tension Reinforcement Strain at Midspan for Beam SB1 212

6.6 Load versus Tension Reinforcement Strain at Midspan for Beam SB2 213

Figure Page

6.7 Load versus Tension Reinforcement Strain at Midspan for Beam SB4 214

6.8 Load versus Midspan Deflection of Type SB Beams 215

6.9 Load versus Deflection for Beam SB1 216

6.10 Load versus Deflection for Beam SB2 217

6.11 Load versus Deflection for Beam SB4 218

6.12 Load versus Deflection for Beam SB1 219

6.13 Load versus Deflection for Beam SB2 219

6.14 Load versus Deflection for Beam SB4 220

6.15 Load versus Deflection for Type SB and RB Beams 221

6.16 Load versus Deflection for SB2, RB2 and Type EB Beams 222

6.17 Load versus Tension Reinforcement Strain at Midspan for Type SB and RB Beams 223

6.18 Load versus Tension Reinforcement Strain at Midspan for SB2, RB2 and Type EB Beams 224

6.19 Load versus Shear Reinforcement Strain for Type SB and RB Beams 225

6.20 Load versus Shear Reinforcement Strain for SB2, RB2 and Type EB Beams 226

6.21 Shear Stress versus Load for Beam SB2 227

6.22 Shear Stress versus Load for Beam SB4 227

6.23 Shear Stress versus Load for Beam RB1 228

6.24 Shear Stress versus Load for Beam RB2 228

6.25 Shear Stress versus Load for Beam RB4 229

6.26 Shear Stress versus Load for Beam EB3 229

6.27 Shear Stress versus Load for Beam EB6 230

6.28 Stress Distribution at End of Beam 231

Figure Page

6.29 Restraining Force versus Load and Compressive Force versus Load for Beam RB1 232

6.30 Restraining Force versus Load and Compressive Force versus Load for Beam RB2 233

6.31 Restraining Force versus Load and Compressive Force versus Load for Beam RB4 234

6.32 Restraining Force versus Load for Type EB Beams 235

List of Plates

Plate Page

3.1 Location of Tension Reinforcement 52

3.2 Stirrup Installation 52

3.3 LVDT's Used for Measuring Vertical Deflections 53

3.4 LVDT's for Measuring Horizontal Strain 53

3.5 Test Set Up 54

3.6 Roller Support 54

3.7 Rocker Support 55

3.8 Horizontal End Restraint 55

4.1 Typical Failure Mode of Prism Loaded Normal to Bed Joints 87

4.2 Failure Mode of Prisms PA and PB Loaded Parallel to Bed Joints 88

4.3 Failure Mode of Prisms PA and PB Loaded Parallel to Bed Joints 89

4.4 Failure Mode of Prisms PLA and PLB Loaded Parallel to Bed Joints 90

5.1 Failure of Beam SB1 170

5.2 Failure of Beam SB2 170

5.3 Failure of Beam SB3 171

5.4 Failure of Beam SB4 171

5.5 Failure of Beam RB1 172

5.6 Cracks at North Support of Beam RB1 173

5.7 Cracks at South Support of Beam RB1 173

5.8 Failure of Beam RB2 174

5.9 Failure of Beam RB3 174

5.10 Cracks at North Support of Beam RB4 175

5.11 Cracks at South Support of Beam RB4 175

Plate Page

5.12 Failure of Beam RB4 176

5.13 Failure of Beam EB1 176

5.14 Beam EB1 after Test 177

5.15 Crack at Interface of Beam EB2 and Supporting Wall 177

5.16 Failure of Beam EB2 178

5.17 Beam EB2 after Test 178

5.18 Failure of Beam EB3 179

5.19 North Supporting Wall of Beam EB3 after Test 179

5.20 Beam EB3 after Test 180

5.21 Cracks above South Support of Beam EB4 180

5.22 Cracks above North Support of Beam EB4 181

5.23 Beam EB4 after Test 181

5.24 South Supporting Wall of Beam EB5 after Test 182

5.25 South Supporting Wall of Beam EB5 after Test 182

5.26 Failure of Beam EB5 183

5.27 Beam EB5 after Test 183

5.28 South Supporting Wall of Beam EB6 after Test 184

5.29 Failure of Beam EB6 184

5.30 Beam EB6 after Test 185

List of Symbols

Dimensions and Section Properties

a = depth of equivalent rectangular stress block

A_s = area of tension reinforcement

A_v = area of web reinforcement

b = width of section

c = distance from extreme compression fiber to neutral axis

d = distance from extreme compression fiber to centroid of tension reinforcement

e = eccentricity of the restraining force measured from the neutral axis

h = height of beam

I = moment of inertia

I_{cr} = moment of inertia of cracked transformed section

I_e = effective moment of inertia

I_g = moment of inertia of gross uncracked section

L = clear span of beam

t = depth of bearing area

y = distance of the restraining force measured from the centriod of longitudinal reinforcement

y_t = distance from centroidal axis of gross section to extreme fiber in tension

Material Properties

E_b = elastic modulus of concrete blocks

E_c = modulus of elasticity of concrete

E_m = modulus of elasticity of masonry

E_{mn} = modulus of elasticity of masonry normal to bed joints

E_{mp} = modulus of elasticity of masonry parallel to bed joints

E_s = modulus of elasticity of reinforcement

Forces and Moments

C = internal resultant compressive force

F = restraining force

H = total thrust

M = moment

M_a = midspan positive moment

M_{cr} = moment at first cracking

M_{max} = maximum service load moment

M_u = ultimate moment

P = applied load

T = internal resultant tension force

Stresses and Strains

ϵ_m = strain in masonry

ϵ_{mu} = ultimate compressive strain in masonry

ϵ_s = strain in reinforcement

ϵ_y = yield strain of reinforcement

f'_b = compressive strength of concrete block unit

f'_c = compressive strength of concrete

f_m = stress in masonry

f'_m = compressive strength of masonry prism

f'_{mn} = compressive strength of masonry prism normal to bed joint

f'_{mp} = compressive strength of masonry prism parallel to bed joint

f_{rm} = modulus of rupture of masonry

f_s = reinforcement stress

f_y = yield stress of reinforcement

v_m = shear resistance of the masonry

v_s = shear resistance of web reinforcement

v_u = maximum shear resistance of a beam

Miscellaneous

a/d = shear span-depth ratio

k = ratio of depth of neutral axis to the effective depth

n = modular ratio = E_s/E_m

q = $\rho f_y/f'_m$

s = spacing of vertical reinforcement

W = unit weight of concrete
= air dry concrete block density

ρ = ratio of tension reinforcement
= A_s/bd

β_1 = factor relating to equivalent compressive rectangular block

Δ = centerline deflection

1. Introduction

1.1 General Remarks

Masonry construction in brick and stone is one of man's oldest types of construction. Even with the inception of modern construction materials such as steel and reinforced concrete, masonry still offers advantages such as pleasing appearance and durability in performance.

Reinforced masonry structures are a recent development. Traditionally, masonry structures were proportioned on the basis of rules of thumb. However there has been a considerable amount of analytical and experimental investigation in recent years and design techniques and construction practices for masonry have been vastly improved.

A considerable number of investigations have focussed on the behavior of load-bearing masonry walls and masonry columns. Relatively few studies have related to the behavior of masonry beams with most of them concentrating on shear behavior.

A masonry lintel beam spanning an opening in a wall is restrained against rotation at its ends by the masonry bordering the opening. The presence of the longitudinal restraining force causes the behavior of the beam to be different from that of an identical unrestrained member. However, lintel beams are often designed on the basis of being simply supported, implying that the member is free to rotate at its ends.

The present study is a preliminary investigation into the behavior of restrained masonry beams. The study is designed to provide a comparison between the behavior of restrained and unrestrained members, and also to provide a basis for developing further studies.

1.2 Object and Scope

The main objectives of this study are:

1. To examine the nonisotropic behavior of concrete masonry.
2. To observe the behavior, cracking pattern, and ultimate capacity of masonry beams under three different support conditions.
3. To determine the effectiveness of tensile and shear reinforcement.
4. To determine if masonry beams can be analysed by reinforced concrete procedures.
5. To predict the capacity of restrained beams by means of an idealized failure mode.
6. To determine the restraining force from test results using idealized and simplified assumptions.
7. To establish a basis for further study of restrained masonry beams.

2. Review of Previous Research and Analysis Methods

2.1 Introduction

Within the last two decades, a large amount of research has been carried out with regard to the performance of masonry walls. However, research related to the flexural behavior and characteristics of masonry beams is very limited, thus the behavior of unrestrained masonry beams is not well defined.

This chapter provides a brief review of previous masonry beam studies related to both unrestrained and restrained members. The behavior of masonry beams is analysed on the basis of analysis employed for reinforced concrete. Procedures for the prediction of ultimate capacity and restraining force in restrained members are developed.

2.2 Review of Previous Investigations

2.2.1 Unrestrained Brick Masonry Beams

In 1933, Withey' conducted a test program involving twenty-five 8x12 in. reinforced brick beams of 8 feet span. Program variables included different types of bricks and different amounts of tension and shear reinforcement. The results indicated that a rather high flexural and shear strength could be developed provided particular attention was paid to mortar bond, coursing, amount and arrangement of reinforcement, and filling of joints. By comparing the test results at working load and ultimate load with values based on formulas for reinforced concrete design, he concluded that those equations used in the calculation of fiber, shear, and bond stresses and deflection, with appropriate constants, could be applied to reinforced brick beams.

In 1934, Hansen[2] summarized test results from six different sources, including his own test results, for beams of different dimensions, joint thickness, and arrangement of bricks. He found that: (1) the deflection of reinforced brick beams was small within working loads, (2) beam shear resistance was affected by the placement of the bricks and the presence of web reinforcement, (3) tensile strength of main reinforcement could be fully developed and (4) the compressive strength of masonry in beam action was greater than that of wall panels in direct compression. He suggested safe stress values to be used in design and he also concluded that elastic analysis similar to that employed in reinforced concrete design could be used in reinforced brick masonry design.

In 1939, Thomas and Simms[3] tested brick beams with high and low longitudinal reinforcement percentages and with stirrups. They concluded that, for a low percentage of tension reinforcement, there was no important difference between reinforced brick beams and the companion reinforced concrete beams in terms of strength, deformation or cracking, providing satisfactory bonding occurred in the brickwork. Beams with a high percentage of tension reinforcement usually failed in shear and the shearing stress at failure increased as the span-depth ratio decreased. The shearing stress at failure was doubled when the span-depth ratio decreased from 6 to 3.

Johnson and Thompson[4] (1963) investigated the relationship between shearing stress in beams and the strength characteristics of masonry disc assemblages. They also studied the effect of depth and beam shape, together with the type and strength of mortar on the shear strength. They concluded that the beam shear strength increased with an increase in mortar tensile strength, mortar compressive strength, and the masonry-disc tensile strength.

Sahlin[5] (1971) studied test results from various sources and found that the ultimate moment for masonry beams could be predicted reasonably well with the aid of the following equation developed for reinforced concrete beams:

$$\frac{M_u}{bd^2 f'_m} = q(1 - 0.59q) \leq 0.4 \qquad (2.1)$$

where

M_u = ultimate moment
b = width of beam
d = effective depth of beam
f'_m = strength of masonry in compression
q = $\rho f_y / f'_m$

ρ = steel area divided by masonry area (width times effective depth)

f_y = steel yield stress

He concluded that absorption of the bricks and the amount of tensile reinforcement affected beam shear strength but the most significant factor was the shear span-depth ratio, (a/d).

In 1975, Suter and Hendry[6] carried out an extensive test program to study the factors influencing the shear strength of masonry beams. The experimental program incorporated steel percentages of 0.24% and 1.46% with the shear span-depth ratio varied from 1 to 5. They found that the ultimate shear strength of reinforced brickwork beams increased only slightly with a large increase in the amount of tensile reinforcement, but increased significantly with decrease in the shear span-depth ratio. Test results indicated that a six-fold increase in tensile reinforcement increased the shear strength by approximately 25%. They suggested that, contrary to the case of reinforced concrete, the effect of steel percentage on beam shear strength could be neglected. They also reported that shorter beams exhibited gradual failure and longer beams exhibited a sudden type of shear failure.

In 1976, Suter and Keller[7] proposed a simplified limit states shear stress criterion based on available experimental results. They recommended a constant shear stress of 50 psi for beams with $(a/d)>2$ and a shear stress of 50(2d/a) psi for those with $(a/d) \leq 2$. This suggested criterion neglects the effects of the amount of reinforcement and the compressive strength of masonry. They also suggested that the current working stress approach was not always safe and the allowable shear stress could not be converted into the ultimate shear stress by simply multiplying by a factor.

In 1976 and 1978, Suter and Keller[8,9] found that the shear resistance of grouted reinforced masonry beams fell between that of reinforced concrete and reinforced masonry beams. They concluded that composite action existed between brickwork wythes and the grouted concrete cores, and the shear capacity of grouted reinforced masonry beams could be predicted using the shear strengths of the grout and brick sections according to their relative widths. They were also able to predict the shear strength of full scale lintels on the basis of results from tests of small scale beams.

2.2.2 Unrestrained Concrete Block Beams

Unlike reinforced brick beams, very little research has been conducted into the flexural behavior of reinforced concrete block beams, and only a few studies have been reported in the past three years.

In 1980, Rathbone[10] tested 36 single-course reinforced concrete blockwork beams to study the effect of amount and arrangement of reinforcement, strength of block and infill, grade of mortar and age at test. He found that the equation for the depth of beam in compression as recommended in the British standard CP110[11] (using a limit states approach without partial safety factors) was not always accurate but acceptable. However, the ultimate failure moment of his specimens could be predicted reasonably well using the ultimate limit state analysis, omitting partial safety factors. He also found that the deflection of the beams at failure was higher than that predicted using the provisions of CP110. However, deflections up to working loads could be predicted accurately or conservatively except for beams that were over-reinforced.

Suter and Keller[12] (1980) tested a total of 60 beams in order to determine the shear capacity of reinforced concrete block beams. Program variables including seven shear parameters with the most significant parameter being the ratio of shear span to effective depth. They verified that a significant increase in shear strength was obtained with a decrease in a/d ratio, a relationship which was already well documented in previous studies of reinforced concrete and reinforced brick masonry beams. In this particular test program, a doubling of the beam depth resulted in a 30% decrease in shear stress. Such a large reduction indicated the size effect for reinforced concrete masonry beams was more pronounced than that predicted by Kani's[13] size effect theory for reinforced concrete beams. They also found that the shear strength of reinforced concrete masonry beams fell between that of reinforced concrete and reinforced brick masonry beams. Other important conclusions included the following: (1) the shear strength was affected by the type but not the slump of fill, (2) joint spacing only affected the shear strength of beams filled with high strength grout, (3) deflections of reinforced concrete masonry beams were not likely to produce serviceability problems.

2.2.3 Restrained Masonry Members

McDowell et al[14] (1956) proposed an arching action theory to explain and predict the increased strength of unreinforced masonry members which are restrained by rigid edge supports. The theory was based on the following assumptions: (1) masonry cannot withstand tensile stress, (2) the mode of failure resembles that for a three-hinged arch due to crushing at mid-span and the ends, (3) the stress distribution is triangular.

Cohen and Liang[15] in the discussion of the above paper described a method of obtaining the capacity of unreinforced masonry walls based on a plastic stress block instead of a triangular stress distribution as suggested by McDowell et al.

Baker[16] in 1978 presented a theory based on arching action to determine the cracking strength of wall panels with in-plane restraints. His theory indicated that the cracking load is more affected by the axial and rotational stiffness of the supports than by the modulus of the materials or the slenderless ratio of the wall.

The most recent research on the effects of restraints on the behavior of concrete block masonry beams was conducted by Hatzinikolas, Longworth and Warwaruk[17] at the University of Alberta. The experimental study consisted of testing four 8 ft. span beams with depths of one to four courses, 2 #5 bars as tension reinforcement and no shear reinforcement. End restraint was provided by large fixed concrete blocks at the ends. All beams failed in shear, but their shear resistance was approximately twice that of unrestrained beams. The ratio of test values to ultimate shear strengths based on provisions of the ACI Building Code[18] (ACI 318-1977) ranged from 1.79 to 3.01. The ratio of test values to allowable values ranged from 3.46 to 5.67 on the basis of CSA S304[19]. Strains in the reinforcement indicated that the capacity of the beams was greatly influenced by the end restraints. It was concluded that design procedures based on simple span action underestimate the capacity of restrained beams since arching action introduced by the horizontal reaction forces is not considered.

2.3 Analysis of Masonry Beams

The following discussion of analysis procedures for masonry beams is based on principles developed for reinforced concrete.

2.3.1 Cracking Moment

The moment at first cracking, M_{cr}, is given by

$$M_{cr} = \frac{f_{rm} I_g}{y_t} \tag{2.2}$$

where

f_{rm} = modulus of rupture of masonry
= $0.6\sqrt{f'_m}$, MPa

I_g = moment of inertia of the gross uncracked section

y_t = distance from centroidal axis of gross section to the extreme tension fiber

2.3.2 Location of Neutral Axis

The position of the neutral axis in singly reinforced rectangular beams can be determined by means of the properties of the transformed section

$$k = \sqrt{2\rho n + (\rho n)^2} - \rho n \tag{2.3}$$

where

k = ratio of depth of neutral axis to the effective depth, d

n = modular ratio = E_s/E_m

2.3.3 Flexure of a Singly Reinforced Masonry Beam Section in the Service Load Range

For a singly reinforced rectangular beam section shown in Figure 2.1(b), the internal resultant compressive force is

$$C = 0.5bkdf_m \tag{2.4}$$

where

kd = depth of neutral axis

f_m = compressive stress in extreme fiber

and the internal resultant tension force is

$$T = A_s f_s \qquad (2.5)$$

where

A_s = area of steel

f_s = steel stress

For equilibrum of forces, T = C, therefore

$$A_s f_s = 0.5bkdf_m \qquad (2.6)$$

The lever arm of the internal force is

$$jd = (d - kd/3) \qquad (2.7)$$

Thus the moment of resistance,

$$M = 0.5bkdf_m(d - kd/3) = A_s f_s(d - kd/3) \qquad (2.8)$$

Equation 2.8 can be used to determine the stresses in the masonry and steel for a given moment, or the moment for a given stress, when the dimensions of the section, the steel area and its location are known.

2.3.4 Ultimate Strength of Masonry Beams

For a singly reinforced section shown in Figure 2.1(c), the resultant internal tensile force at ultimate load is $T=A_s f_y$, for a yielding failure. Using Whitney's rectangular stress block, the resultant internal compressive force is

$$C = 0.85f'_m ab \qquad (2.9)$$

where

a = depth of the equivalent rectangular stress block

The internal lever arm is given by

$$jd = (d - 0.5a) \qquad (2.10)$$

For a yielding failure, by equilibrum of forces, we have

$$a = \frac{A_s f_y}{0.85f'_m b} \qquad (2.11)$$

Therefore, the ultimate moment is

$$M_u = T(jd) = C(jd)$$

or

$$M_u = A_s f_y (d - 0.5a) = 0.85f'_m ab(d - 0.5a) \qquad (2.12)$$

Equation 2.12 can be used to predict the capacity of a simply supported beam.

2.3.5 Effective Moment of Inertia

An empirical equation proposed by Branson[20] is used to predict the effective moment of inertia, I_e, for a reinforced concrete member

$$I_e = \left(\frac{M_{cr}}{M_{max}}\right)^3 I_g + \left[1 - \left(\frac{M_{cr}}{M_{max}}\right)^3\right] I_{cr} \leq I_g \qquad (2.13)$$

where

$M_{cr} = f_r I_g / y_t$

M_{max} = maximum service load moment under which deflection is computed

I_{cr} = moment of inertia of cracked transformed section

If we consider that the cracking of a reinforced masonry beam is similar to that of a reinforced concrete beam, Equation 2.13 may be used to predict the effective moment of inertia of a simply supported masonry beam, where the modulus of rupture, $f_r = f_{rm}$, the modulus of rupture of masonry.

2.3.6 Shear Resistance

The maximum shear resistance of a masonry beam (v_u) may be expressed as

$$v_u = v_m + v_s \tag{2.14}$$

where

v_m = shear resistance of the masonry

v_s = shear resistance of web reinforcement

The shear resistance of the masonry may be expressed as

$$v_m = 0.17\sqrt{f'_m} \quad \text{(MPa)} \tag{2.15}$$

If the web reinforcement is in the form of vertical stirrups then

$$v_s = \frac{A_v f_s}{bs} \tag{2.16}$$

where

A_v = area of stirrup

f_s = f_y when steel yield

s = spacing of stirrups

2.4 Three-Hinged Arch Failure Model

In a lintel beam restrained at its ends by masonry walls, longitudinal forces are developed in the lower portion of the beam cross section as the beam seeks to deflect under the action of lateral loads. Thus an arching action is developed, providing increased capacity as compared with a simply supported beam. When the restraint is rigid, complete arching action is developed. However, such conditions do not occur in actual construction, and the degree of arching, which depends on the amount of restraint, is indeterminate. The magnitude of the longitudinal restraining force and its location are both unknown except under controlled laboratory conditions.

As suggested by various investigators[14,15,16,21] in the study of restrained structures, a three-hinged arch model provides the simplest approach to an analysis of arching action.

An unreinforced restrained beam subjected to third-point loads is shown in Figure 2.2(a). The axial force, H, developed by the end restraints produces arching action. The maximum possible arching occurs when the rise in the thrust line is equal to the depth of the beam as shown. Thus

$$Hh = P(L/3) \tag{2.17}$$

where

H = total thrust
h = depth of beam
P = applied load
L = clear span

However, it is impossible to have a thrust line having zero thickness. Practically, the thrust would spread over a finite depth as in Figure 2.2(b). Failure at points A, B and C would be a function of the thrust, the bearing area and the strength of masonry.

For beams with longitudinal reinforcement, the restraining force at the ends of the beam, points A and C, would be less than the thrust at point B, due to the contribution of the longitudinal reinforcement. For simplification and by equilibrium, we can assume that the thrusts at points A, B and C all have the same magnitude implying that the thrust at the ends is actually the sum of the restraining force and the force in the longitudinal reinforcement.

For a bearing depth of t, the arch rise becomes (h-t). Considering the deflection (Δ) at mid-span, the arch rise is then reduced to ($h-t-\Delta$). Therefore, for three-hinged arch action, we have the following moment equation

$$H(h - t - \Delta) = P(L/3) \qquad (2.18)$$

In order to evaluate the arch thrust, both the stress at the failure points and the depth t have to be estimated. With appropriate assumptions, Equation 2.18 can be used to predict the maximum applied load for a restrained member.

2.5 Prediction of End Restraint

The difference between a restrained and an unrestrained flexural member is the existence in the former of an longitudinal compressive force whose magnitude varies with the applied load and deformation. Usually this force acts below the centroid of the beam.

Analyses of the behavior of restrained structures have been performed by some investigators[22,23]. Although the approaches in these analyses were quite different, the resulting governing equations are similar.

Consider the beam shown in Figure 2.3(a) subjected to two concentrated loads and a longitudinal force F located at a distance y above the tensile reinforcement. The free body diagram shown in Figure 2.3(b) represents one half of the beam. For equilibrum,

$$P(L/3) = Fe + M_a \qquad (2.19)$$

where

e = eccentricity of the restraining force measured from the neutral axis
= $(d - kd - y)$

M_a = mid-span positive moment

or

$$P(L/3) = F(d - kd - y) + M_a \qquad (2.20)$$

If we include the effect of deflection,

$$P(L/3) = F(d - kd - y) + M_a - F\Delta \qquad (2.21a)$$

or

$$P(L/3) = F(d - kd - y - \Delta) + M \qquad (2.21b)$$

Using a straight line - no tension stress distribution at the mid-span section as shown in Figure 2.3(c). We have

$$M_a = (0.5bkdf_m)(2kd/3) + A_s f_s (d - kd) \qquad (2.22)$$

By force equilibrum for the free body shown in Figure 2.3(b)

$$C = F + T$$

or

$$0.5bkdf_m = F + A_s f_s \qquad (2.23)$$

By substituting Equations 2.22 and 2.23 into Equation 2.21, we have

$$P(L/3) = F(d - kd/3 - y - \Delta) + A_s f_s (d - kd/3) \qquad (2.24)$$

At ultimate load, using a Whitney's rectangular stress block shown in Figure 2.3(d),

$$M_a = 0.85f'_m ab(c - a/2) + A_s f_s (d - c) \qquad (2.25)$$

and

$$0.85f'_m ab = F + A_s f_s \qquad (2.26)$$

Similarly

$$P(L/3) = F(d - a/2 - y - \Delta) + A_s f_s (d - a/2) \qquad (2.27)$$

where

$f_s = f_y$ for a yielding failure

Equations 2.24 and 2.27 can be used to predict the magnitude of the restraining force if the location of this axial force is known.

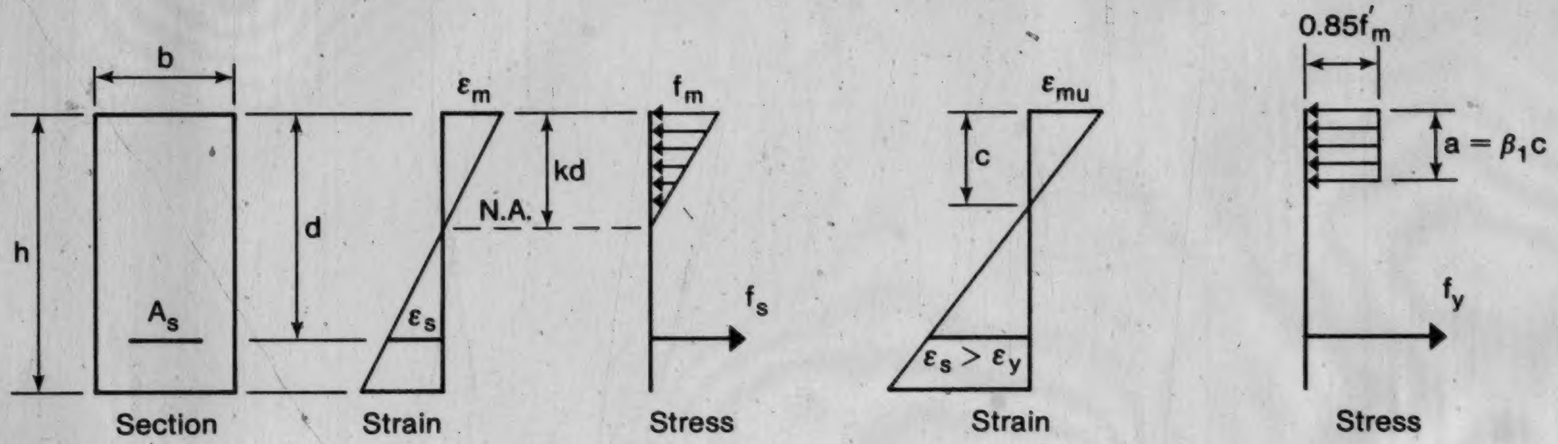
b
h
A_s
Section
d
ε_m
ε_s
Strain
kd
N.A.
f_m
f_s
Stress
ε_{mu}
c
$\varepsilon_s > \varepsilon_y$
Strain
$0.85f'_m$
$a = \beta_1 c$
f_y
Stress

(a) (b) Service Load (c) Ultimate Load

Figure 2.1 Stress and Strain Distributions in a Singly Reinforced Section

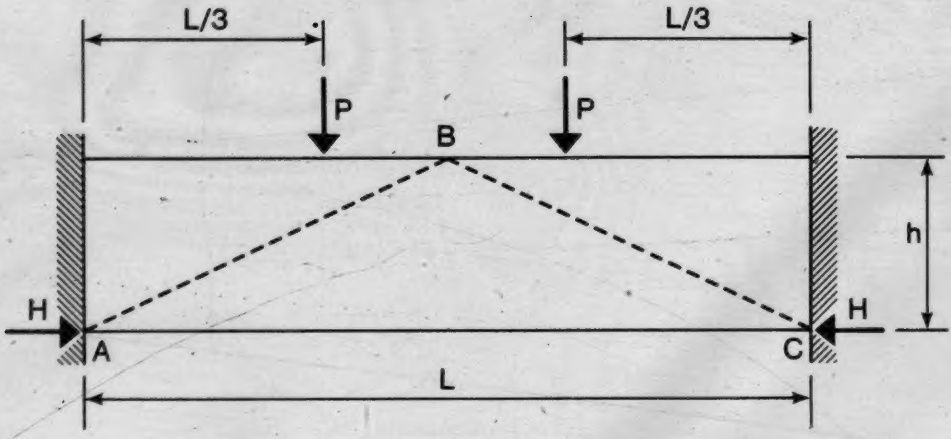
L/3
L/3
P
P
B
h
H
H
A
C
L

(a) Simplified Line of Thrust

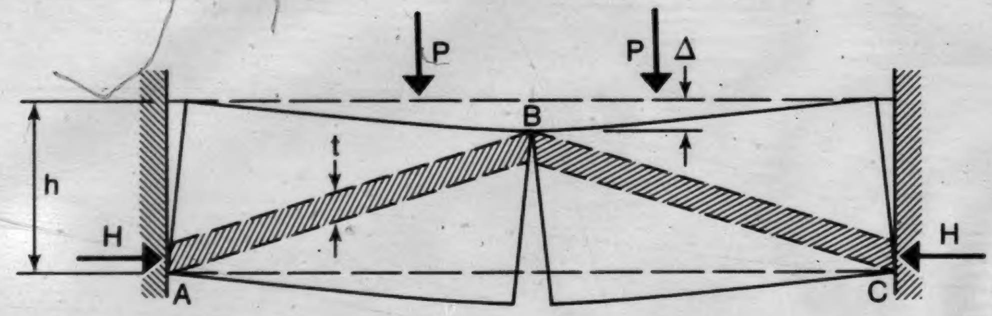
P
P
Δ
B
t
h
H
H
A
C

(b) Distribution of Thrust

Figure 2.2 Distribution of Thrust in a Restrained Beam

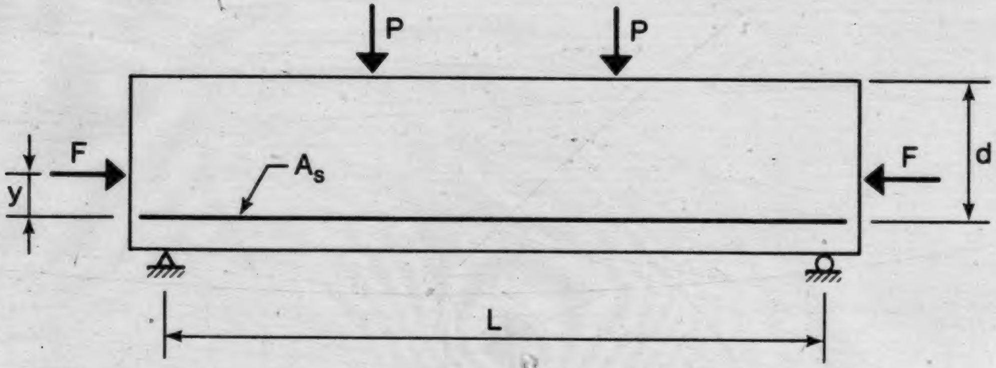

(a) Forces Acting on a Restrained Beam

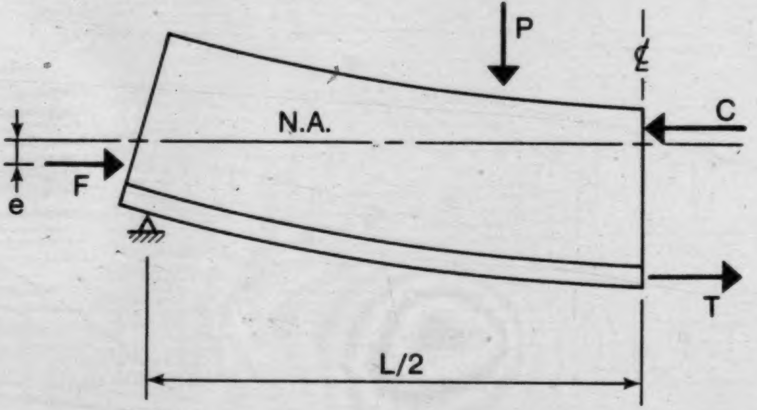

(b) Free Body Diagram of Half Span

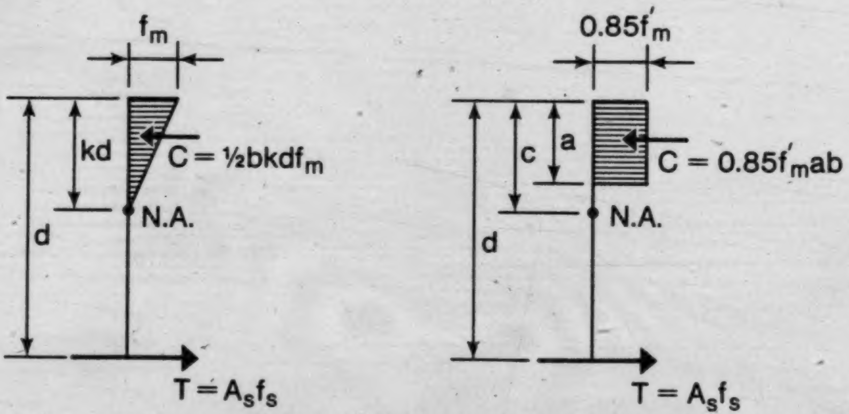
f_m
kd
C = ½bkdf_m
N.A.
d
T = A_sf_s
0.85f′_m
c
a
C = 0.85f′_mab
N.A.
d
T = A_sf_s

(c) Linear Stress Distribution (d) Conditions at Failure

Figure 2.3 Equilibrum Conditions for a Restrained Beam

3. Experimental Program

3.1 Materials

Materials used in the construction of the test specimens are commercially available in the Edmonton area, and are typical of those presently being used in building construction.

3.1.1 Concrete Block Units

All the blocks were in metric sizes and were supplied by one manufacturer. The common units used for the construction of all the specimens were the 200x200x400 mm Standard blocks (Stretcher and Mixed End), the 200x200x400 mm Bond Beam Lintel blocks and the 200x200x200 mm Half blocks. The units are shown schematically in Figure 3.1. The dimensions of the units are listed in Table 3.1.

3.1.2 Mortar

The mortar used throughout the test program was ready-mix mortar supplied by one manufacturer. The mortar was delivered to the laboratory in a large steel container either in half cubic metre or one-third of a cubic metre quantities. The mortar was covered with a plastic sheet to prevent evaporation and resultant stiffening. It was frequently retempered using a shovel in order to maintain a uniform consistency. The mason was permitted to add some water required for reasonable workability according to his own judgement.

50 mm test cubes were made from the batches of mortar used by the mason in specimen preparation (not directly from mortar in the container). After the mortar cubes were cast, the moulds were covered with a thin plastic sheet for at least 48 hours. The moulds were then stripped and the mortar cubes were cured either in a lime saturated water solution or under the same environment as that of the beam specimens.

Since the test program was divided into three parts, three batches of ready-mix mortar were ordered at about two month intervals. The 28 day compressive strengths of the mortar cubes from the first two batches were not low (9.16 MPa and 12.16 MPa). However, the strength of the cubes from the third batch was only 6.66 MPa at approximately 26 days.

The mortar cubes for the first two series were both tested at 7 or 28 days. The cubes for the third series were tested at the same age as the corresponding prisms, either at 13 or 26 days.

3.1.3 Grout

The grout used in casting the test specimens in the first two series was ready-mix concrete obtained from a local supplier. Initially, it was intended to maintain the same concrete strength for both series. However, cylinder tests indicated that the strength of the concrete for the first series was 31.27 MPa and 19.39 MPa for the second series. During grouting, water was added to the grout to make it more workable in order to fill the voids, especially those in which shear reinforcement was located.

150 mm diameter concrete cylinders made in non-absorptive moulds and 75x75x150 mm block moulded concrete prisms were cast in accordance with CSA Standard A179M-1976[24]. These control specimens were either moist cured or air cured in the laboratory under the same environment as the beam specimens.

In the third series of prism tests, two different grouts, grout A and grout B, were batched in the laboratory using normal portland cement and aggregate obtained from a local supplier. The mix proportions of these two mixes are shown in Table 3.2. Three 150 mm concrete cylinders were cast from each batch of approximately 0.2 m^3 in volume.

The cylinders and prisms were either tested at 7 days or at the same age as the beam or block prism specimens.

3.1.4 Reinforcement

20M bars were used for tension reinforcement and 10M bars were used for shear reinforcement. The bars were cut to the require length in the laboratory.

Coupon tests were conducted to determine the yield and ultimate strength for both bar sizes. All coupons exhibited a well defined yield point and yield plateau. The stress-strain relationships for the reinforcing bars are shown in Figure 3.2. The physical properties of the bars are shown in Table 3.3, wherein each value is the average of 3 specimens tested.

3.2 Test Specimens

A detailed description of the prism and beam specimens and the method of specimen fabrication are presented in this section.

3.2.1 Prisms

Prisms were used as control specimens throughout the test program. It has been suggested that the common practice of testing two course high prisms would result in a higher compressive strength due to the lateral confinement at the tops and bottoms of the prisms. Therefore, three course high prisms were used in this test program. They were constructed in running bond, with one and a half standard blocks in each course. No vertical or lateral reinforcement was used. Mortar was applied only to the face shells and the joints were tooled. For grouted prisms, the grout was trowelled level with the top of the prism so as to provide a plane load surface. Figure 3.3(a) illustrates schematically the prism dimensions.

In the first and second beam test series, six prisms were constructed at the same time as the beams, using the same mortar and grout as for the corresponding beams. These prisms were tested vertically with a load applied normal to the bed joints.

In the third series, nineteen prisms were built (3 courses high) in running bond. Eleven of these prisms had the same dimensions as the control prisms described previously, the remaining eight prisms were larger, with two and a half blocks in each courses. The dimensions of these prisms are shown in Figure 3.3. The object of the third series was to obtain information about the difference in compressive strength and modulus of elastically of the masonry tested with load applied normal or parallel to the bed joints. Two different prism sizes and two different grout strengths for the prisms were used. Half of the prisms were tested under uniform load applied normal to the bed joints and the remaining half were tested under load applied parallel to the bed joints. Table 3.4 summarizes the prism classification, the time of test and the direction of load.

All the prisms in the three series were air cured in the laboratory environment which was maintained at 70°F and 40% relative humidity.

3.2.2 Full Scale Beam Specimens

3.2.2.1 General

Fourteen full scale beam specimens were constructed to provide a clear span of 3.6 m. The height of the beams varied from 2 to 4 courses and the width for all beams was 190 mm. Of these fourteen beams, four were simply supported and four were restrained at both ends by means of large concrete blocks prestressed to the laboratory concrete floor. These eight beams were constructed in the first series of the test program. The remaining six, constructed in the second series, were supported at both ends by walls with varying lengths. The simply supported beams are designated as Type SB beams, those restrained by fixed concrete blocks at both ends are Type RB beams and those supported on walls are Type EB beams.

3.2.2.2 Reinforcement Details

Tension reinforcement in each beam consisted of two 20M bars located at the same level 100 mm from the bottom of the beam. The bars terminated at 25 mm from the ends of the beam. Plate 3.1 shows the location of bars in a typical beam.

Shear reinforcement was in the form of single-leg stirrups fabricated from 10M bar. The stirrups were cold bent in the shop to an accurate pattern.

Before placing the reinforcement, all electrical resistance strain gauges were mounted on the bars and waterproofed. The strain gauges on the stirrups were located at d/2 from the top of the beam with the stirrups in their correct position. The strain gauges on the tension bars were positioned to face the near side of the beams.

3.2.2.3 Beam Fabrication

All beams were constructed in running bond by an experienced mason. The bed and head joints were 10 mm with mortar applied only to the face shells, cut flush and then tooled. Blocks with cracks or large chips were not used and blocks with pre-drilled holes were located to accomodate wires from the strain gauges. The bottom block courses were built using bond beam lintel blocks and the remaining courses were built using standard (stretcher or mixed end) and half blocks. The mason kept the beams straight and plumb using a horizontal line and level. Grouting was performed approximately four days after the masonry work was completed, so that the mortar had developed sufficient strength to withstand the stresses due to pouring. The grout was vibrated using a mechanical vibrator with a one inch diameter shaft. The open ends at the lowest course of the beams were closed with plywood pieces during grouting. The grout was trowelled level with the top of the concrete blocks.

Type SB Beams

The four Type SB beams were simply supported. the overall length was 4.0 m and the clear span was 3.6 m. One beam was 2 courses high, two were 3 courses high and one was 4 courses high. All specimens except one of the 3 course beams were reinforced with shear reinforcement. Sketches of the four specimens are shown in Figure 3.4. The following construction procedures were used.

1. The first course was laid on the laboratory floor using only bond beam units.
2. The tension reinforcement was positioned the following day, with the lead wires pulled through the pre-drilled holes in the blocks.
3. The remaining courses were constructed using standard and half blocks.
4. Stirrups were located at every hole along the shear spans and were supported by tying them to a horizontal bar lying along the top of the beam, lead wires from the stirrup gauges were pulled through the holes in the blocks. Plate 3.2 shows the way how the stirrup was supported.
5. All electrical wires were secured to prevent them from being drawn inward during grouting and mortar droppings at the bottom of the beams were removed as much as possible.
6. The beams were grouted in one lift. The top surface was smoothed and the stirrup support bars were removed.

Type RB Beams

The four Type RB specimens were restrained by fixed concrete blocks at both ends. The overall length of the beams was 5.2 m and the clear span was 3.6 m. One beam was 2 courses high, two were 3 courses high and one was 4 courses high. The reinforcement was exactly the same as for the corresponding Type SB beams. Figure 3.5 shows the details of the Type RB specimens. The construction sequence was as follows:

1. Two large concrete blocks which were to provide the end restraint were positioned and prestressed to the laboratory floor.
2. The end supports consisting of one course of two blocks were laid on the floor adjacent to the concrete blocks.
3. To provide temporary support during construction of the beams, one course of blocks and a 6 mm sheet of plywood were laid between the end supports.

The remainder of the procedure was the same as that for construction of the Type SB beams. The gaps between the ends of the beams and the concrete blocks were grouted to ensure full contact. Two weeks after grouting, the support blocks were removed.

Type EB Beams

The six Type EB specimens were supported at both ends on walls 3 courses high. All six beams were 4 courses high with a clear span of 3.6 m. Two beams were supported on walls 4 blocks long. One of these beams contained no stirrups. One beam was supported on walls 3 blocks long. Two beams were supported on walls 2 blocks long and one of these contained no stirrups. One beam was supported on walls 1 block long. Shear reinforcement was exactly the same as for Type SB and Type RB specimens. Figure 3.6 shows details of these beams. The construction sequence was as follows:

1. The walls at both ends of the beams were constructed.
2. To provide temporary support during construction, 3 courses of blocks together with a 6 mm sheet of plywood were laid between the walls.

The remainder of the procedure was the same as for Type SB beams. The support blocks were removed two weeks after grouting.

The same mortar and grout were used in the construction of both Type SB and Type RB beams, but different batch of mortar and grout were used for Type EB beams. All the specimens were cured in the laboratory at a temperature of 70°F and a relative humidity of 40%.

3.3 Instrumentation

3.3.1 Prisms

In the first and second series of the test program, all the prisms were tested in vertical compression with the load applied normal to the bed joints. For measuring vertical deformation over a 400 mm gauge length, linear variable differential transducers (LVDT's) were located on both faces of the prisms and centered at mid-height.

In the third series of prism tests, vertical deformations were measured by LVDT's on a gauge length of 400 mm for all prisms except those larger prisms (PLA and PLB) tested with load parallel to the bed joints, whereas a gauge length of 600 mm was used.

3.3.2 Full Scale Beam Specimens

Vertical deflections were measured at 5 points which were equally spaced at 600 mm along the length of the beams using LVDT's calibrated to read in increments of 1/100 mm. The location of the LVDT's is shown in Figure 3.7(a). Plate 3.3 shows the support system for the LVDT's.

Horizontal strains in the constant moment region and in one of the shear spans were also measured by LVDT's positioned on the face of the beams with a gauge length of 600 mm. Two of the LVDT's were located in the constant moment region with one located 25 mm below the top surface and the other at the level of the tension reinforcement. A second pair of LVDT's was located in one of the shear spans and at the same vertical positions as the pair in the constant moment region. The locations of these LVDT's are also shown in Figure 3.7(a). Plate 3.4 shows the attachment of the LVDT's to the surface of the beam.

The strains in the stirrups were measured by strain gauges. Three stirrups were instrumented in each beam. These stirrups were located at one end, the first one at 100 mm from the face of support and the others placed in alterate block cores as shown in Figure 3.7(b). All gauges were d/2 below the top of the beam.

The strains in the main reinforcement at midspan of all beams were measured by strain gauges. For all Type RB beams, three strain gauges were mounted near one end of the bar, with the first located at the face of the support and the others spaced at 330 mm toward the end of the beam. The locations of these strain gauges are shown in Figure 3.8(a). For the Type EB beams, strain gauges were also mounted near the ends of the bars with one always located at the face of the supporting wall and the remainder spaced at 330 mm towards the end of the beam. Figure 3.8 shows the locations of these strain gauges.

In order to avoid possible damage, all lead wires from the strain gauges were led out of the beams through pre-drilled 10 mm holes in the blocks at the location of the gauges.

The two vertical loads on the beams were measured by load cells with a capacity of 450 kN each. The horizontal restraining force in the Type EB beams was measured by a load cell with a capacity of 180 kN.

Loads, deflections, and strains were monitored and recorded automatically in the Nova Computer. After each test was completed, the data stored in the Nova Computer was transferred to a permanent file in the AMDAHL 470 computer for further processing.

3.4 Test Procedure

3.4.1 Prisms

All prisms were tested in axial compression using a MTS hydraulic testing machine which is capable of providing a vertical compression load of 6.23 MN. A fork lift was used to transport the prisms to the MTS machine for testing. Prisms tested with load normal to the bed joints were located under the head of the machine in the same orientation as they were constructed. Those tested with load parallel to the bed joints were rotated 90 degrees before they were moved to the machine. All the prisms were capped top and bottom with high strength plaster of paris and 6 mm steel plates so that the load was applied uniformly over the total area of the prisms. The LVDT's were removed when the applied load reached 80% of the maximum load.

3.4.2 Full Scale Beam Specimens

All beam specimens were tested at an age of 28 to 35 days. Two symmetrically placed concentrated loads were applied at the third point of the 3.6 m span. The loads were achieved by two manually controlled air-compression jacks. Plate 3.5 shows the test set up.

The supports for Type SB specimens consisted of a roller which provided free rotation and horizontal movement of one end, and a rocker which provided free rotation for the other end. Plates 3.6 and 3.7 show these two supports.

For Type EB specimens, the horizontal restraint was provided by two 19 mm high strength steel rods holding the bottom course of the supporting walls at both ends, with a load cell measured the restraining force. Plate 3.8 shows the arrangement.

The vertical loads were transmitted to the beam through 25x100x200 mm steel plates set in plaster of paris. After the loading apparatus was in place, all measuring devices (transducers and strain gauges) were positioned and connected.

At the beginning of a test, a load of 10 kN was applied to the beam and then released. Initial readings of all the measuring devices were then taken. The loads were slowly applied in increments of approximately 5 kN. After each load increment, all readings were taken and stored and surface cracks were marked. To prevent damage to the instrumentation, the LVDT's located in the constant moment region were removed just prior to beam failure. Generally, each beam test was completed within a two hour period.

Table 3.1 Dimensions of Concrete Block Units

Masonry Unit	Modular Dimensions			Actual Dimensions		
	Width (mm)	Height (mm)	Length (mm)	Width (mm)	Height (mm)	Length (mm)
Stretcher	200	200	400	190	190	390
Mixed End	200	200	400	190	190	390
Half	200	200	200	190	190	190
Bond Beam Lintel	200	200	400	190	190	390

Table 3.2 Grout Mix Design

Mix Designation	28 Day Design Strength (MPa)	Slump (mm)	Mix Proportions by Weight (Kg/m³)	Air Entrainment
A	34	150	C : 415 S : 730 1/2 A : 500 3/4 A : 540 H_2O : 151	No
B	28	125	C : 340 S : 715 3/4 A : 1080 H_2O : 160	No

Table 3.3 Physical Properties of Reinforcing Steel

Bar Type	Yield Strength (MPa)	Yield Strain (mm/mm)	Ultimate Strength (MPa)	Modulus of Elasticity (MPa)
10M Series 1	545	0.00252	864	216000
20M Series 1	417	0.00220	650	189000
10M Series 2	473	0.00254	776	186000
20M Series 2	434	0.00224	728	193000

Table 3.4 Properties of Prisms

Prism	Dimension	Grout	Load Direction	Test Time*
PS 1-6	S**	ready-mix	N#	same as beam spec.
PE 1-6	S	ready-mix	N	same as beam spec.
PA 1,3,5	S	A	P##	12
PA 4,6	S	A	N	13
PB 1,3,5	S	B	P	26
PB 2,4,6	S	B	N	26
PLA 1,3	L***	A	P	13
PLA 2,4	L	A	N	14
PLA 5	L	A	P	26
PLA 6	L	A	N	26
PLB 1	L	B	P	27
PLB 2	L	B	N	27

* Days after casting
** Dimension is shown in Fig. 3.3(a)
*** Dimension is shown in Fig. 3.3(b)
# Normal to bed joints
## Parallel to bed joints

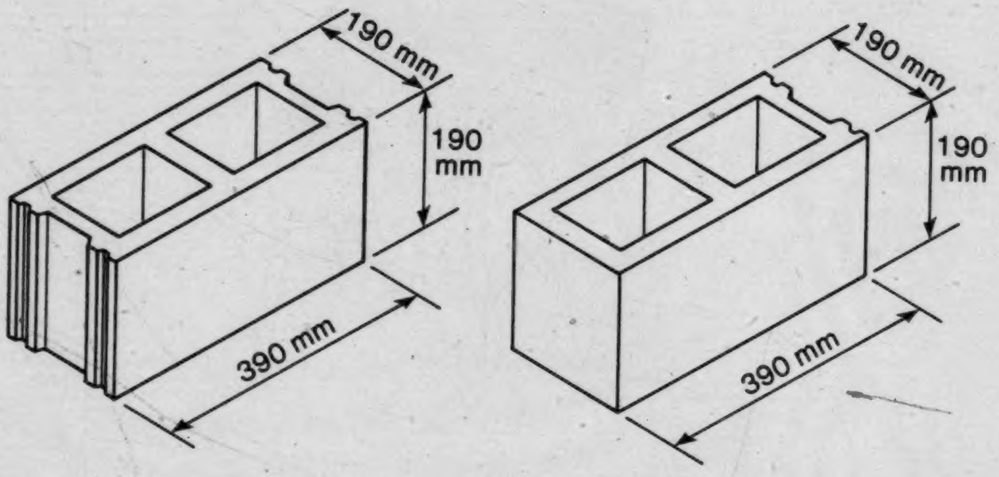
190 mm
190 mm
390 mm
190 mm
190 mm
390 mm

(a) Stretcher (b) Mixed End

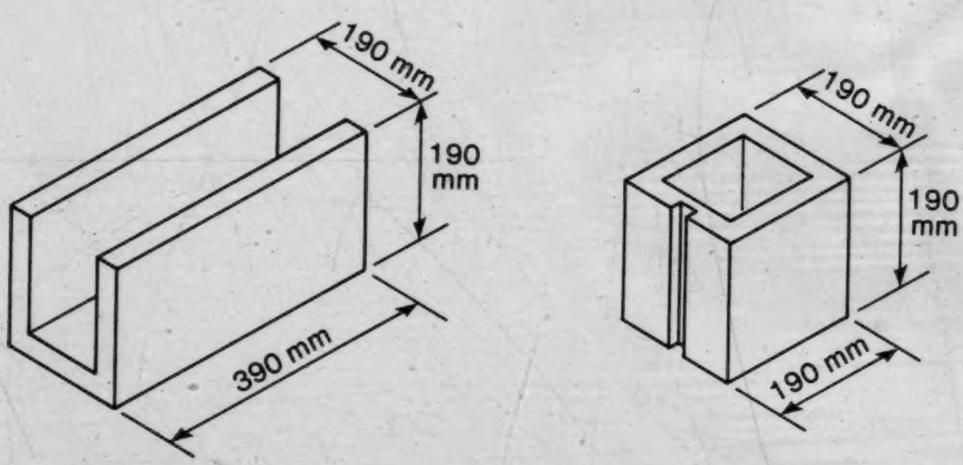
190 mm
190 mm
390 mm
190 mm
190 mm
190 mm

(c) Bond Beam Lintel (d) Half Block

Figure 3.1 Masonry Units

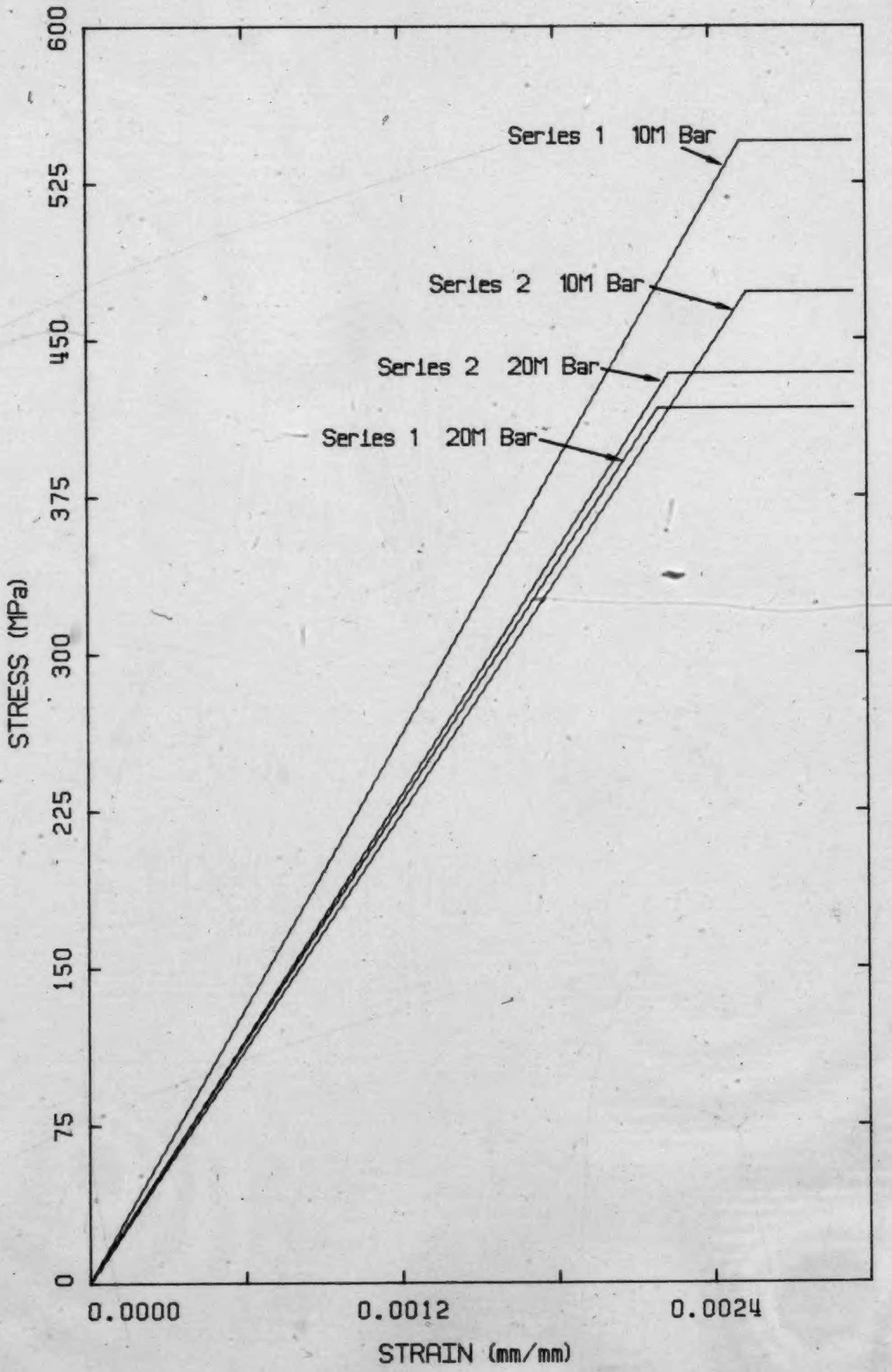

Figure 3.2 Stress-Strain Relations for Reinforcing Steel

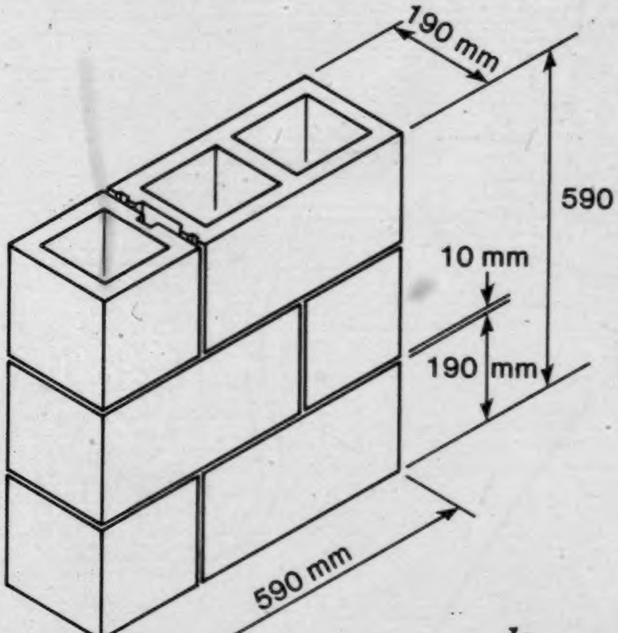
190 mm
590 mm
10 mm
190 mm
590 mm

(a) Small Prism

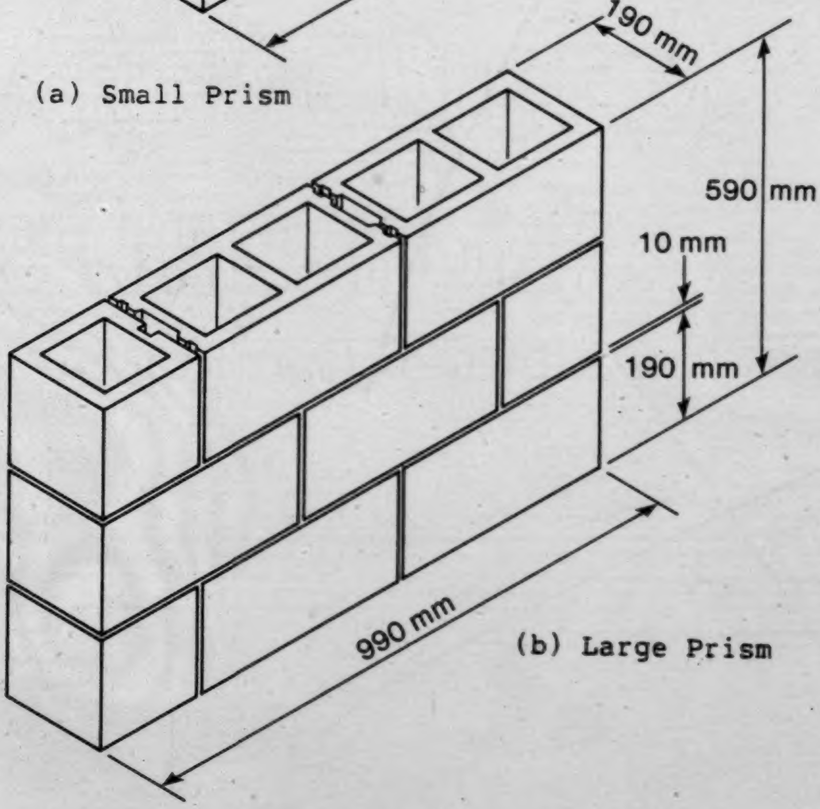
190 mm
590 mm
10 mm
190 mm
990 mm

(b) Large Prism

Figure 3.3 Masonry Prisms

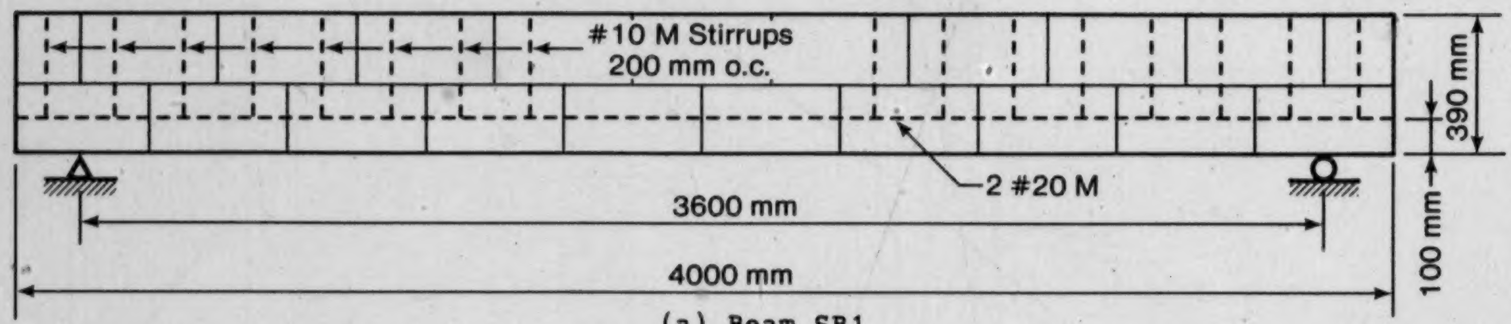
#10 M Stirrups
200 mm o.c.
390 mm
100 mm
2 #20 M
3600 mm
4000 mm

(a) Beam SB1

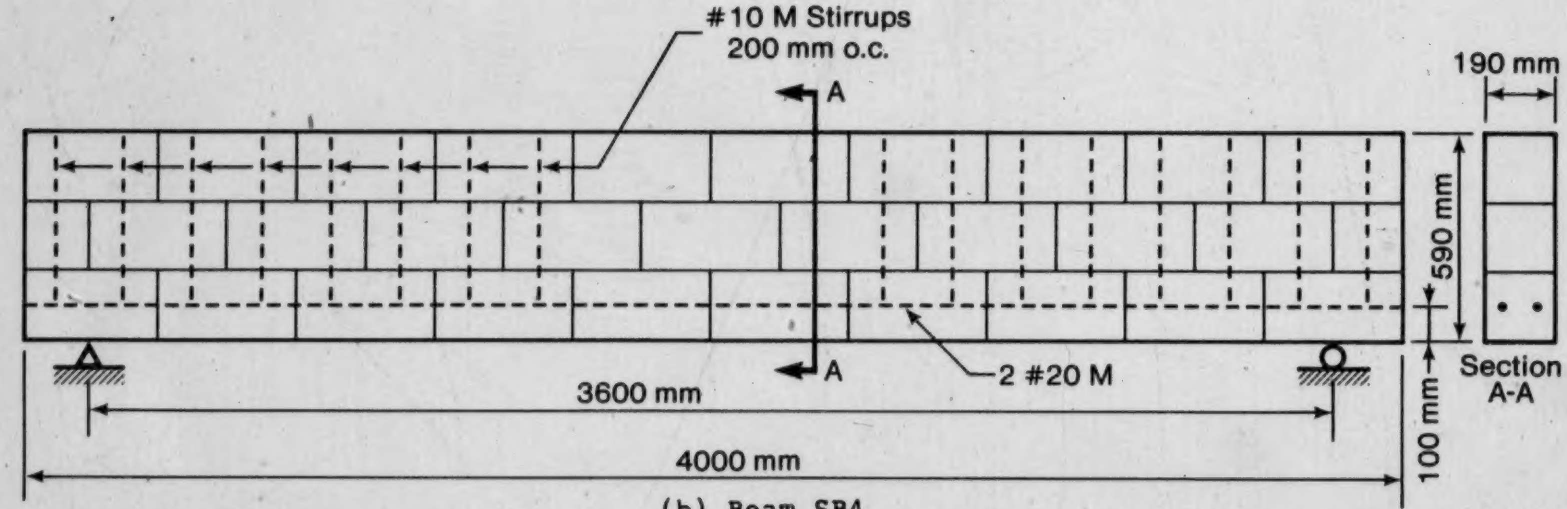
#10 M Stirrups
200 mm o.c.
A
A
190 mm
590 mm
100 mm
2 #20 M
3600 mm
4000 mm
Section
A-A

(b) Beam SB4

Figure 3.4a Type SB Beam Details

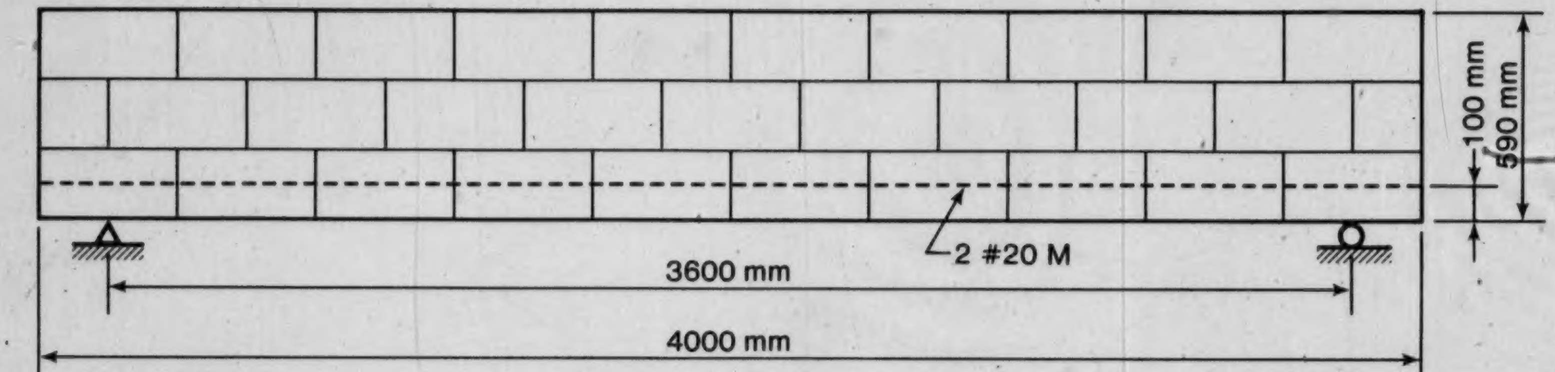
100 mm
590 mm
2 #20 M
3600 mm
4000 mm

(c) Beam SB3

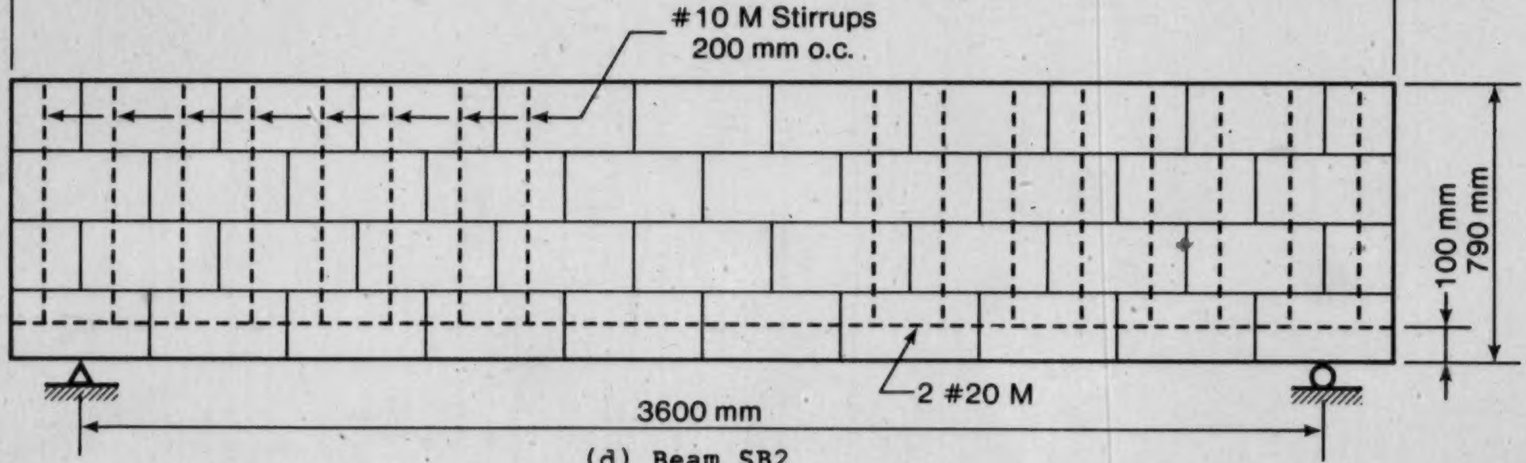
#10 M Stirrups
200 mm o.c.
100 mm
790 mm
2 #20 M
3600 mm

(d) Beam SB2

Figure 3.4b Type SB Beam Details

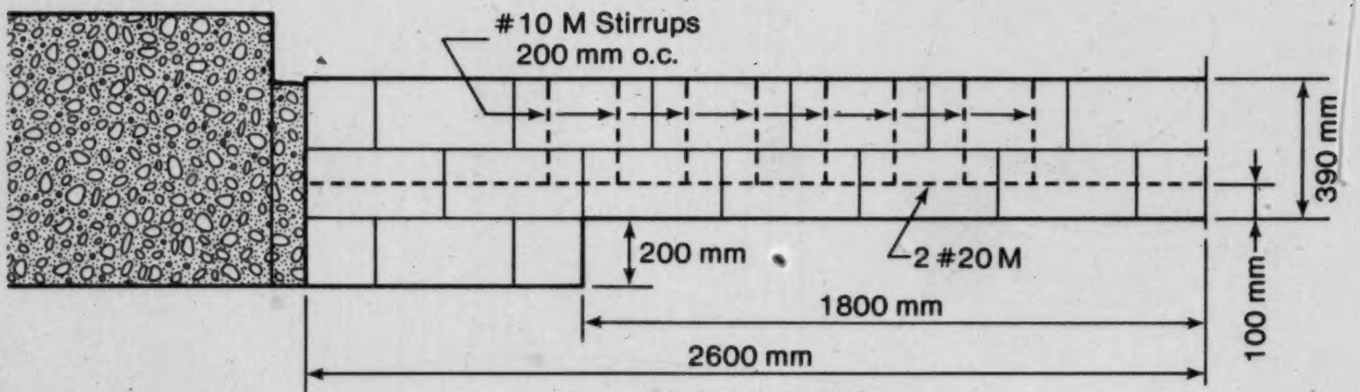
#10 M Stirrups
200 mm o.c.
390 mm
100 mm
200 mm
2 #20 M
1800 mm
2600 mm

(a) Beam RB1

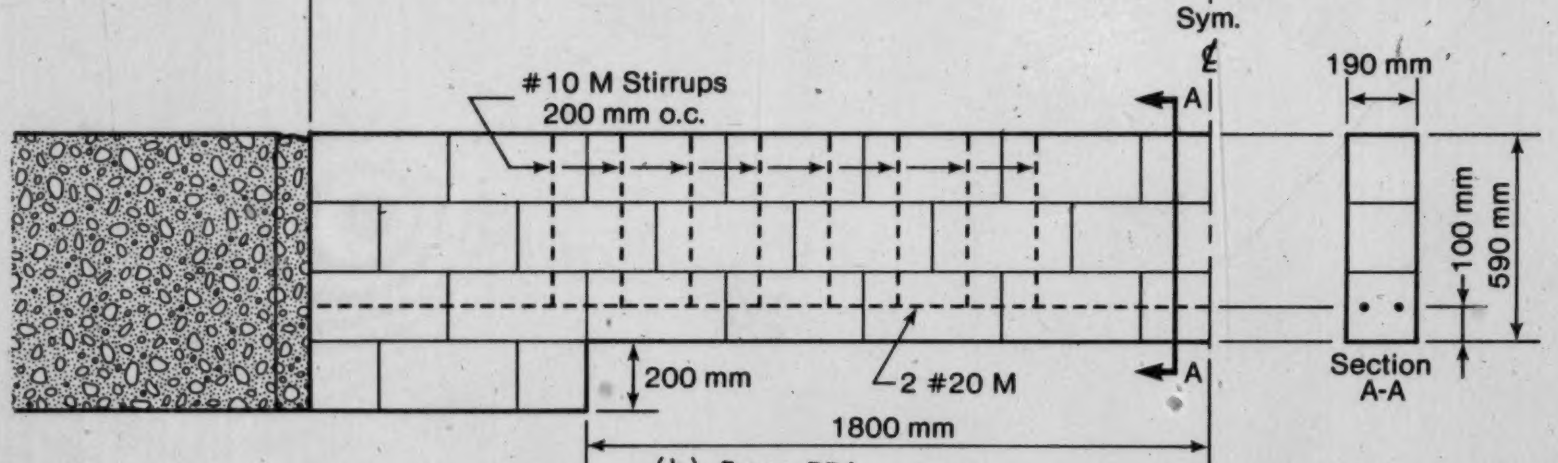
Sym.
℄
#10 M Stirrups
200 mm o.c.
A
A
190 mm
100 mm
590 mm
200 mm
2 #20 M
1800 mm
Section
A-A

(b) Beam RB4

Figure 3.5a Type RB Beam Details

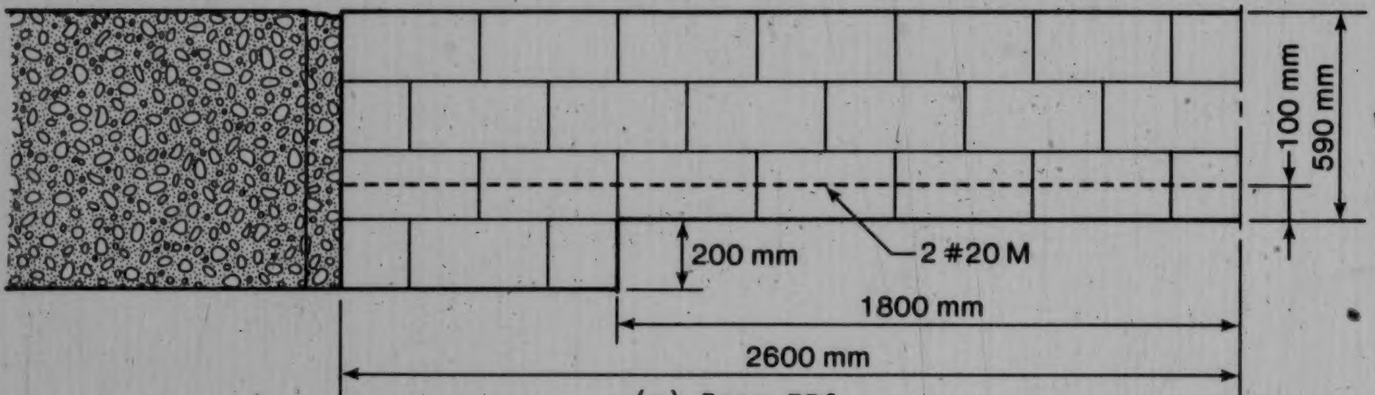
100 mm
590 mm
200 mm
2 #20 M
1800 mm
2600 mm

(c) Beam RB3

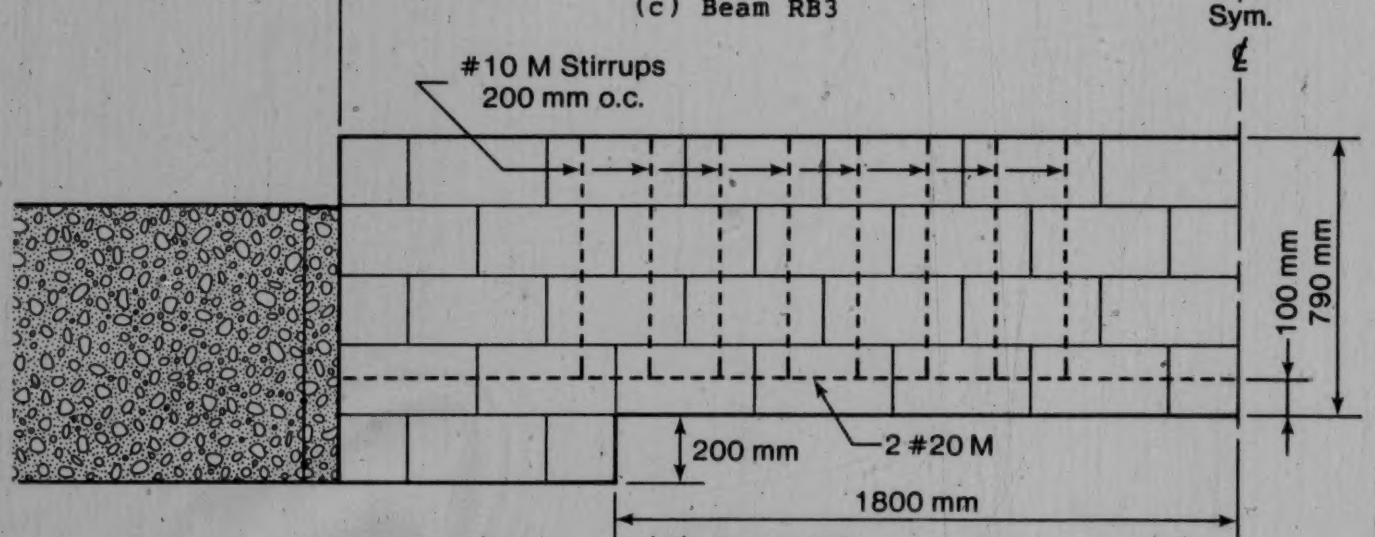
Sym.
℄
#10 M Stirrups
200 mm o.c.
100 mm
790 mm
200 mm
2 #20 M
1800 mm

(d) Beam RB2

Figure 3.5b Type RB Beam Details

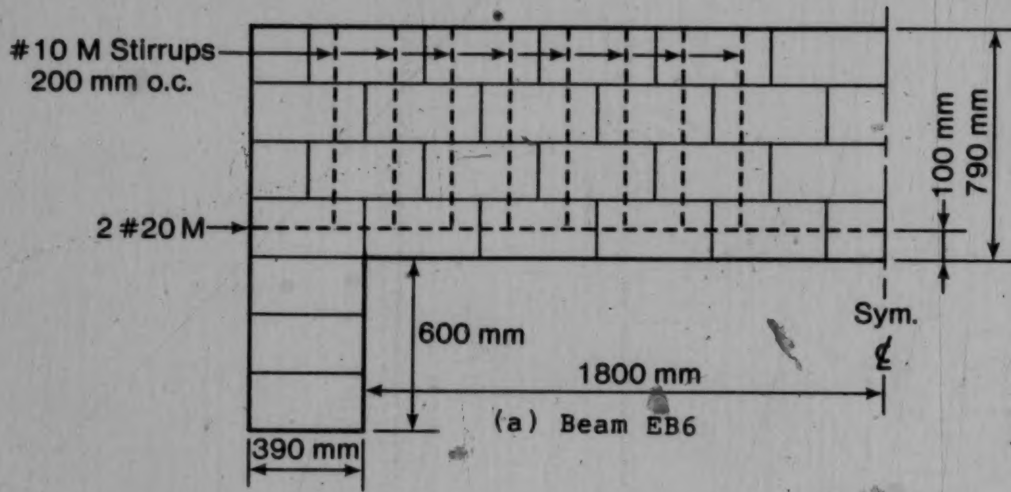
#10 M Stirrups
200 mm o.c.
2 #20 M
100 mm
790 mm
Sym.
℄
600 mm
1800 mm
390 mm

(a) Beam EB6

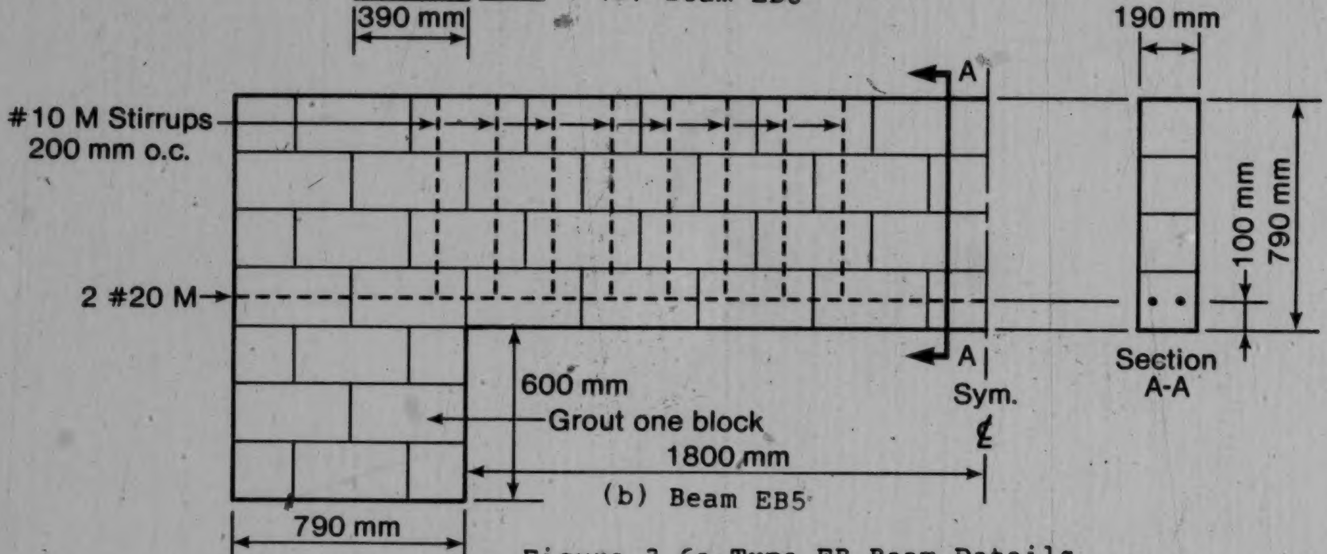
190 mm
A
#10 M Stirrups
200 mm o.c.
2 #20 M
100 mm
790 mm
A
Section
A-A
Sym.
℄
600 mm
Grout one block
1800 mm
790 mm

(b) Beam EB5

Figure 3.6a Type EB Beam Details

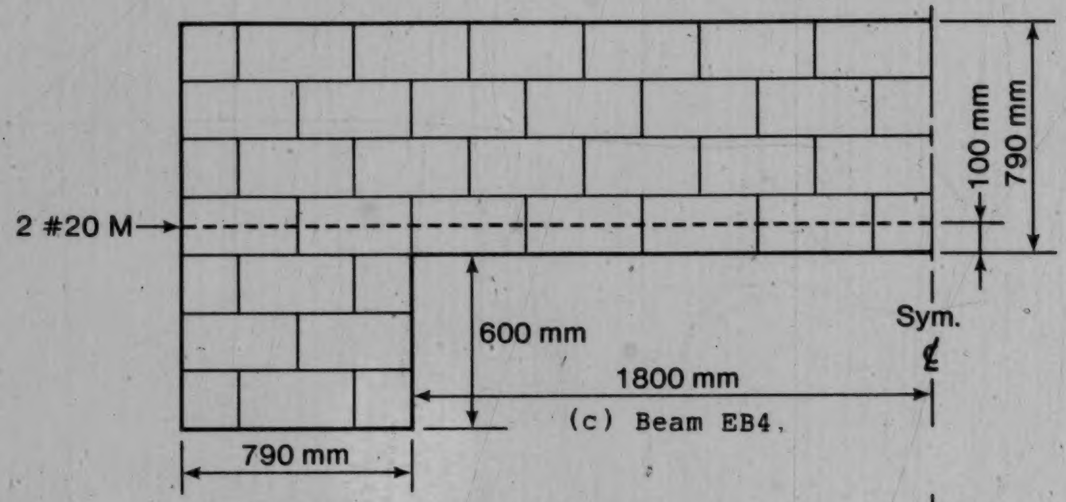
2 #20 M
100 mm
790 mm
Sym.
℄
600 mm
1800 mm
790 mm

(c) Beam EB4.

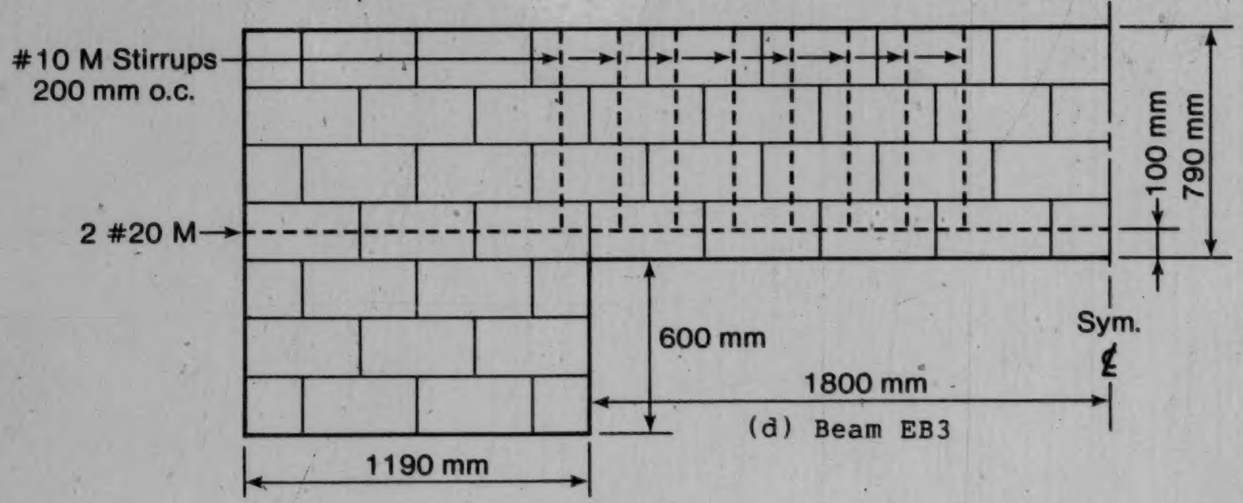
#10 M Stirrups
200 mm o.c.
2 #20 M
100 mm
790 mm
Sym.
℄
600 mm
1800 mm
1190 mm

(d) Beam EB3

Figure 3.6b Type EB Beam Details

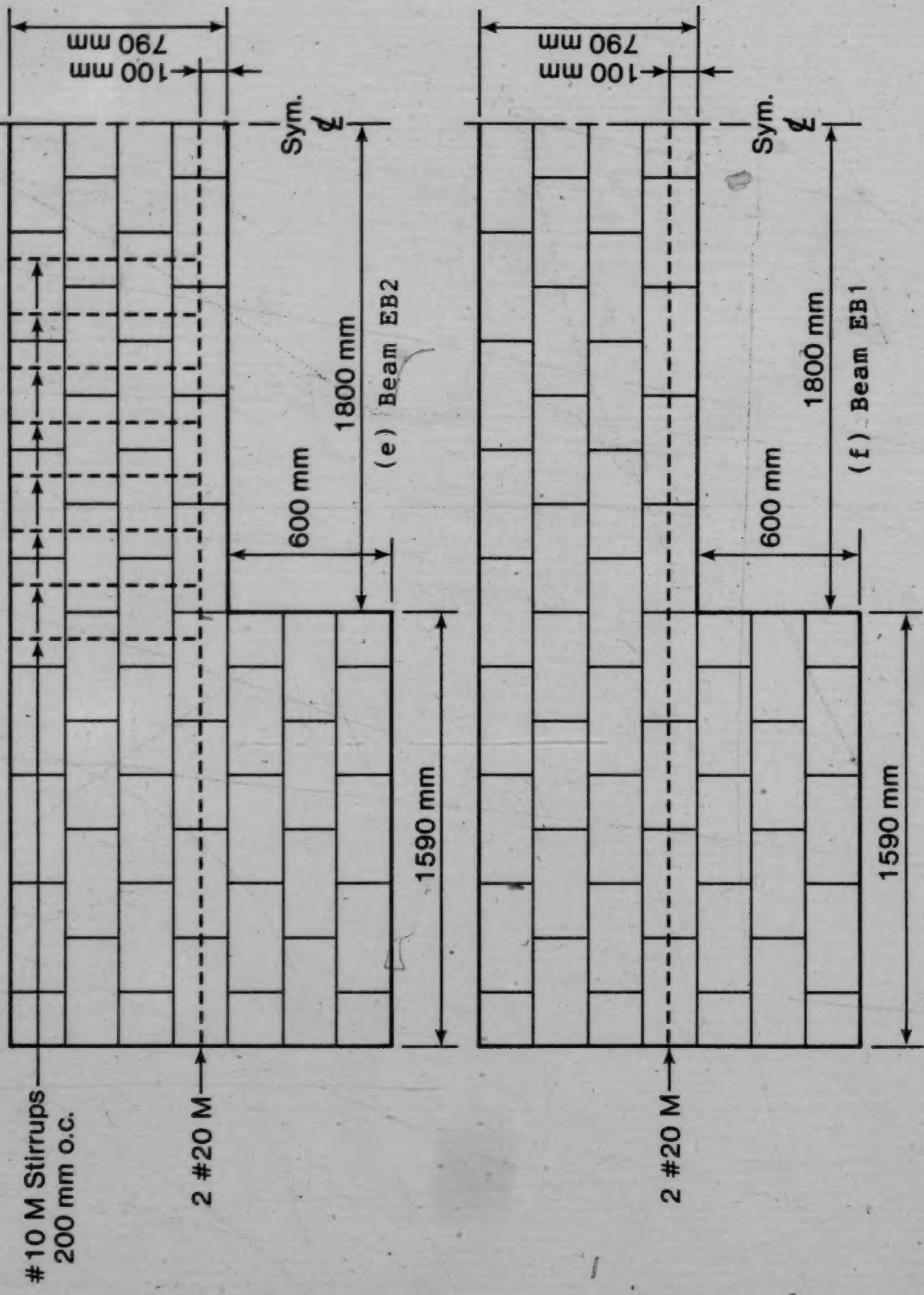
#10 M Stirrups
200 mm o.c.
2 #20 M
2 #20 M
790 mm
100 mm
790 mm
100 mm
Sym. ℄
Sym. ℄
1800 mm
600 mm
1590 mm
1800 mm
600 mm
1590 mm

(e) Beam EB2

(f) Beam EB1

Figure 3.6c Type EB Beam Details

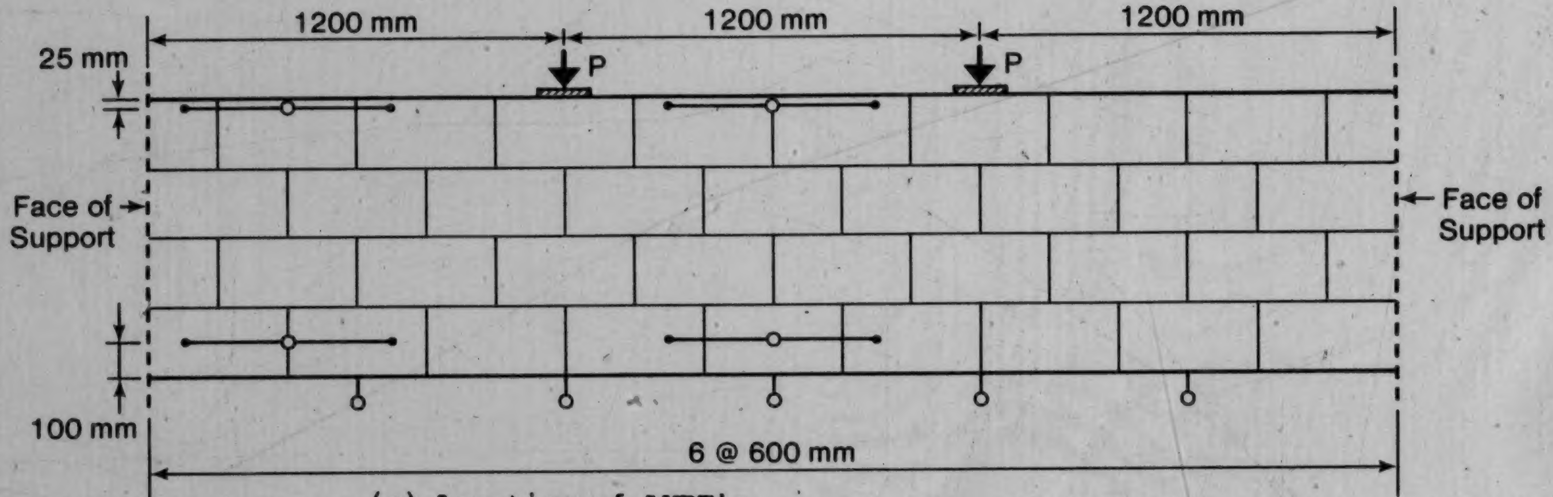
1200 mm
1200 mm
1200 mm
P
P
25 mm
Face of Support
Face of Support
100 mm
6 @ 600 mm

(a) Location of LVDT's

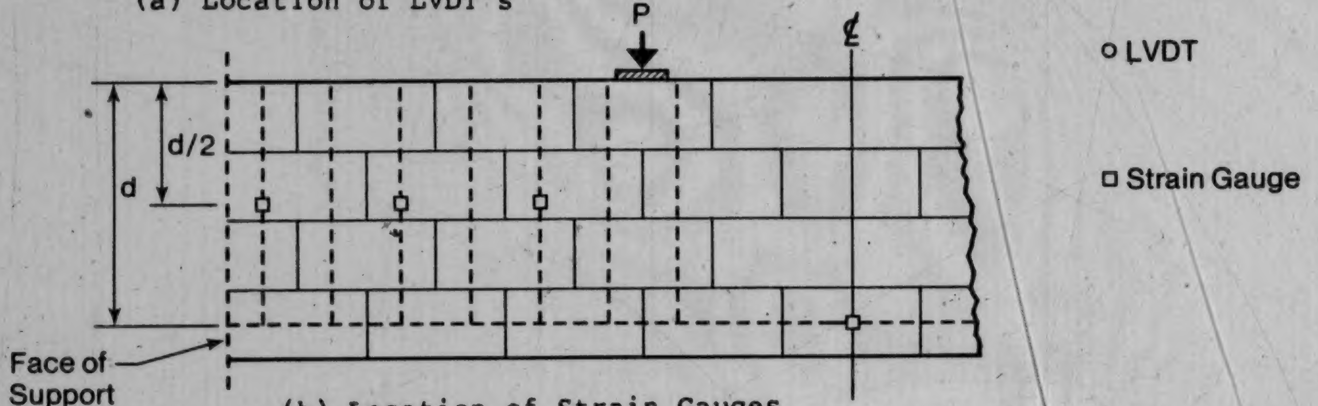
P
℄
○ LVDT
□ Strain Gauge
d/2
d
Face of Support

(b) Location of Strain Gauges

Figure 3.7 Location of Beam Instrumentation

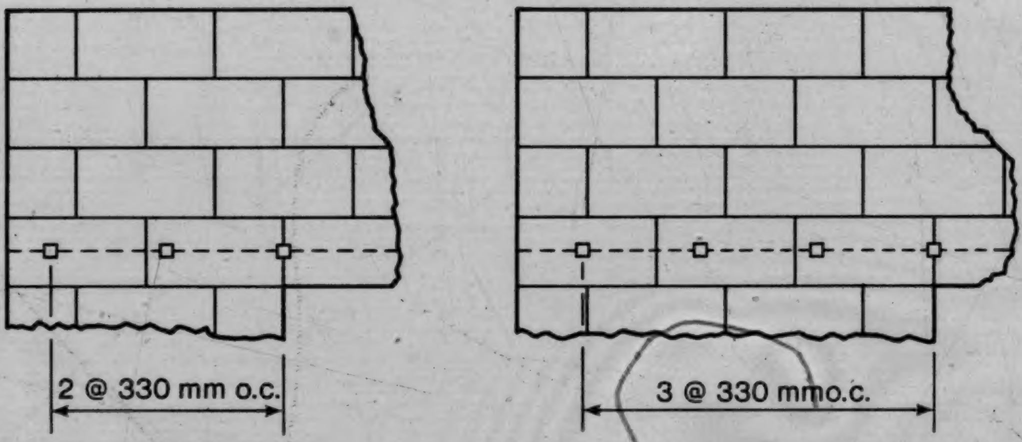
2 @ 330 mm o.c.
3 @ 330 mmo.c.

(a) Beams EB4, EB5 and Type RB Beams

(b) Beam EB3

□ Strain Gauge

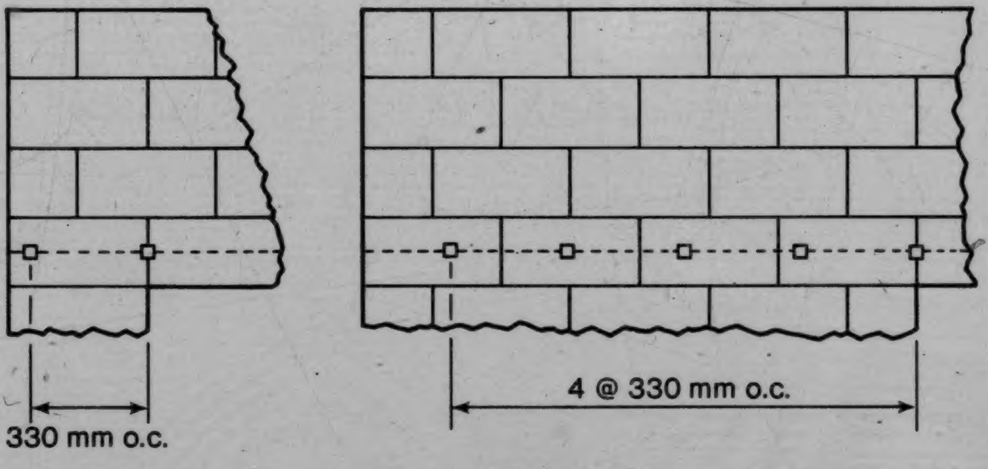
330 mm o.c.
4 @ 330 mm o.c.

(c) Beam EB6

(d) Beams EB1 and EB2

Figure 3.8 Location of Strain Gauges on Tension Reinforcement at End of Type EB and RB Beams

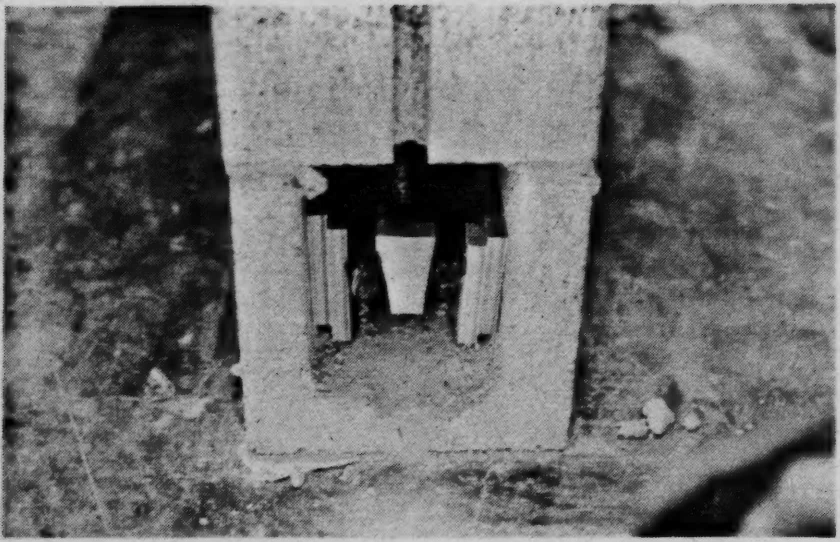

Plate 3.1 Location of Tension Reinforcement

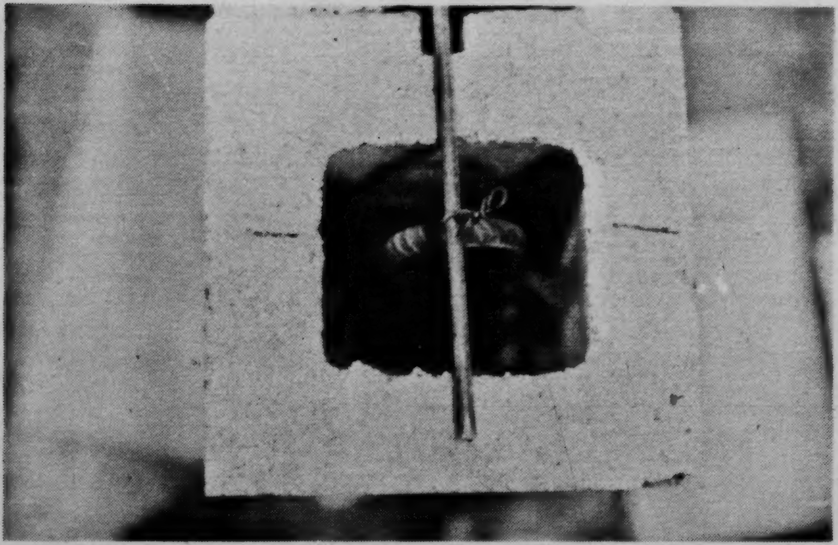

Plate 3.2 Stirrup Installation

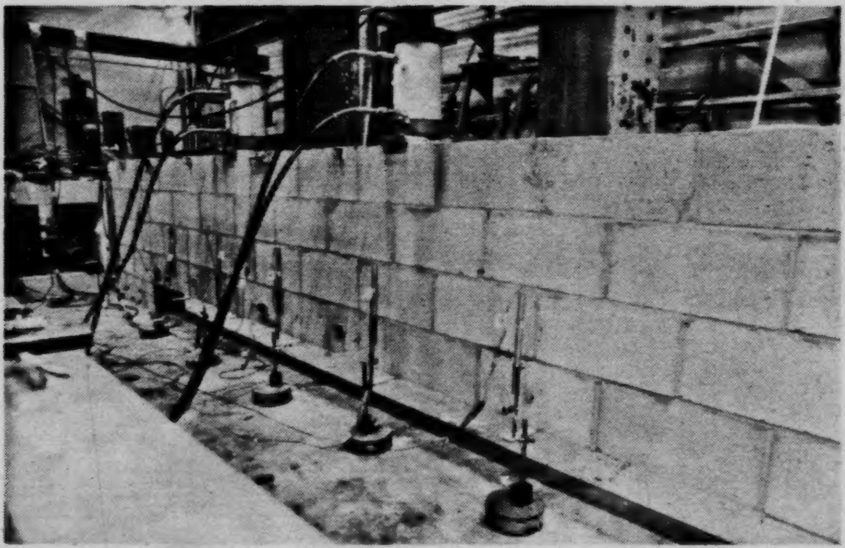

Plate 3.3 LVDT's Used for Measuring Vertical Deflections

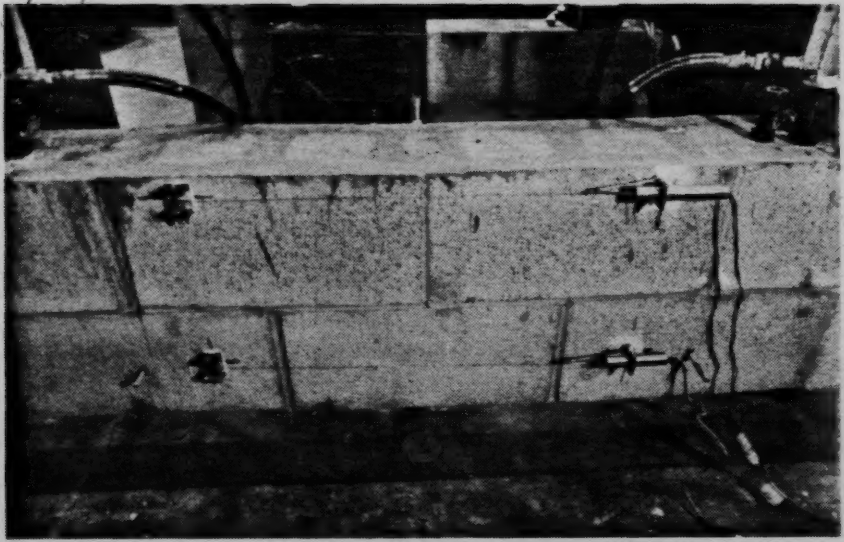

Plate 3.4 LVDT's for Measuring Horizontal Strain

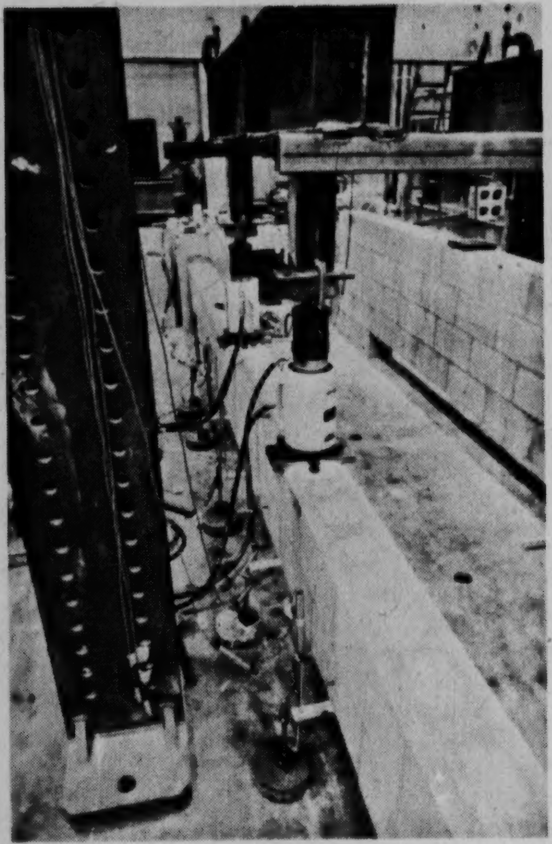

Plate 3.5 Test Set Up

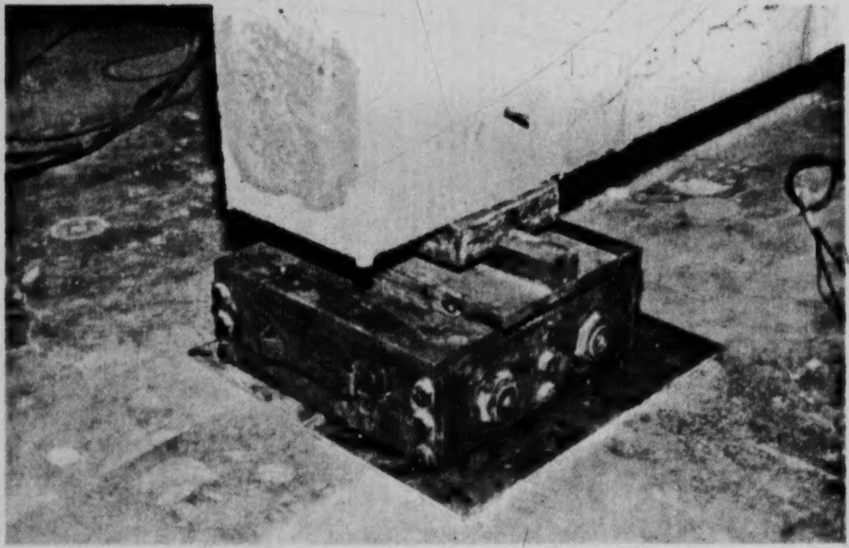

Plate 3.6 Roller Support

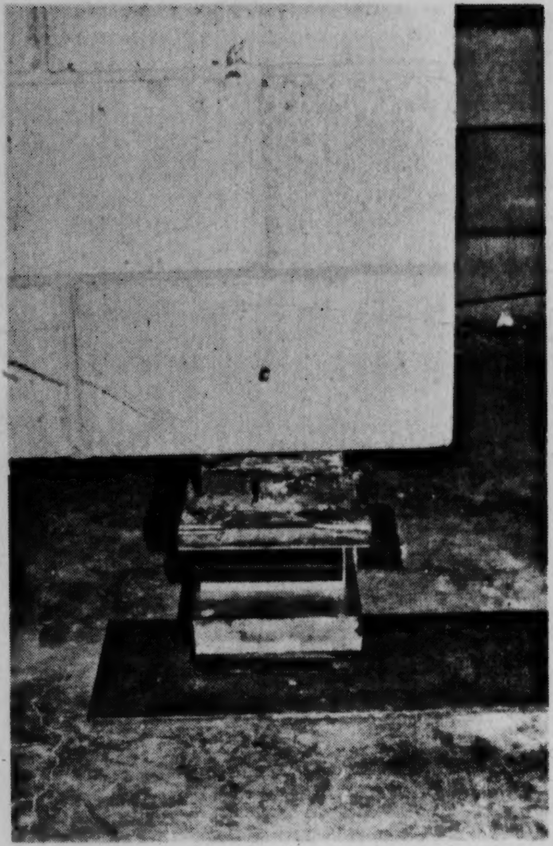

Plate 3.7 Rocker Support

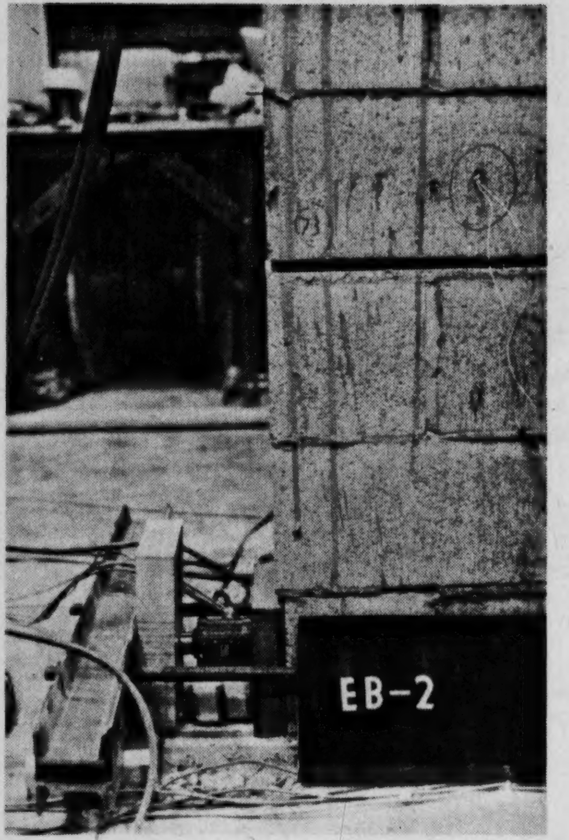

Plate 3.8 Horizontal End Restraint

4. Material Tests and Prism Tests

4.1 Introduction

In this chapter, the properties of the constituents of a masonry assemblage are examined experimentally. The nonisotropic nature of masonry is discussed on the basis of the experimental results of tests on grouted concrete masonry prisms.

4.2 Properties of Mortar Cubes

The most important properties of mortar are its workability, water retentivity, modulus of elasticity and strength. In this study, only the compressive strength of the mortar was examined and no attempt was made to measure any of the other properties. In actual construction practice, mortar is cured in air rather than in saturated lime water, which is a standard curing procedure for 50x50x50 mm mortar cubes. Therefore, the air cured strength of mortar cubes should give a better indication of the actual strength of mortar in a masonry assemblage.

Three batches of ready-mix mortar were used in the construction of the test specimens. For each batch of mortar, at least twenty 50x50x50 mm cubes were cast and cured either in saturated lime water or in the laboratory environment similar to that for the beams and prisms. The cubes were tested vertically to obtain the compressive strengths. A complete set of cube strength results is given in Table 4.1.

4.3 Properties of Grout

As mentioned in Section 3.1.3, the grouts used in the first two series of the experimental program were ready-mix concretes and those used in the third series were batched in the laboratory. Standard cylinder and block moulded prisms were cast and either laboratory cured or moist cured. A complete set of test results, together with the coefficients of variation and standard deviations, for standard cylinders and block moulded prisms is shown in Table 4.2 and Table 4.3 respectively.

The difference between the air cured and moist cured cylinder strengths is rather insignificant. The difference between the cylinder strengths for the first two series was quite large, but there was no significant difference in the strengths of the corresponding prisms. Also in the third series, there was no significant difference in prism strengths although there was a considerable difference in the cylinder strengths.

4.4 Properties of Masonry Units

4.4.1 Compressive Strength

The compressive strength of masonry units is obtained by testing pre-capped single masonry units, with the capping applied only to the net area for hollow masonry units. However, the lateral restraint due to friction at the interface of the specimen and the testing machine tends to increase the compressive strength of the units. Moreover, the stress state developed in the test and the failure mode of the test units differ from those in actual construction. The influence of these and other factors on masonry unit tests have been discussed in detail by some investigators[25,26].

In this study, the compressive strength of the masonry units normal to the bed joints was obtained by testing stretcher blocks with modular dimensions of 200x200x400 mm. All the units were capped top and bottom with high strength plaster of paris to provide smooth surfaces. The mean net area failure stress was 19.56 MPa. A complete set of test results is given in Table 4.4. Generally, the units failed by extensive spalling along the sides and by the development of vertical tension cracks.

In order to obtain the compressive strength of the masonry units placed in the same service orientation as in the beam specimen, stretcher units, which were capped with fiberboard, were tested with the load applied to the head joints. The mean compressive strength obtained in these tests was 9.50 MPa. Complete test results are also shown in Table 4.4. In these tests, the failure of the units was caused by splitting of the block webs without any spalling from the sides.

Results indicated that there was a significant difference in the compressive strengths of the units tested in the two orientations. However, because of the differences in capping conditions, h/t ratio, the geometry of the blocks in the two directions and the failure modes, no definite conclusions can be drawn. More testing is required in order to clearly establish the relationship between properties for the two block orientations.

4.4.2 Modulus of Elasticity

The modulus of elasticity of masonry units is affected by a number of factors. However, on the basis of experimental studies, empirical relationships have only been developed to express the modulus, E_b, as a function of compressive strength, f'_b.

Richart et al[27] proposed a value of the elastic modulus of concrete block as expressed by

$$E_b = 1000f'_b \tag{4.1}$$

where

E_b = block elastic modulus, psi

f'_b = block compressive strength, psi

The ACI equation for hardened concrete as proposed by Pauw is

$$E_c = 33W^{3/2}\sqrt{f'_c} \tag{4.2}$$

where

W = unit weight of concrete, lb./cu.ft.

f'_c = compressive strength of concrete, psi

Holm[24] suggested a similar equation for the elastic modulus of block units:

$$E_b = 22W^{3/2}\sqrt{f'_b} \tag{4.3}$$

where

W = air dry block density, lb./cu.ft.

In the present study, vertical compressive strains in 3 specimens, B8 to B10, were measured over a gauge length of 2 in. at 5 locations on the faces of each block. Table 4.4 contains the values of the secant modulus at $0.5f'_m$. The mean elastic modulus reported is 10950 MPa. Figure 4.1 is a plot of the stress-strain relationships for the three specimens.

Based on a unit weight of 1590 Kg/m³ and an average compressive strength of 19.56 MPa of the specimens, the values of the elastic modulus of the concrete block units as predicted by Equations 4.1 to 4.3 are 20750, 12270 and 8205 MPa respectively. These values are also plotted in Figure 4.1. It is clearly indicated that the use of Equation 4.1 is unconservative while Equations 4.2 and 4.3 provide more reasonable values.

4.5 Prism Investigation

4.5.1 General

Prisms are small test specimens used to determine structural properties such as the compressive strength, modulus of elasticity, etc. of a full size masonry assemblage. Although there has been extensive work related to masonry characteristics using small scale prism specimens, theoretical treatment of the various structural properties is still not well developed. This is due to the fact that the influence of the various components on the behavior of a masonry assemblage is complex due to the different behavior of each element.

In this study, only the compressive strength (f'_m) and modulus of elasticity (E_m) were studied experimentally. Since the direction of the compressive force in a masonry beam with respect to the orientation of the masonry unit is different from that in a masonry wall or column, a series of prism tests was conducted to investigate the nonisotropic behavior of grouted concrete masonry.

4.5.2 Prism Failure Modes

The failure mode for all grouted prisms with compressive load applied normal to the bed joints was characterised by tensile splitting of the block shells and the grout cores. Shell cracking usually occurred before the ultimate load was reached. This phenonemon might be explained by the significant lateral tensile strains in the grout at high vertical compressive force resulting in extensive microcracking and increased Poissons Ratio. This lateral expansion of the grout created tension in the block shells and resulted in the typical splitting failure of the prism. Plate 4.1 shows typical tensile splitting in a prism loaded normal to the bed joints.

The prisms loaded parallel to the bed joints all experienced serious crushing of the head mortar joints followed by face shells spalling away from the grout cores and cracking or crushing of the grout. Crushing of the head mortar joints and cracking at the bed joints were occurred well in advance of the ultimate load. The mortar failed in crushing first because of lower strength compared with other components. As a result of crushing, the mortar tended to expand in the lateral direction thus developing shear forces at the joints. These forces were large enough to pull the face shells of the blocks away from the grout cores. Failure of the prisms was very slow and joint failure could be seen clearly as shown in Plate 4.2. Typical failures of these prisms are shown in Plate 4.2 and Plate 4.3.

For both test orientations, it can be argued that the grout and the blocks did not function as an integral unit as the face shells always spalled away from the grout core at or below the failure load. For the prisms loaded normal to the bed joints, no mortar joint failure was observed, probably because of the continuity provided by the concrete grout cores which functioned as short columns. However, such continuity of the grout core is not available when the prisms are loaded in the other orientation.

4.5.3 Compressive Strength of Prism

Determination of the compressive strength of the nonhomogeneous grouted masonry assemblage is a difficult problem due to the complex interactions of the various components which have widely different material properties. Although some theoretical analyses have been developed, most are based on idealized assumptions whose validity in actual construction practice are questionable.

Previous investigations[29,30,31,32] indicated that the factors influencing the prism compressive strength are the block unit strength, mortar strength, grout strength, prism dimensions and slenderness, bond pattern and thickness, capping, workmanship, curing condition, test age and loading rate. Considering the nonisotropic behavior of a masonry assemblage, loading orientation is another important factor.

Presently, design provisions such as those in CAN3-S304-M78[33] "Masonry Design and Construction for

Buildings" permit the determination of masonry strength based either on block and mortar strength or on prism tests. The first method is known to be conservative and neglects the nonisotropic behavior of masonry. The prism test method provides more accurate values for the compressive strength. However, as noted above, there are a number of factors which influence the results of prism tests. The CAN3-S304-M78 requires that a height-to-thickness correction factor be applied to prisms whose slenderness ratio is more than 2. However, recent investigations[30,31,32] indicate that such correction factors are not required and they also suggested that the confining effect of platten restraint results in increasing the strength of 2 course prisms. By increasing the prism height, this effect can be diminished.

In the present study, 3-course prisms were used as control specimens with details as described in Section 3.2.1. For the prisms loaded normal to the bed joints, the average compressive strength, f'_{mn}, was 16.43 MPa and 13.75 MPa for prisms in the first and second series (PS and PE) respectively. In the third series, the compressive strength of PA prisms was 12.64 MPa when loaded normally (f'_{mn}) but 6.81 MPa when loaded parallel to the bed joint (f'_{mp}), while that of PB prisms was 16.52 MPa and 7.09 MPa respectively. A complete set of test results is shown in Table 4.5.

Figure 4.2 shows values of the prism strength, f'_{mn}, as a function of the mortar cube strength for the PB and PS prisms having similar grout strengths (30.62 MPa and 31.27

MPa respectively). Although data is insufficient for definite conclusions, results tend to indicate that prism strength, f'_{mn}, is independent of the mortar strength. This behavior is in agreement with that suggested by Hamid and Drysdale.

Figure 4.3 shows the values of prism strength, f'_{mn}, in terms of the strength of air cured concrete cylinders. The figure indicates that an increase in grout strength results in an increase in prism strength, f'_{mn}. Using a linear regression analysis, the strength of the prisms can be related to the grout strength by:

$$f'_{mn} = 9.4 + 0.23f'_c \quad \text{(MPa)} \qquad (4.4)$$

Similar empirical equations have been suggested by other investigators[34,35]. However, because of the difference in block units and prism size used in their studies, comparison of their empirical equations with Equation 4.4 is not valid.

Figure 4.4 shows the relation between prism strength, f'_{mp}, and concrete cylinder strength (grout strength) for the PA and PB prisms loaded parallel to the bed joints. Clearly, the increase in prism strength is small compared with the increase in grout strength.

From the recorded compressive strength of the prisms, it is observed that:

1. There is a big difference in the compressive strength for the prisms loaded in the two directions.

2. The effect of grout strength (f'_c) on the compressive strength of prisms loaded normally (f'_{mn}) is more important than on the compressive strength of prisms loaded parallel to the bed joints (f'_{mp}).

Obviously, nonisotropic behavior of masonry is existed. Although no tests were done to investigate the influence of mortar strength on the strength of prisms loaded parallel to the bed joint, the failure mode indicated that prism strength, f'_{mp}, depends on mortar strength as failure always initiated by crushing of the mortar joints. Nevertheless, more tests should be carried out to investigate the influence of grout and the mortar strength on f'_{mp} before definite conclusions can be reached.

The slenderness effect for prisms loaded parallel to the bed joint is indicated in the test values reported in Table 4.5. The failure stress is between 6.2 to 6.3 MPa for the taller prisms with a slenderness ratio of 5 compared with 6.8 to 7.1 MPa for the shorter prisms with a slenderness ratio of 3.

4.5.4 Modulus of Elasticity of Prisms

The modulus of elasticity is an important parameter affecting both strength and deflection calculations. Determination of the modulus of a composite masonry assemblage is complicated as it is governed by the widely varying moduli of the individual components. Theoretical treatment and experimental information on this important engineering parameter are lacking. In this section, the modulus of elasticity of the masonry prisms is examined experimentally in terms of the secant modulus at one-half of the maximum stress.

The vertical stress-strain relationships for PE, PA and PB prisms loaded normally are shown in Figures 4.5 and 4.6. It can be seen that the PB prisms are slightly stiffer than the PE prisms. Considering that mortar strength is unimportant for this type of loading, the increased stiffness is due to higher grout strength (30.62 MPa for PB prisms versus 19.39 MPa for PE prisms). However, the stiffness is not affected by grout strength for the prisms loaded parallel to bed joint. This is shown in the stress-strain relationships for PA and PB prisms in Figure 4.7. The difference in deformation characteristics for masonry prisms loaded in the two different orientations is shown in Figures 4.8 and 4.9 for PA and PB prisms respectively. These figures indicate that the stiffness of the prisms loaded parallel to the bed joint is approximately one half the stiffness of prisms loaded normal to the bed joints.

The average modulus of elasticity for PE prisms in the second series was 9750 Mpa, while that of PA and PB prisms loaded normally (E_{mn}) was 8420 and 11700 MPa respectively. The average modulus for the PA and PB prisms loaded parallel to the bed joint (E_{mp}) was 4200 MPa and 4150 MPa respectively.

Figure 4.11 shows the prism modulus of elasticity as a function of prism compressive strength for prisms loaded normal to the bed joint. Using linear regression analysis, the elastic modulus can be expressed as

$$E_{mn} = 478 + 676f'_{mn} \quad \text{(MPa)} \tag{4.5}$$

The modulus of elasticity of masonry as defined in CSA-S304-M78 is also shown in Figure 4.11. It can be seen that the modulus is significantly over-estimated by the CSA provision.

Figure 4.12 is similar to Figure 4.11 except that the results for the prisms loaded parallel to the bed joint are also plotted in Figure 4.12. It can be observed that most of the values of parallel loaded prisms are within one standard deviation of Equation 4.5. It seems that the empirical equation obtained for normally loaded prisms might also be used for prisms loaded parallel to the bed joint.

The stress-strain relationships for the larger prisms (PLA and PLB) loaded parallel to the bed joint (slenderness ratio equal to 5) are shown in Figure 4.10. A comparison of Figure 4.7 and Figure 4.10 indicates that for this type of loading, the stress-strain relationships are very similar, regardless of the slenderless ratio. However, the strains in the smaller prisms (PA and PB) were measured over a gauge length of 400 mm with one mortar joint included, while those in the larger prisms were measured over a gauge length of 600 mm with two mortar joints included. This indicates that strain measurements are not affected by the number of mortar joints included in the measurements.

Table 4.1 Compressive Strength of 50x50x50 mm Mortar Cubes

Series	No.	Cure	Failure Stress (MPa)	Ave.Fail. Stress (MPa)	Standard Deviation (MPa)	Coef.of Variation (%)
1	1	SL*	11.72	10.96	0.79	7.2
	2	"	11.55			
	3	"	9.74			
	4	"	11.72			
	5	"	11.46			
	6	"	11.29			
	7	"	10.34			
	8	"	9.83			
	1	L**	10.95	9.16	1.08	11.8
	2	"	10.00			
	3	"	8.10			
	4	"	10.77			
	5	"	9.83			
	6	"	8.70			
	7	"	8.79			
	8	"	8.70			
	9	"	11.12			
	10	"	8.79			
	11	"	8.70			
	12	"	10.51			
	13	"	9.14			
	14	"	8.19			
	15	"	7.93			
	16	"	8.27			
	17	"	9.05			
	18	"	7.41			
2	1	L	8.96	12.16	2.59	21.3
	2	"	10.69			
	3	"	10.00			
	4	"	10.95			
	5	"	8.27			
	6	"	10.08			
	7	"	9.91			
	8	"	10.00			
	9	"	8.96			
	10	"	15.00			
	11	"	8.96			
	12	"	15.51			
	13	"	9.57			
	14	"	13.79			
	15	"	13.45			
	16	"	14.13			
	17	"	14.91			
	18	"	15.96			
	19	"	9.14			
	20	"	16.20			
	21	"	11.89			
	22	"	10.86			
	23	"	12.50			
	24	"	13.62			
	25	"	13.45			
	26	"	15.60			
	27	"	15.94			
3	1	SL	7.07	7.24#		
	2	"	7.93			
	3	"	6.72			
	4	SL	9.14	8.79##		
	5	"	8.96			
	6	"	8.27			
	1	L	6.21	6.53#	1.27	19.5
	2	"	6.55			
	3	"	4.83			
	4	"	5.17			
	5	"	5.52			
	6	"	7.93			
	7	"	8.62			
	8	"	7.41			
	1	L	5.69	6.66##	0.94	14.1
	2	"	8.53			
	3	"	7.07			
	4	"	5.60			
	5	"	7.24			
	6	"	5.34			
	7	"	6.72			
	8	"	6.81			
	9	"	6.90			

* Saturated lime cured specimens ** Lab. cured specimens # 13 day strength ## 26 day strength

Table 4.2 Compressive Strength of Concrete Cylinders

Series	No.	Cure	Failure Stress (MPa)	Ave.Fail. Stress (MPa)	Standard Deviation (MPa)	Coef.of Variation (%)
1	1	ML*	34.26	34.68		
	2	"	34.82			
	3	"	33.77			
	4	"	35.85			
	1	L**	31.31	31.27	1.12	3.6
	2	"	32.80			
	3	"	30.43			
	4	"	29.53			
	5	"	31.34			
	6	"	31.65			
	7	"	30.18			
	8	"	32.90			
2	1	L	18.65	19.39	0.93	4.8
	2	"	18.53			
	3	"	17.68			
	4	"	19.26			
	5	"	19.14			
	6	"	20.12			
	7	"	19.26			
	8	"	20.12			
	9	"	18.90			
	10	"	20.85			
	11	"	20.73			
3	A1	ML	22.31	24.43#		
	A2	"	26.46			
	A3	"	24.51			
	A1	L	19.75	24.53#	2.66	10.8
	A2	"	23.41			
	A3	"	23.78			
	A4	"	28.17			
	A5	"	25.97			
	A6	"	26.09			
	A7	L	26.82	26.74##		
	A8	"	26.95			
	A9	"	26.46			
	B1	ML	30.97	29.55##		
	B2	"	27.92			
	B3	"	29.75			
	B1	L	30.12	30.62##	1.07	3.5
	B2	"	30.48			
	B3	"	28.90			
	B4	"	30.60			
	B5	"	32.43			
	B6	"	31.21			

* Moist cure
** Lab. cure
# 13 day strength
## 26 day strength

Table 4.3 Compressive Strength of 75x75x150 mm Concrete Prisms

Series	No.	Cure	Failure Stress (MPa)	Ave.Fail. Stress (MPa)	Standard Deviation (MPa)	Coef.of Variation (%)
1	1	ML	38.69	38.91		
	2	ML	37.35			
	3	ML	39.84			
	4	ML	39.76			
	1	L	41.94	41.48	2.43	5.9
	2	L	36.77			
	3	L	40.91			
	4	L	41.94			
	5	L	42.44			
	6	L	44.89			
2	1	L	18.16	20.11	1.41	7.0
	2	L	22.83			
	3	L	20.61			
	4	L	20.91			
	5	L	19.61			
	6	L	19.00			
	7	L	21.53			
	8	L	18.62			
	9	L	19.69			

Table 4.4 Compressive Strength and Modulus of Elasticity of Masonry Units

No.	Load Direction	f'_b (MPa)	E_b (MPa)	No.	Load Direction	f'_b (MPa)
B1	N*	17.89	-	B11	P**	9.21
B2	N	16.94	-	B12	P	10.18
B3	N	22.76	-	B13	P	9.01
B4	N	20.66	-	B14	P	9.61
B5	N	14.82	-			
B6	N	19.64	-			
B7	N	20.52	-			
B8	N	19.86	13400			
B9	N	23.37	10260			
B10	N	19.11	9190			
Ave.		19.56	10950			9.50

* Normal to bed joints
** Parallel to bed joints .

Table 4.5 Results of Prism Tests

Prism No.	Load Dir.	Comp.Strength		f'_m	E_m	Average	
		Grout (MPa)	Mortar (MPa)	(MPa)	(MPa)	f'_m (MPa)	E_m (MPa)
PS1	N*	31.27	9.16	17.00	-	16.43	-
PS2	"			14.84	-		
PS3	"			16.89	-		
PS4	"			15.70	-		
PS5	"			19.73	-		
PS6	"			14.42	-		
PE1	N	19.39	12.16	13.86	10370	13.75	9750
PE2	"			13.34	12043		
PE3	"			12.96	8921		
PE4	"			12.69	8522		
PE5	"			14.18	8921		
PE6	"			15.49	-		
PA1	P**	24.53	6.53	6.22	4213	6.81	4200
PA3	"			7.07	4273		
PA5	"			7.15	4108		
PB1	P	30.62	6.66	6.90	4357	7.09	4150
PB3	"			7.13	3734		
PB5	"			7.23	4366		
PA4	N	24.53	6.53	14.15	9460	12.64	8420
PA6	"			11.12	7383		
PB2	N	30.62	6.66	14.78	10539	16.52	11700
PB4	"			17.77	11227		
PB6	"			17.02	13328		
PLA1	P	24.53	6.53	5.54	5442	6.23	4370
PLA3	"			6.92	3294		
PLA2	N	24.53	6.53	11.75	8914	11.70	8710
PLA4	"			11.64	8506		
PLA5	P	26.74	6.66	6.20	4941		
PLB1	P	30.62	6.66	6.29	5140		
PLA6	N	26.74	6.66	11.92	6743		
PLB2	N	30.62	6.66	11.28	6049		

* Normal to bed joints
** Parallel to bed joints

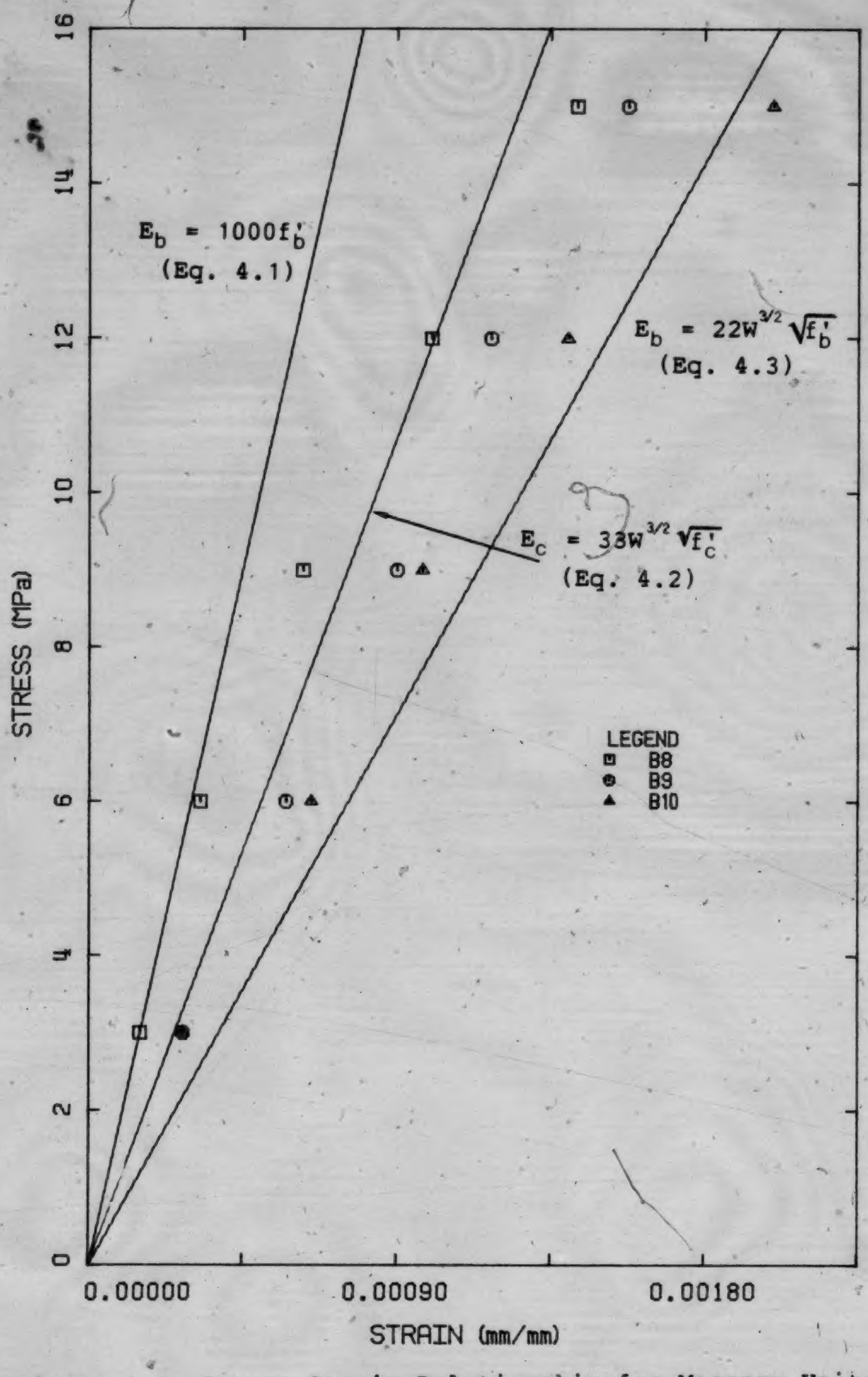

Figure 4.1 Stress-Strain Relationship for Masonry Units

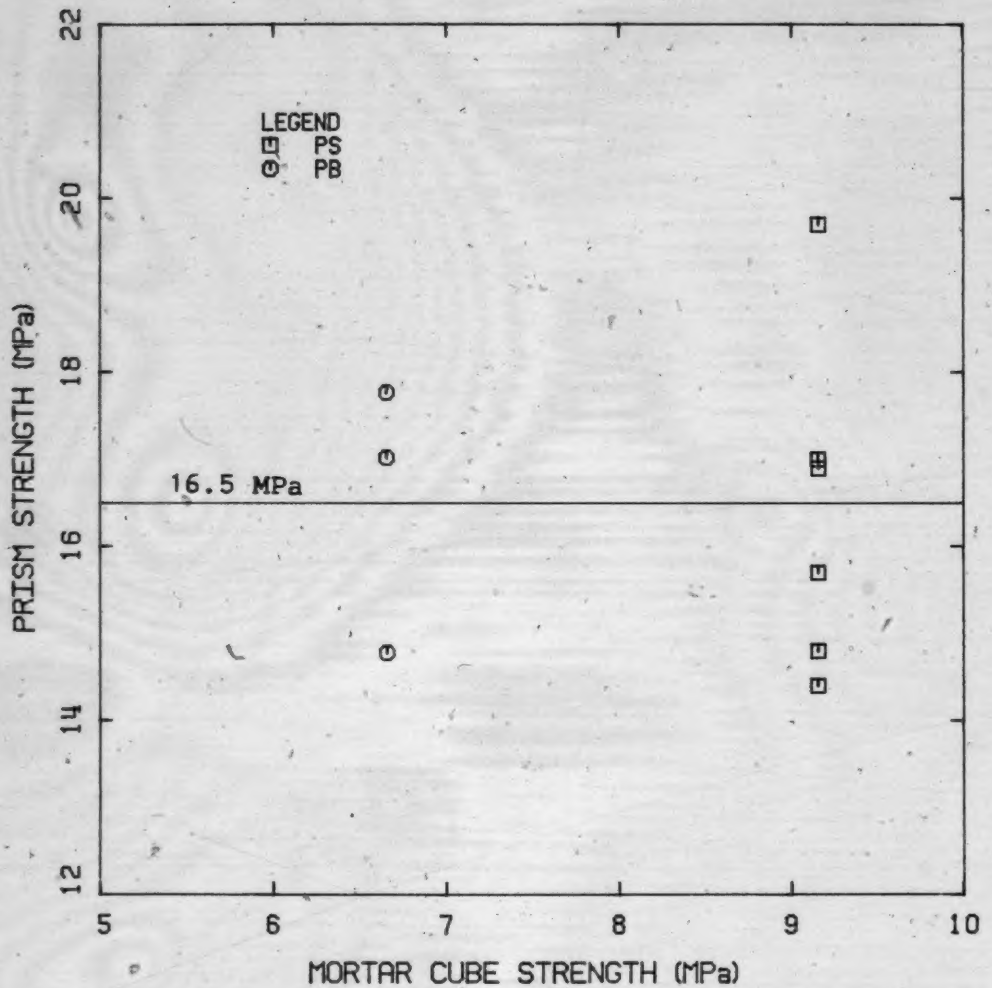

Figure 4.2 Comparison of Masonry Prism Strength and Mortar Cube Strength

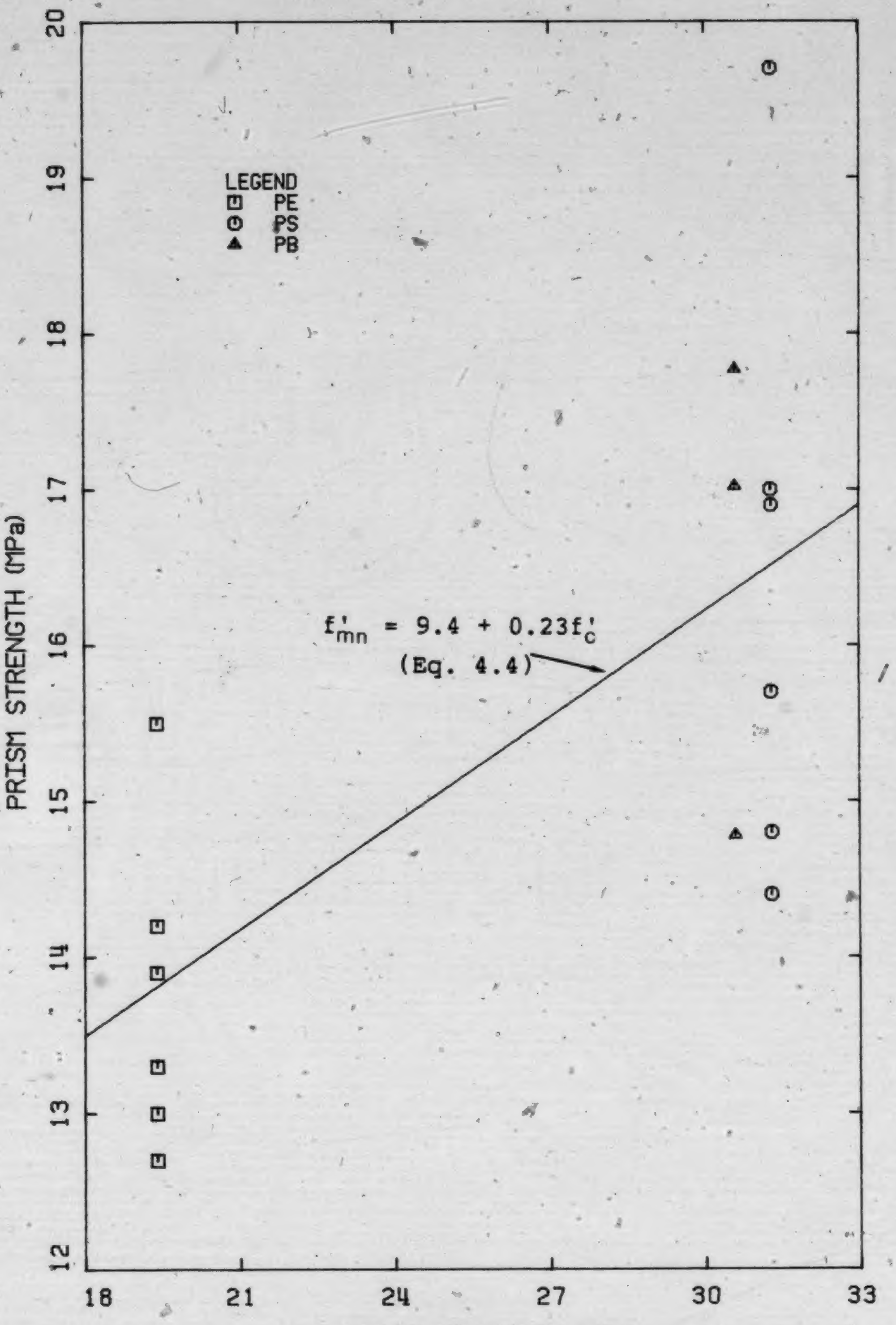

Figure 4.3 Comparison of Prism and Cylinder Strengths for Grout

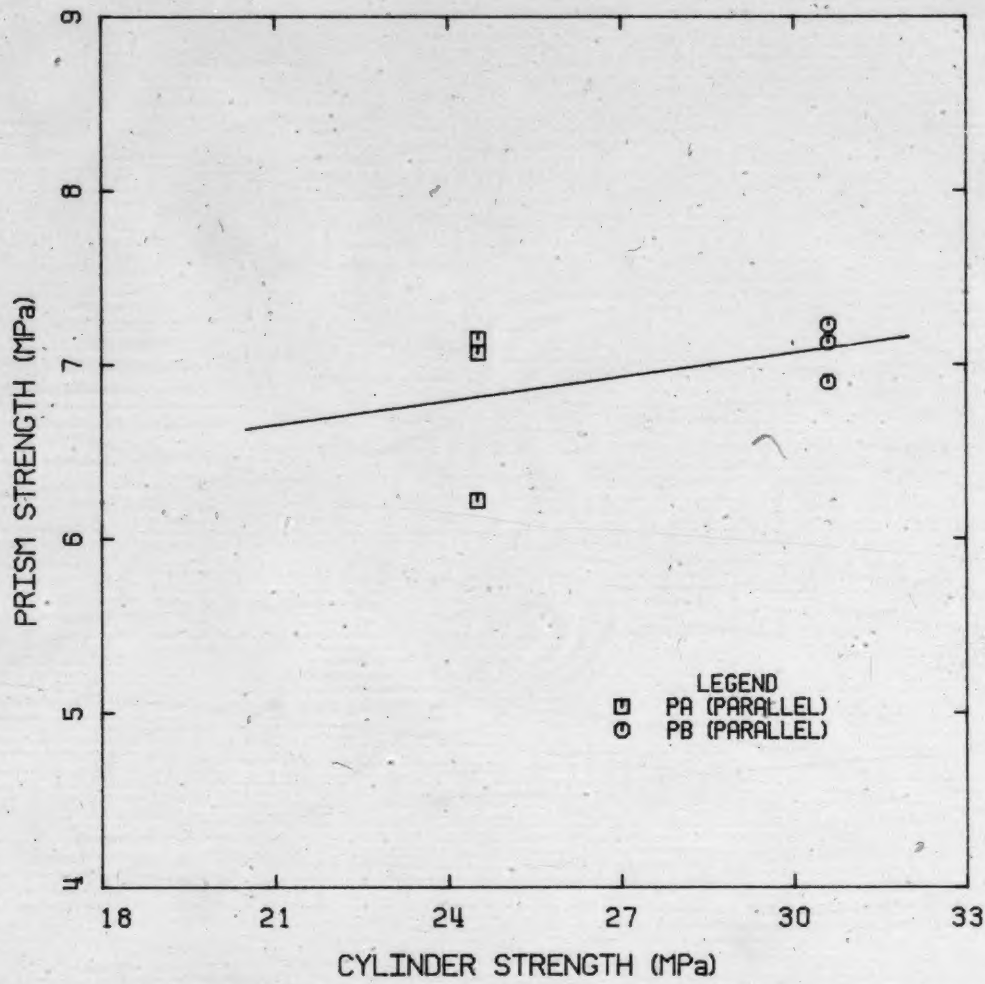

Figure 4.4 Comparison of Prism and Cylinder Strengths for Grout

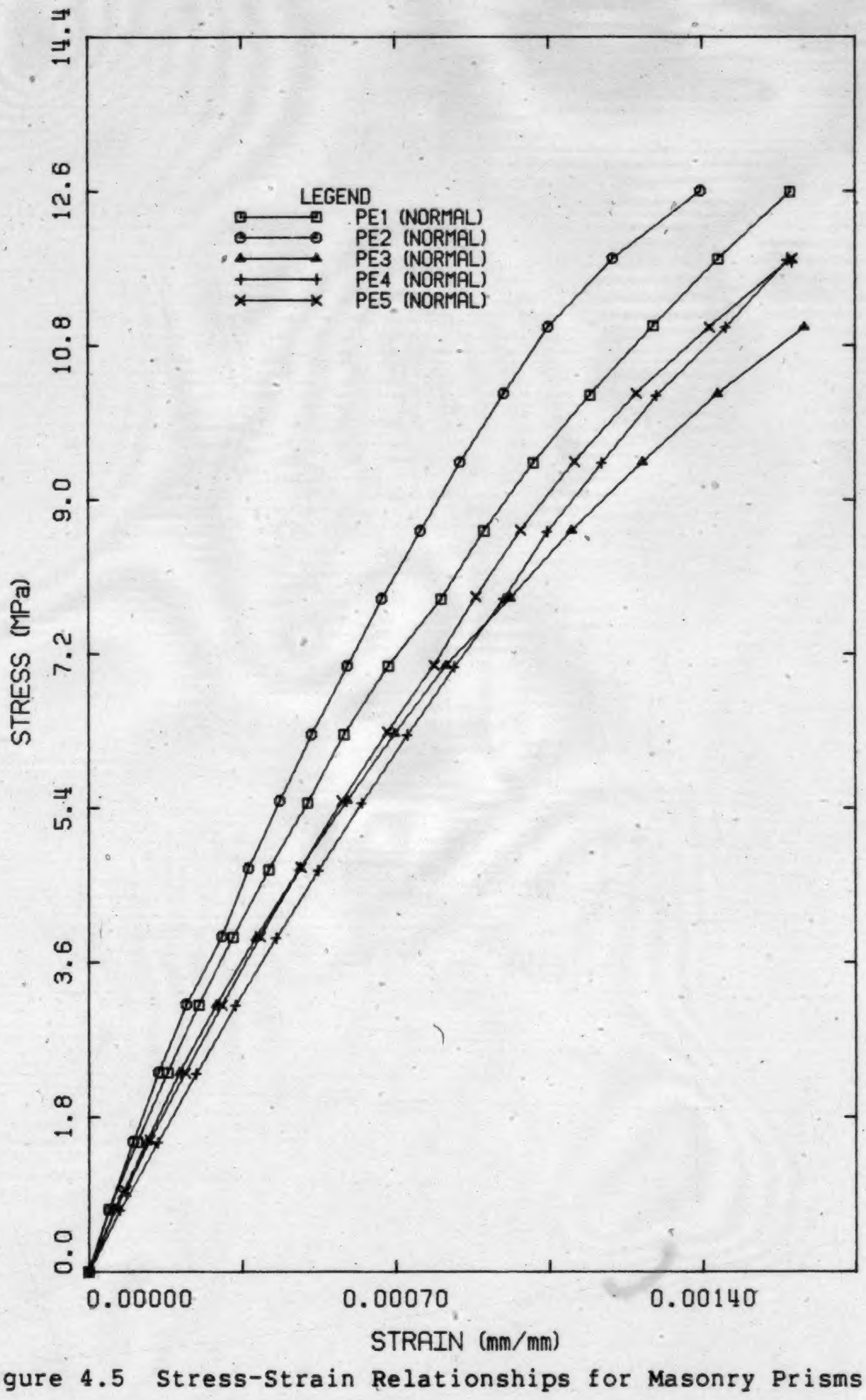

Figure 4.5 Stress-Strain Relationships for Masonry Prisms

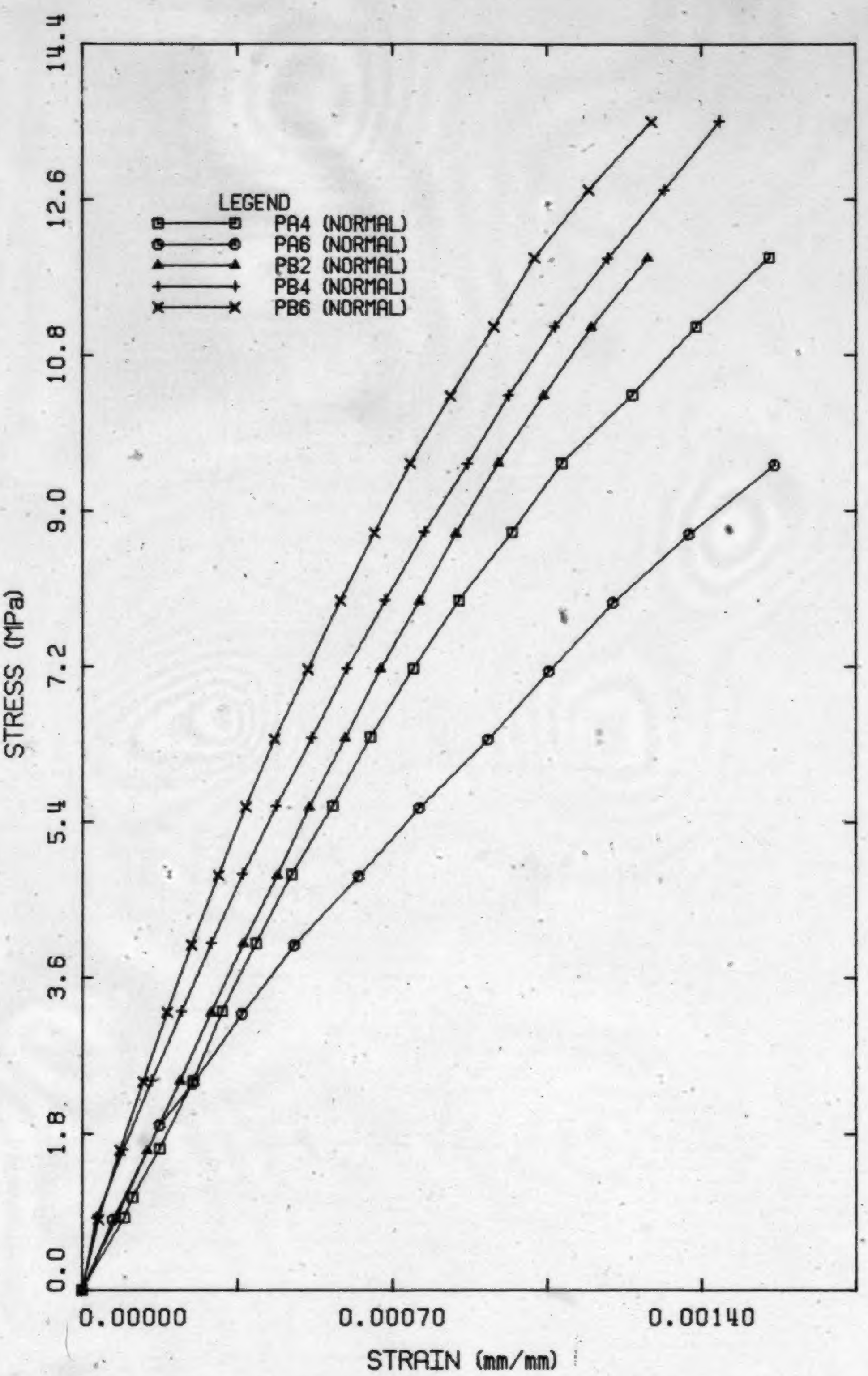

Figure 4.6 Stress-Strain Relationships for Masonry Prisms

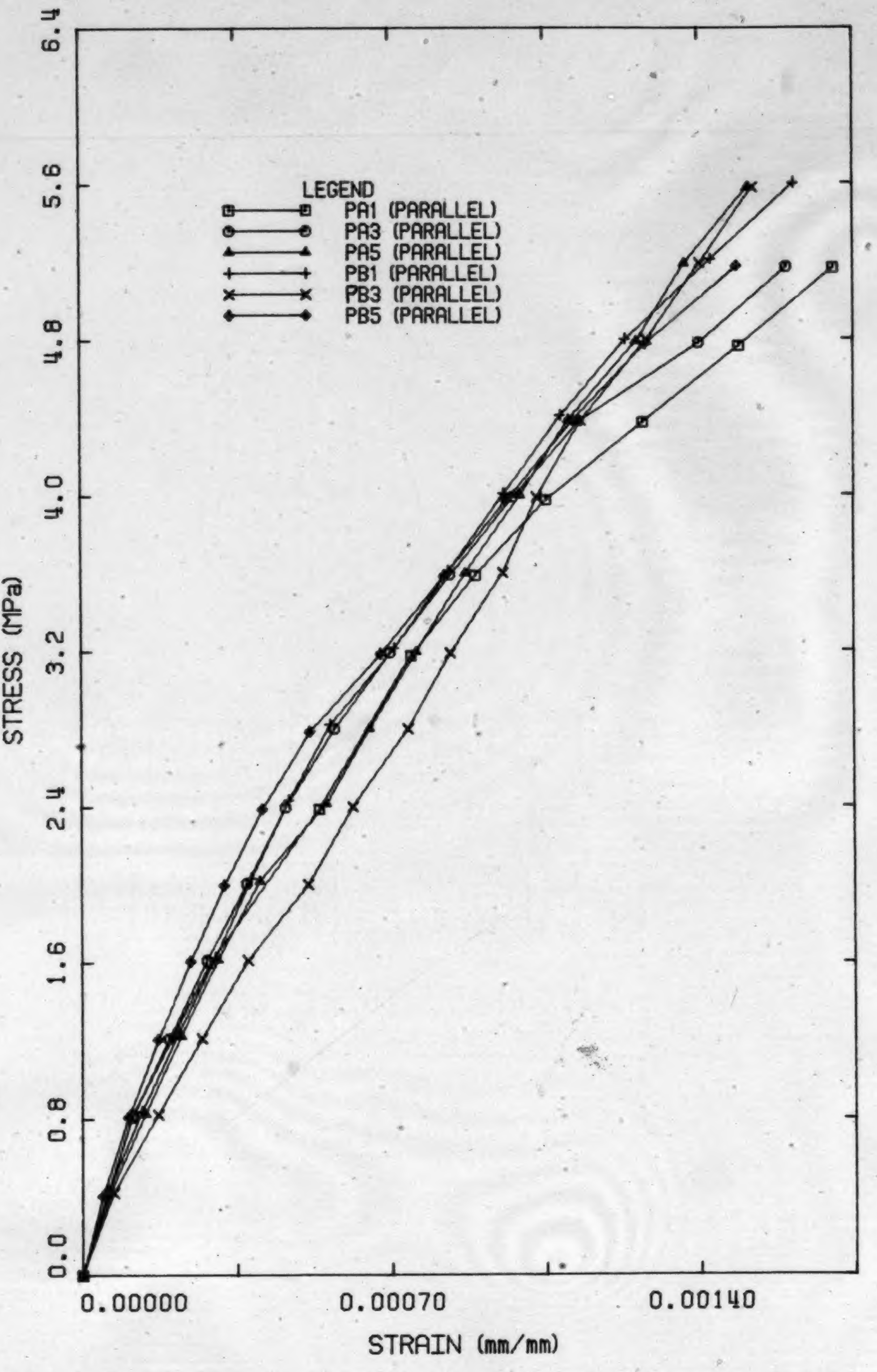

Figure 4.7 Stress-Strain Relationships for Masonry Prisms

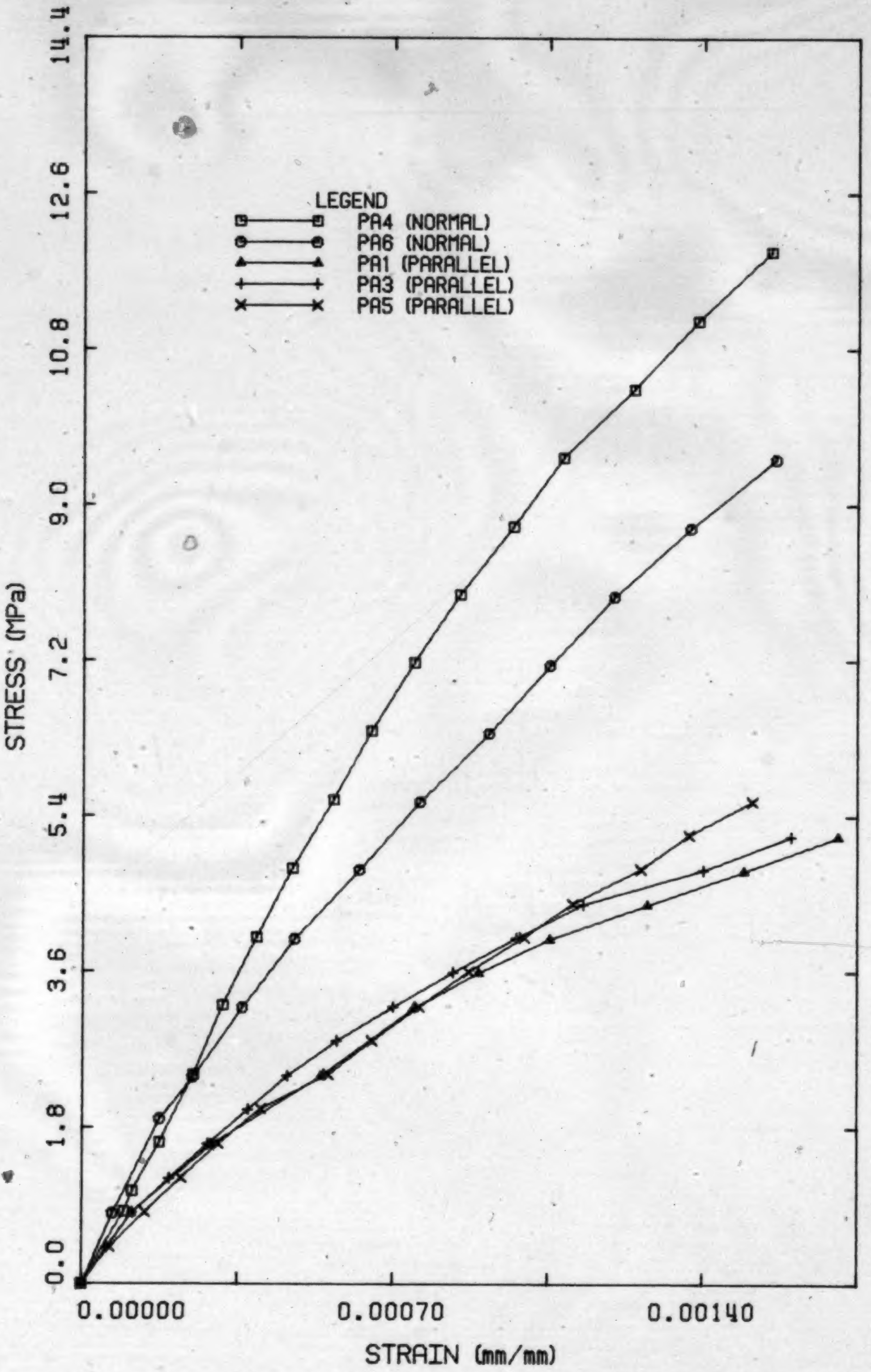

Figure 4.8 Stress-Strain Relationships for Masonry Prisms

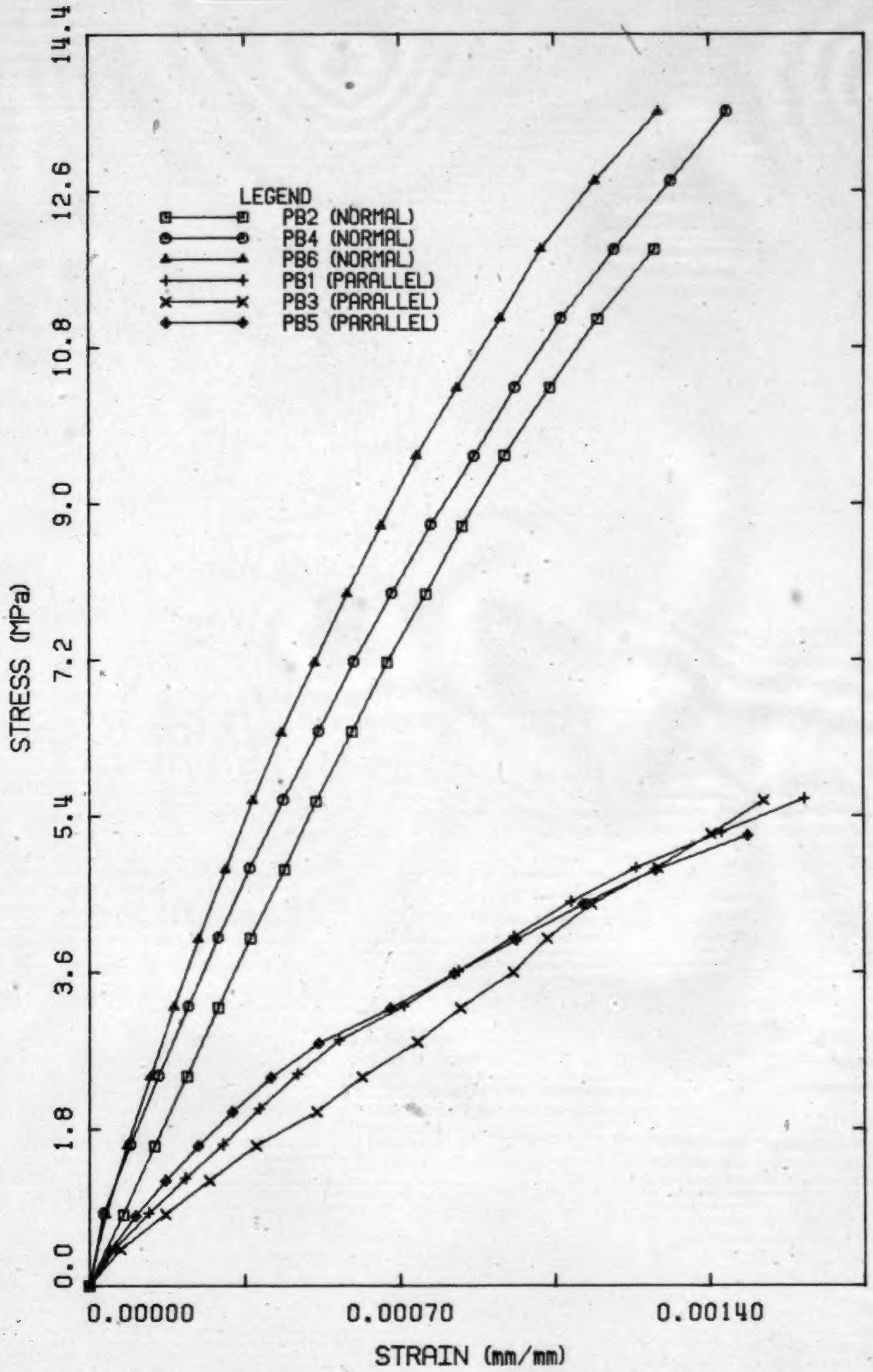

Figure 4.9 Stress-Strain Relationships for Masonry Prisms

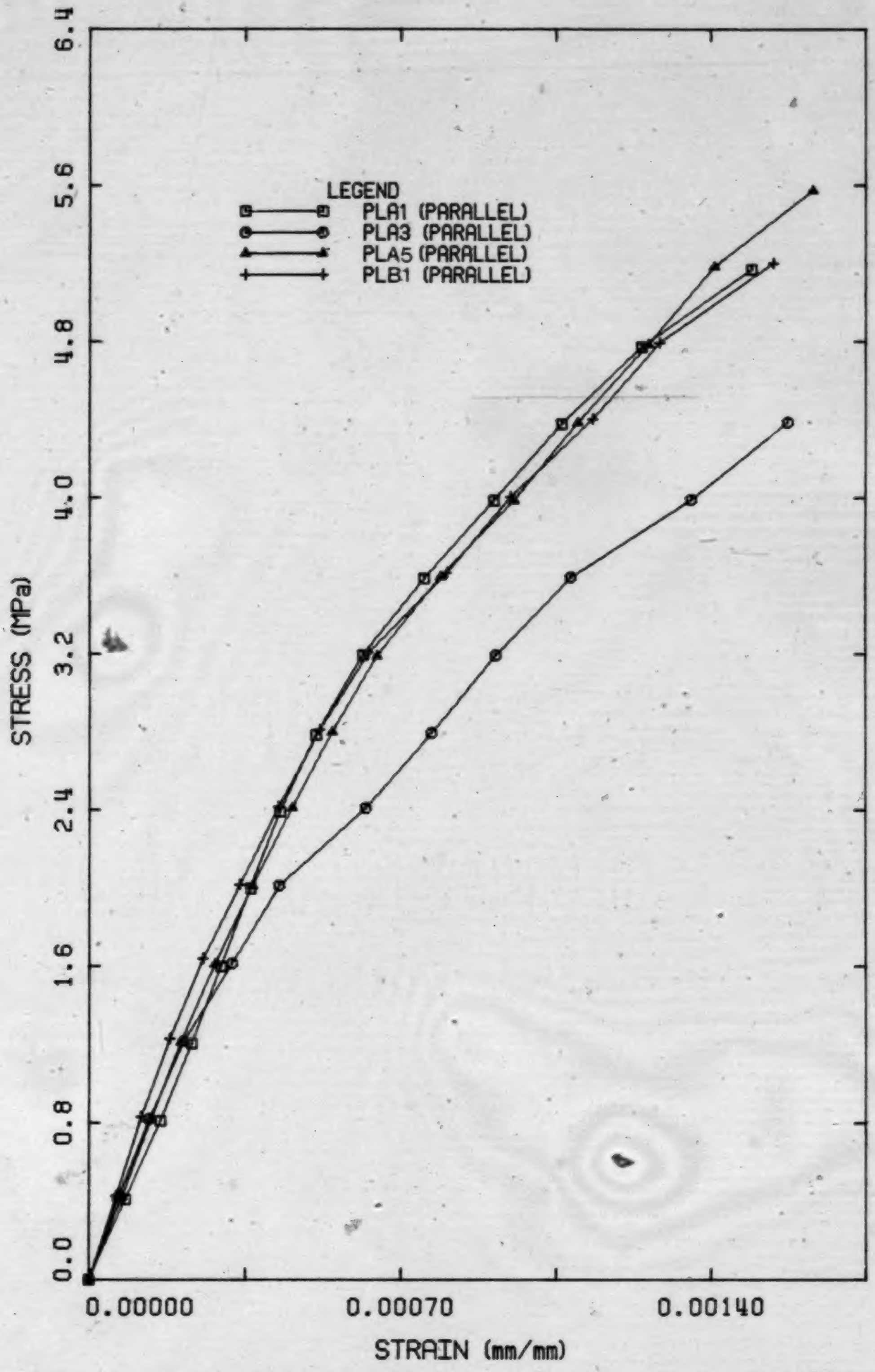

Figure 4.10 Stress-Strain Relationships for Masonry Prisms

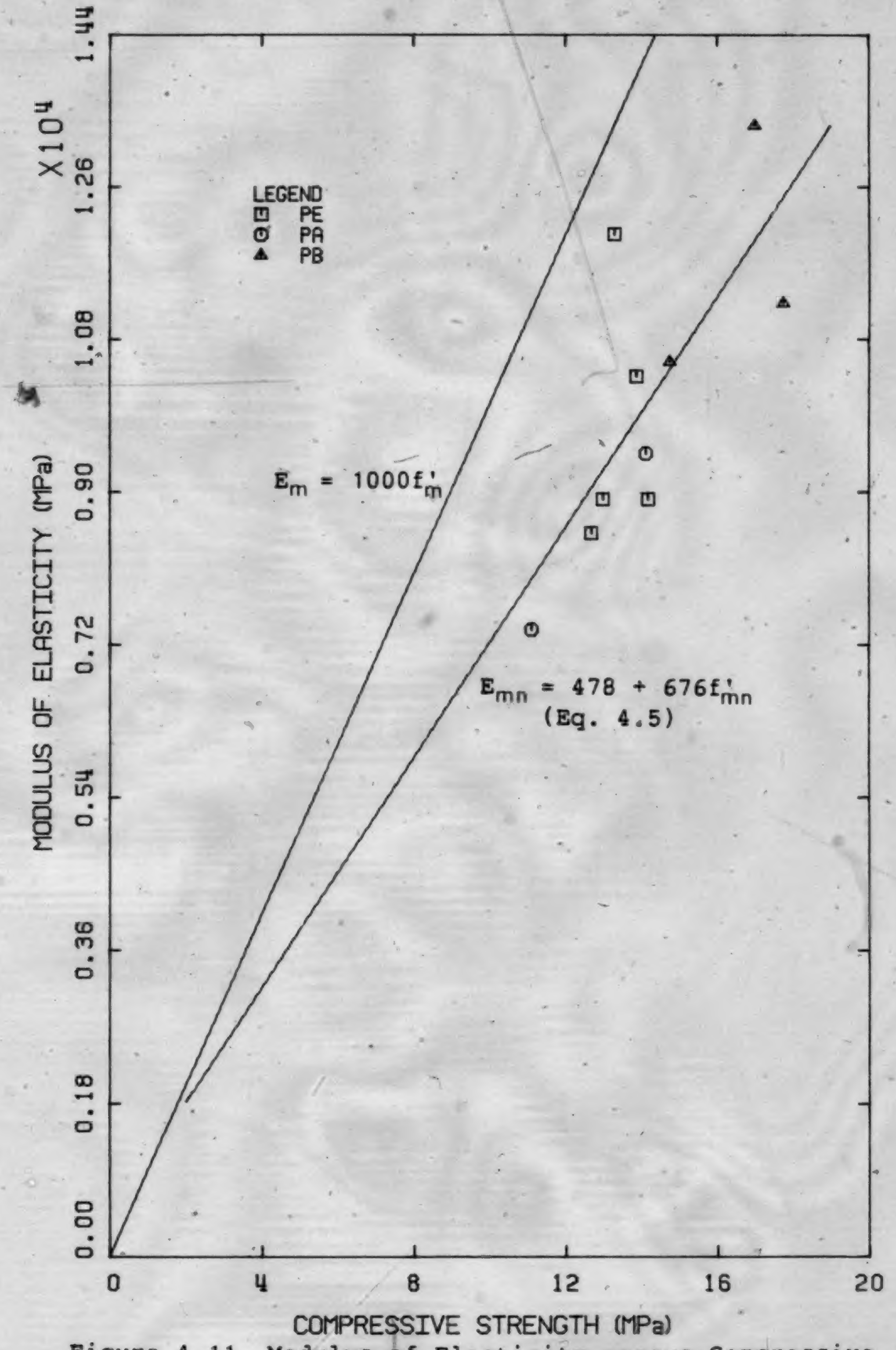

Figure 4.11 Modulus of Elasticity versus Compressive Strength for Masonry Prisms

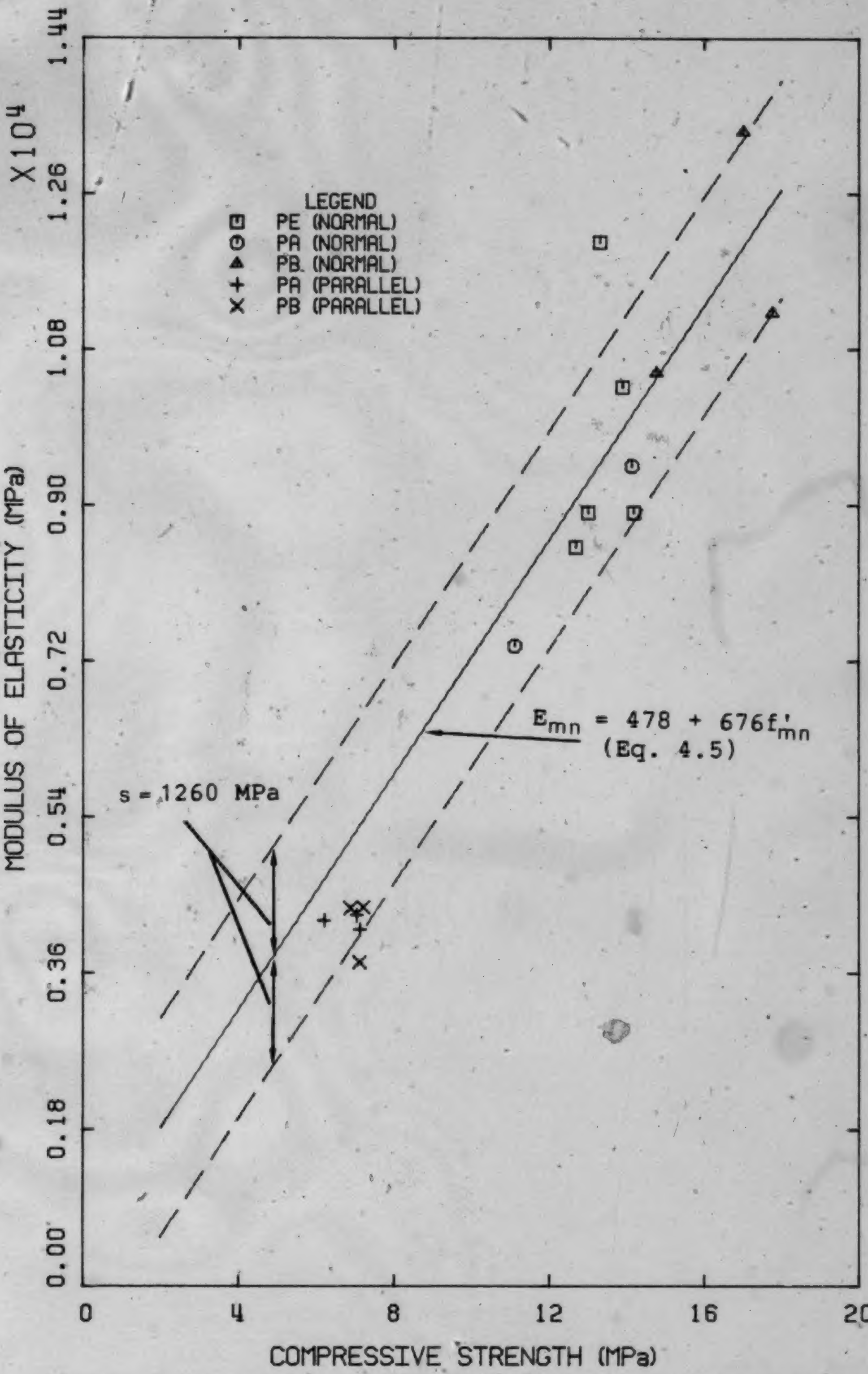

Figure 4.12 Modulus of Elasticity versus Compressive Strength for Masonry Prisms

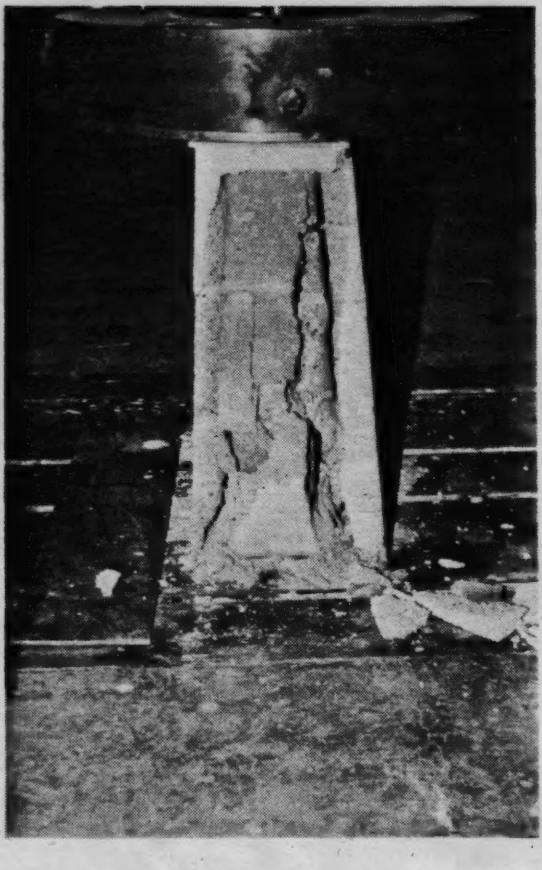

Plate 4.1 Typical Failure Mode of Prism Loaded Normal to Bed Joints

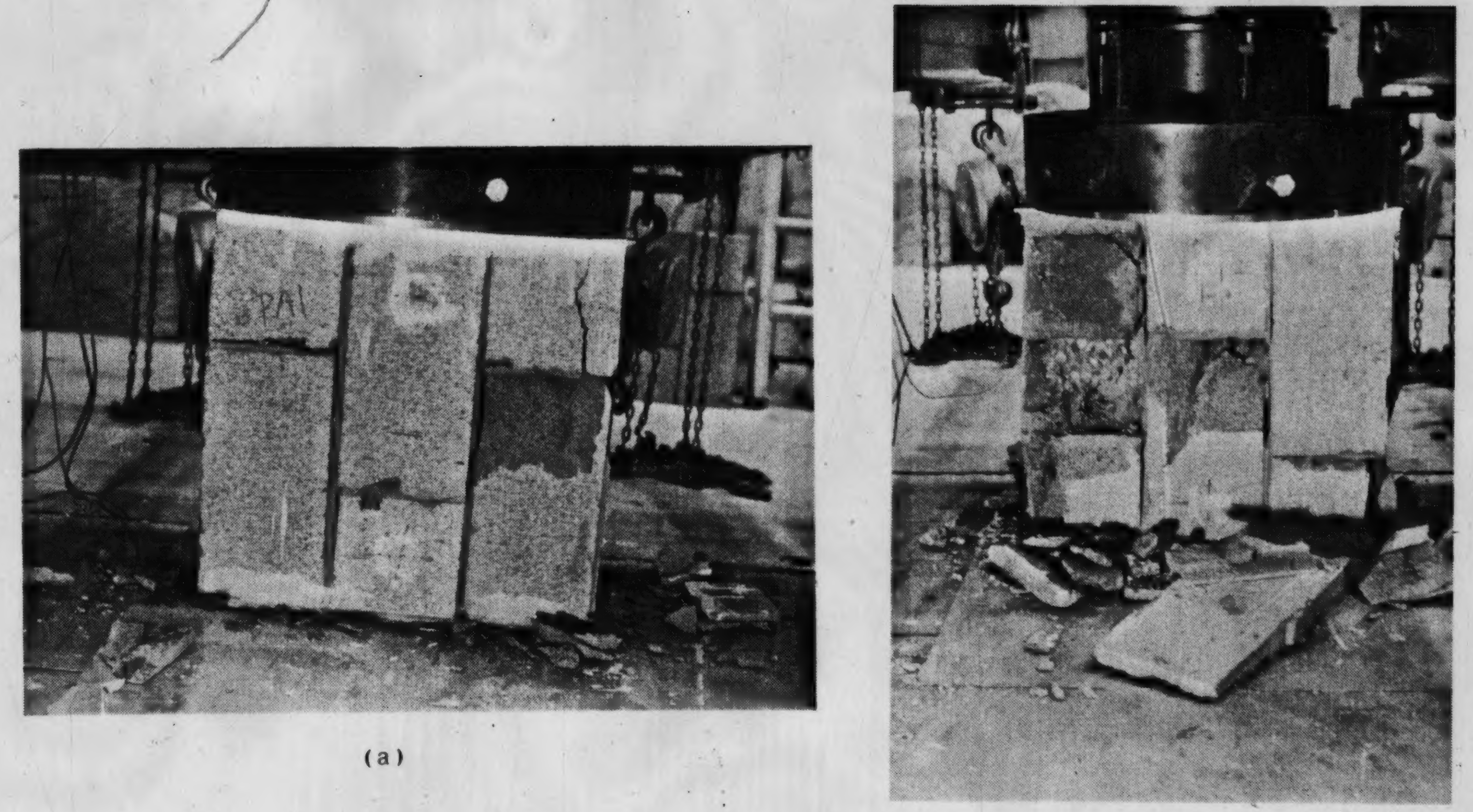

(a)

(b)

Plate 4.2 Failure Mode of Prisms PA and PB Loaded Parallel to Bed Joints

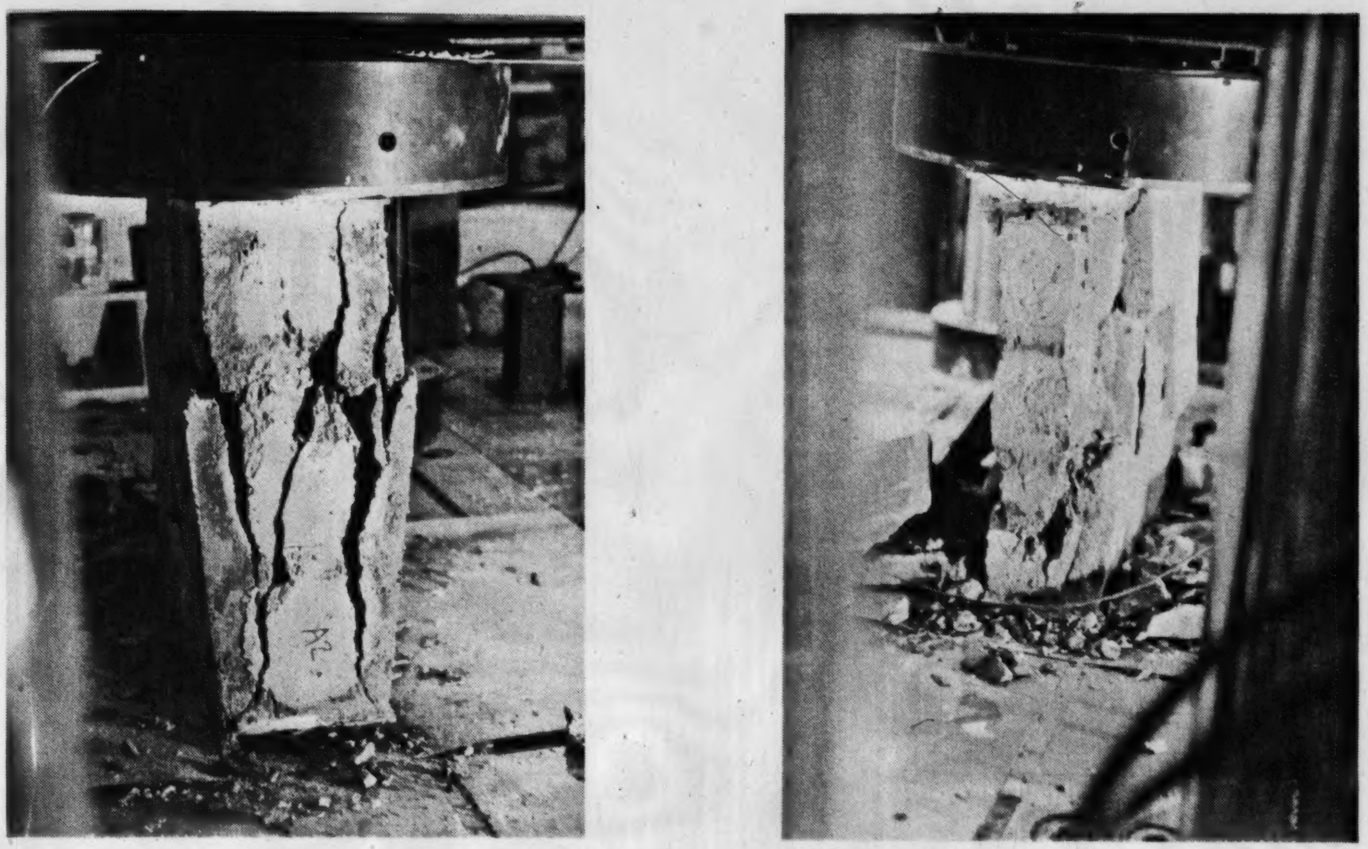

(a) (b)

Plate 4.3 Failure Mode of Prisms PA and PB Loaded Parallel to Bed Joints

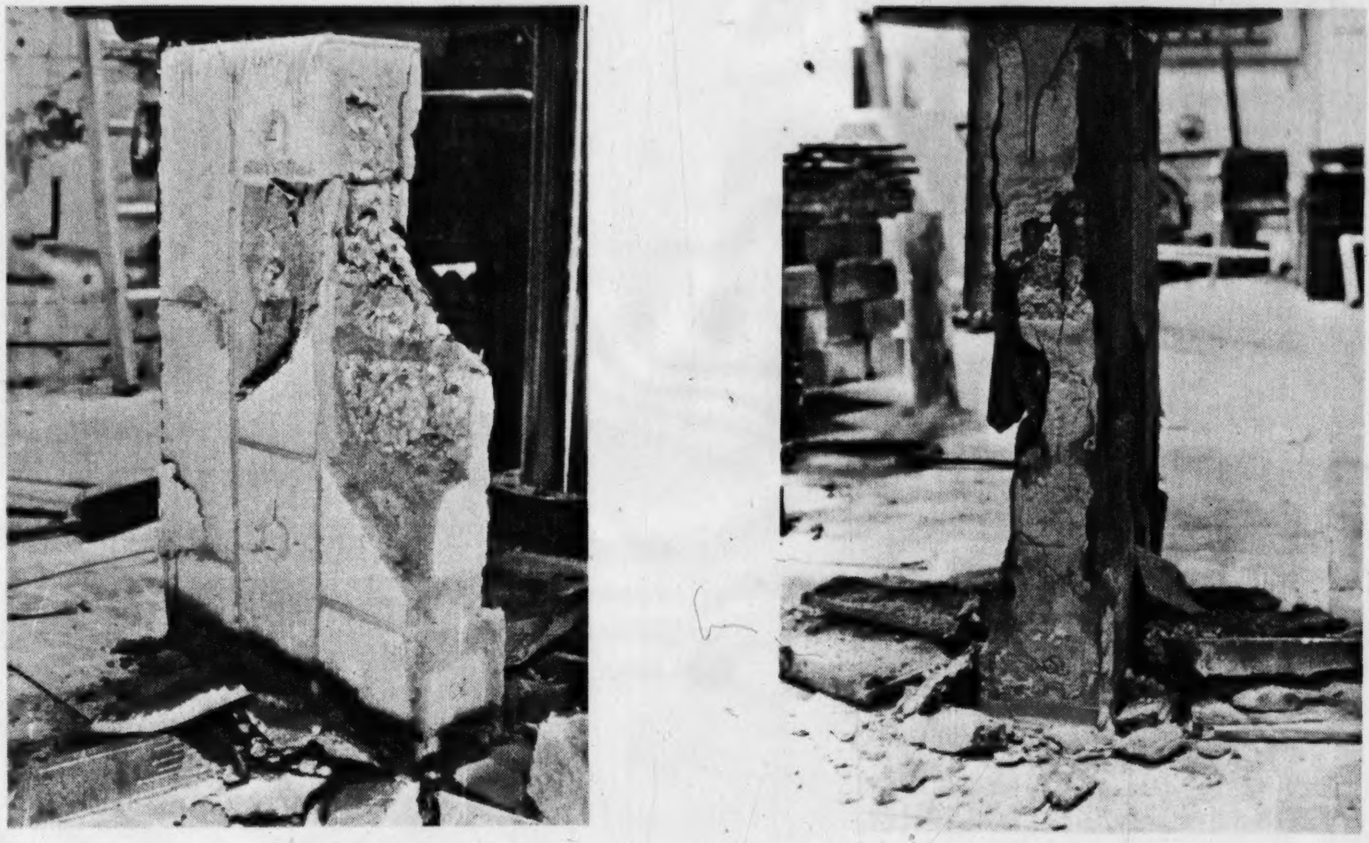

(a)

(b)

Plate 4.4 Failure Mode of Prisms PLA and PLB Loaded Parallel to Bed Joints

5. Test Results

5.1 Introduction

In this chapter results of full scale beam tests are summarized and presented in tabular, graphic and photographic form. Identification of the beams is shown in Table 5.1. Geometric properties of the beams are not included here, since they have been presented in Chapter 3. Beam loads are defined in terms of the average of the two applied loads. All plots involving loads are terminated at maximum loads. Crack patterns are included in Appendix A. Table 5.2 gives the principal test results for all beam series. These include yielding and ultimate capacities, and centerline deflection at steel yield and at ultimate load.

5.2 General Behavior

Beam SB1

At a load of 20 kN, vertical tension cracks appeared at most mortar joints in the bottom course along the beam, but they all terminated at the horizontal joint at the top of this course. At 35 kN, more tension cracks began to appear in the middle of the lintel blocks under the head joints of the upper course. Approximately at tension steel yielding, hairline shear cracks appeared in the south shear span sloping approximately 45° across the blocks or following the horizontal joint. After steel yielding, the beam sustained additional load. Crushing at the head joint and cracking of the blocks were observed at the top of the beam as load was increased. The beam finally failed when a block of masonry at the top of the beam lifted as shown in Plate 5.1.

Beam SB2

At a load of 60 kN, visible flexural cracks were observed in the vertical mortar joints and also through the middle of the lintel blocks in the maximum moment region. Stair-stepped cracks appeared in the two shear spans when the load was increased from 90 to 125 kN. These cracks extended upwards from the existing flexural cracks, following the vertical mortar joints and then travelled along the horizontal joint to the next vertical joint. After the tension steel yielded, two head joints at the top of the beam between the load points showed evidence of crushing. No further load could be applied when all three top course blocks between the loads were cracked longitudinally and large flexural cracks extended up to the top course. Plate 5.2 shows the crushing of the head joint.

Beam SB3

Visible tension cracks appeared in the maximum moment region at a load of 38 kN. These cracks extended above the lower horizontal joint. At a load of 65 kN, diagonal cracks appeared in both shear spans. As the load increased, these diagonal cracks propagated through the beam from the load points to the supports. At 85 kN, when the tension steel began to yield, serious cracking was observed under the south load point and at the level of the steel near the north support. When the beam failed, the load immediately dropped off and it was observed that large size cracks had formed under the north load point. Plate 5.3 shows the shear cracks in the beam at failure.

Beam SB4

Initially, the development of tension cracks was similar to that in Beam SB3. Beginning at a load of 55 kN, more tension cracks formed in the shear spans, either in the head joints or extending upward from the middle of the lintel blocks. A number of cracks appeared in the horizontal joints at or after the tension steel yielded. Most of these cracks extended from the existing vertical tension cracks. When the beam approached failure, a head joint near the north load point crushed and a large piece of face shell spalled off. The condition of the beam at failure is shown in Plate 5.4.

Beam RB1

At a load of 37 kN, cracks along the vertical mortar joints and horizontal bed joints were observed to exist in the constant moment region. Cracks also developed in the head joints at the top of the beam near the supporting edges and extended vertically downward to the level of the tension reinforcement as load increased. At 46 kN, cracks opened up at the interfaces between the beam and the supporting blocks and the edges of the supports were slightly crushed. No further load could be applied when all the top mortar joints between the loads crushed, followed by opening up of the cracks at the interfaces between the blocks and grout, and by spalling of the face shell. Plate 5.5 shows conditions at failure. The cracks at the top of the beam above the supports are shown in Plate 5.6 and 5.7 which also show clearly the existence of horizontal cracks at the level of the reinforcement.

Beam RB2

This beam was first tested using a load cell with inadequate capacity and the test was terminated. After a larger load cell was introduced, the beam was loaded to failure without difficulty. Results for the two separate tests were recorded.

Flexural cracks were first observed at 105 kN. A head joint crack at the top of the beam above the north support appeared at a load of 105 kN and a similar crack above the south support appeared at 190 kN. The north support edge began to crush at 80% of maximum load. Stair-stepped shear cracks, similar to those in Beam SB2, appeared at 190 kN. The failure mode was a typical crushing failure as the reinforcement had not yielded when maximum capacity of the beam was reached. Plate 5.8 shows the compressive zone of the beam after the test.

Beam RB3

Tension cracks developed mainly in the vertical mortar joints. Cracks appeared at the second mortar joint from each of the support edges at the top of the beam at a load of 55 kN and extended vertically downward as load increased. Shear cracks first appeared at a load of approximately 95 kN, running across the blocks and along the horizontal joints towards the load points and the support edges. At 110 kN, another large shear crack appeared above the existing crack in the south shear span and the load dropped suddenly. However, conditions stabilized and loading was continued. Further shear cracks appeared in the north shear span. The beam finally failed when a large piece of masonry fell off as shown in Plate 5.9. Since the strain gauge on the tension reinforcement malfunctioned, it was not possible to ascertain whether or not the reinforcement had yielded before failure.

Beam RB4

Visible tension cracks appeared in the vertical mortar joints at a load of 80 kN and also appeared in the middle of the lintel blocks at 95 kN. The cracking above the beam supports similar to that in Beam RB3 already appeared at a load of 40 kN. At a load of 85 kN, a crack appeared immediately above the north support edge. Plates 5.10 and 5.11 show clearly that these cracks extended down to the level of the reinforcement. Hairline shear cracks began to propagate in both shear spans at 100 kN. Most of these shear cracks propagated across the blocks. After the tension reinforcement yielded, the top course split longitudinally and the face shell spalled off, resulting in a sudden drop in the load. Plate 5.12 shows the compressive zone of the beam after failure.

Beam EB1

Flexural cracks mainly formed in the vertical mortar joints and were visible at a load of 85 kN. At 125 kN, inclined cracks started to develop, running across the blocks. Near maximum load, serious cracking was observed at the level of the reinforcement close to both supports and large inclined cracks formed above the existing shear cracks. No signs of cracking or crushing were observed in the support walls at the end of the test. The large inclined cracks are shown in Plate 5.13 and Plate 5.14 shows the beam after test.

Beam EB2

Visible tension cracks were observed at a load of 90 kN and hairline inclined cracks appeared at 170 kN. The support wall cracked and crushed near maximum load and a crack appeared between the beam and wall as shown in Plate

5.15. The longitudinal reinforcement was close to yield when the beam was loaded to its maximum capacity. Plate 5.16 shows the failure condition in the compressive zone and Plate 5.17 shows the beam after test.

Beam EB3

Visible tension cracks were observed at a load of 100 kN and hairline inclined cracks formed at 125 kN. Cracks occurred at the interfaces between the beam and support walls at a very early stage of loading. The reinforcement reached yield followed by crushing of the compressive zone as shown in Plate 5.18. The north support wall also cracked and crushed extensively with the blocks in the second and third layer moving out. The condition of the support wall after the beam failed is shown in Plate 5.19. Plate 5.20 shows the beam after test.

Beam EB4

This beam failed suddenly and the record of the cracking pattern is incomplete. Flexural cracks were observed at a load of 75 kN. Large shear cracks developed at 115 kN. At a load of 125 kN, further inclined cracks formed in the north shear span. Near maximum load, cracks appeared in the mortar joints above the support walls and extended downward towards the support edges as shown in Plates 5.21 and 5.22. The beam suddenly fractured along the inclined crack with the tension reinforcement still below yielding. Plate 5.23 shows the beam after test.

Beam EB5

Visible tension cracks were first recorded at a load of 85 kN and shear cracks started to develop at 135 kN running across the blocks or along the vertical or horizontal joints. Cracks at the interface of beam and support walls were visible at 93 kN. Near maximum load, the south support wall cracked and crushed seriously. The blocks in the second and third layer were dislodged and moved outwards. The failure of the wall is shown in Plates 5.24 and 5.25. At maximum load, the masonry in the compressive zone cracked and crushed extensively as shown in Plate 5.26. This was a typical crushing failure as the longitudinal reinforcement had not yielded at maximum load. Plate 5.27 shows the beam after failure.

Beam EB6

Visible flexural cracks appeared at a load of approximately 75 kN and extended upward and toward the center of the beam. Hairline shear cracks running mainly across the blocks developed at a load of 125 kN. Cracks developed at the interfaces between the beam and the support walls at a load of 60 kN and extended towards the support edges. After the tension reinforcement yielded, the south support wall cracked and crushed suddenly as shown in Plate 5.28. The load was suddenly reduced when the blocks in the compressive zone crushed as shown in Plate 5.29. Numerous hairline shear cracks were evident at the end of the test. Plate 5.30 shows the beam after failure.

5.3 Load-Deflection Relationships

The relationships between load and vertical deflection at 5 locations along the beams are shown in Figures 5.1 to 5.14. Since one of the LVDT's malfunctioned in Beam RB3, the deflection at that location could not be recorded. The deflected shapes of the beams for various loads are plotted in Figures 5.15 to 5.28.

5.4 Load-Strain Relationships

Strains were measured in one of the tension reinforcing bars at mid-span of each beam specimen and at various locations near the ends for Type RB and EB beams. Figures 5.29 to 5.31 show the relationship between load and reinforcement strain at mid-span for different series. Figures 5.32 to 5.39 show the relationship between load and reinforcement strains at various locations near the ends of the beams. For Type EB beams, only the strains at the edge of the support are plotted.

Strain readings from gauges mounted at mid-depth on the web reinforcement are shown in Figures 5.40 to 5.47. Load-strain relationships are not presented for Beam EB2 and EB5 since the strain gauges near the loading point for these two beams malfunctioned.

Horizontal surface strains were also measured by LVDT's located 25 mm from the top of the beams and at the level of tension reinforcement in the constant moment region. Figures 5.48 to 5.61 show the relationship between load and these surface strains.

5.5 Load-Restraining Force and Load-Displacement Relationships

The horizontal restraining force in the bottom course of the supporting walls for Type EB specimens is plotted against load and shown in Figure 5.62.

The displacements in the second course of each support wall for Type EB beams were recorded. However, since only one end showed significant displacement while the maximum displacement at the other end was always less than 1 mm, the relationship between load and horizontal displacement is presented in Figure 5.63 only for the ends with large displacement.

5.6 Crack Patterns

Crack patterns for all beam specimens are presented in Appendix A. Beam EB4 is not included since crack patterns were damaged when the beam failed. The numbers beside the cracks refer to the loads in kN at which the cracks were observed to reach the positions marked.

Table 5.1 Beam Classification

Beam	Courses	Reinforcement		Support Condition
		Tension	Shear*	
SB1	2	2 #20M	#10M	S
SB2	4	2 #20M	#10M	S
SB3	3	2 #20M	-	S
SB4	3	2 #20M	#10M	S
RB1	2	2 #20M	#10M	F
RB2	4	2 #20M	#10M	F
RB3	3	2 #20M	-	F
RB4	3	2 #20M	#10M	F
EB1	4	2 #20M	-	W 4**
EB2	4	2 #20M	#10M	W 4
EB3	4	2 #20M	#10M	W 3
EB4	4	2 #20M	-	W 2
EB5	4	2 #20M	#10M	W 2
EB6	4	2 #20M	#10M	W 1

S = Simply supported
F = Restrained by fixed concrete blocks
W = Support on masonry walls

* Single-leg stirrups
** Support wall length (in terms of no. of full blocks)

Table 5.2 Test Results

Beam	Average Load		Midspan Deflection	
	Yield (kN)	Maximum (kN)	Yield (mm)	Maximum (mm)
SB1	45.0	50.9	22.0	33.5
SB2	123.5	153.0	8.4	20.3
SB3	80.0	93.2	16.4	24.5
SB4	80.0	90.3	13.0	23.2
RB1	-	63.4	-	27.3
RB2	-	241.1	-	19.7
RB3	*	110.3	*	19.0
RB4	120.0	135.3	14.0	21.6
EB1	-	156.8	-	13.9
EB2	-	208.9	-	14.1
EB3	196.3	196.3	14.5	14.5
EB4	-	167.3	-	14.6
EB5	-	183.9	-	15.3
EB6	175.3	191.0	10.7	17.9

* Strain gauge on tension reinforcement non-functional

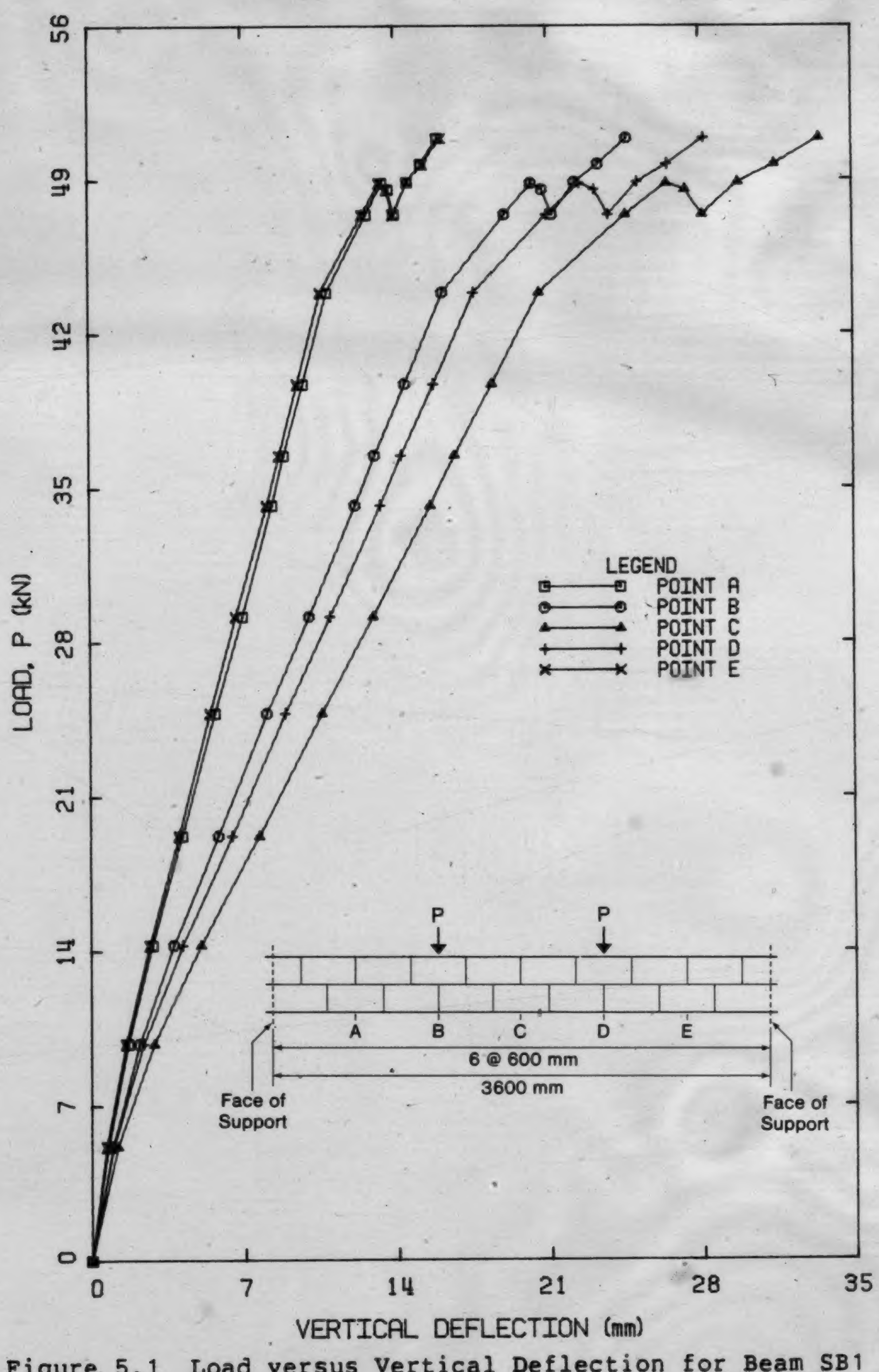

Figure 5.1 Load versus Vertical Deflection for Beam SB1

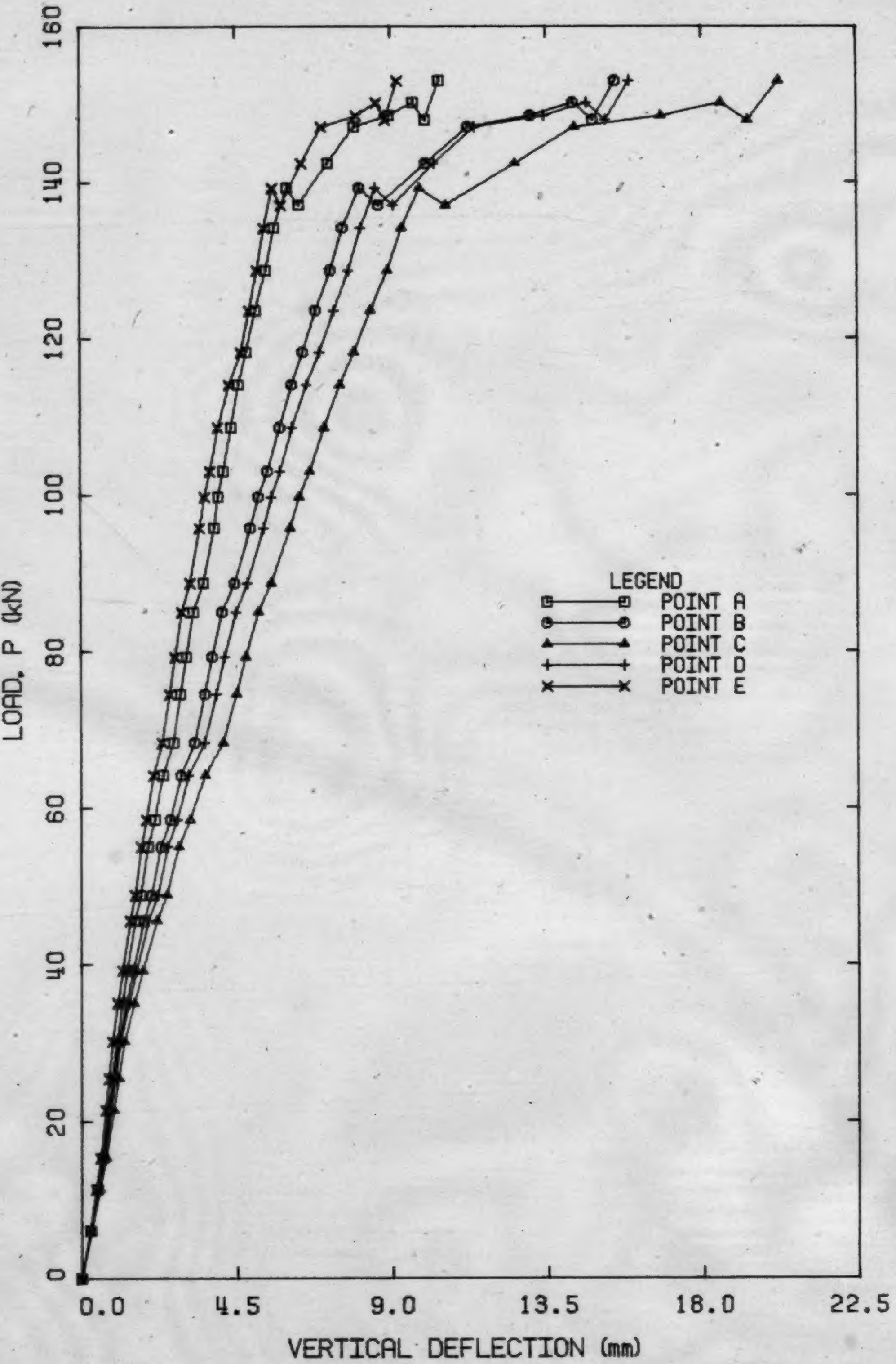

Figure 5.2 Load versus Vertical Deflection for Beam SB2

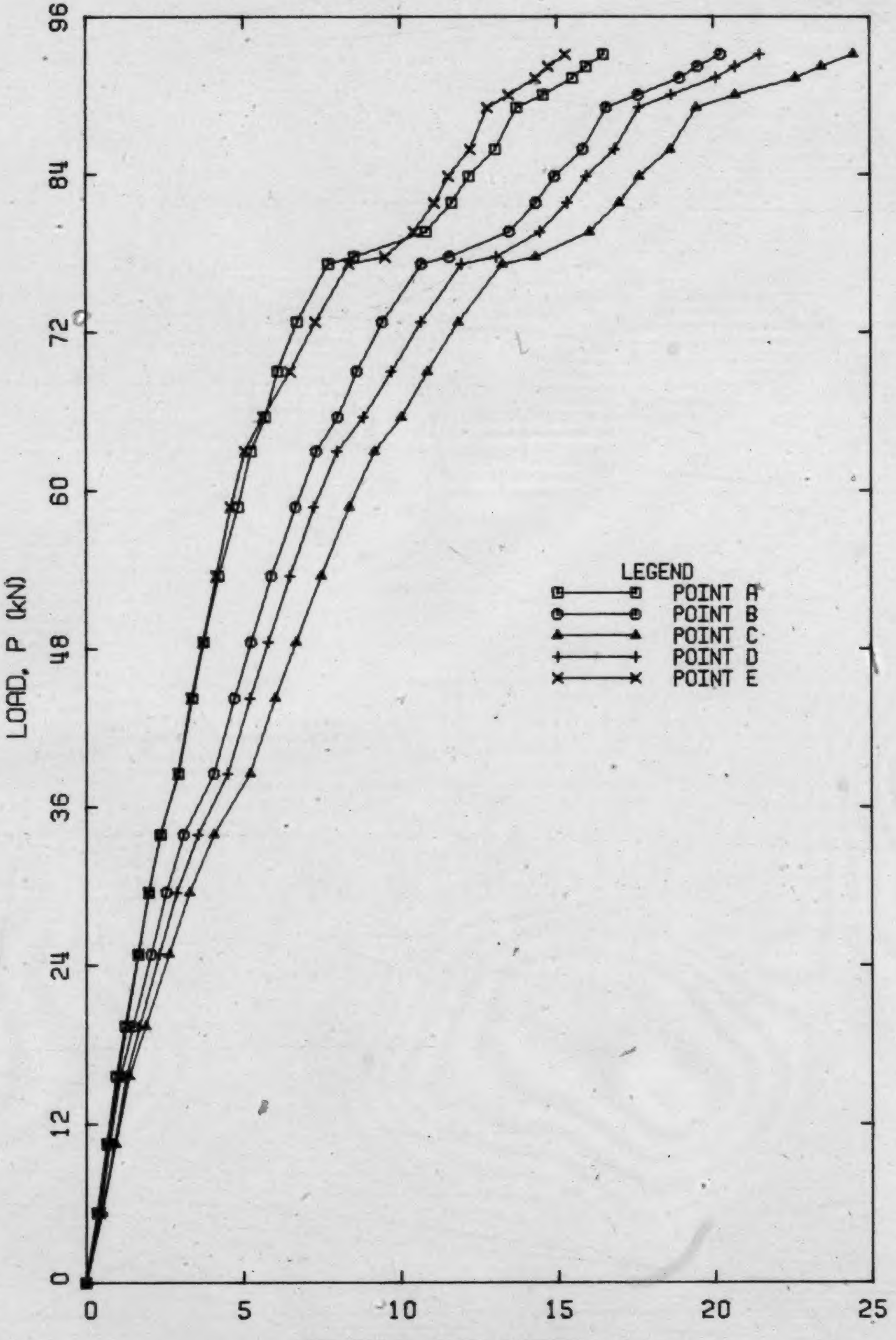

Figure 5.3 Load versus Vertical Deflection for Beam SB3

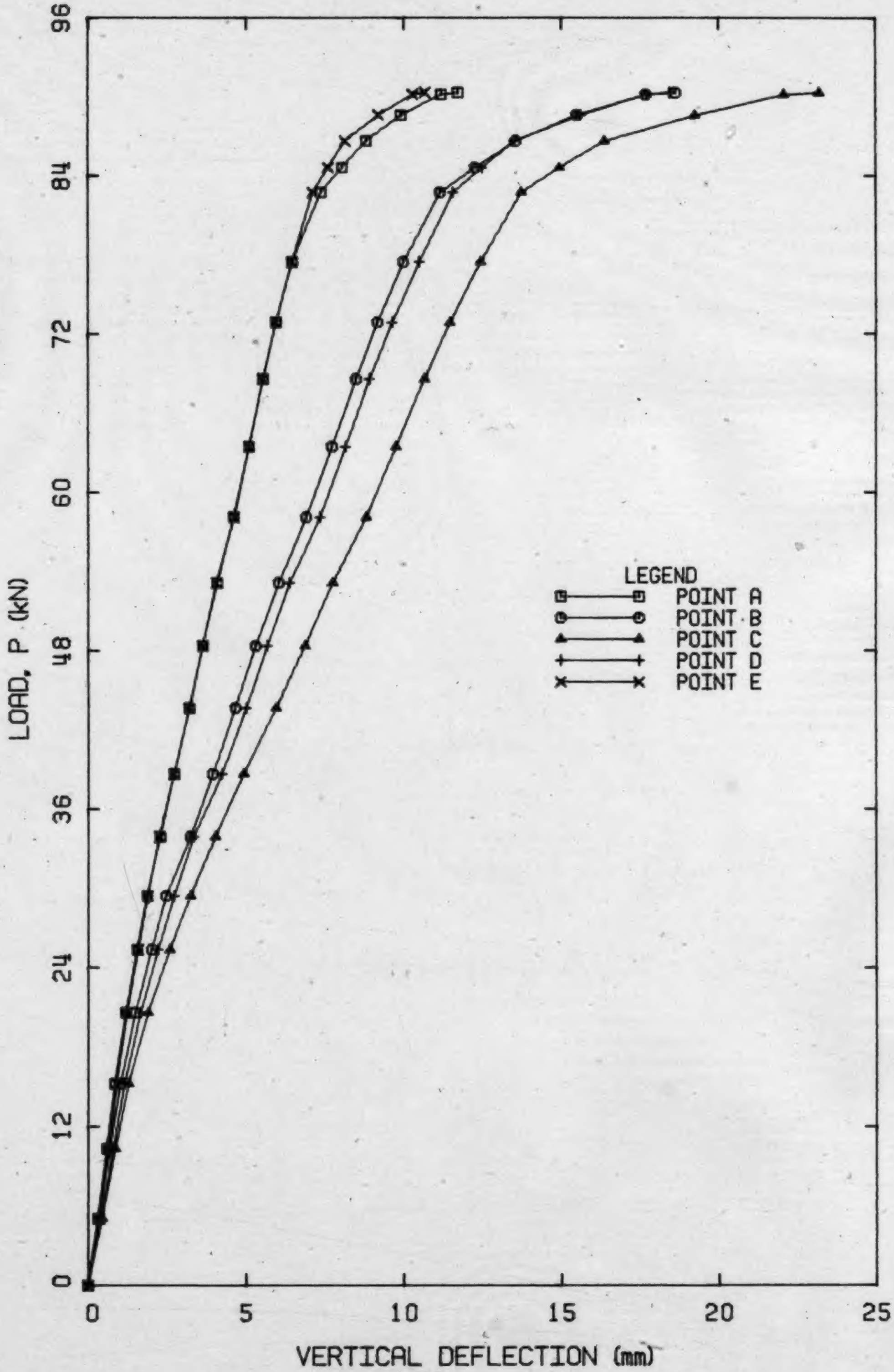

Figure 5.4 Load versus Vertical Deflection for Beam SB4

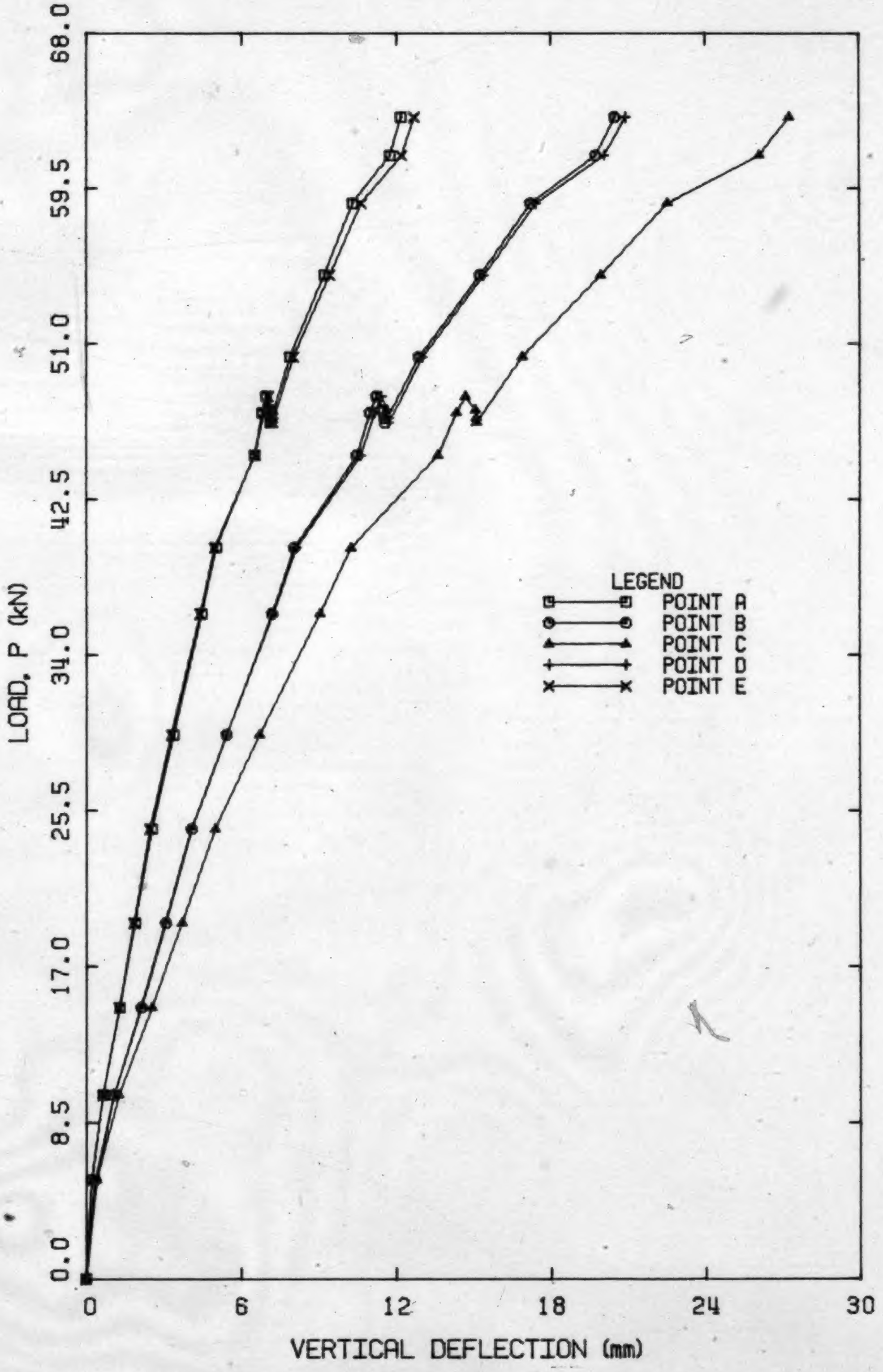

Figure 5.5 Load versus Vertical Deflection for Beam RB1

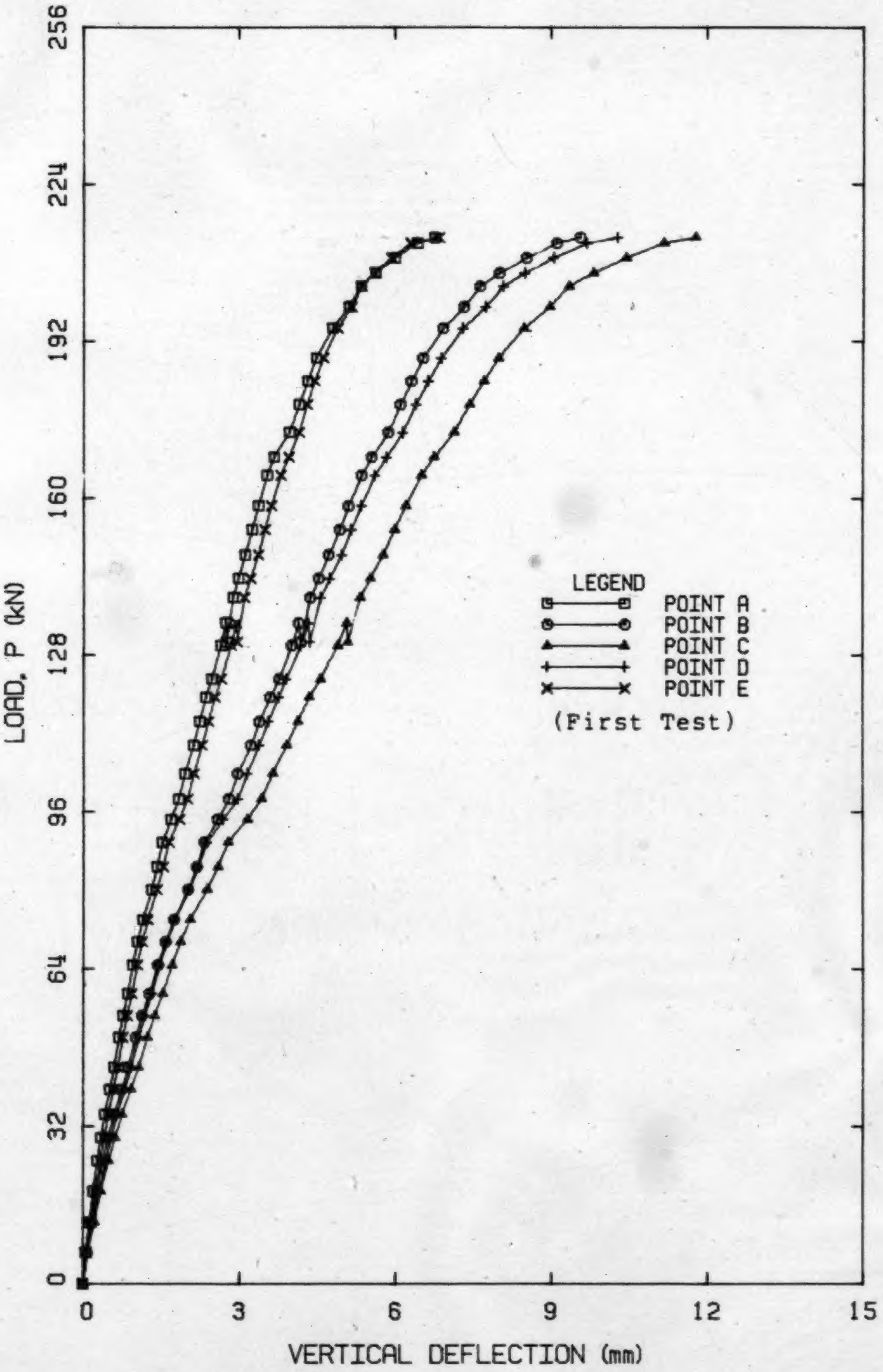

Figure 5.6 Load versus Vertical Deflection for Beam RB2

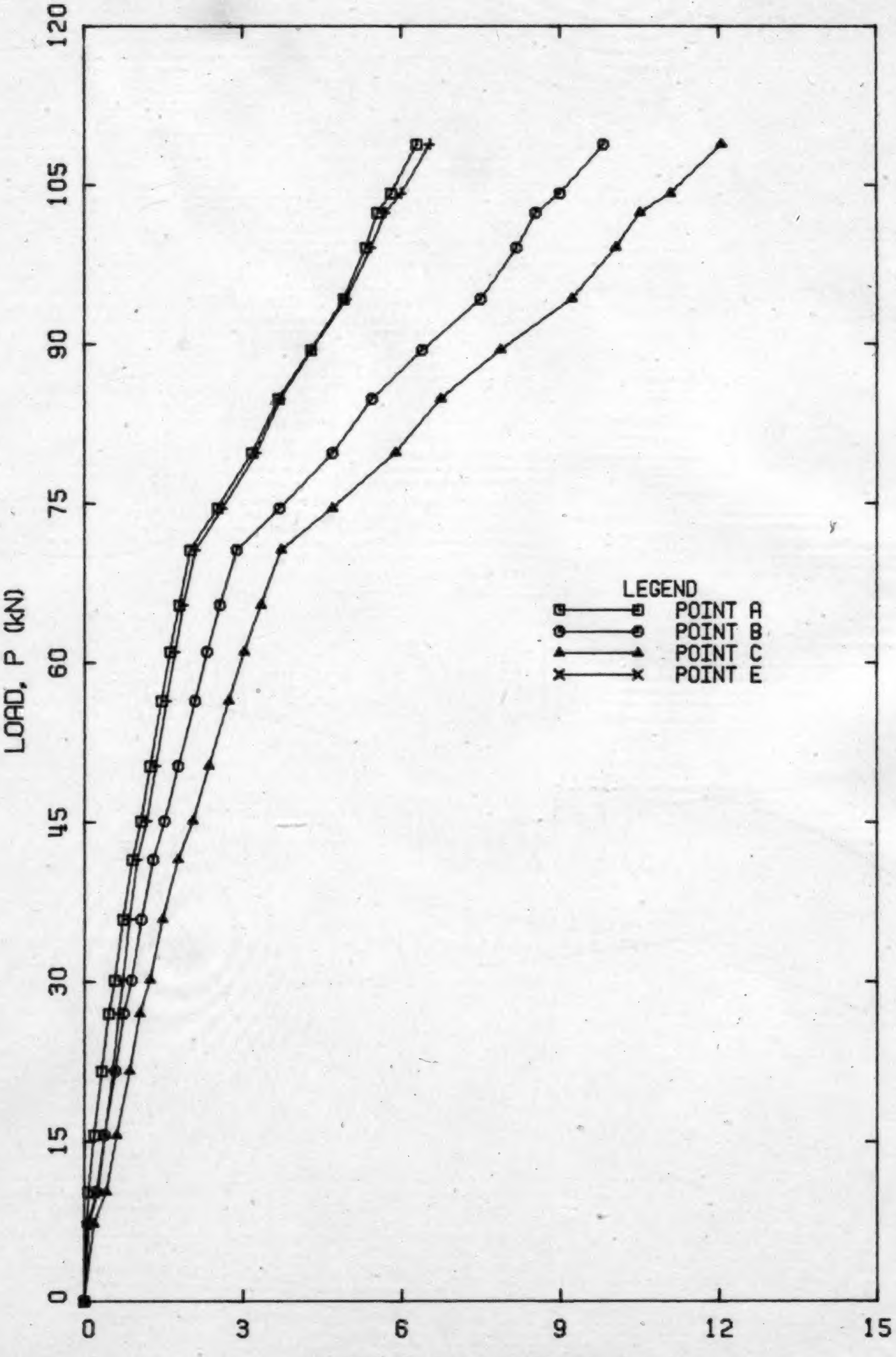

Figure 5.7 Load versus Vertical Deflection for Beam RB3

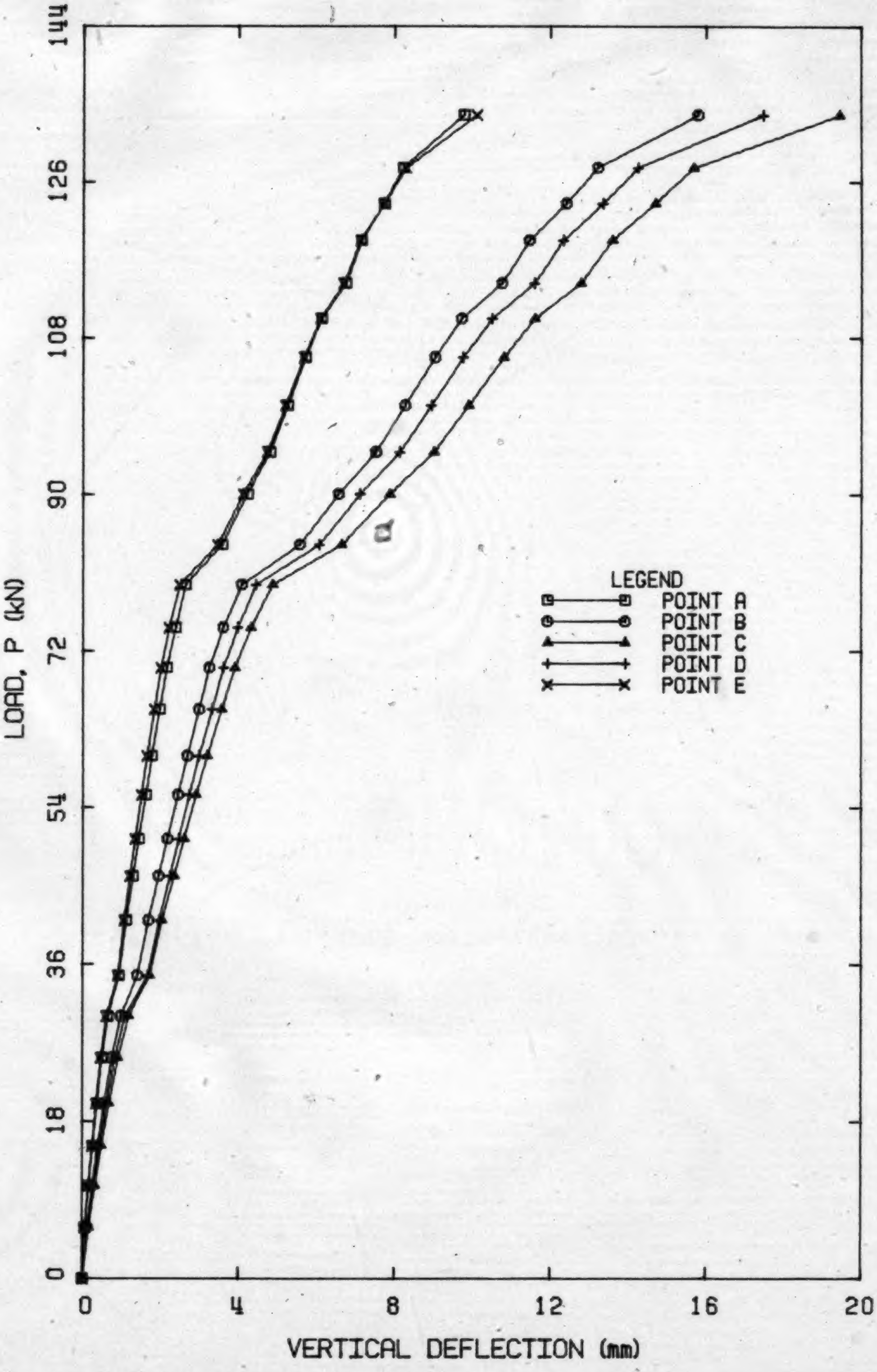

Figure 5.8 Load versus Vertical Deflection for Beam RB4

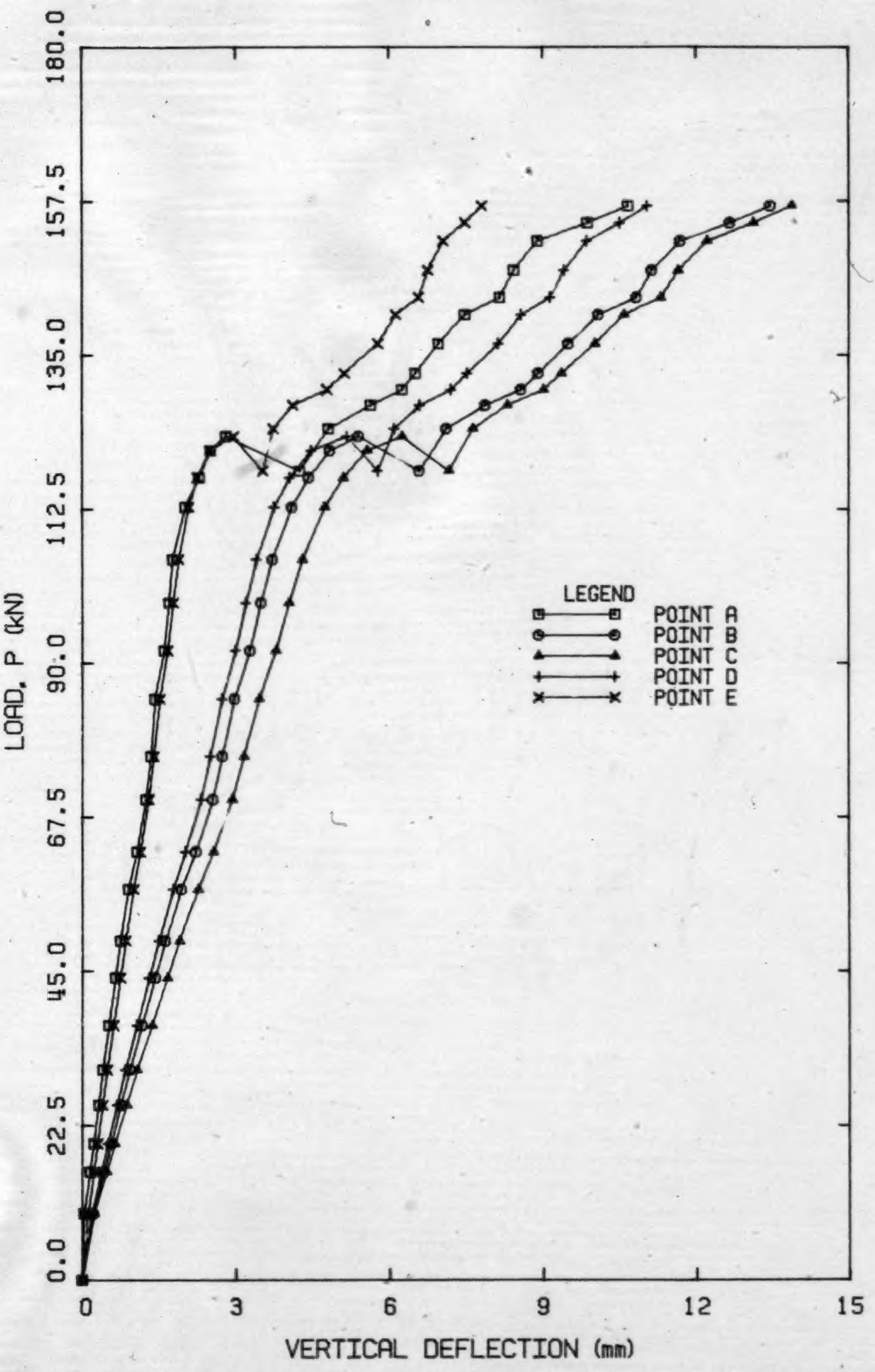

Figure 5.9 Load versus Vertical Deflection for Beam EB1

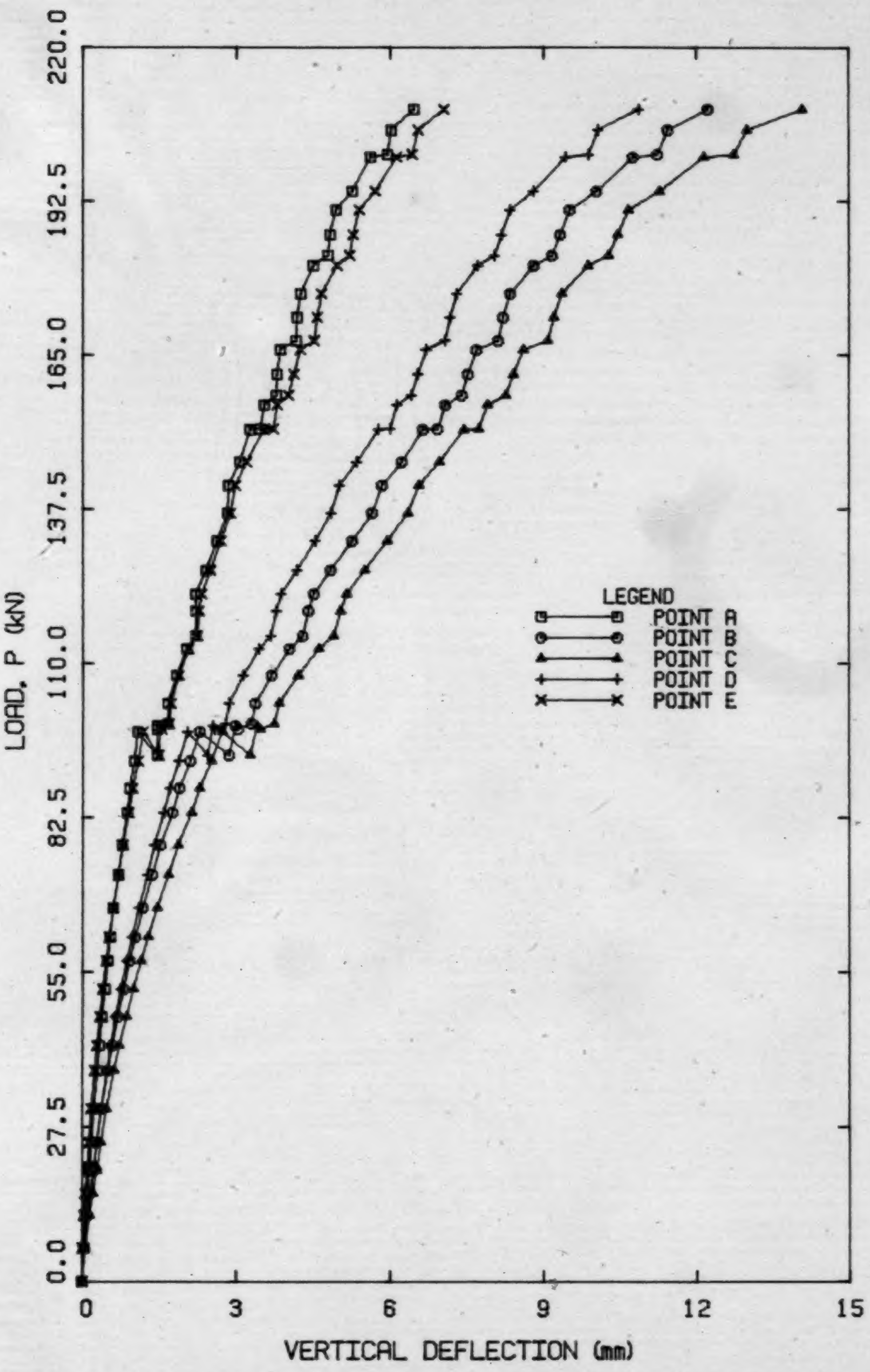

Figure 5.10 Load versus Vertical Deflection for Beam EB2

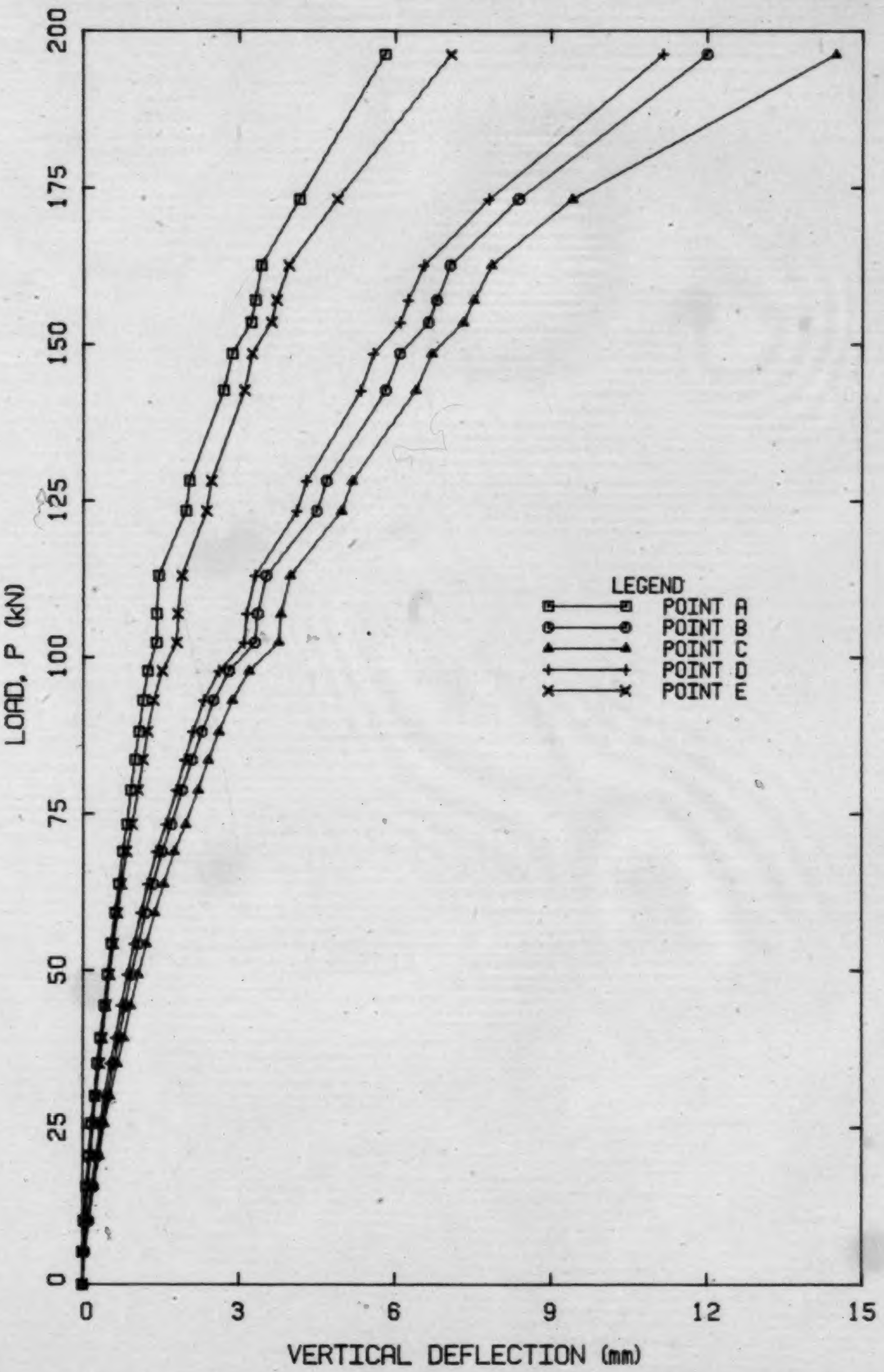

Figure 5.11 Load versus Vertical Deflection for Beam EB3

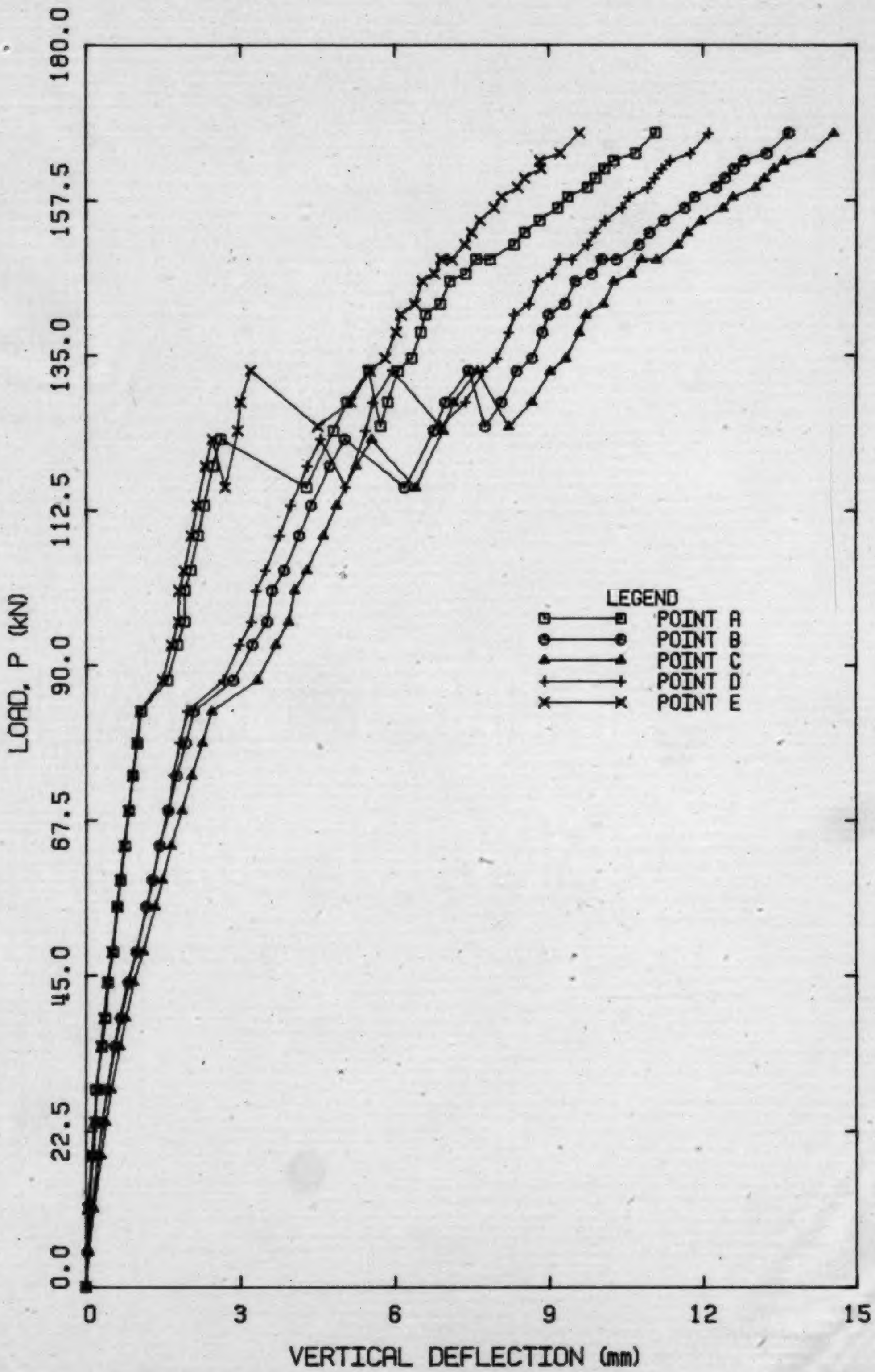

Figure 5.12 Load versus Vertical Deflection for Beam EB4

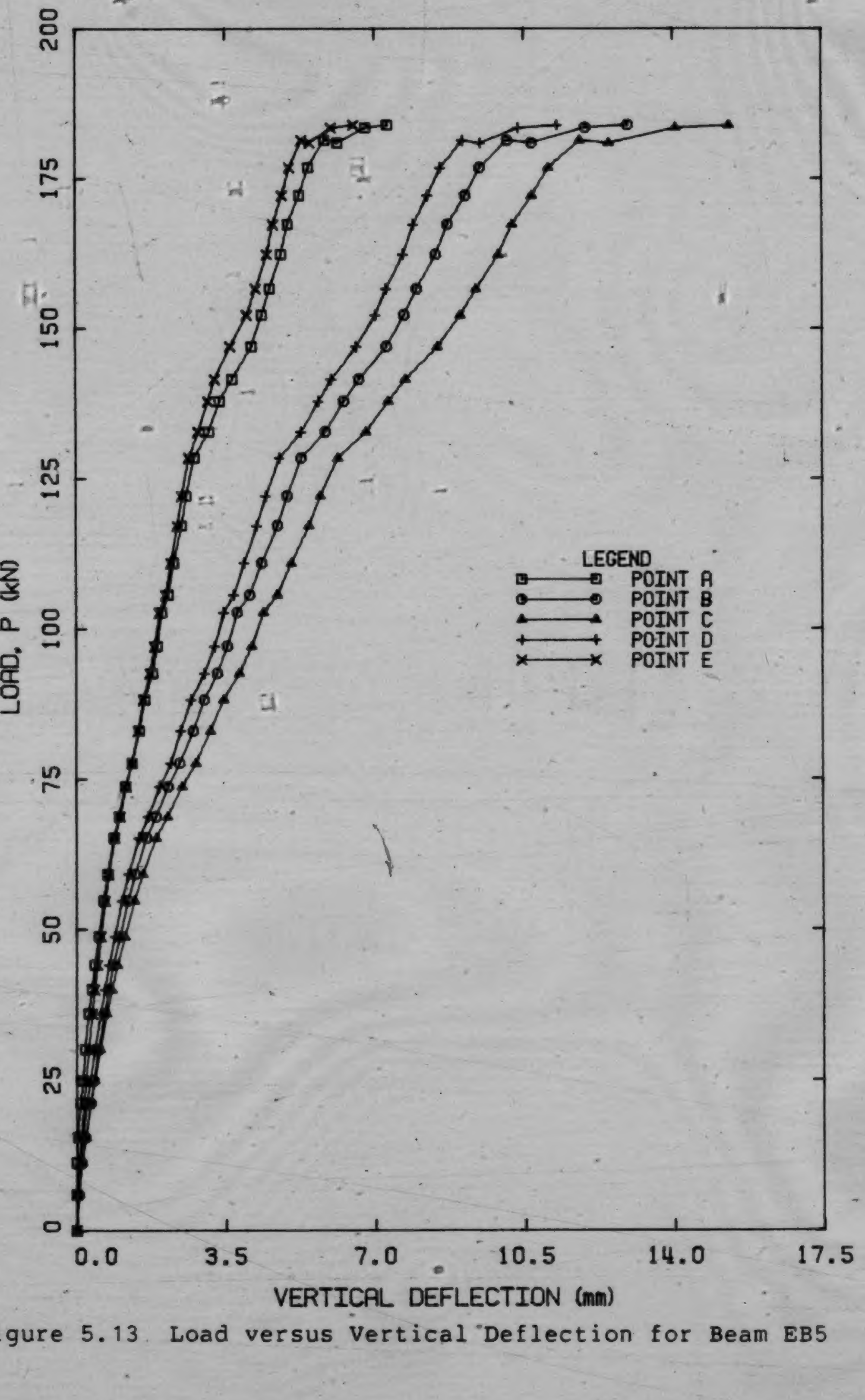

Figure 5.13 Load versus Vertical Deflection for Beam EB5

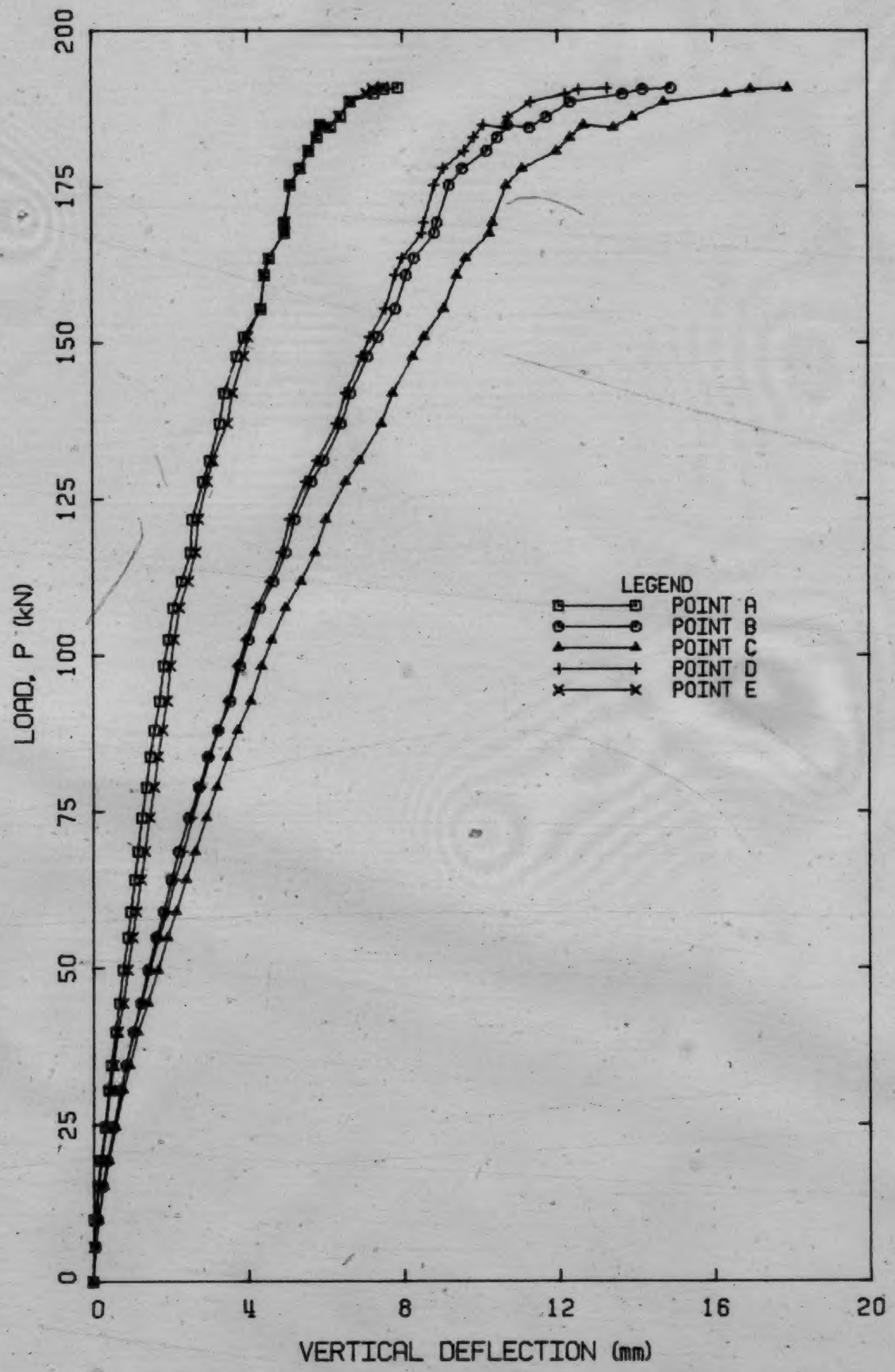

Figure 5.14 Load versus Vertical Deflection for Beam EB6

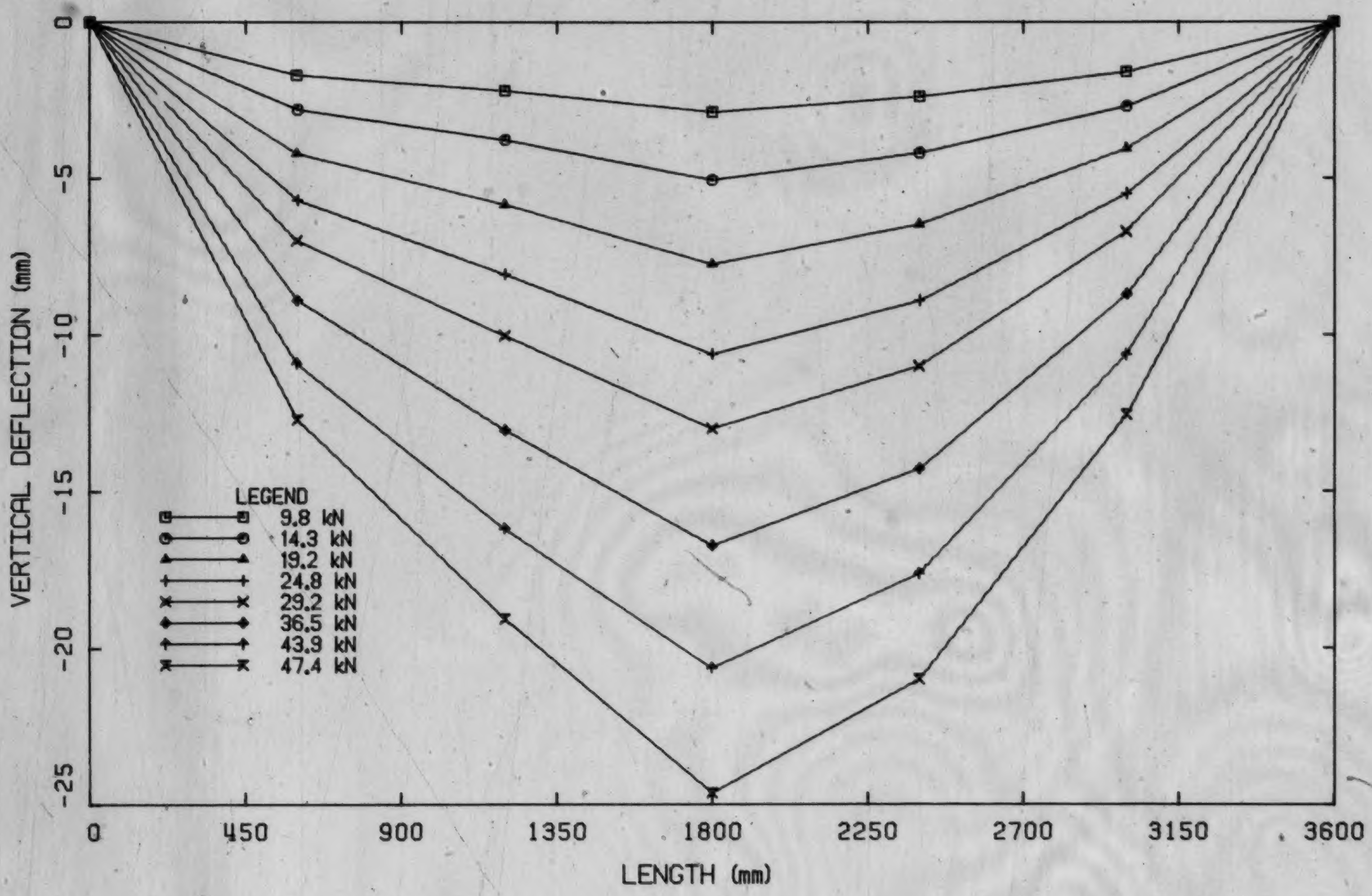

Figure 5.15 Deflected Shape of Beam SB1

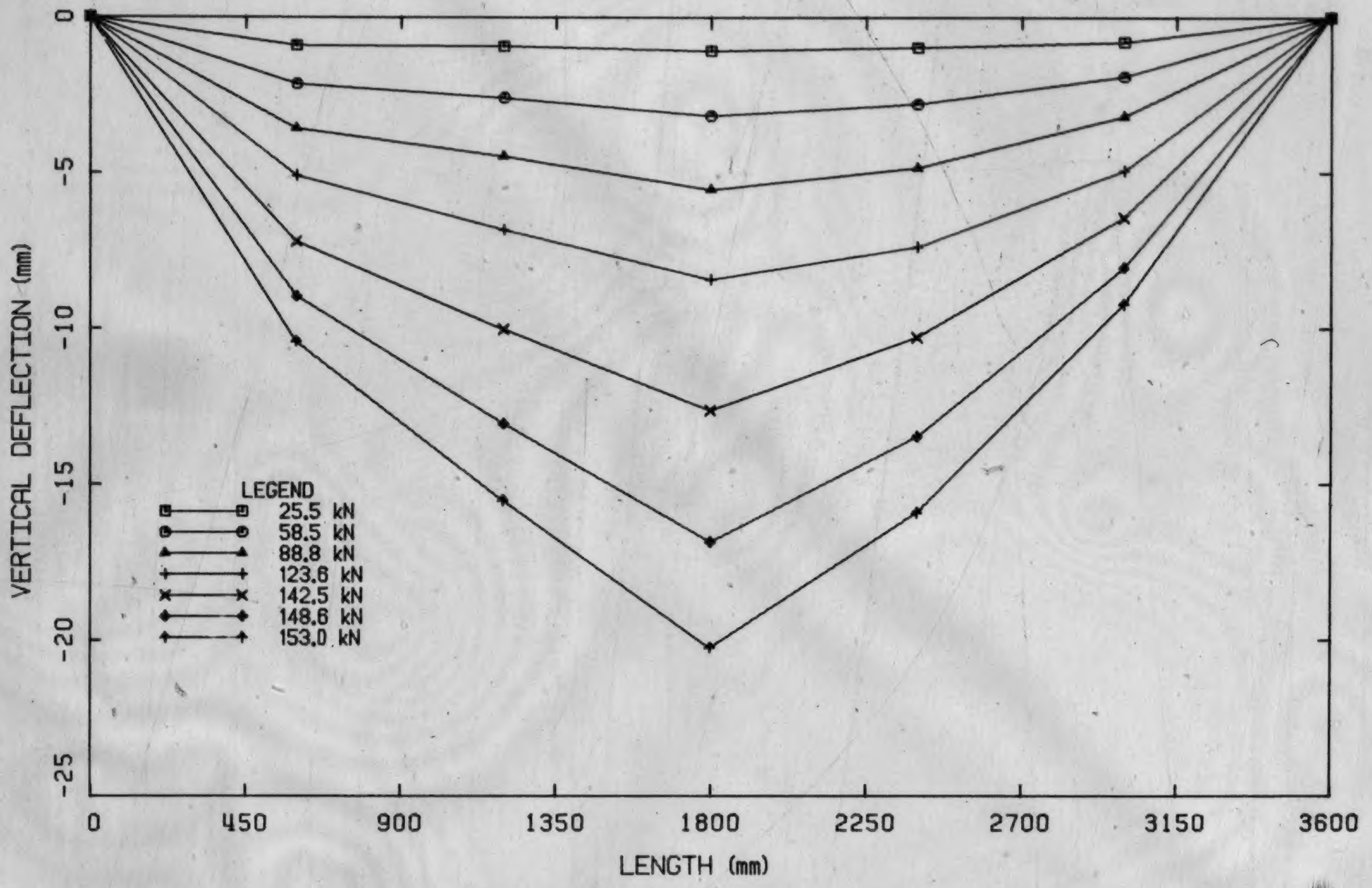

Figure 5.16 Deflected Shape of Beam SB2

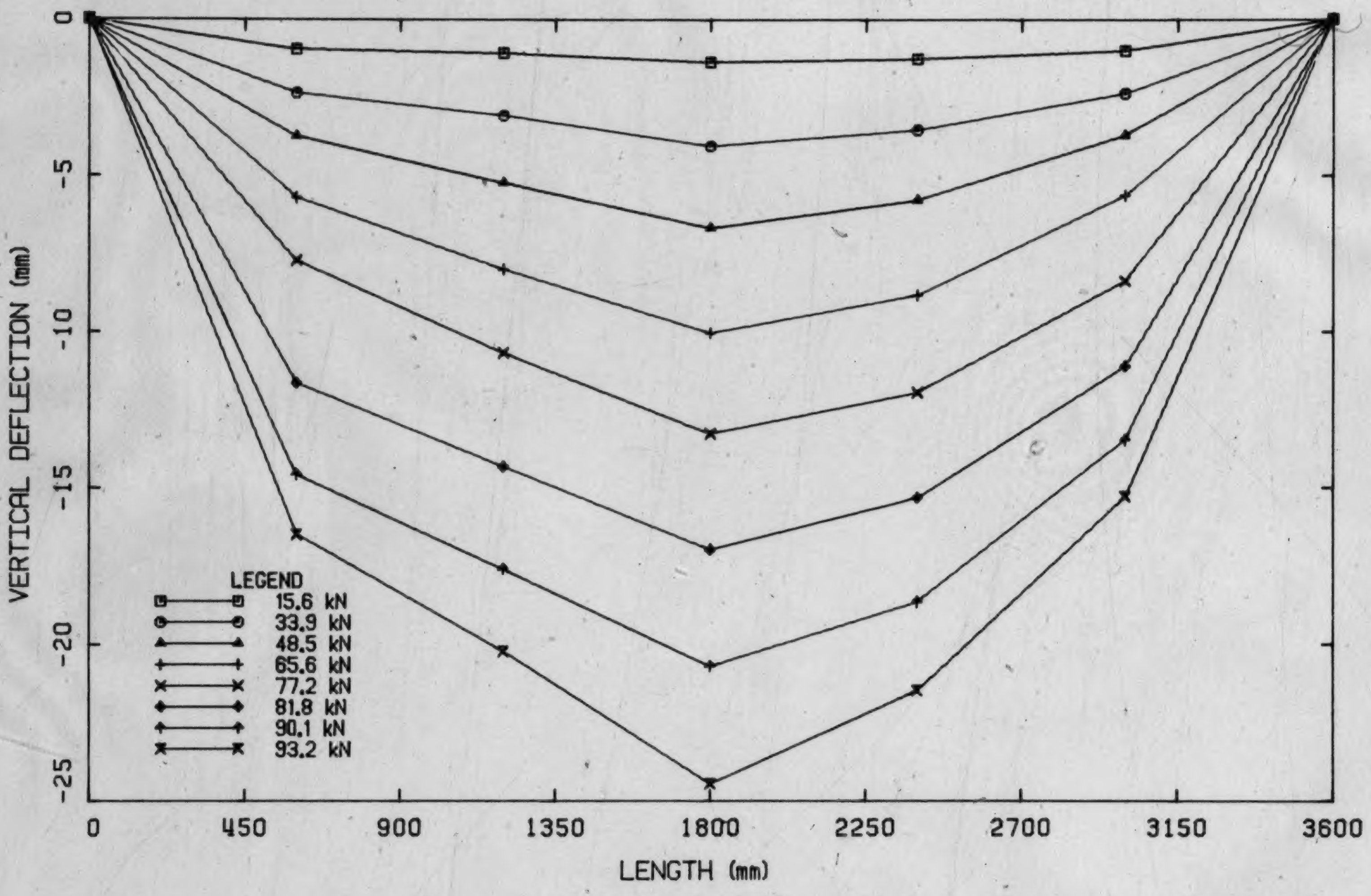

Figure 5.17 Deflected Shape of Beam SB3

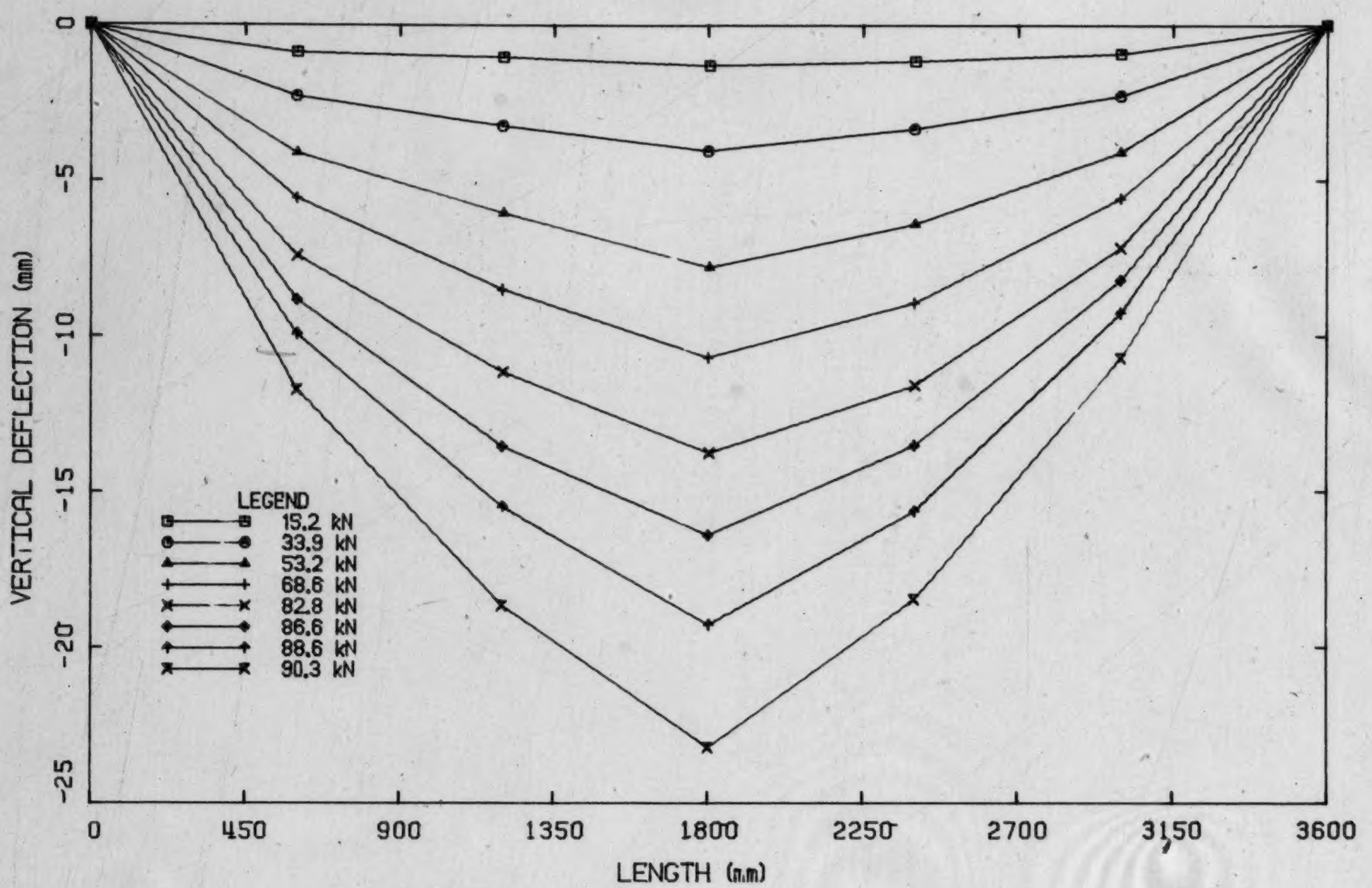

Figure 5.18 Deflected Shape of Beam SB4

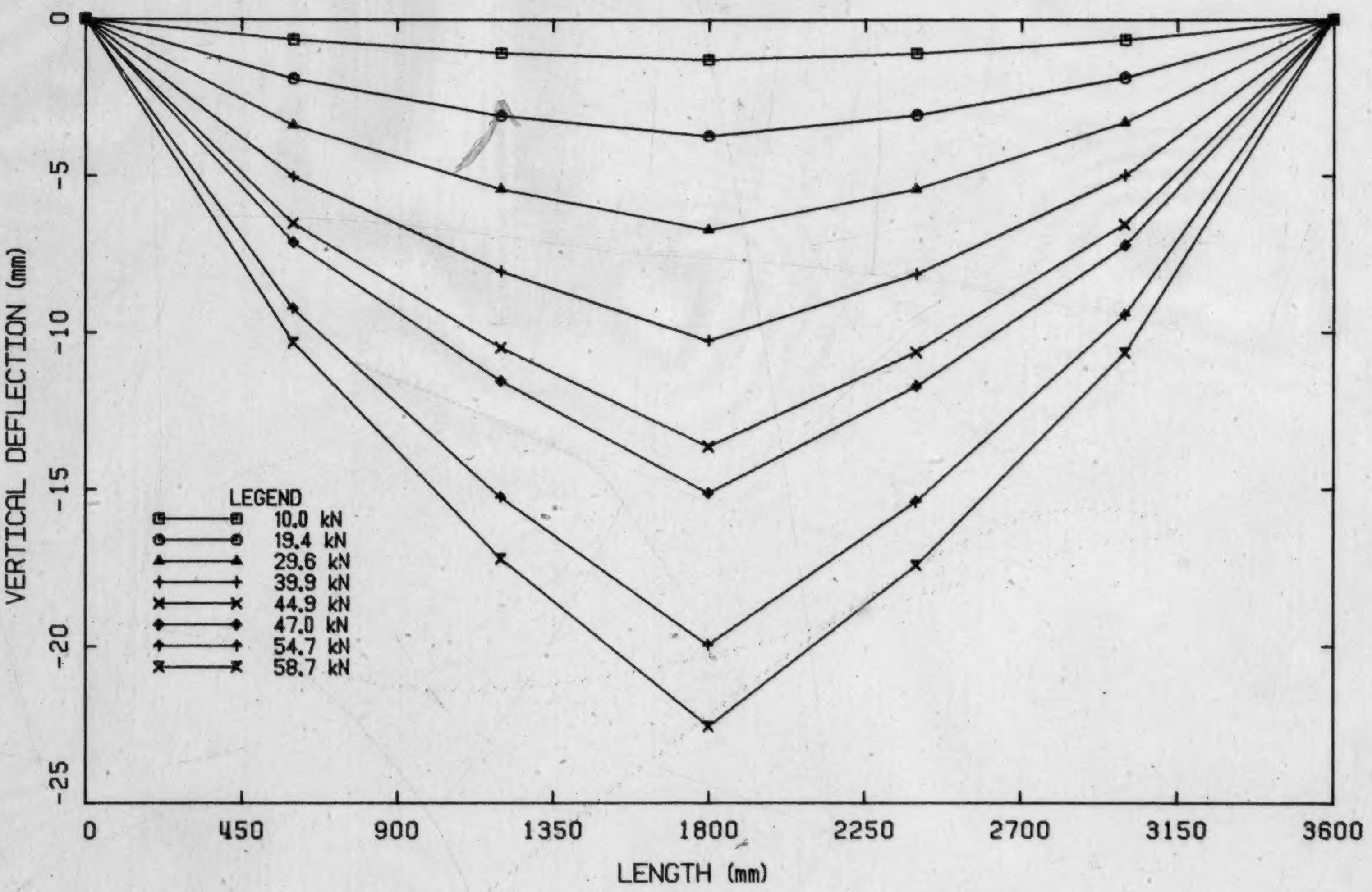

Figure 5.19 Deflected Shape of Beam RB1

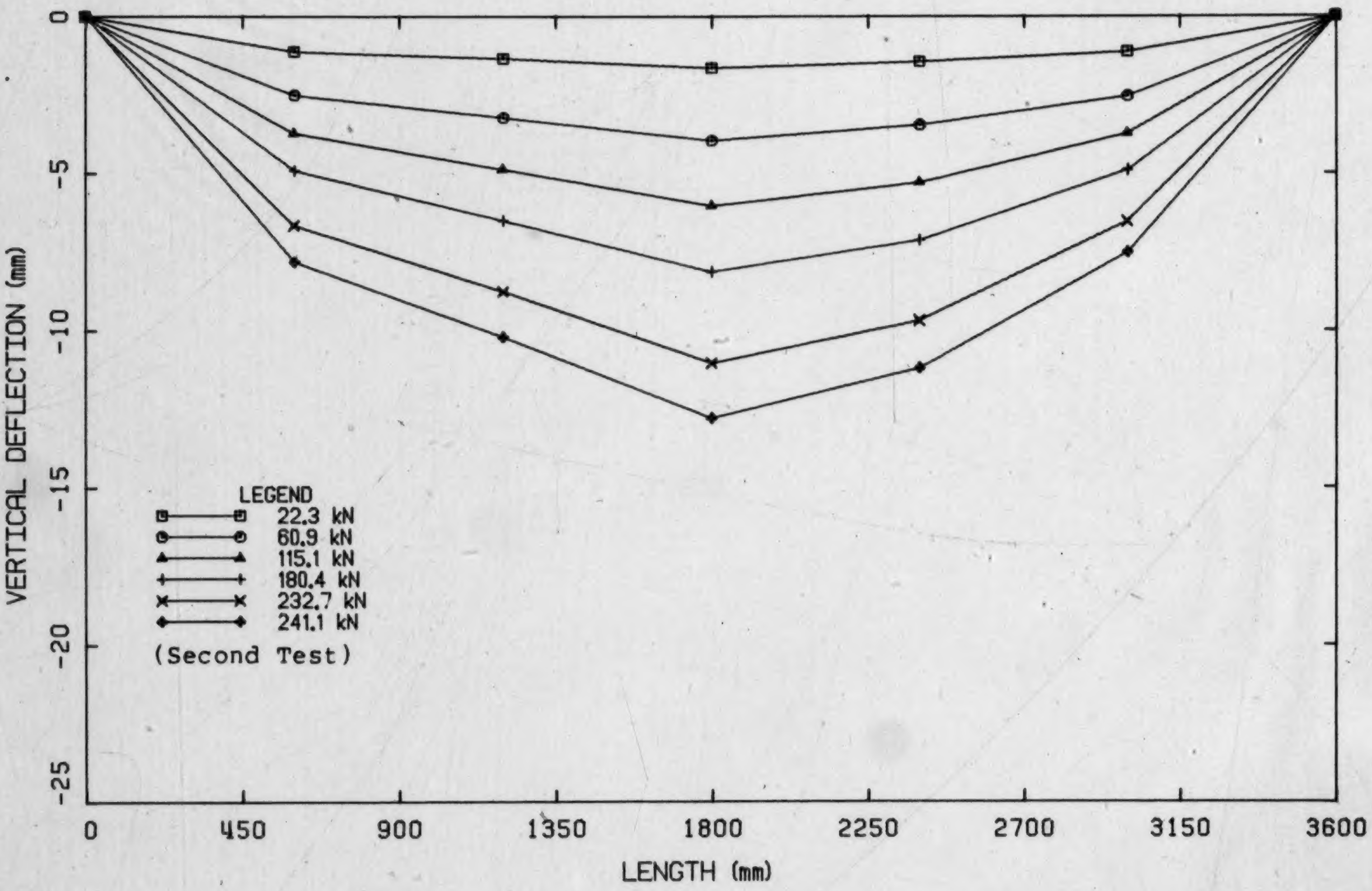

Figure 5.20 Deflected Shape of Beam RB2

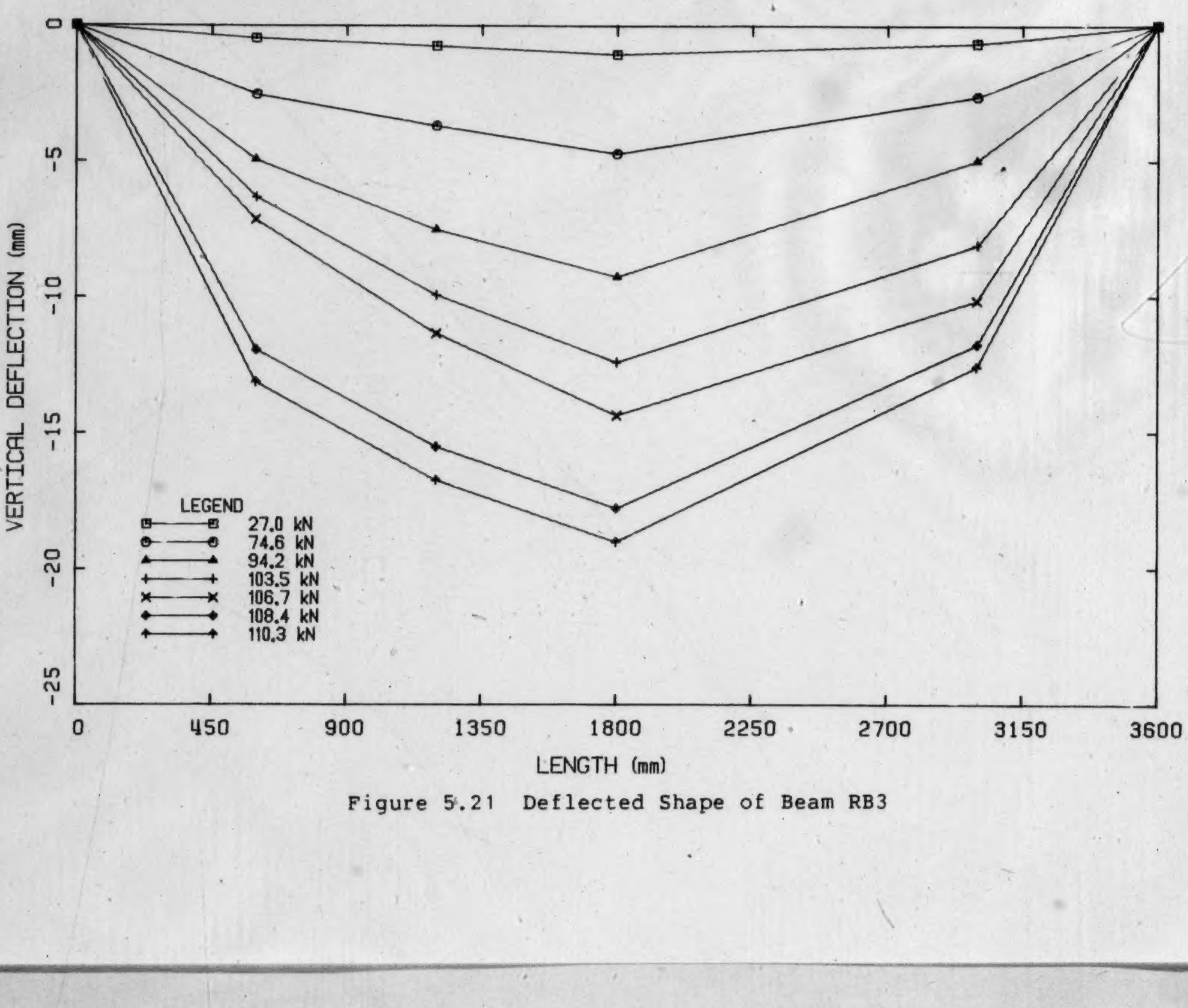

Figure 5.21 Deflected Shape of Beam RB3

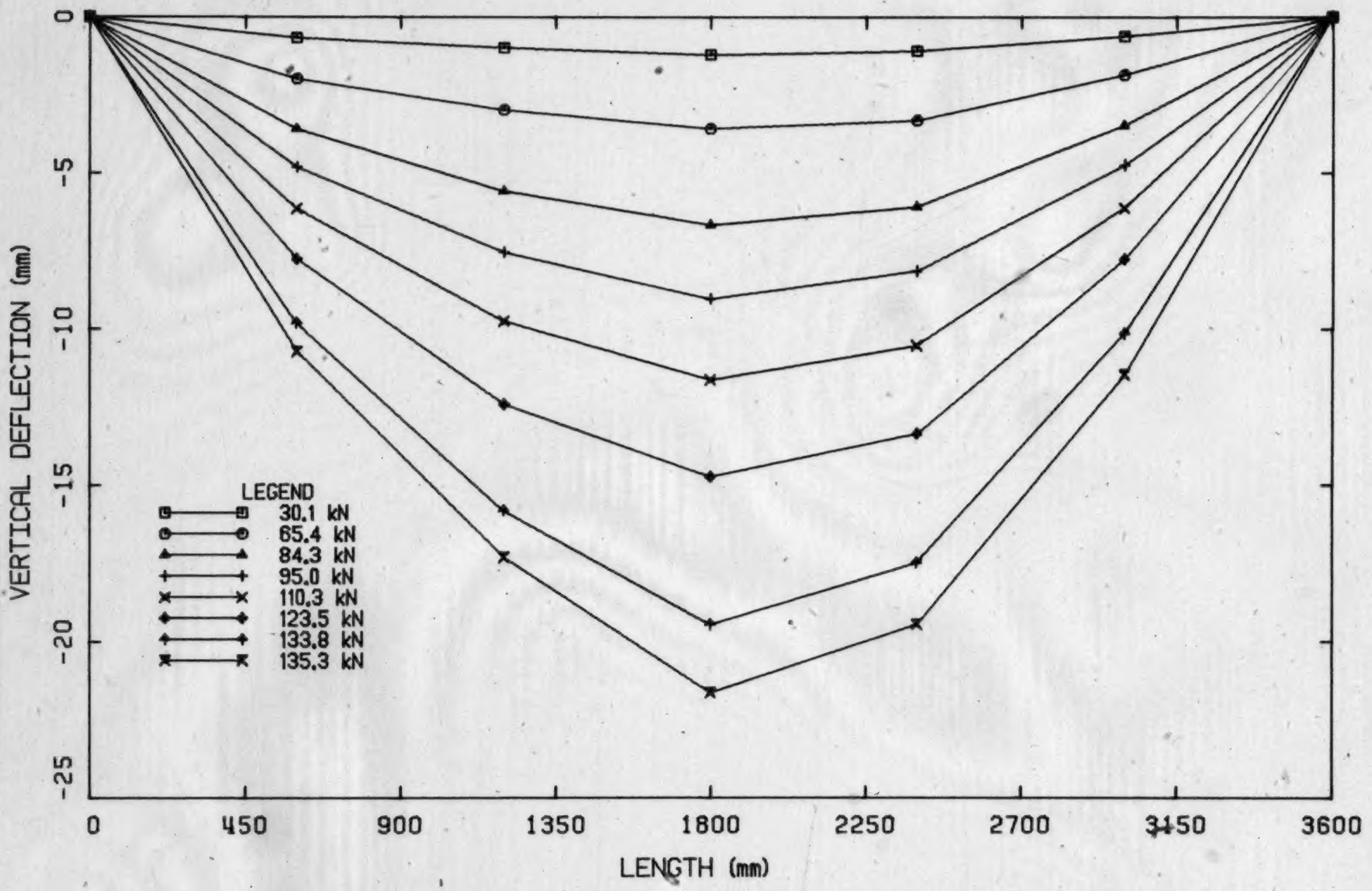

Figure 5.22 Deflected Shape of Beam RB4

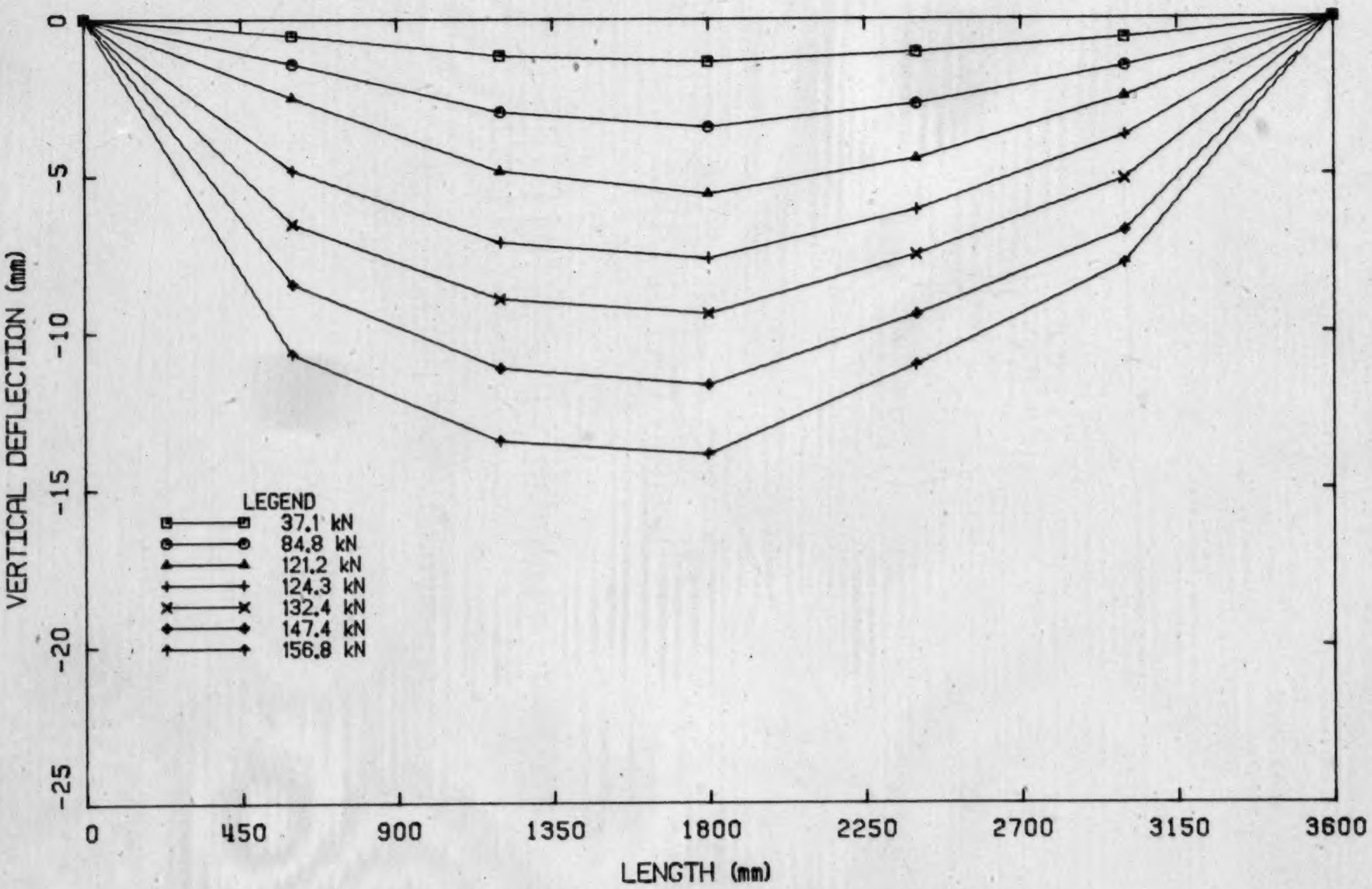

Figure 5.23 Deflected Shape of Beam EB1

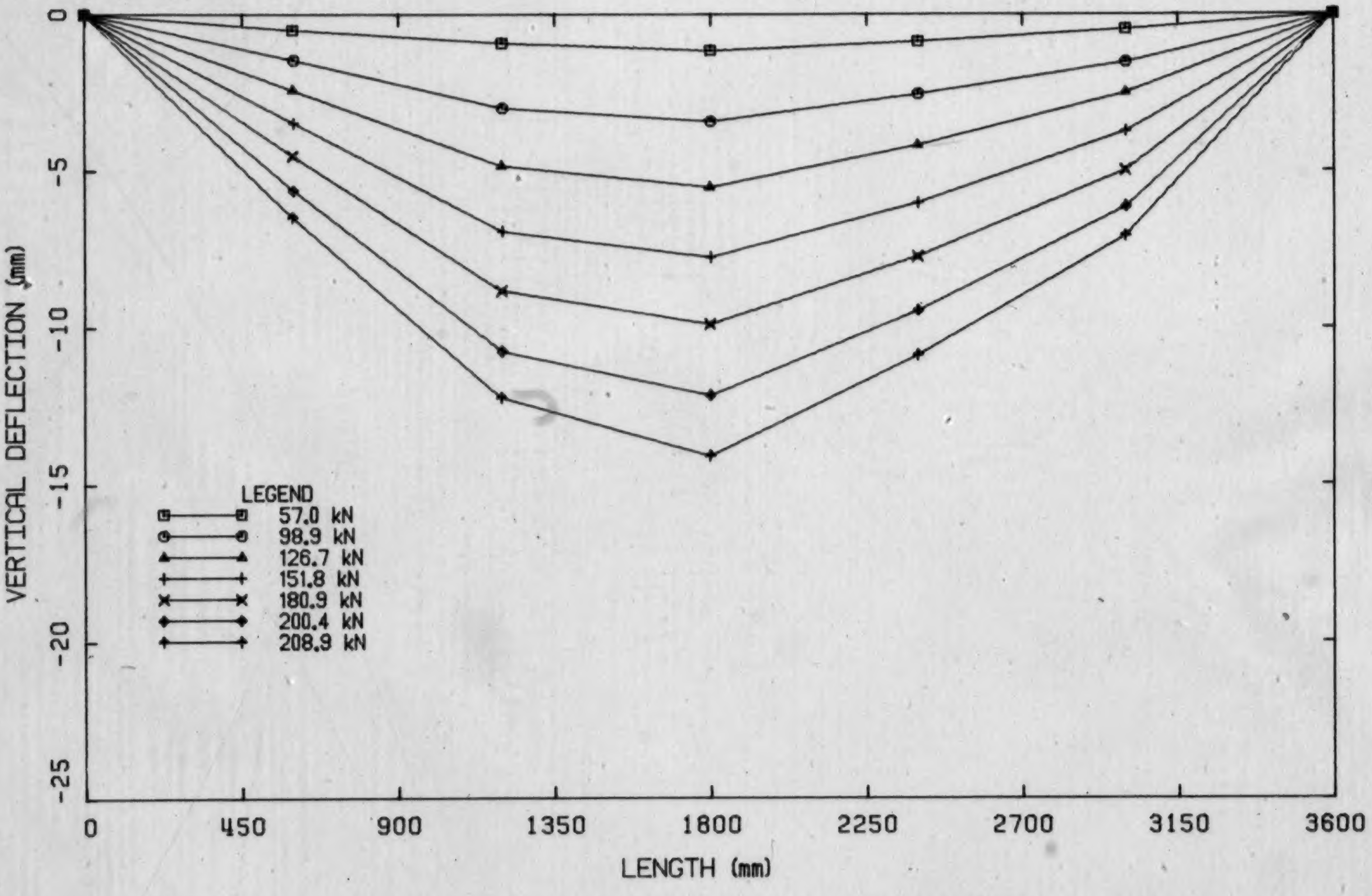

Figure 5.24 Deflected Shape of Beam EB2

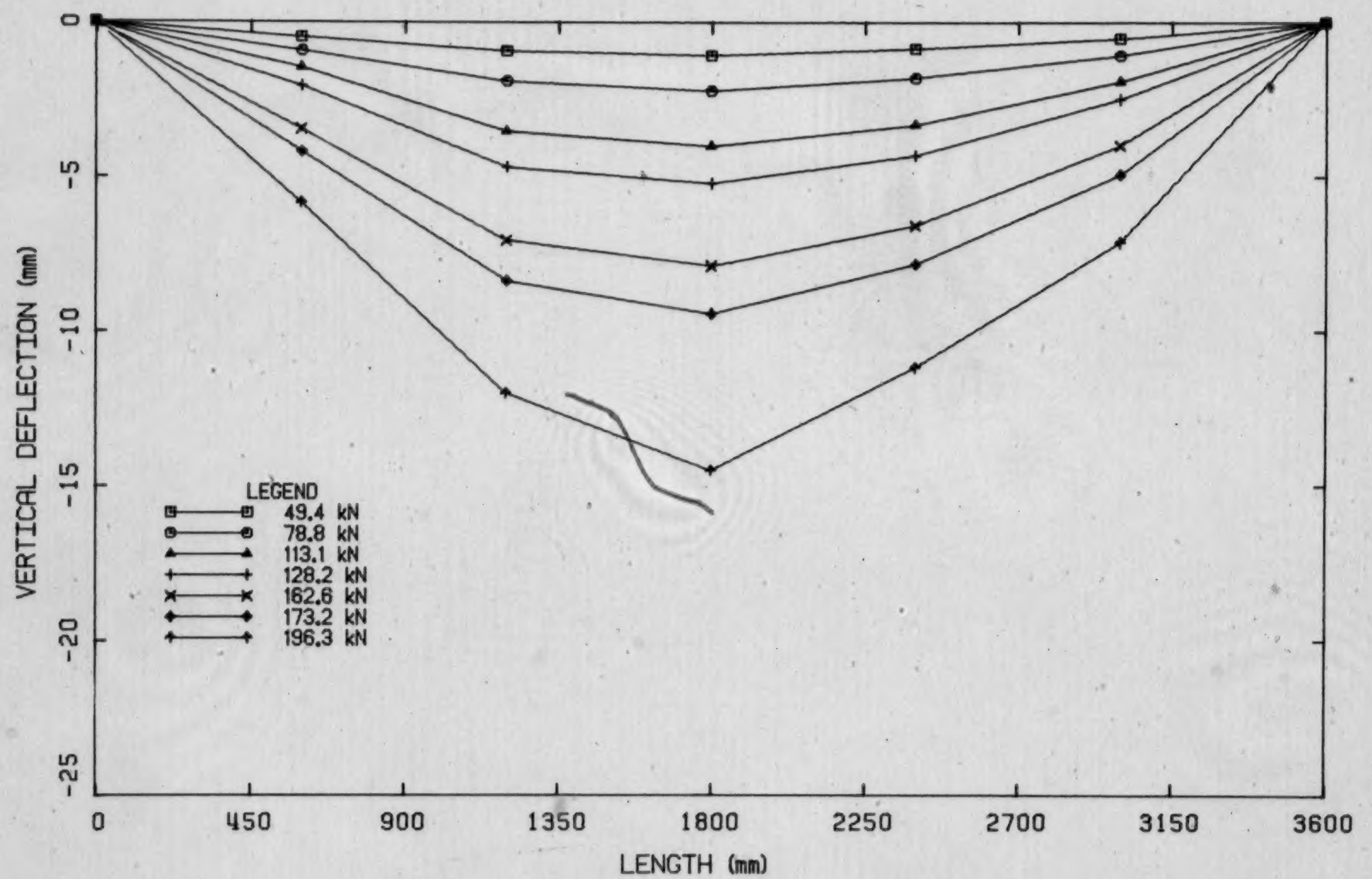

Figure 5.25 Deflected Shape of Beam EB3

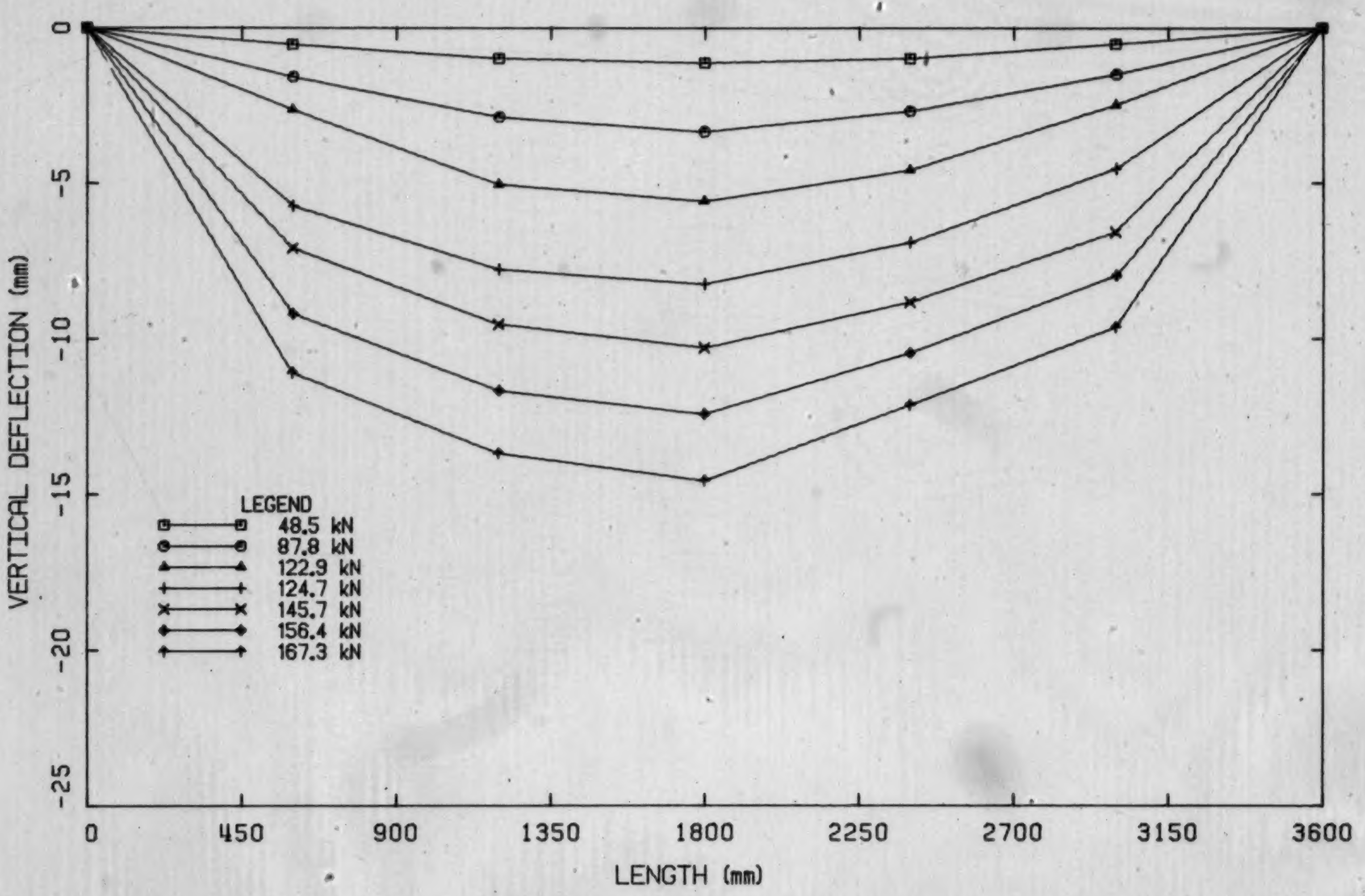

Figure 5.26 Deflected Shape of Beam EB4

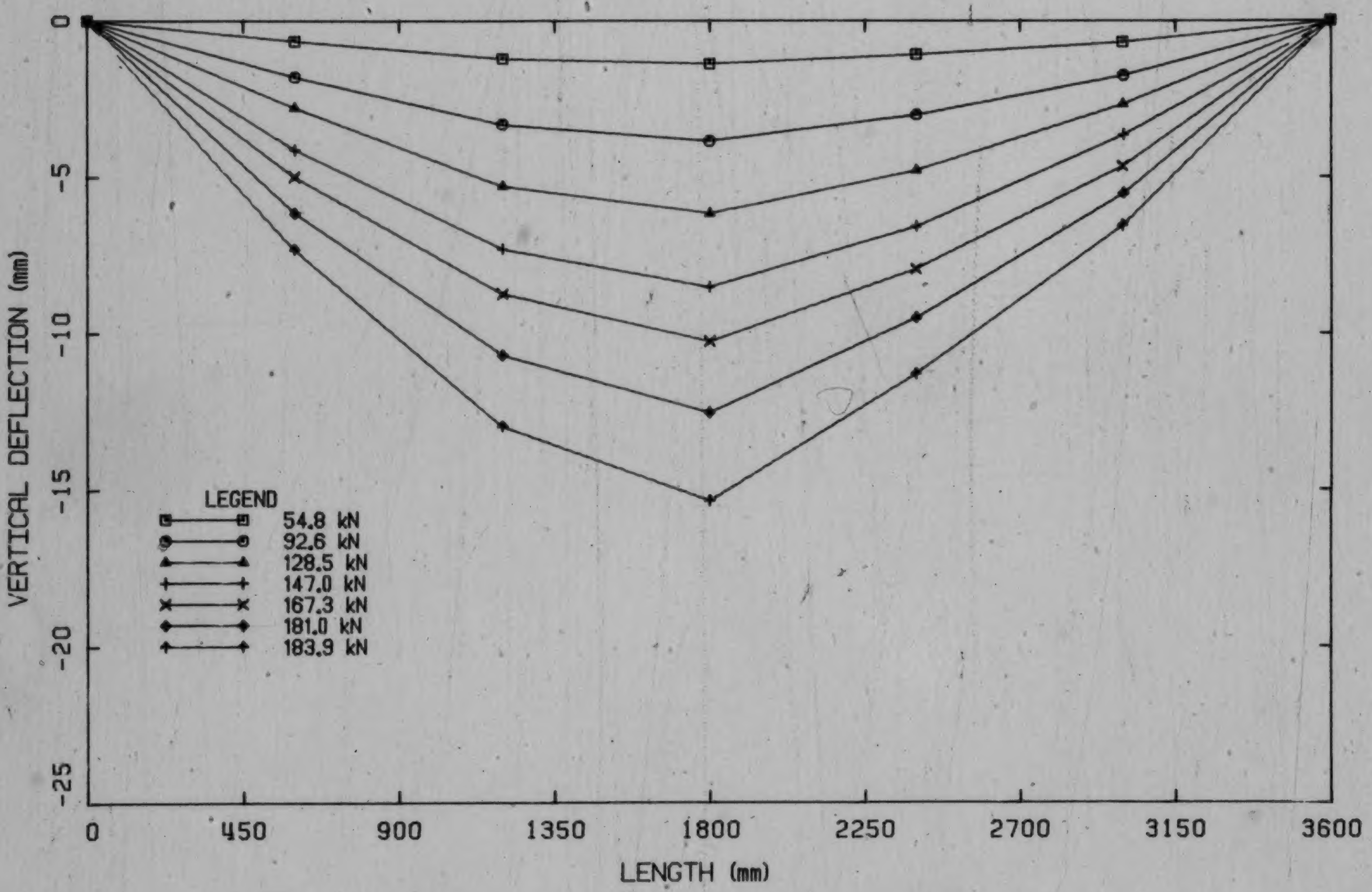

Figure 5.27 Deflected Shape of Beam EB5

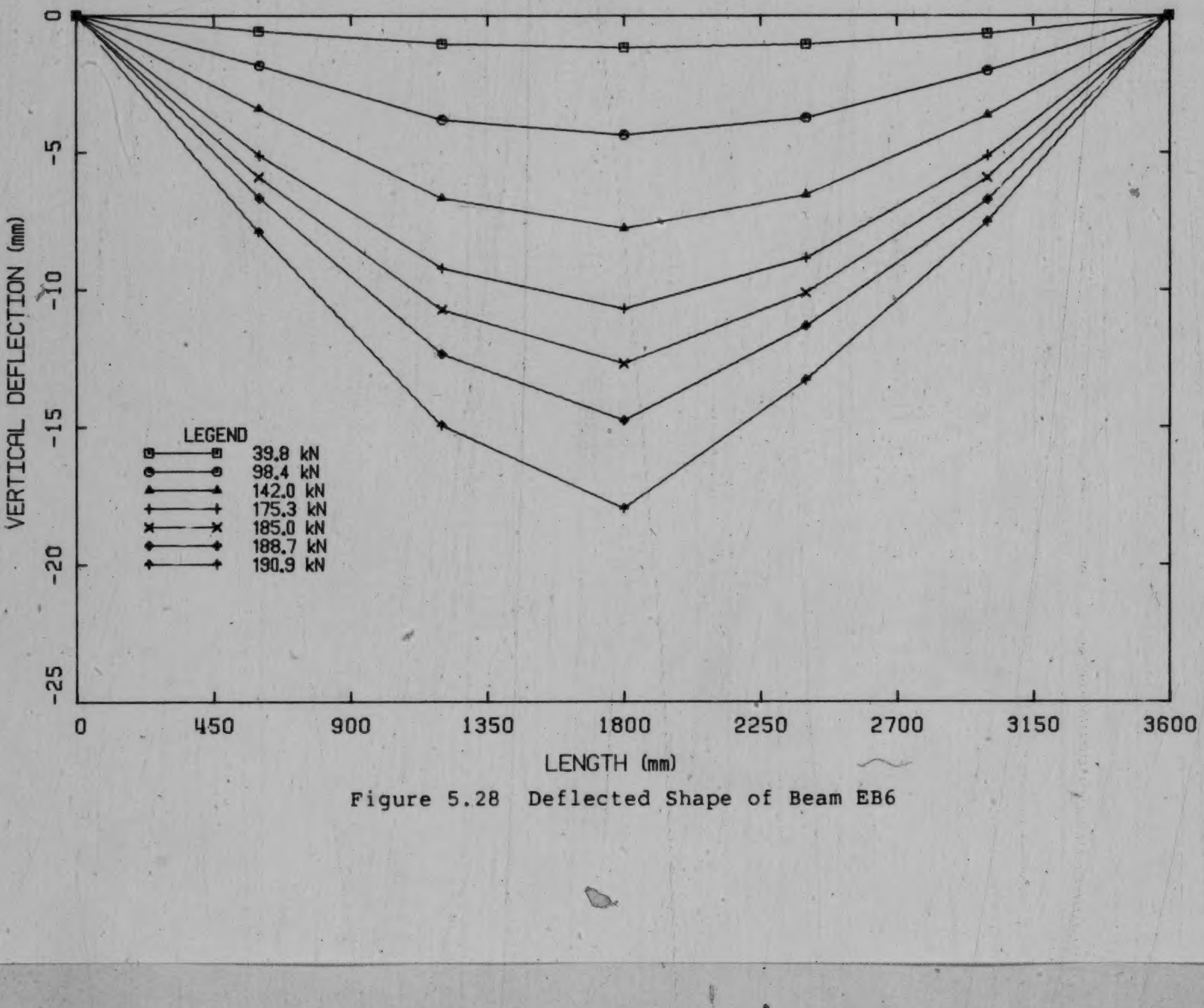

Figure 5.28 Deflected Shape of Beam EB6

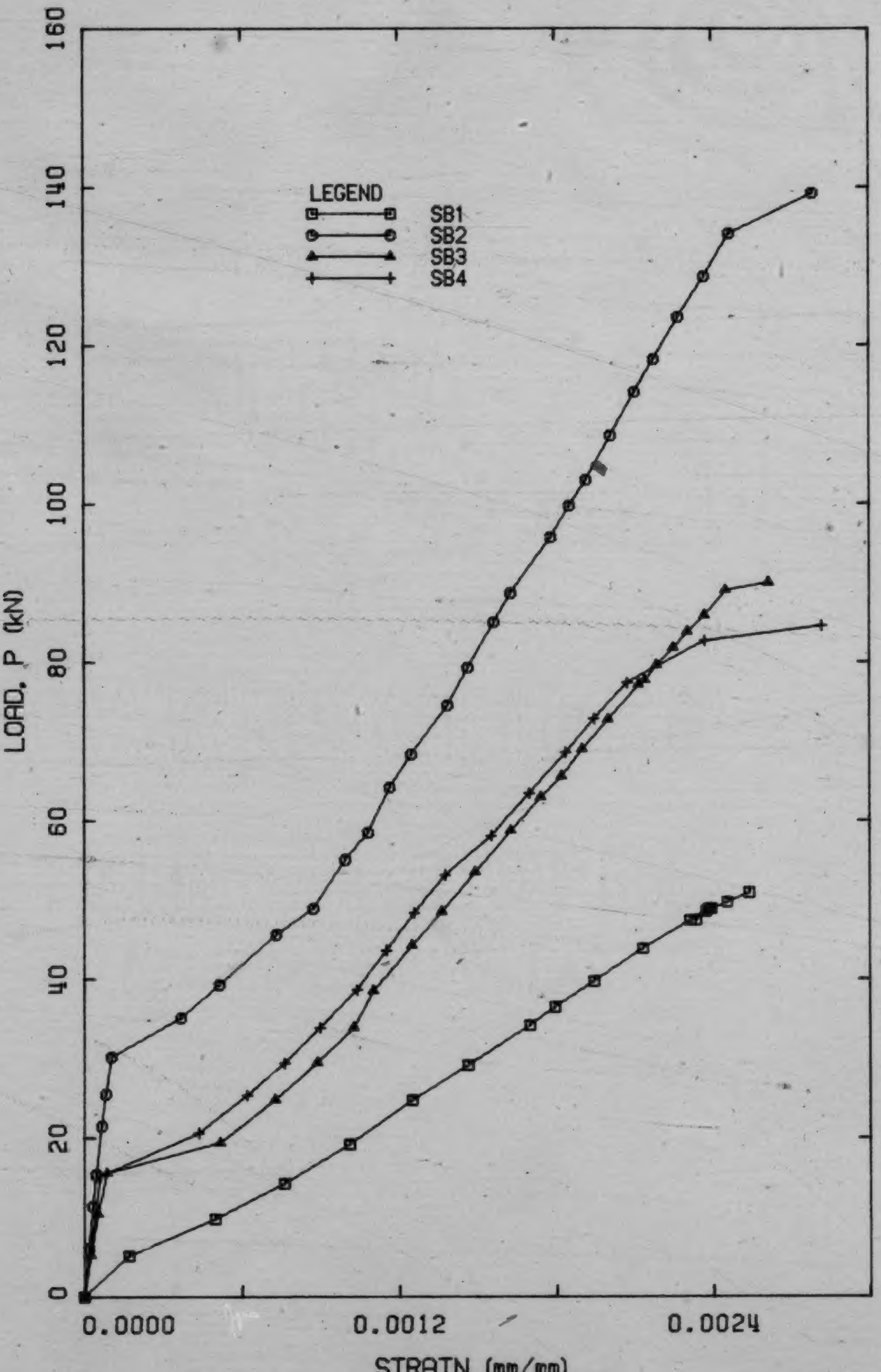

Figure 5.29 Load versus Tension Reinforcement Strain at Midspan for Type SB Beams

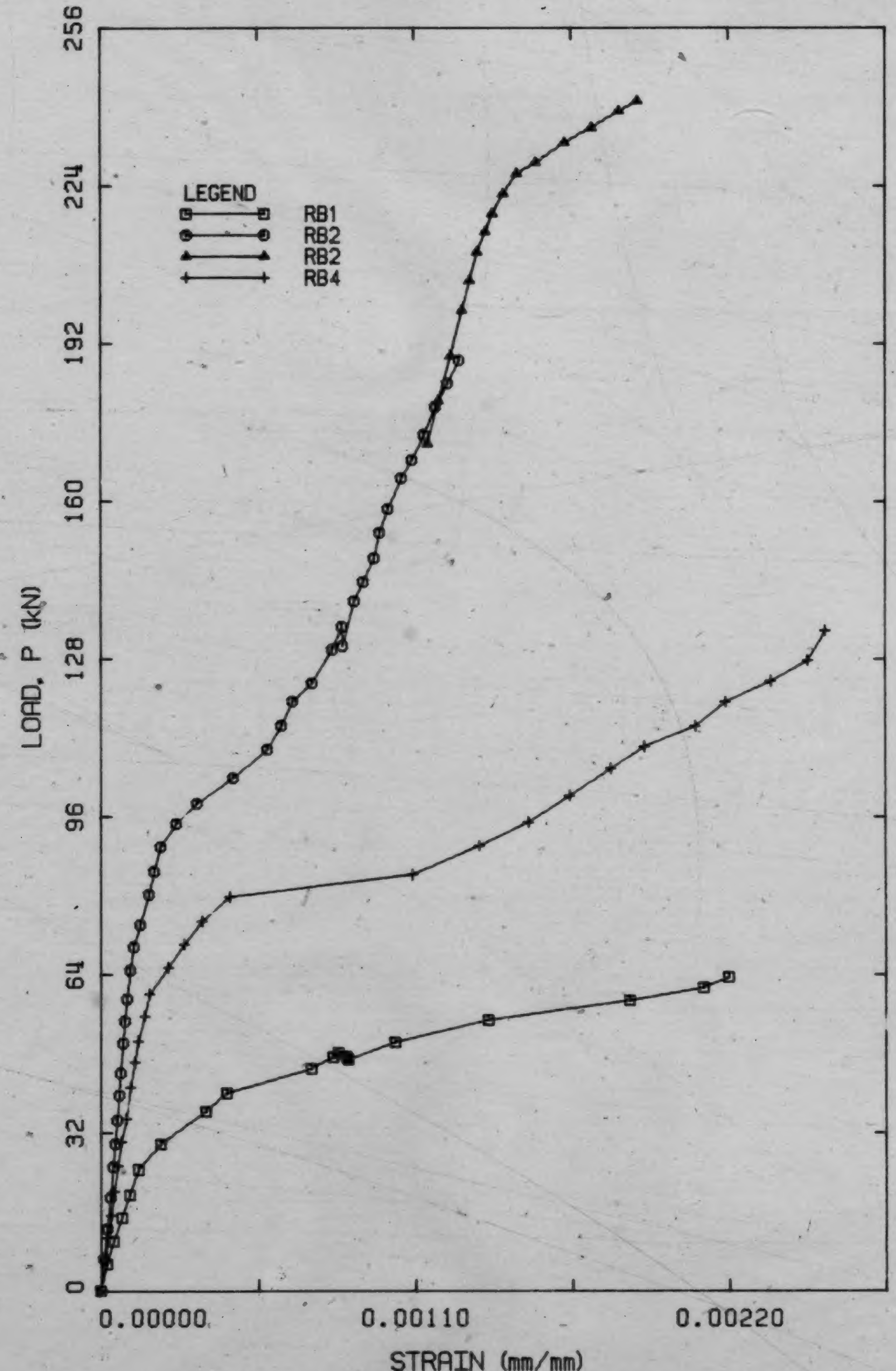

Figure 5.30 Load versus Tension Reinforcement Strain at Midspan for Type RB Beams

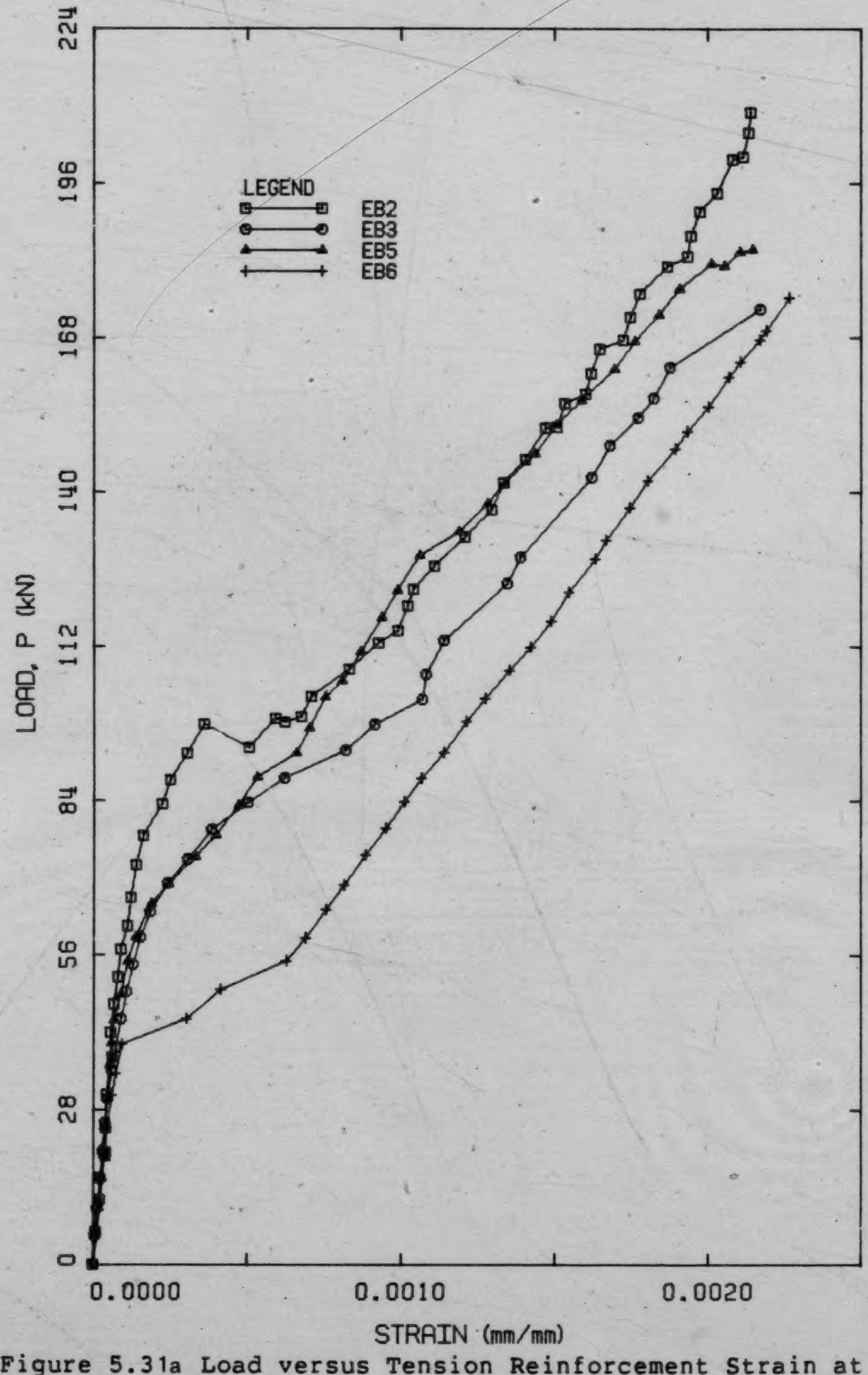

Figure 5.31a Load versus Tension Reinforcement Strain at Midspan for Type EB Beams

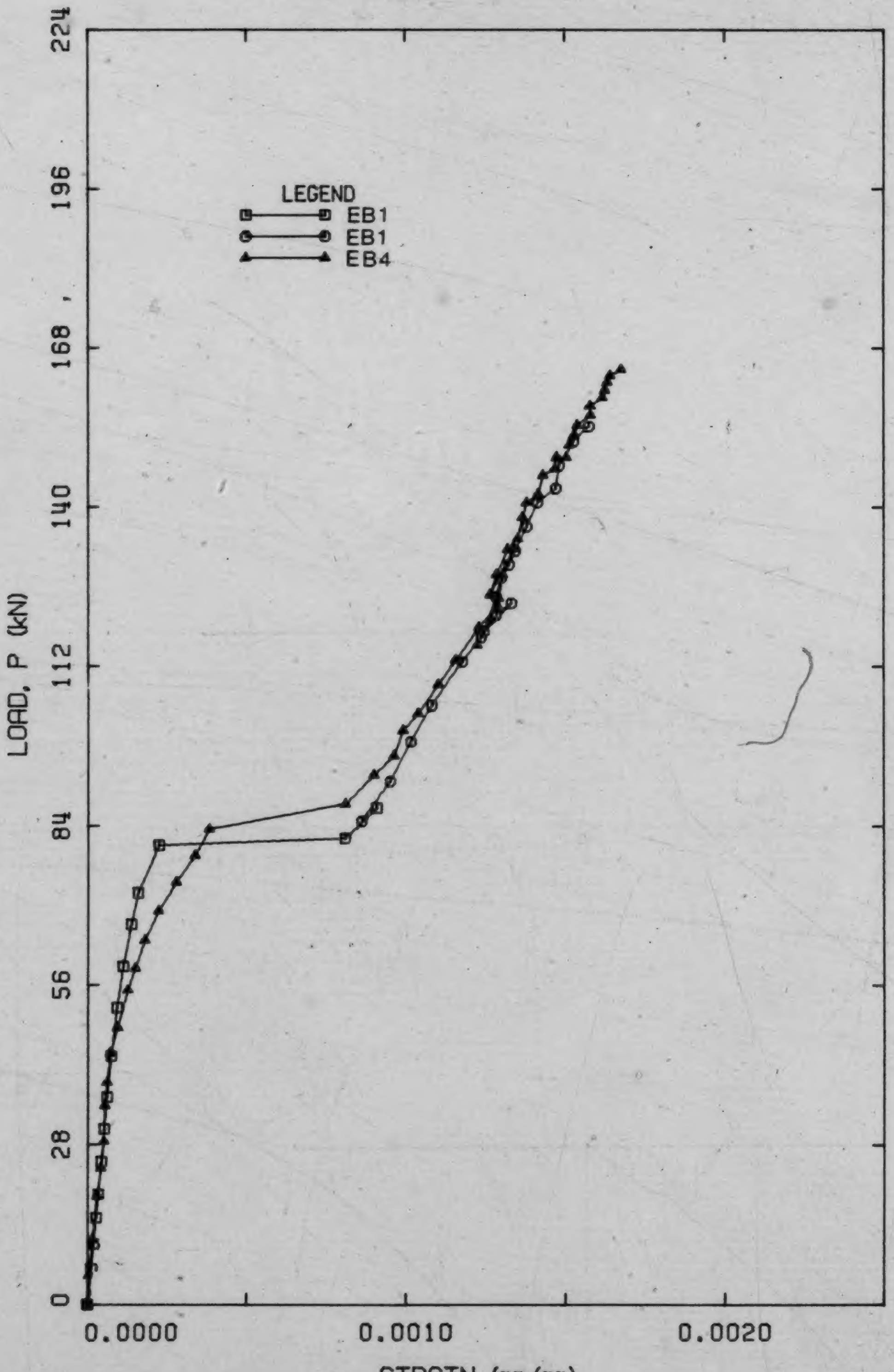

Figure 5.31b Load versus Tension Reinforcement Strain at Midspan for Type EB Beams

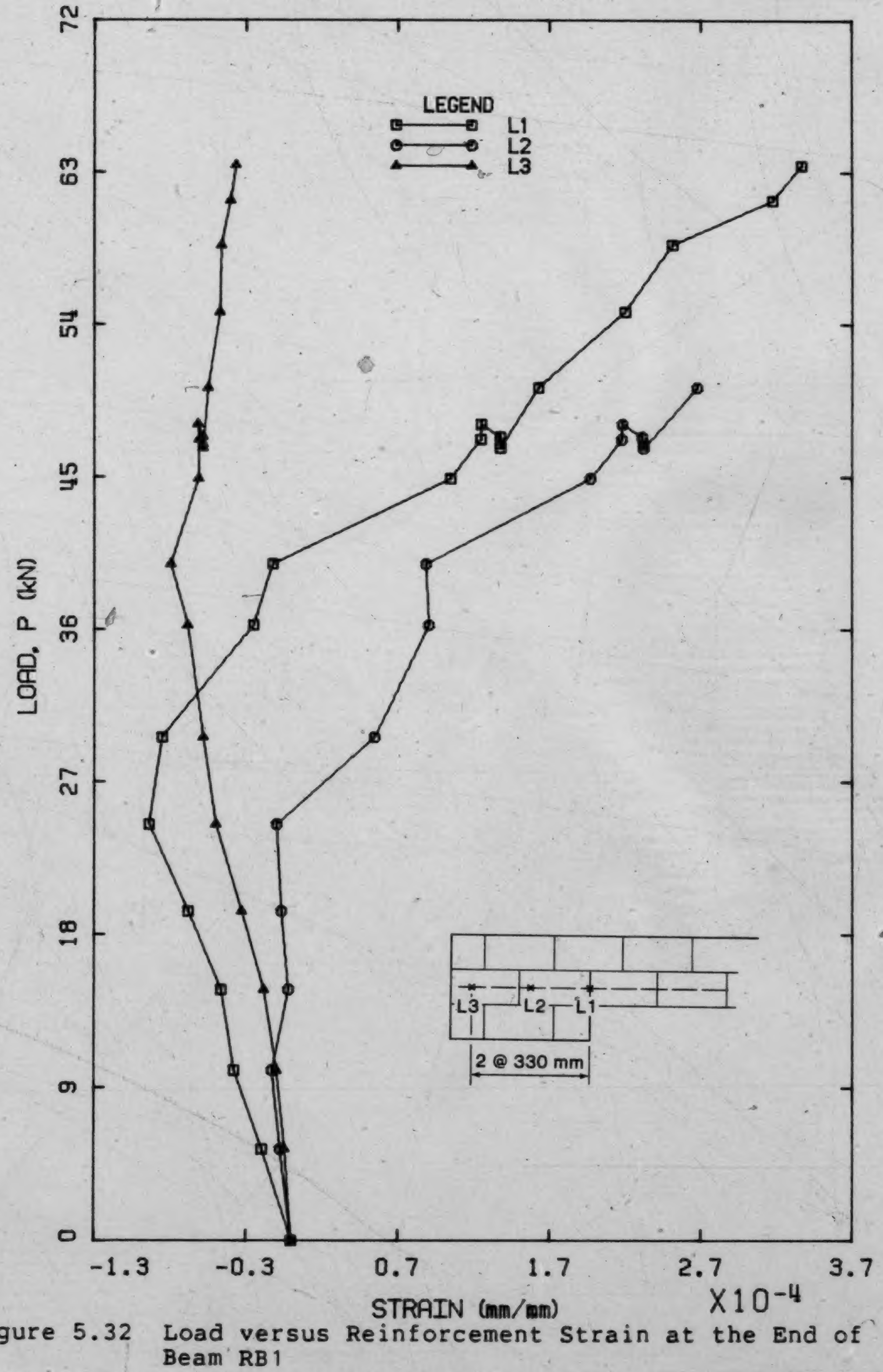

Figure 5.32 Load versus Reinforcement Strain at the End of Beam RB1

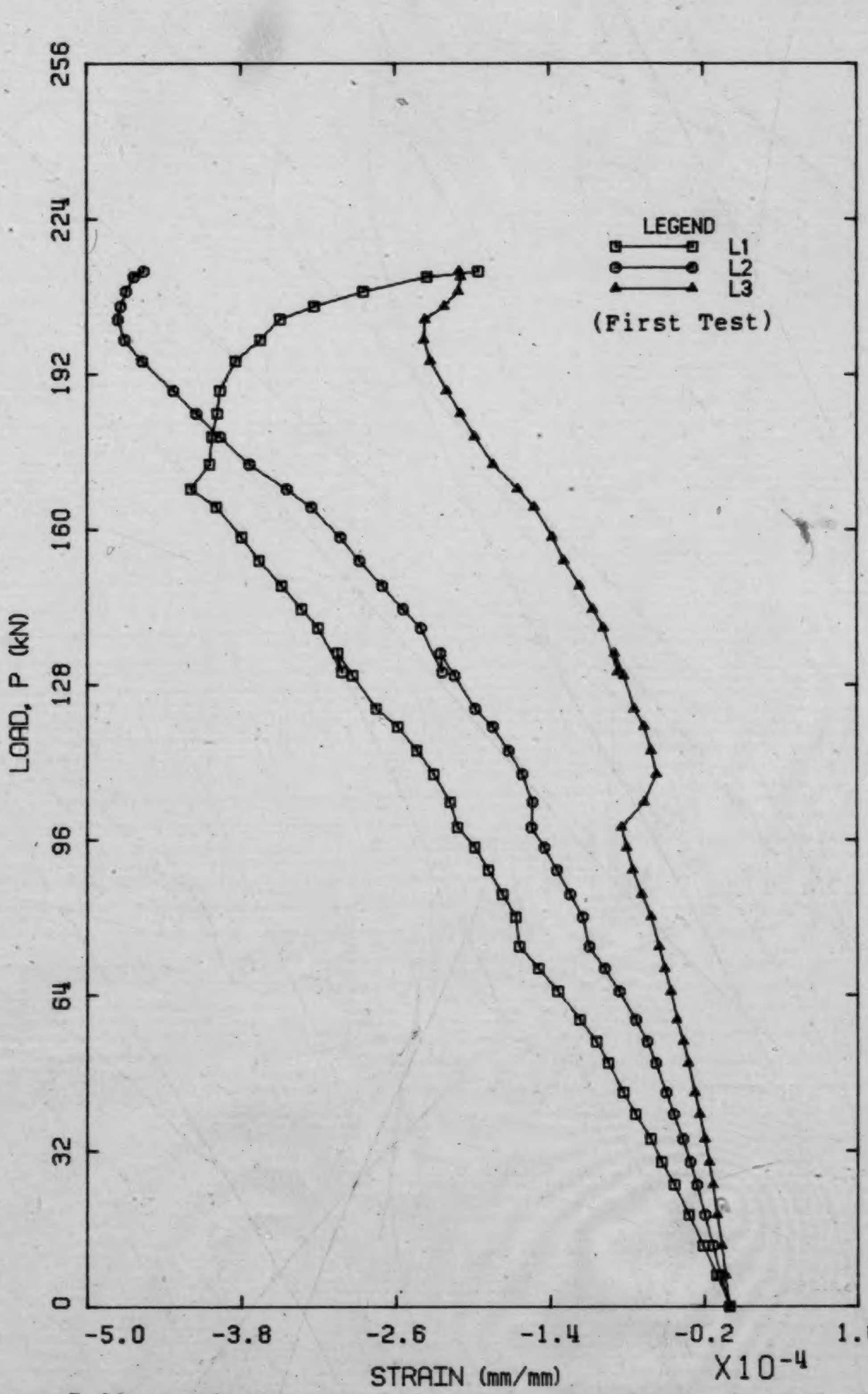

Figure 5.33a Load versus Reinforcement Strain at the End of Beam RB2

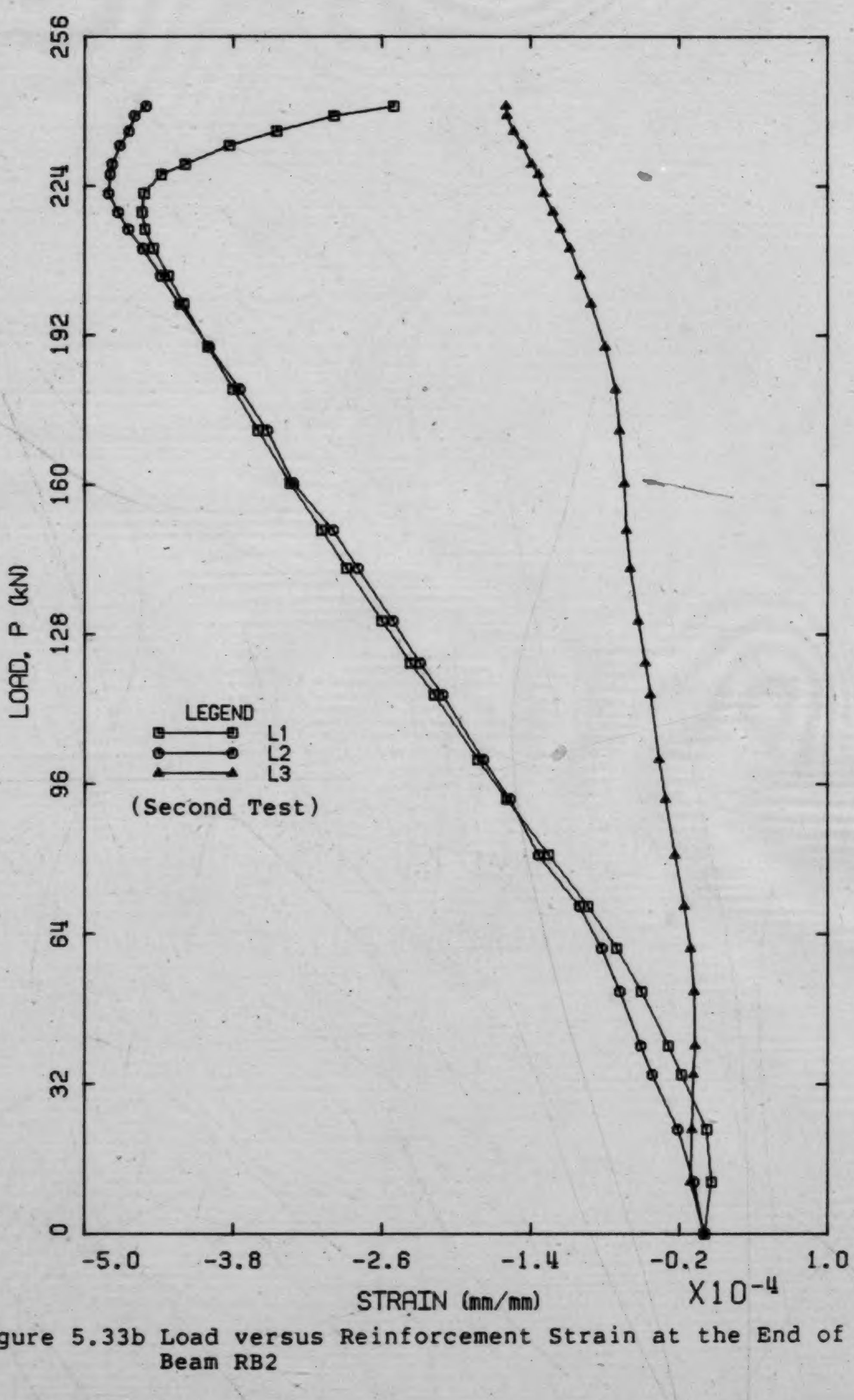

Figure 5.33b Load versus Reinforcement Strain at the End of Beam RB2

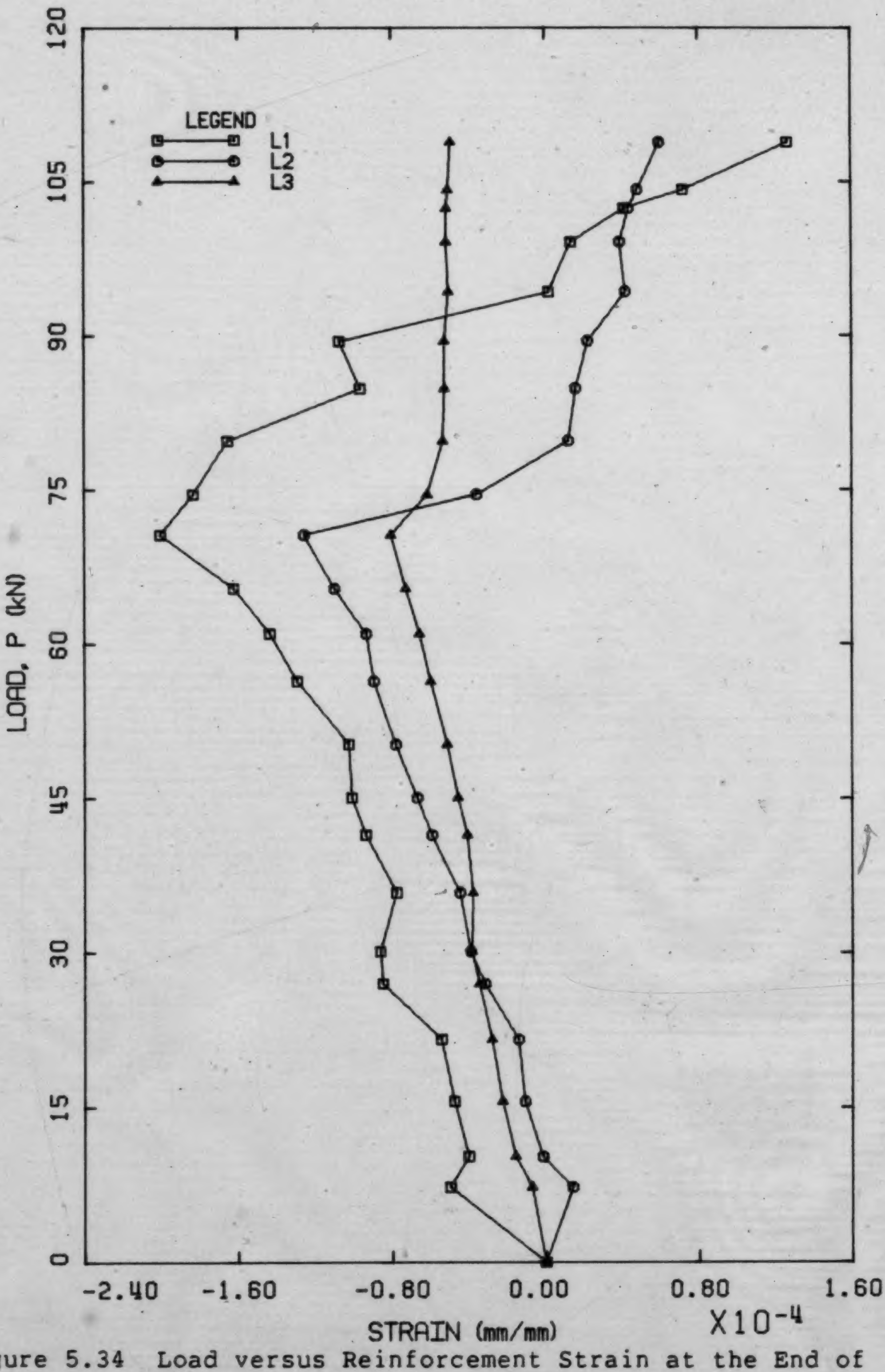

Figure 5.34 Load versus Reinforcement Strain at the End of Beam RB3

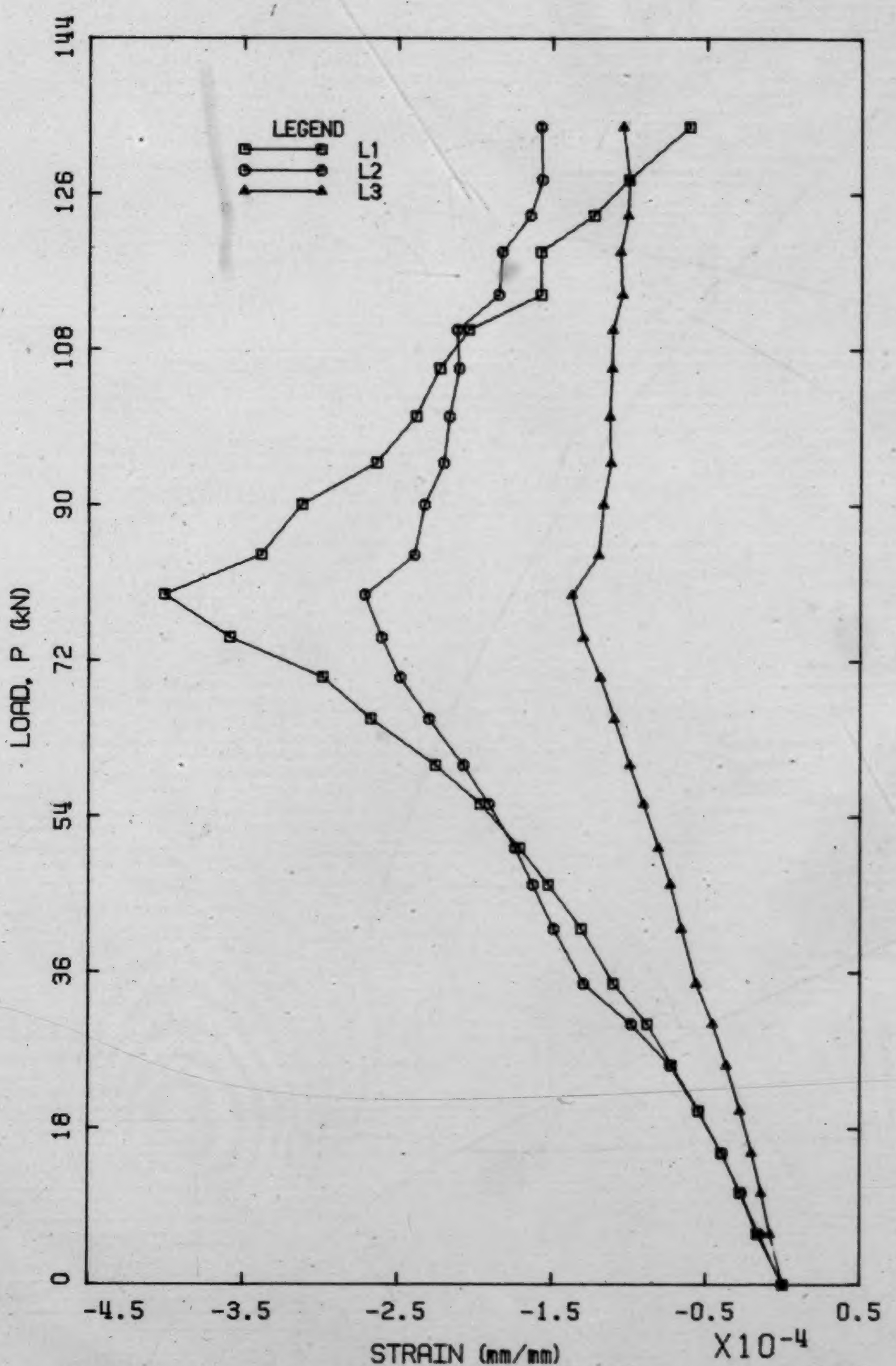

Figure 5.35 Load versus Reinforcement Strain at the End of Beam RB4

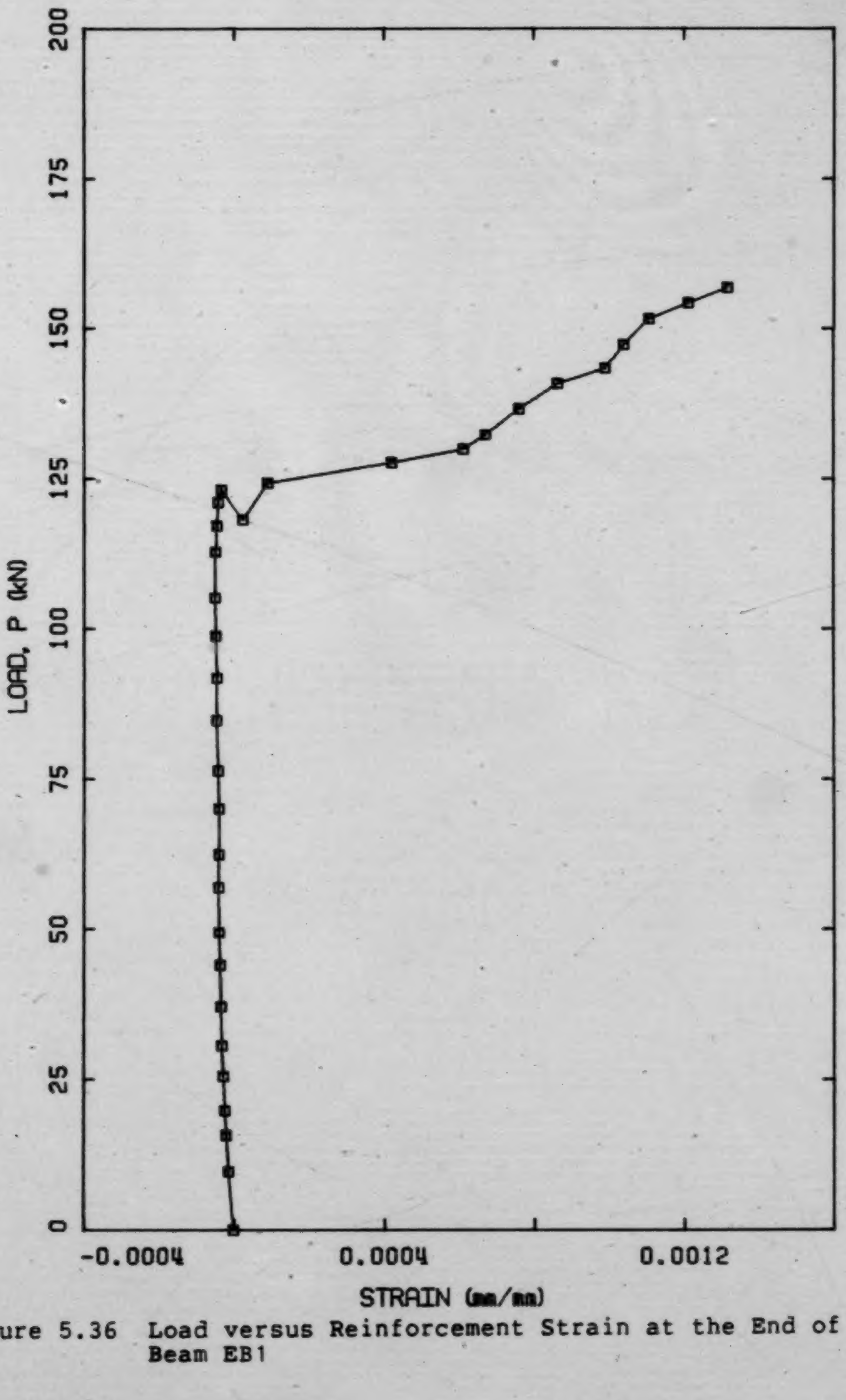

Figure 5.36 Load versus Reinforcement Strain at the End of Beam EB1

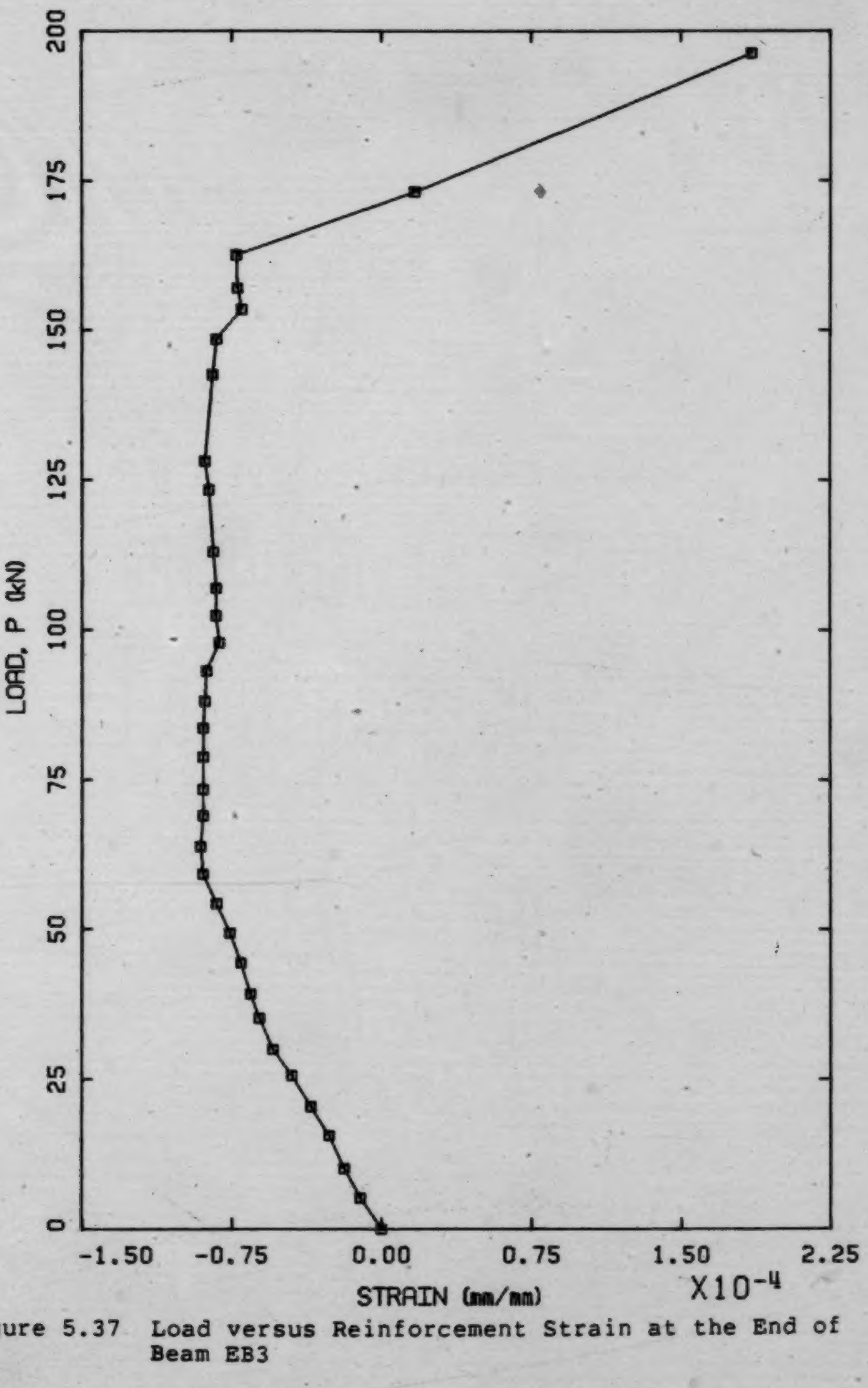

Figure 5.37 Load versus Reinforcement Strain at the End of Beam EB3

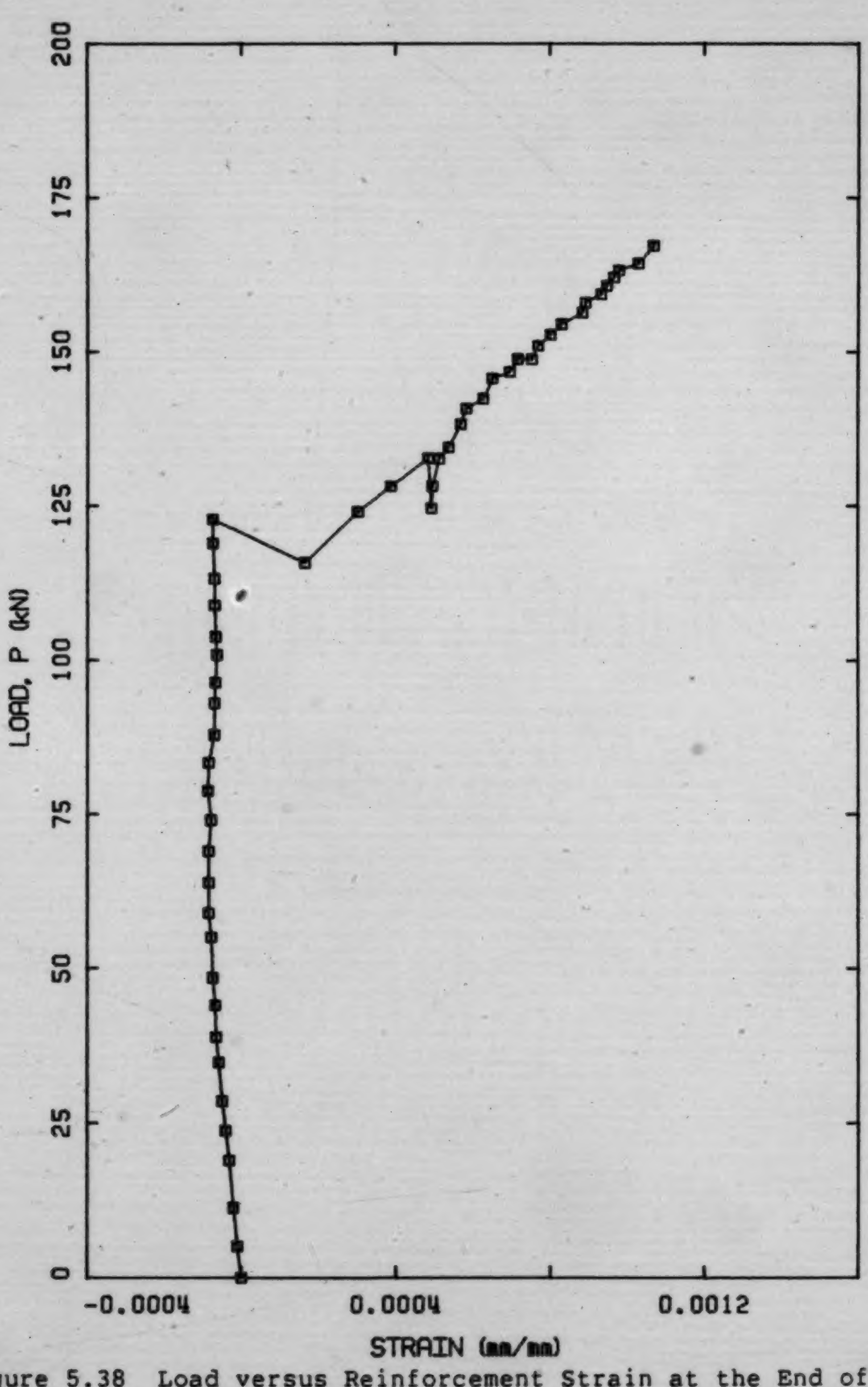

Figure 5.38 Load versus Reinforcement Strain at the End of Beam EB4

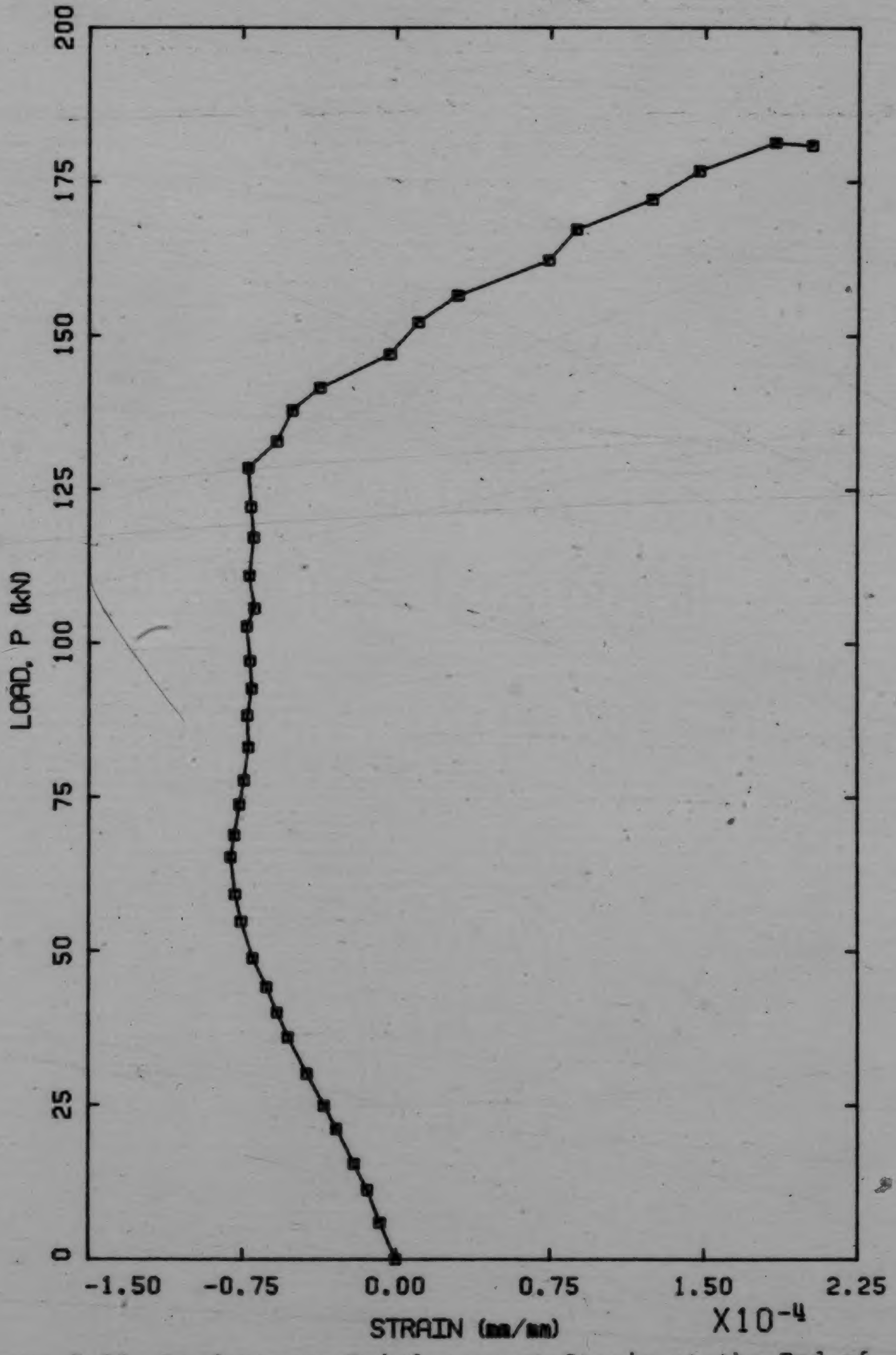

Figure 5.39 Load versus Reinforcement Strain at the End of Beam EB5

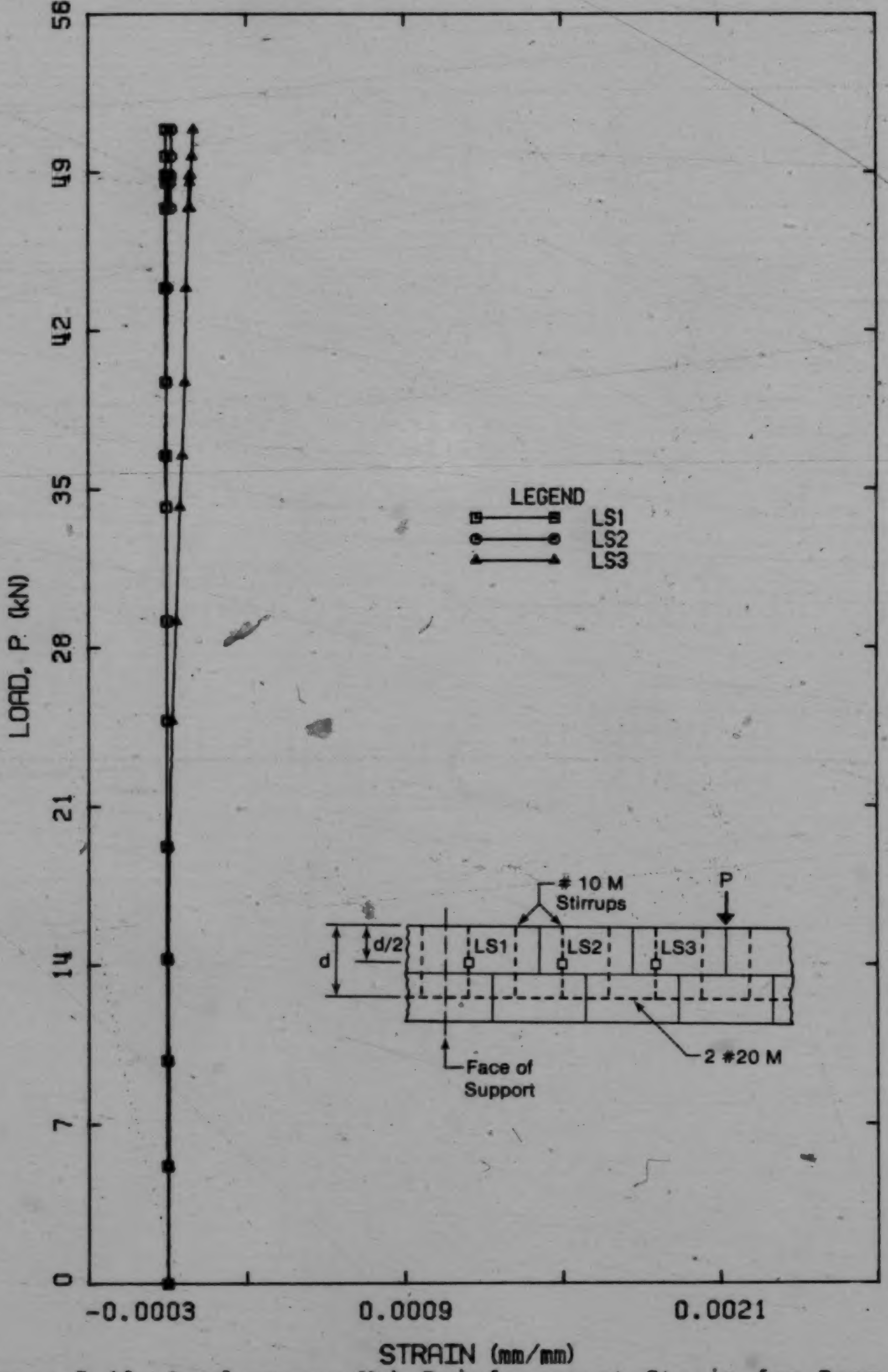

Figure 5.40 Load versus Web Reinforcement Strain for Beam SB1

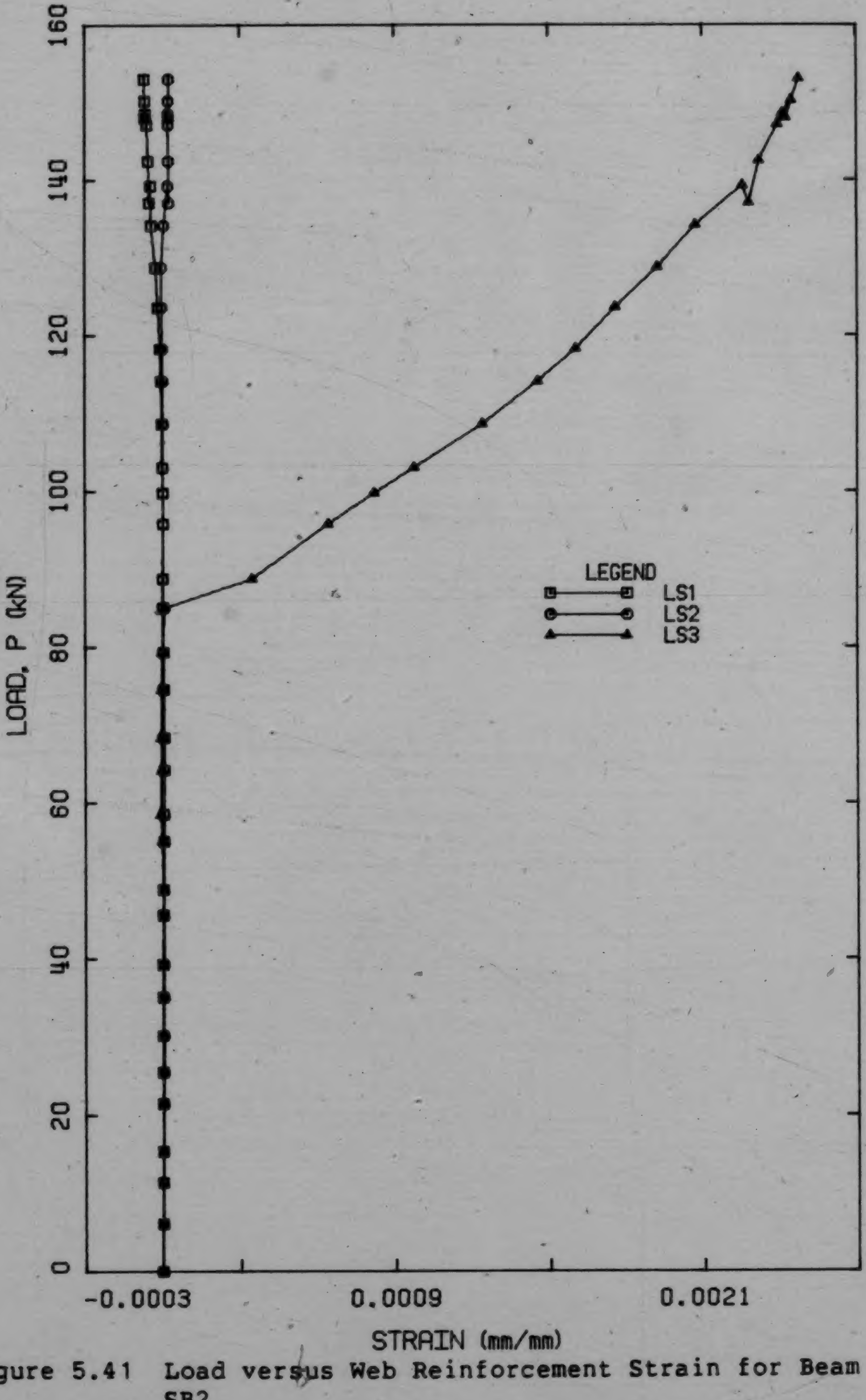

Figure 5.41 Load versus Web Reinforcement Strain for Beam SB2

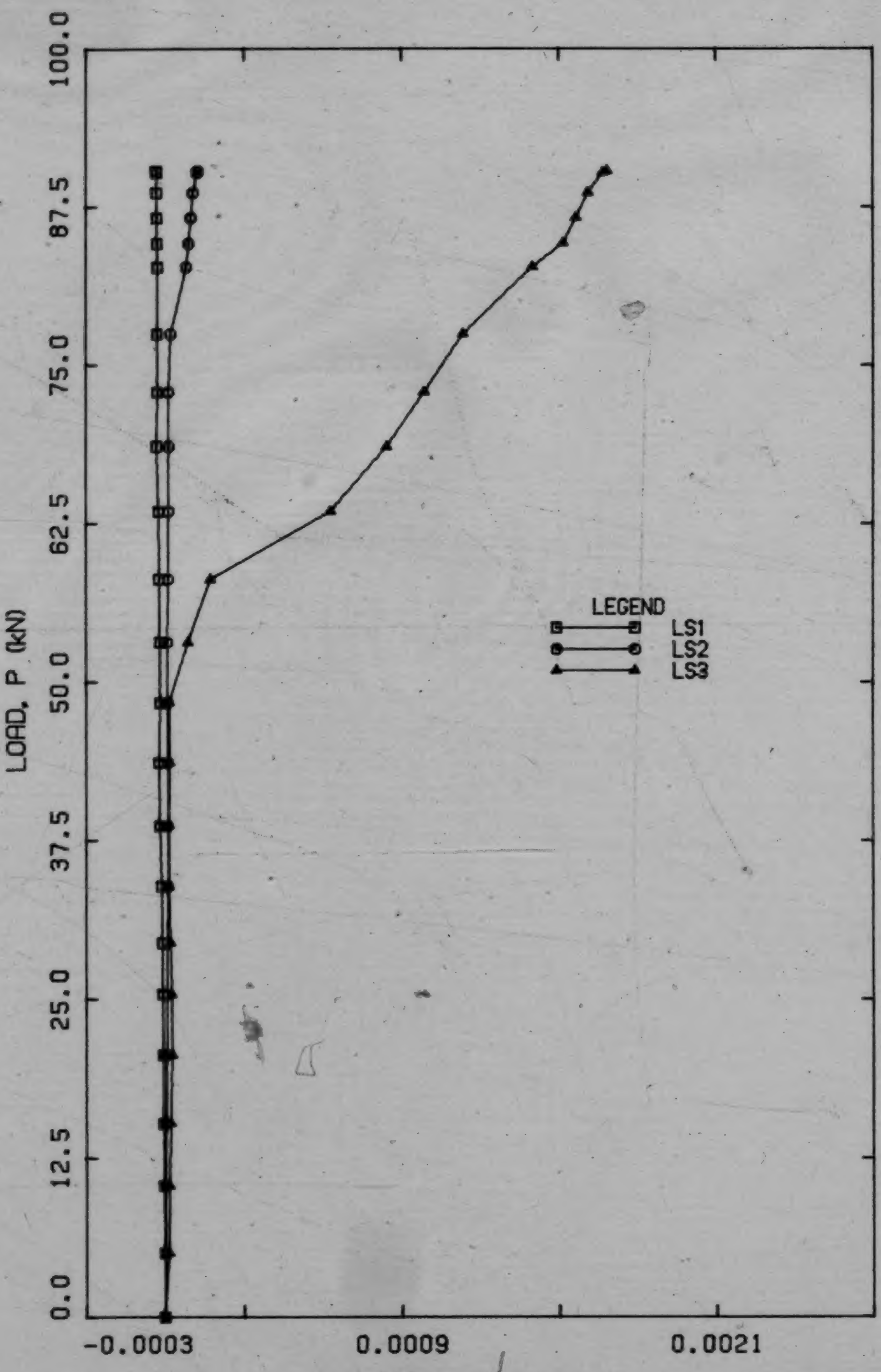

Figure 5.42 Load versus Web Reinforcement Strain for Beam SB4

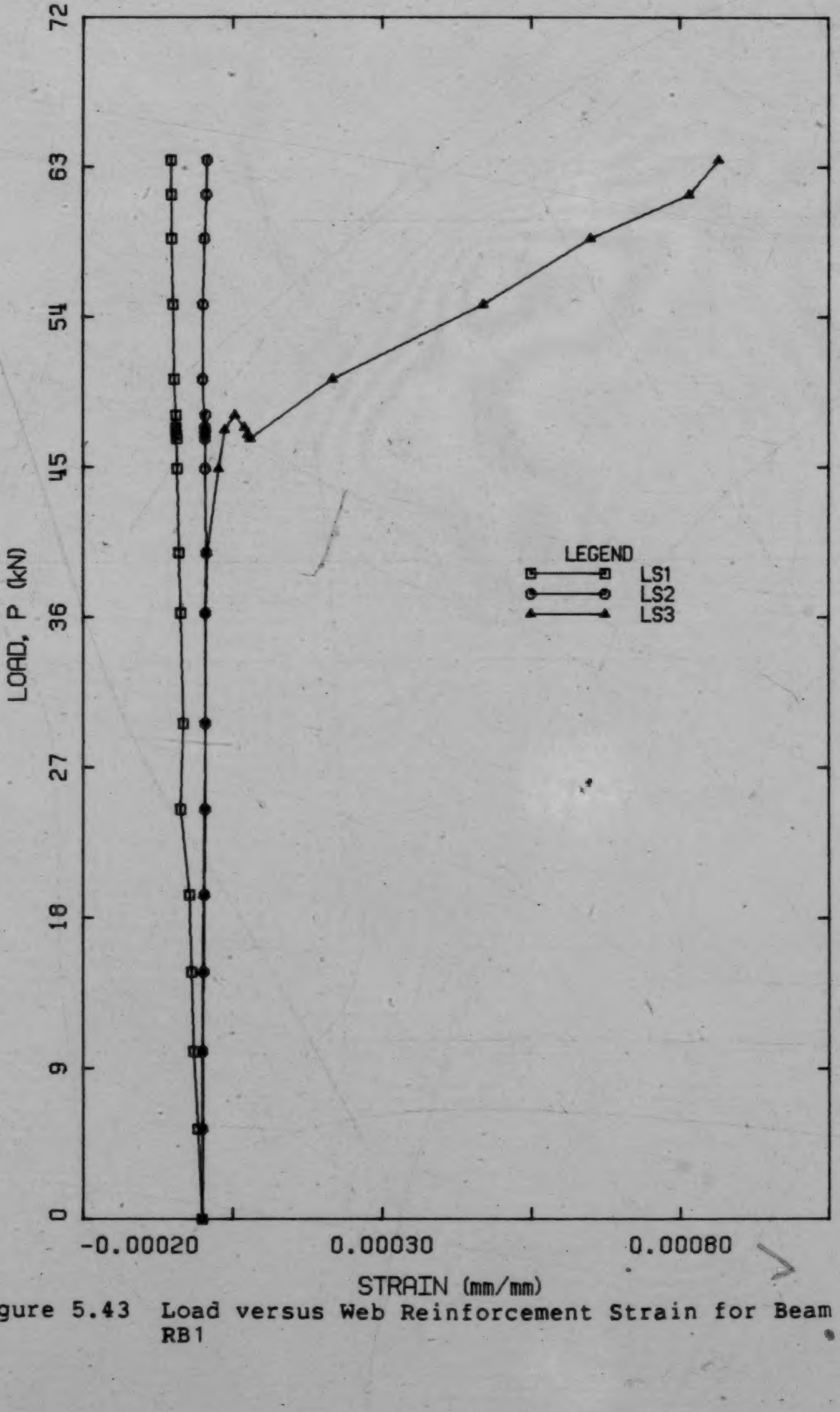

Figure 5.43 Load versus Web Reinforcement Strain for Beam RB1

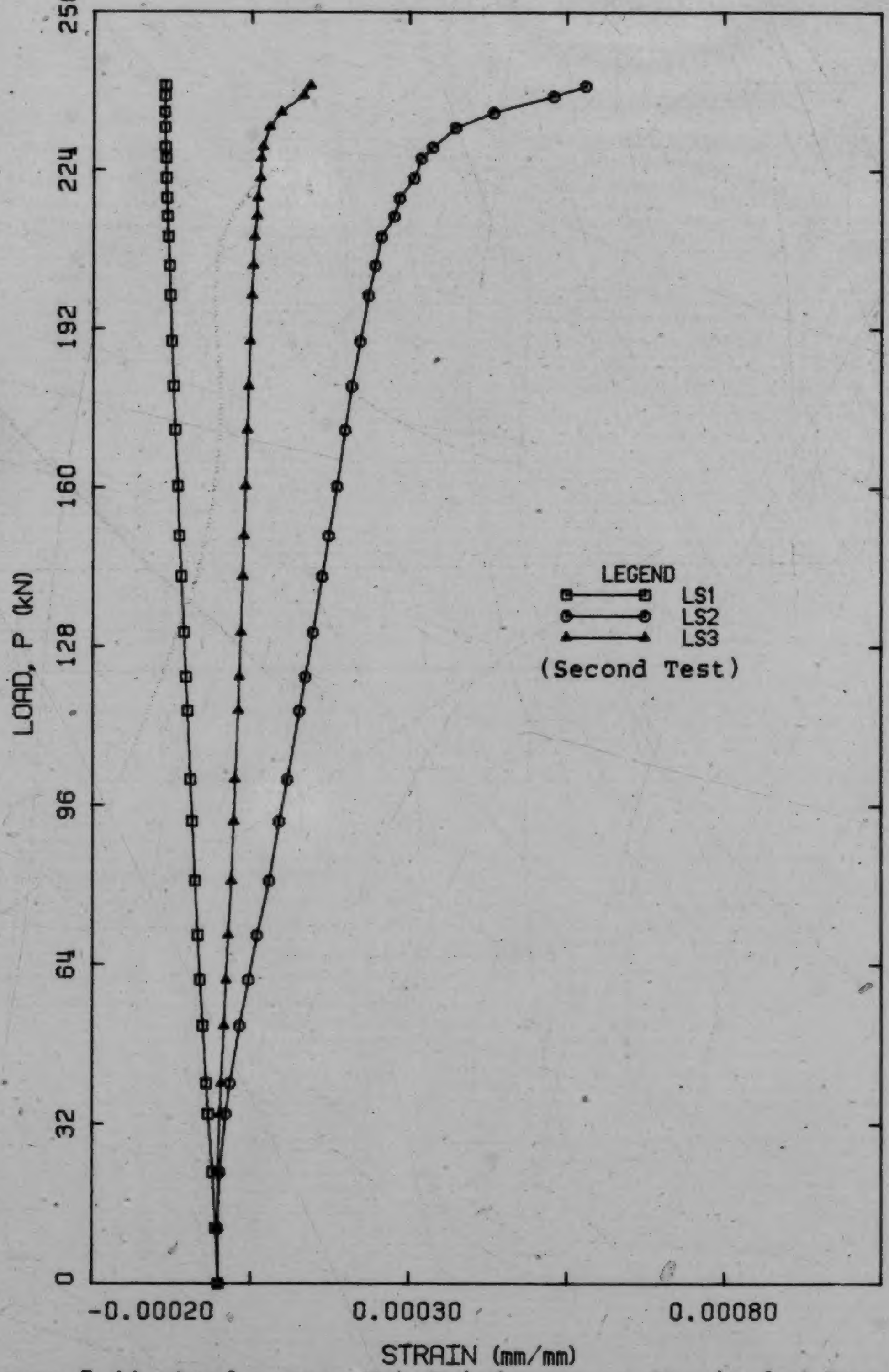

Figure 5.44 Load versus Web Reinforcement Strain for Beam RB2

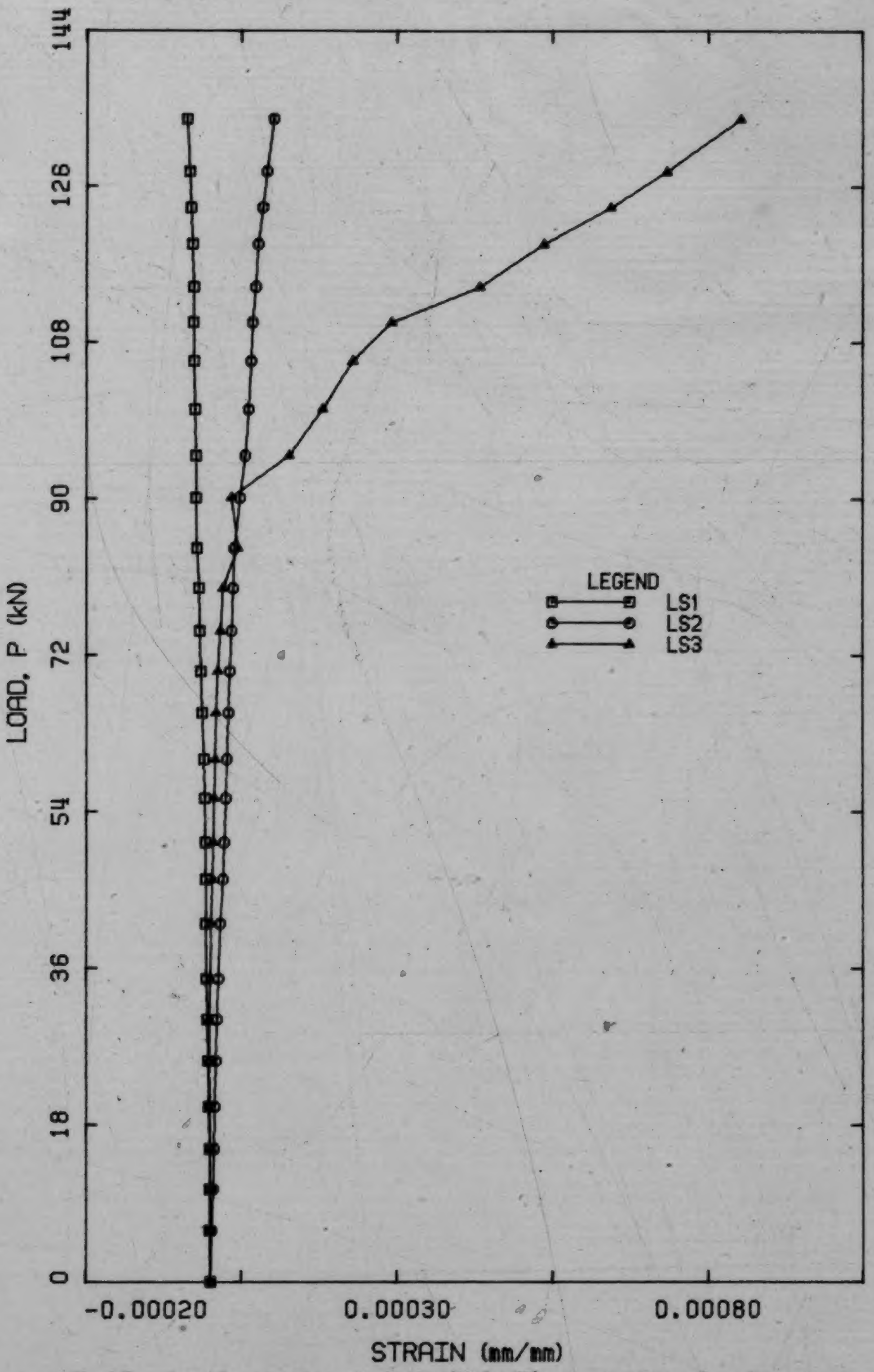

Figure 5.45 Load versus Web Reinforcement Strain for Beam RB4

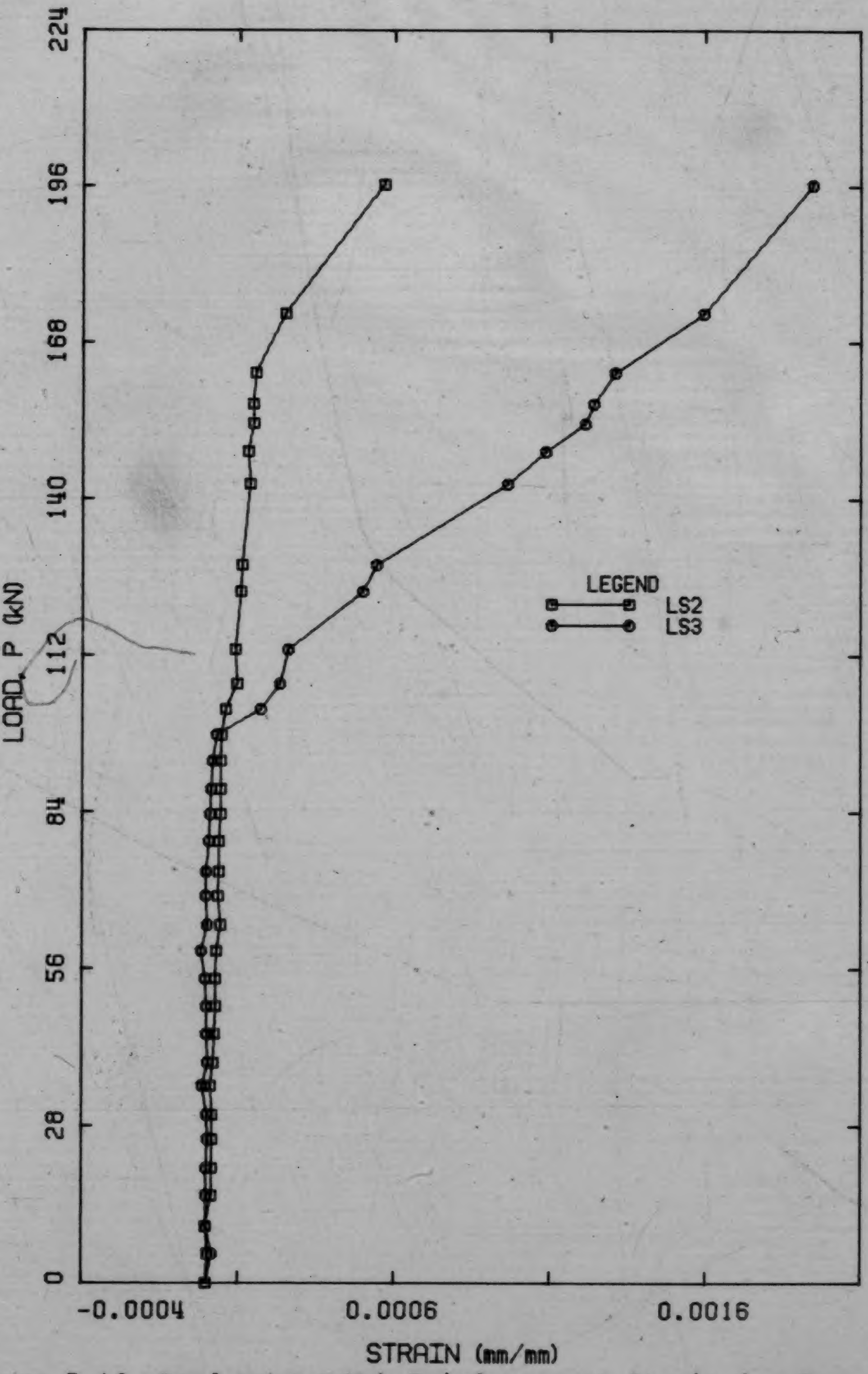

Figure 5.46 Load versus Web Reinforcement Strain for Beam EB3

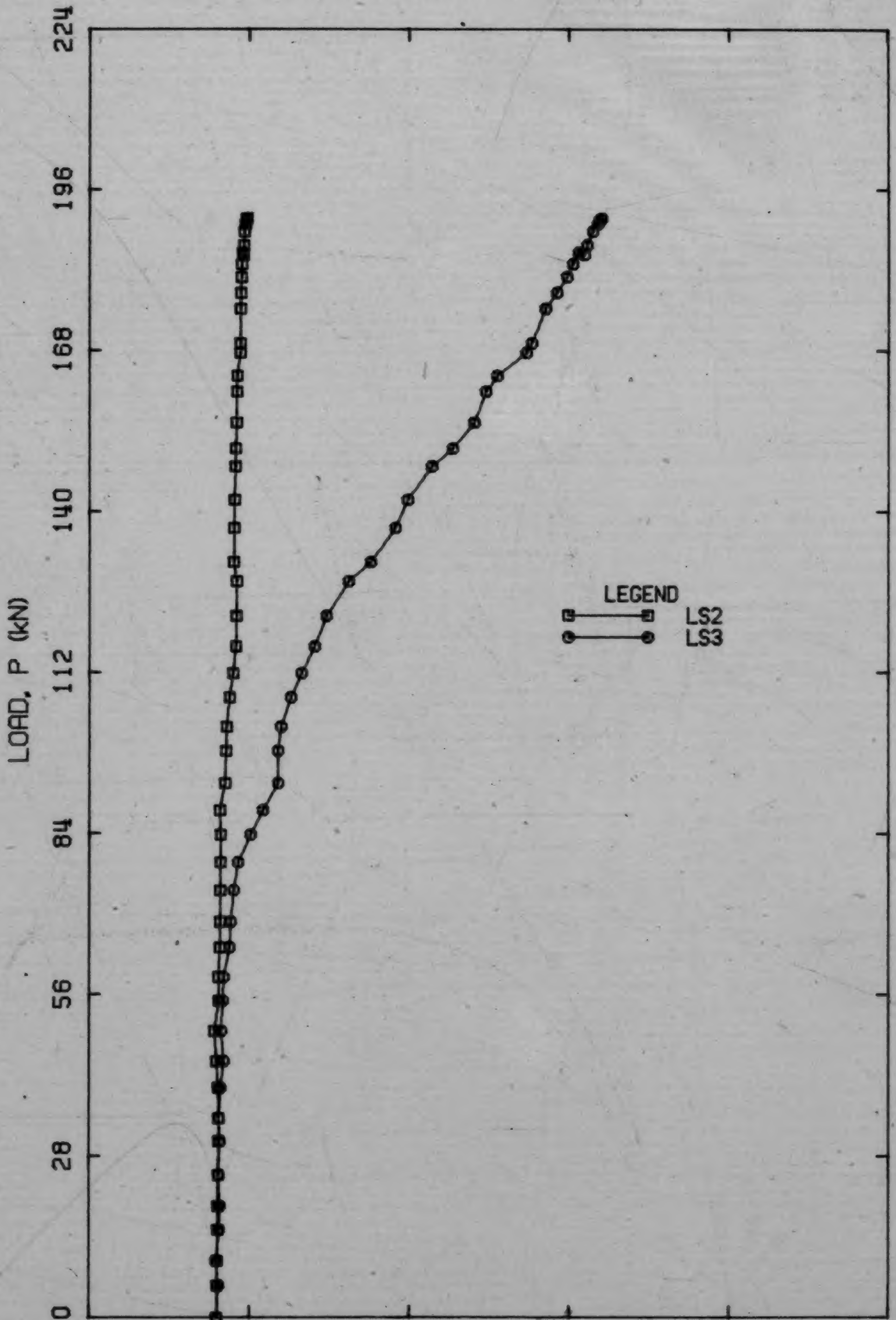

Figure 5.47 Load versus Web Reinforcement Strain for Beam EB6

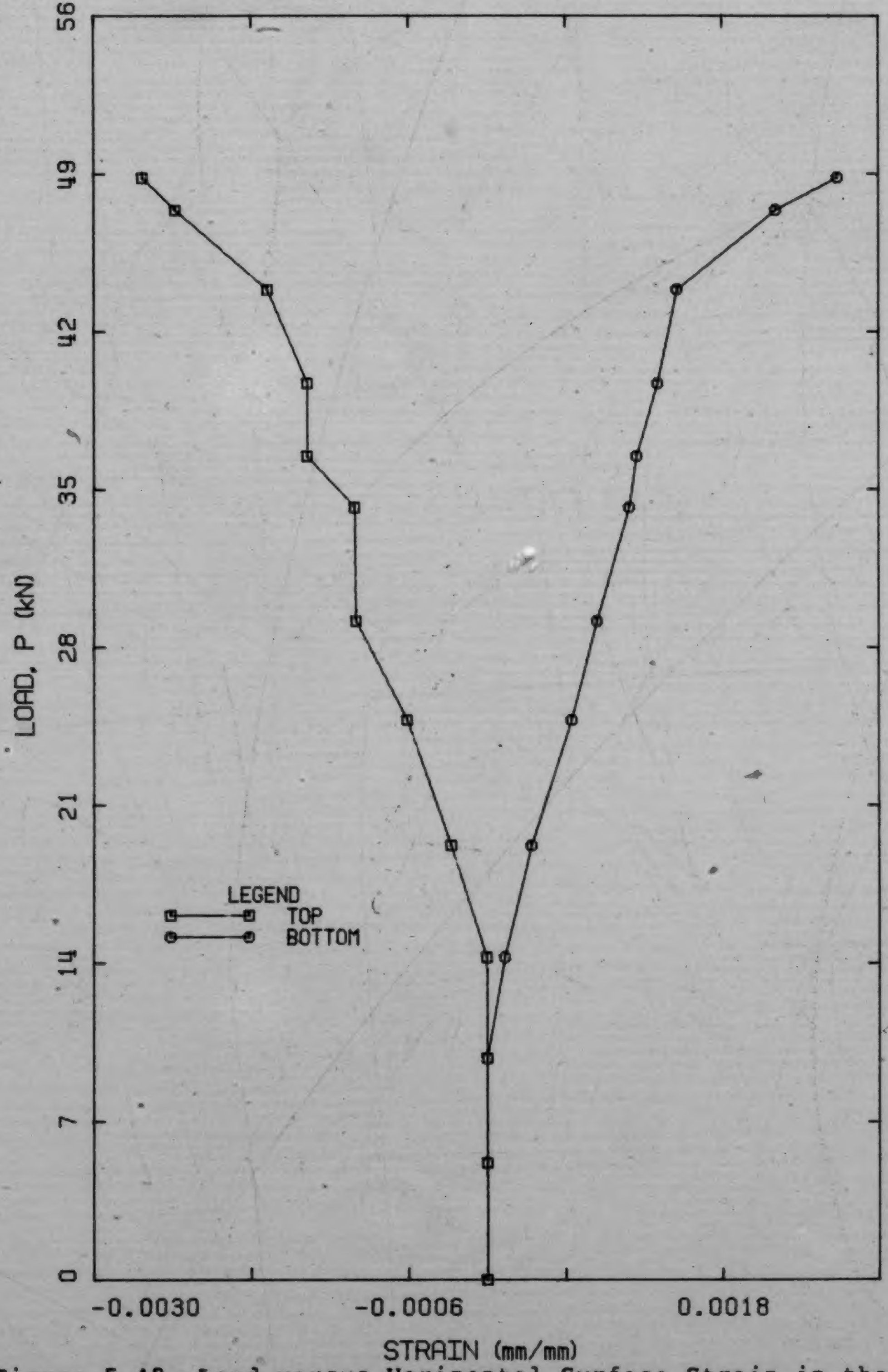

Figure 5.48 Load versus Horizontal Surface Strain in the Constant Moment Region for Beam SB1

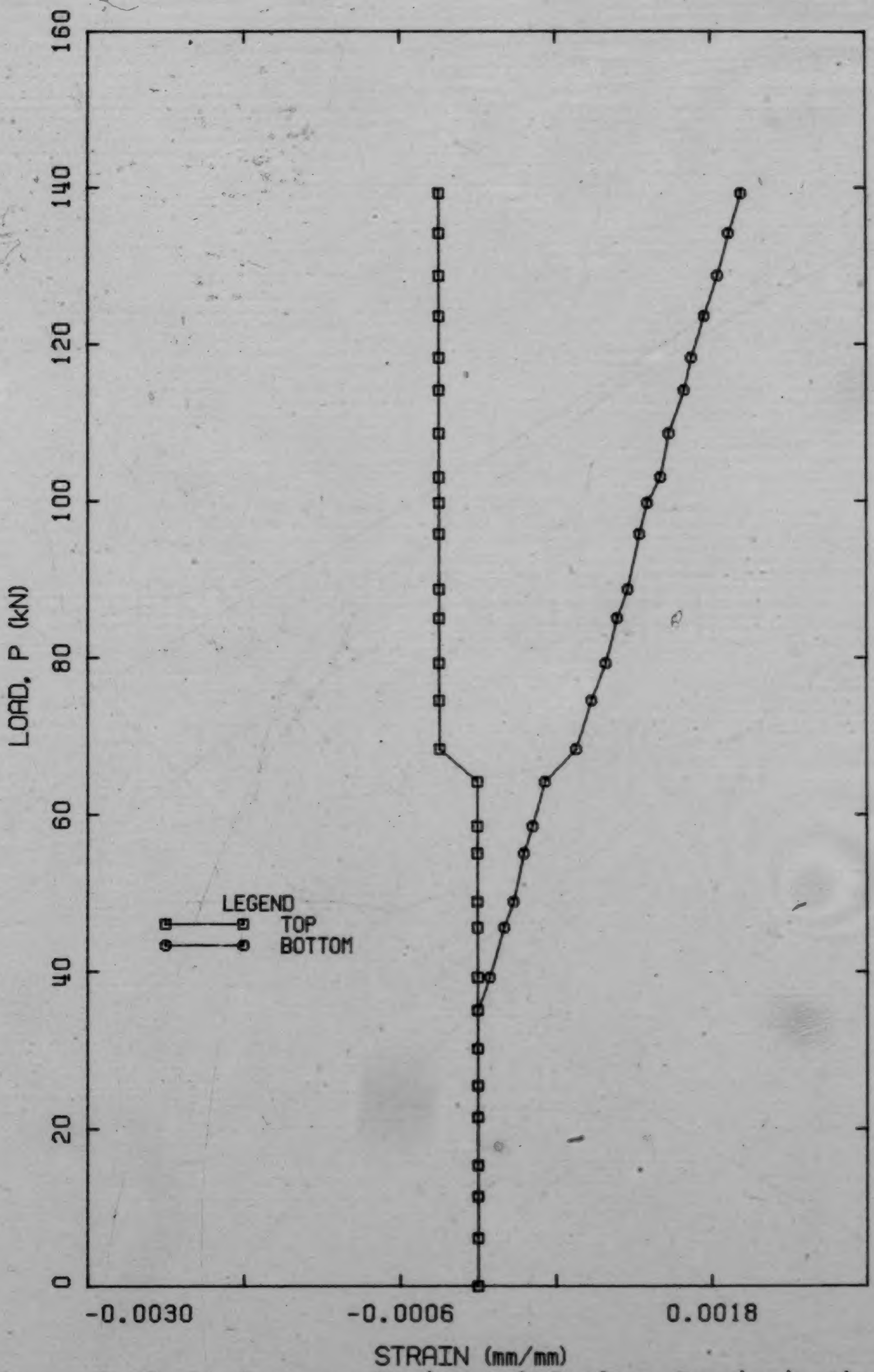

Figure 5.49 Load versus Horizontal Surface Strain in the Constant Moment Region for Beam SB2

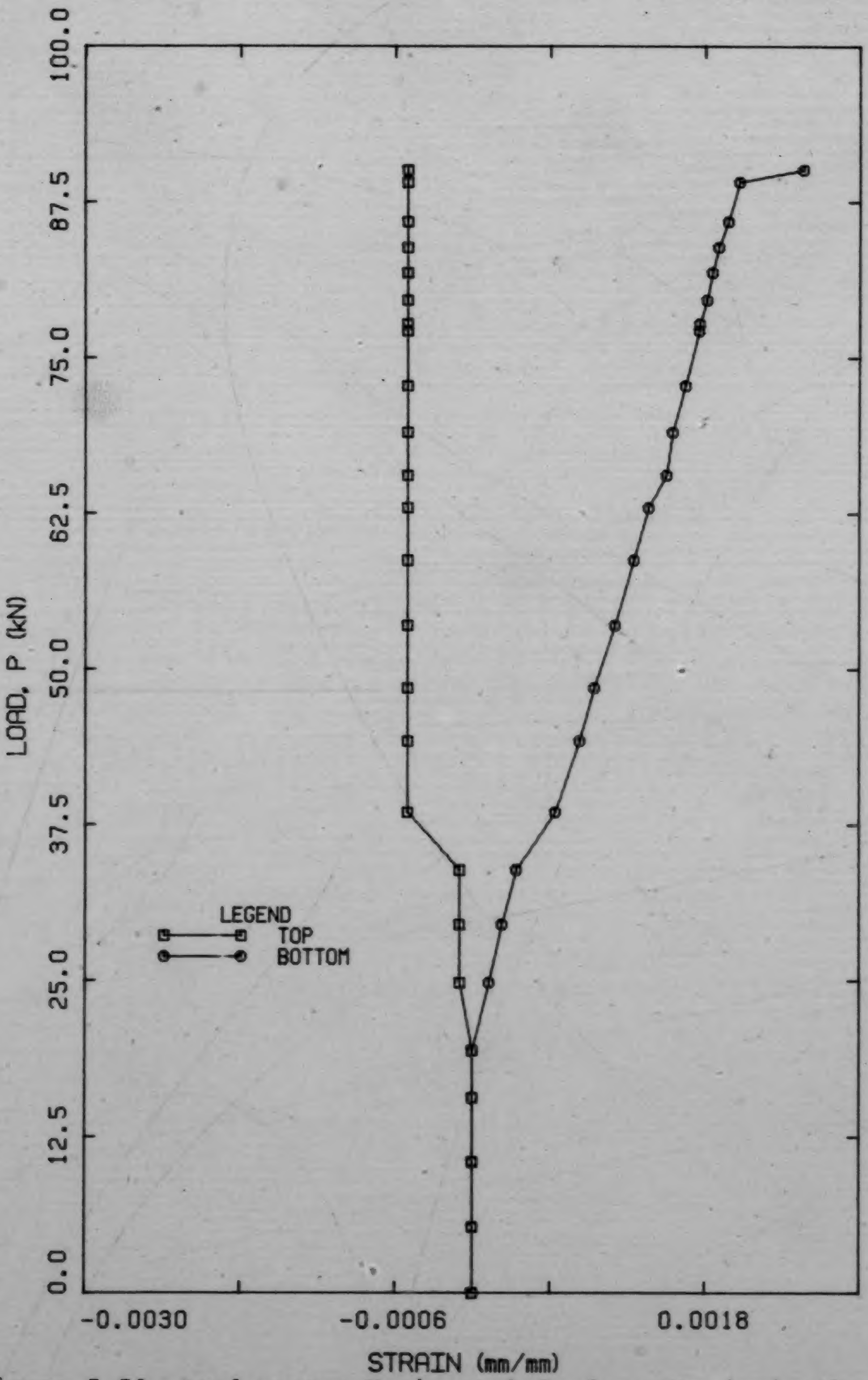

Figure 5.50 Load versus Horizontal Surface Strain in the Constant Moment Region for Beam SB3

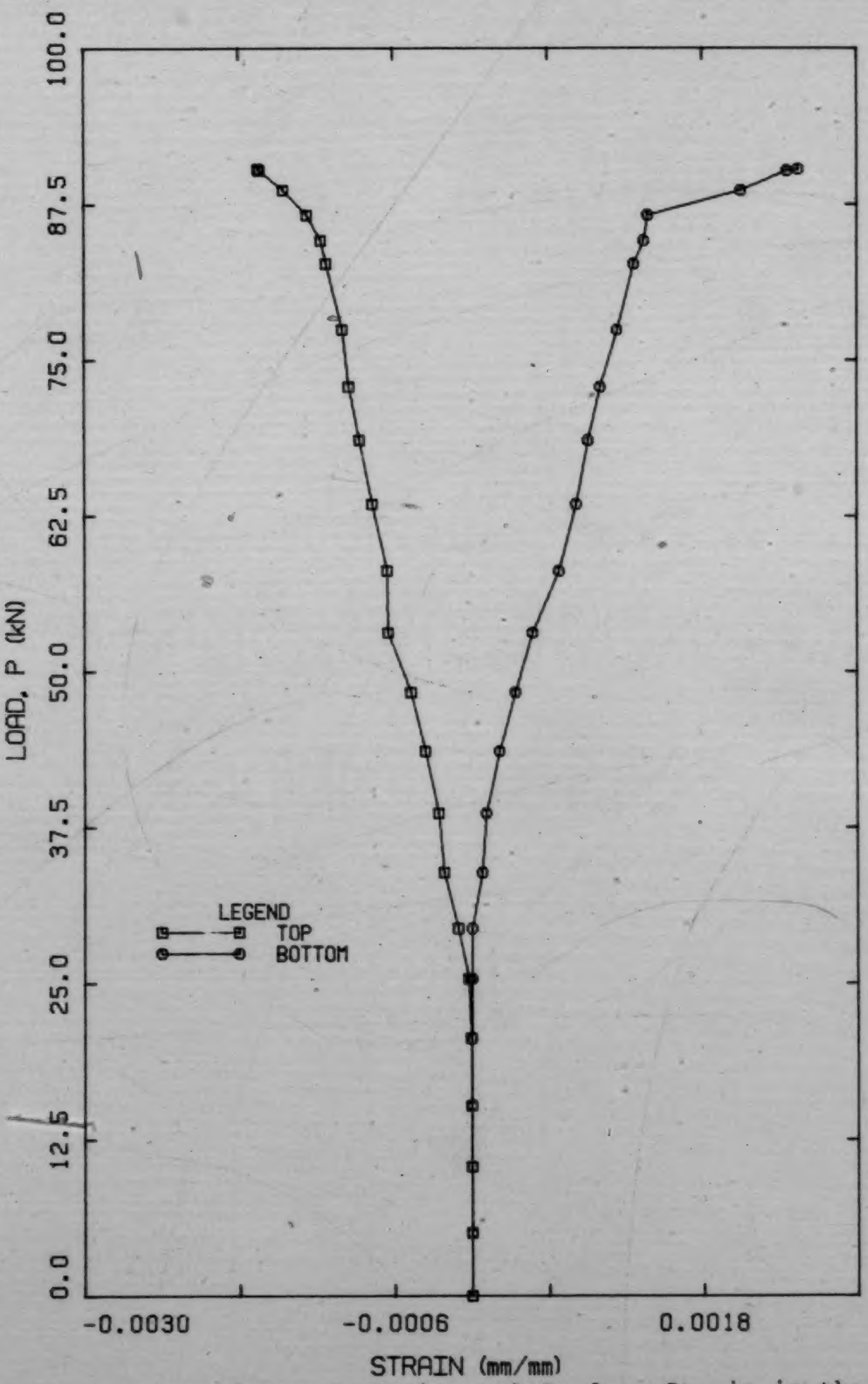

Figure 5.51 Load versus Horizontal Surface Strain in the Constant Moment Region for Beam SB4

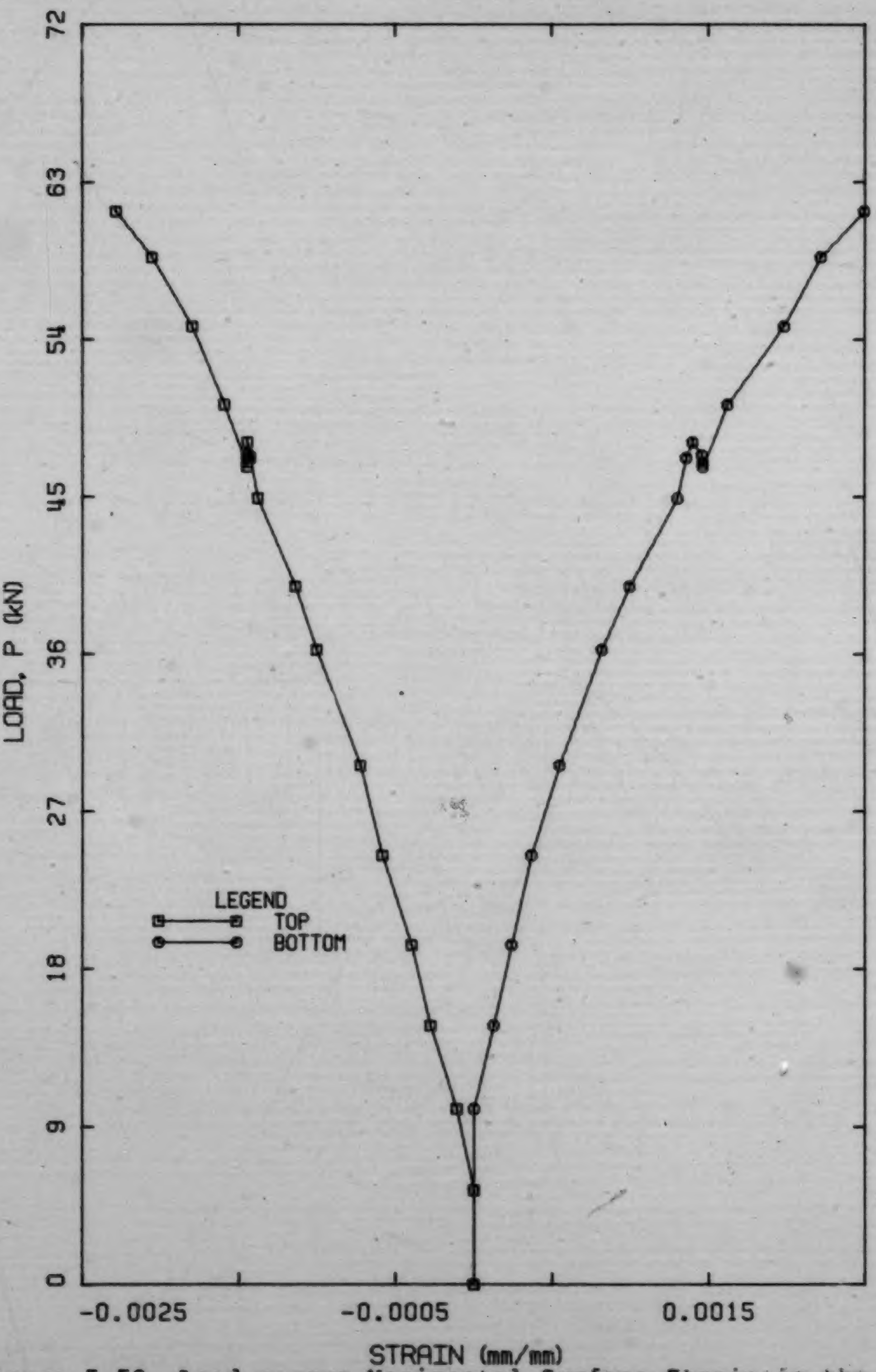

Figure 5.52 Load versus Horizontal Surface Strain in the Constant Moment Region for Beam RB1

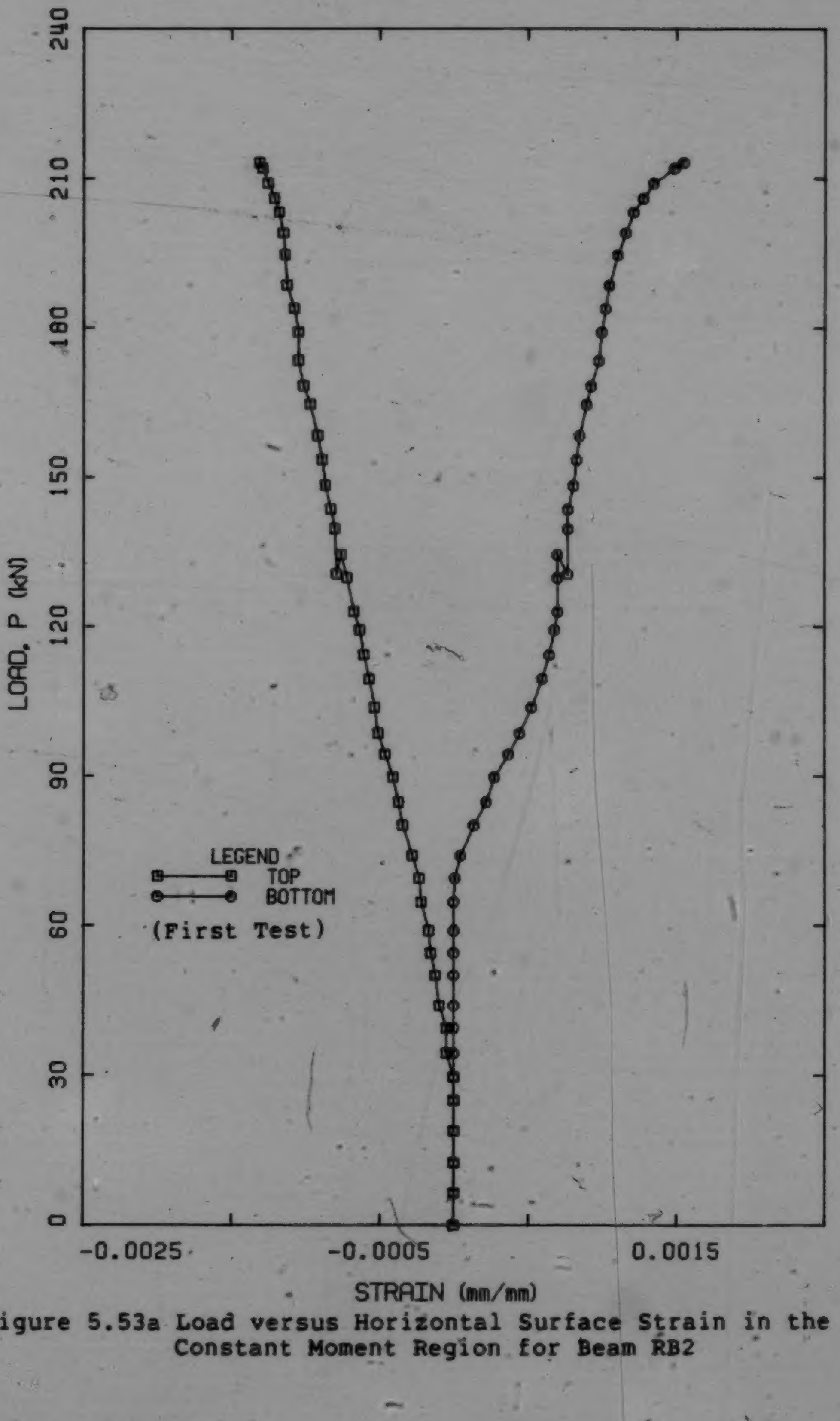

Figure 5.53a Load versus Horizontal Surface Strain in the Constant Moment Region for Beam RB2

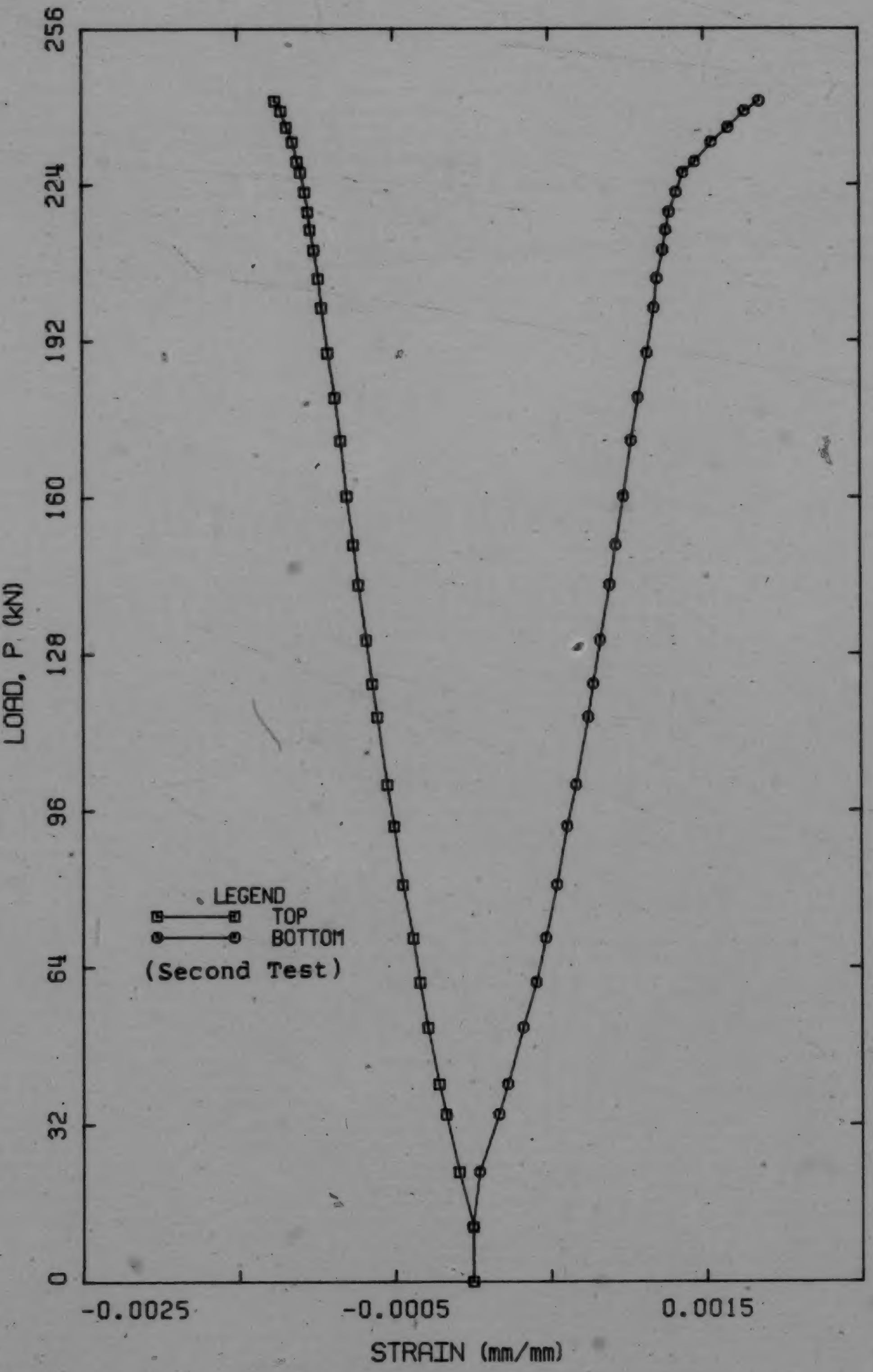

Figure 5.53b Load versus Horizontal Surface Strain in the Constant Moment Region for Beam RB2

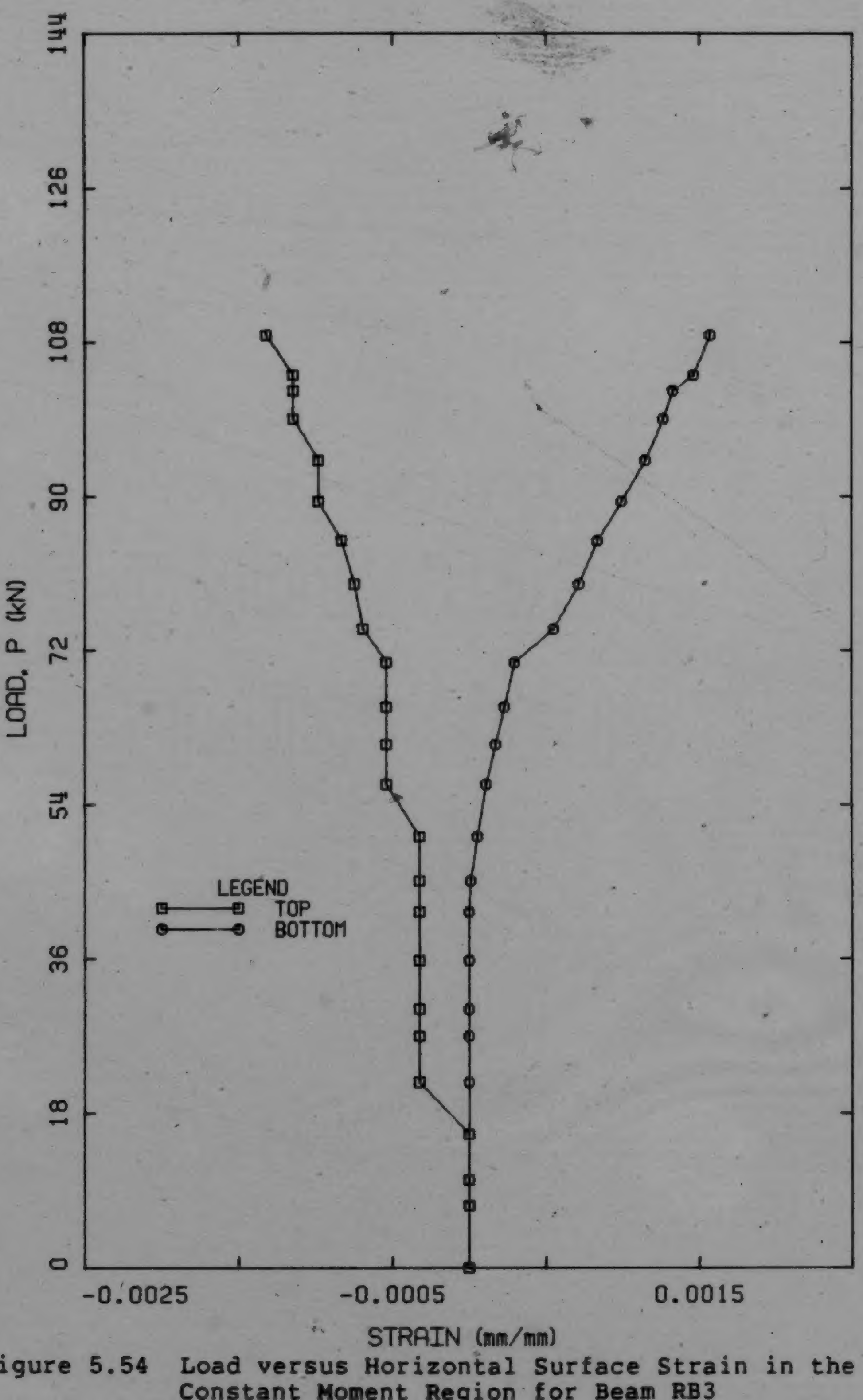

Figure 5.54 Load versus Horizontal Surface Strain in the Constant Moment Region for Beam RB3

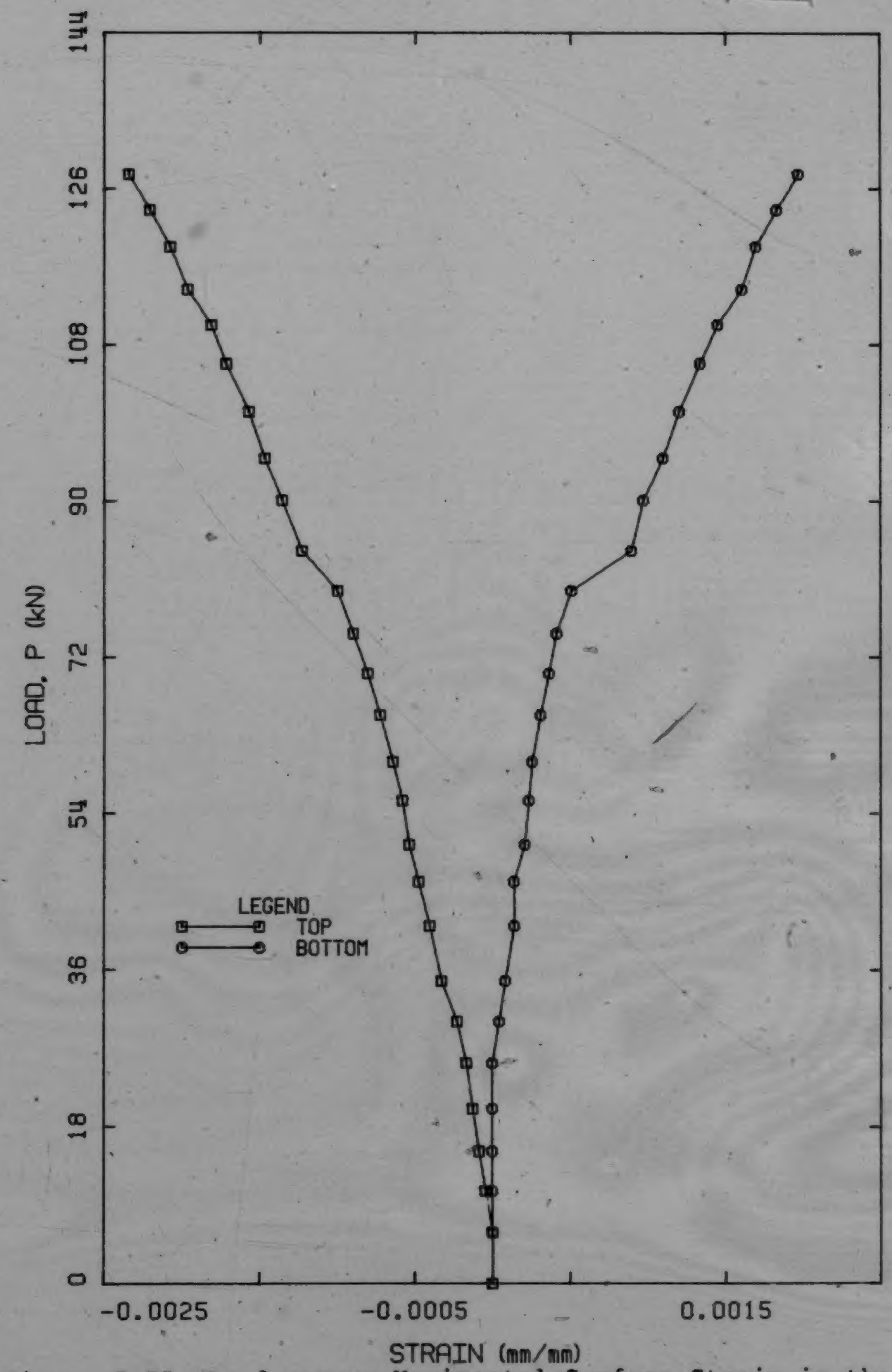

Figure 5.55 Load versus Horizontal Surface Strain in the Constant Moment Region for Beam RB4

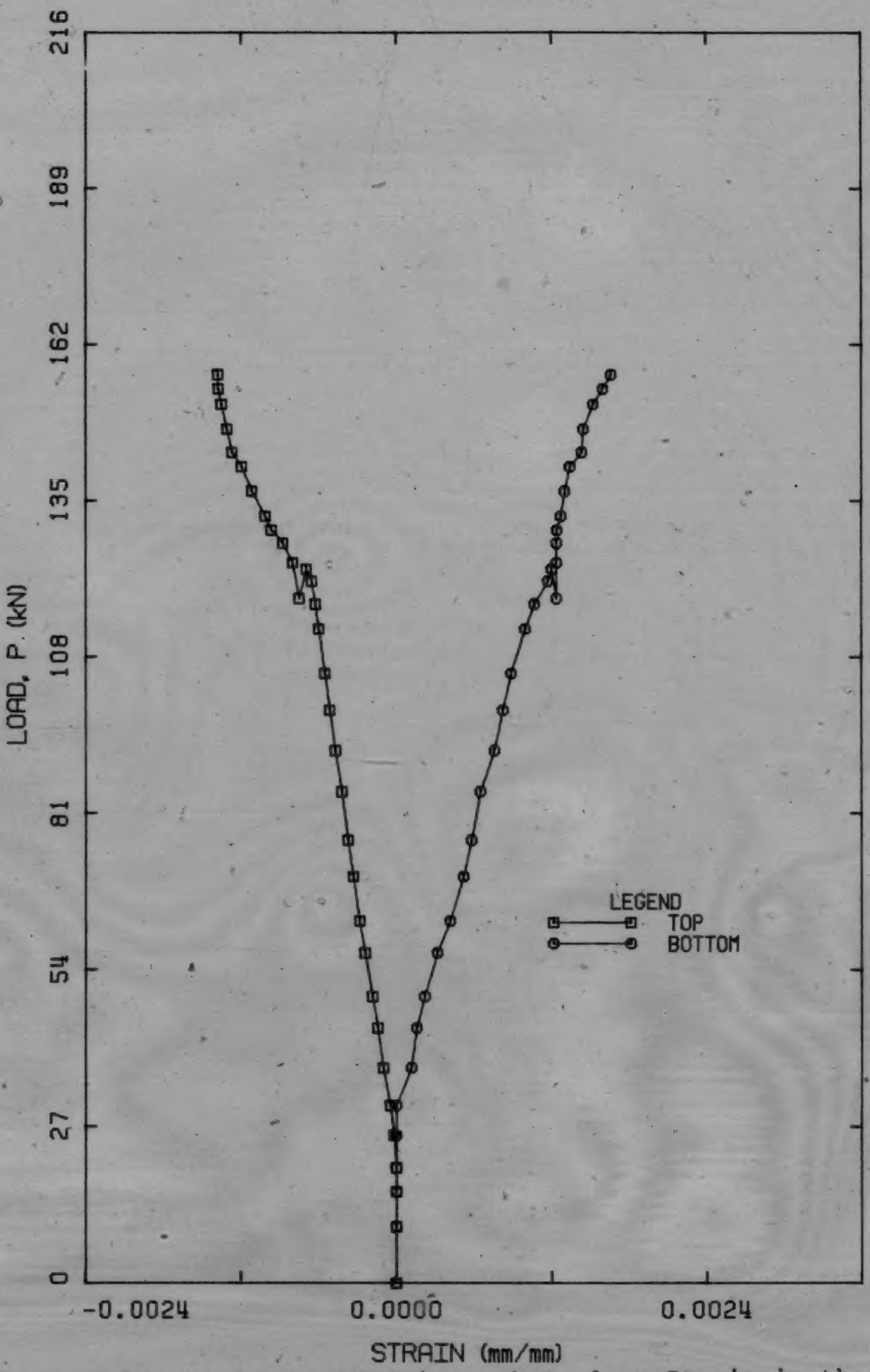

Figure 5.56 Load versus Horizontal Surface Strain in the Constant Moment Region for Beam EB1

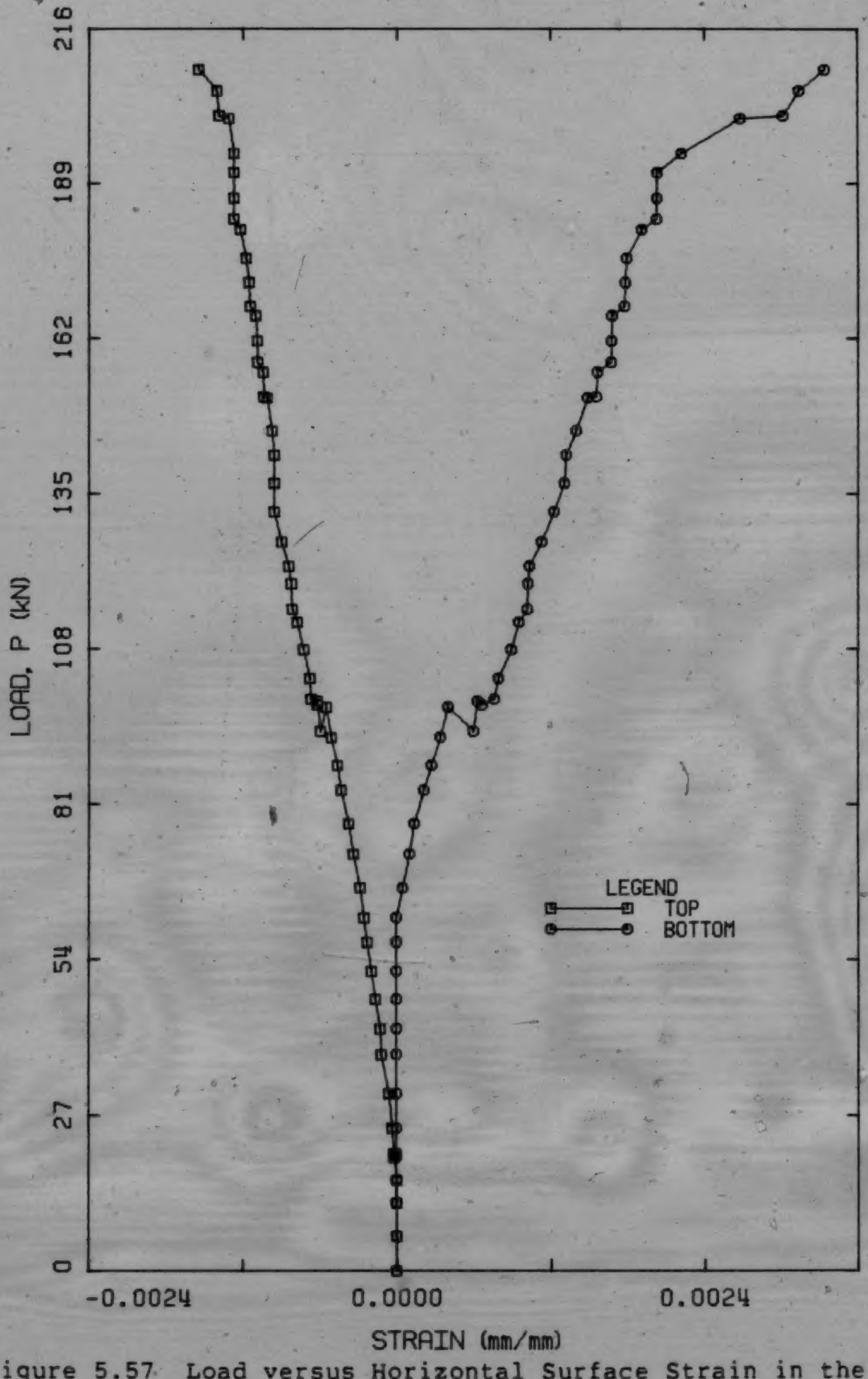

Figure 5.57 Load versus Horizontal Surface Strain in the Constant Moment Region for Beam EB2

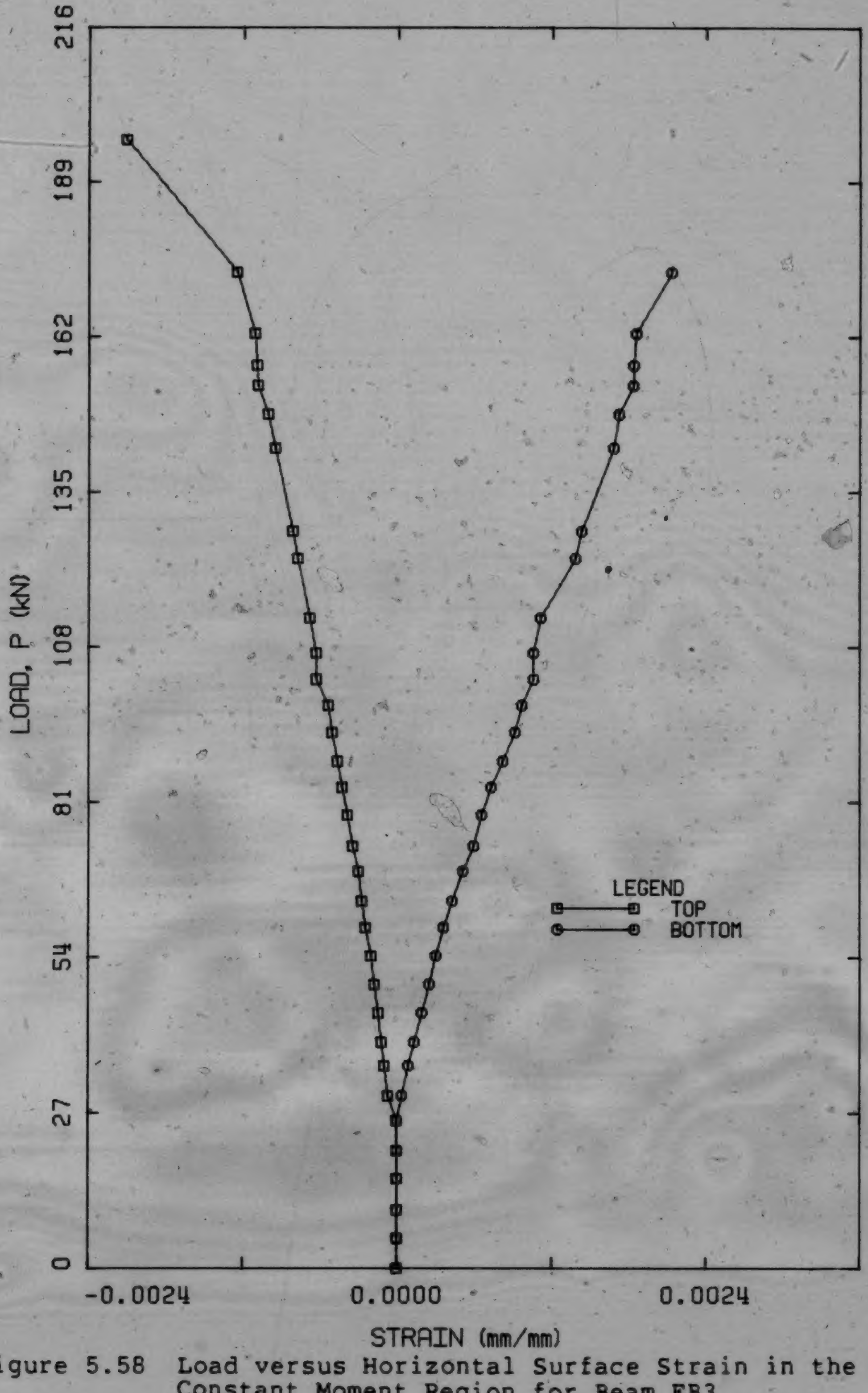

Figure 5.58 Load versus Horizontal Surface Strain in the Constant Moment Region for Beam EB3

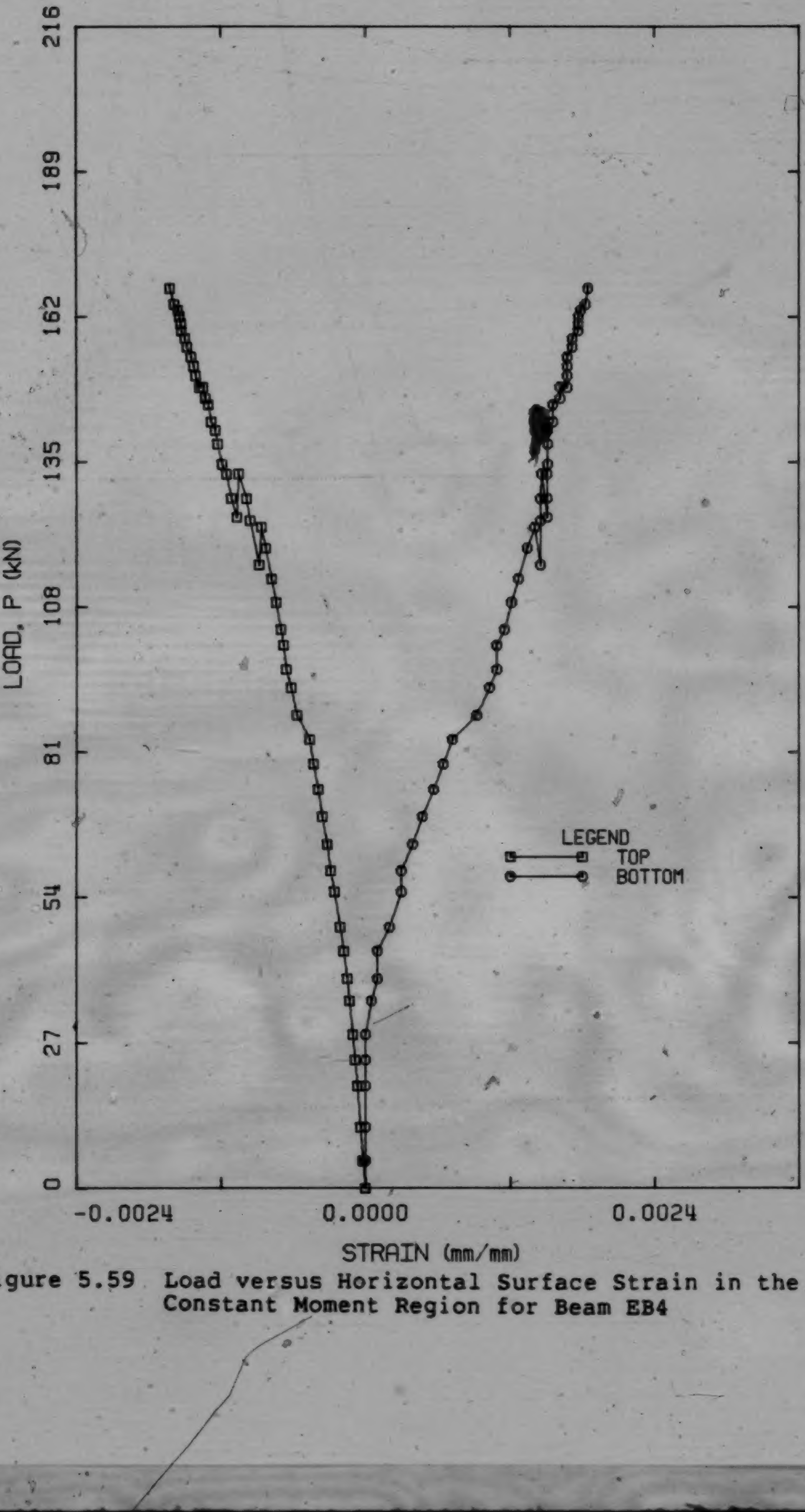

Figure 5.59 Load versus Horizontal Surface Strain in the Constant Moment Region for Beam EB4

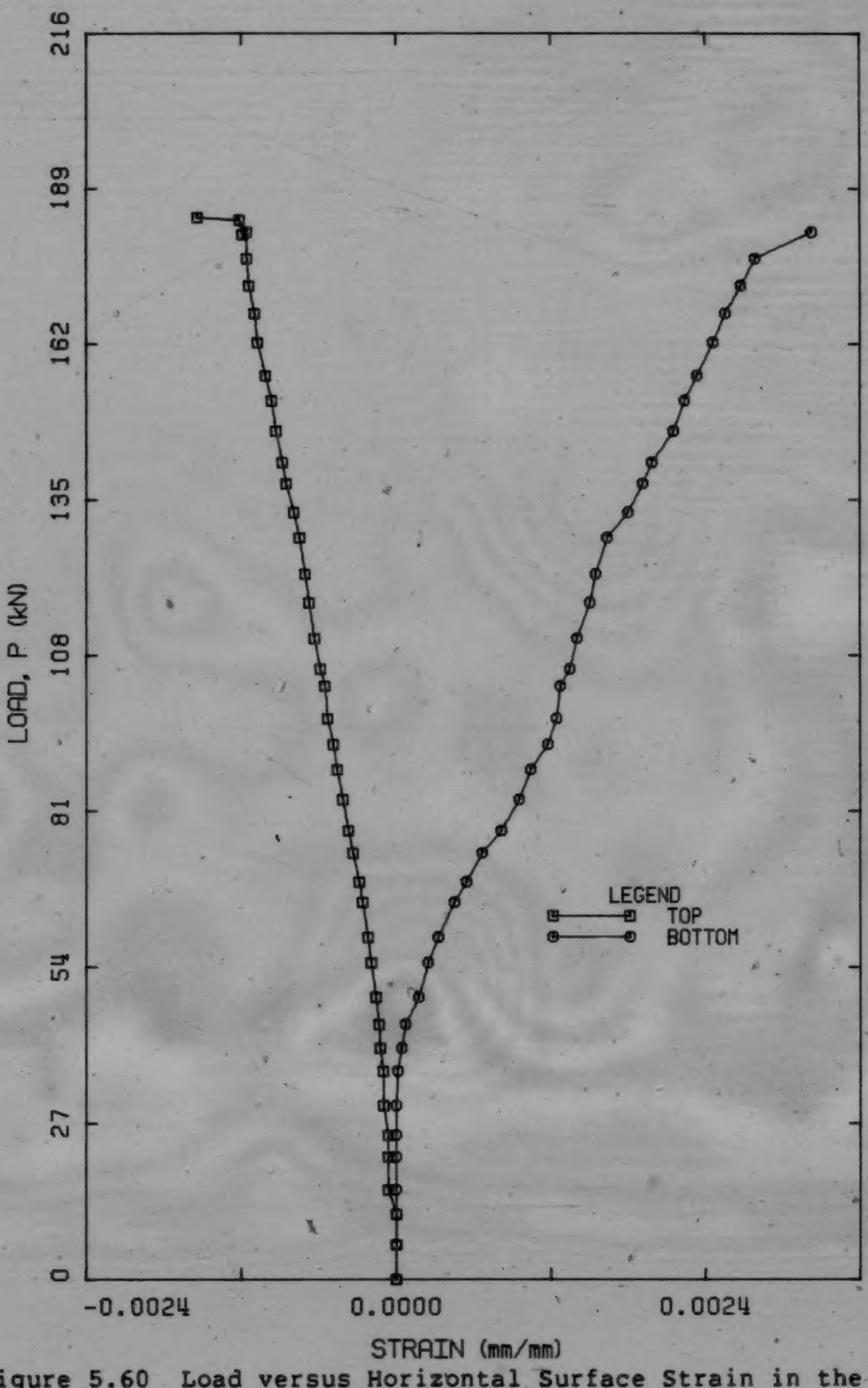

Figure 5.60 Load versus Horizontal Surface Strain in the Constant Moment Region for Beam EB5

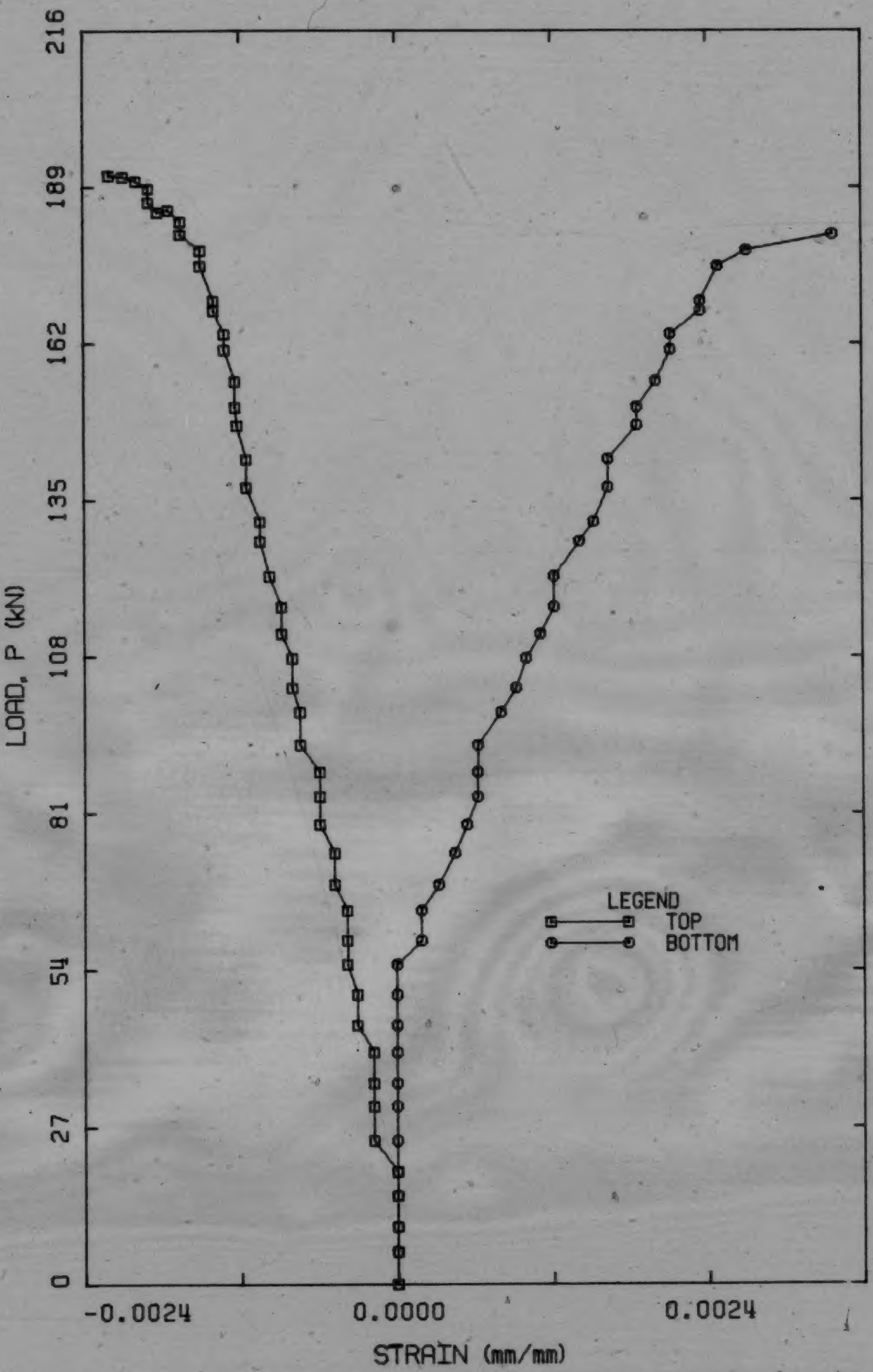

Figure 5.61 Load versus Horizontal Surface Strain in the Constant Moment Region for Beam EB6

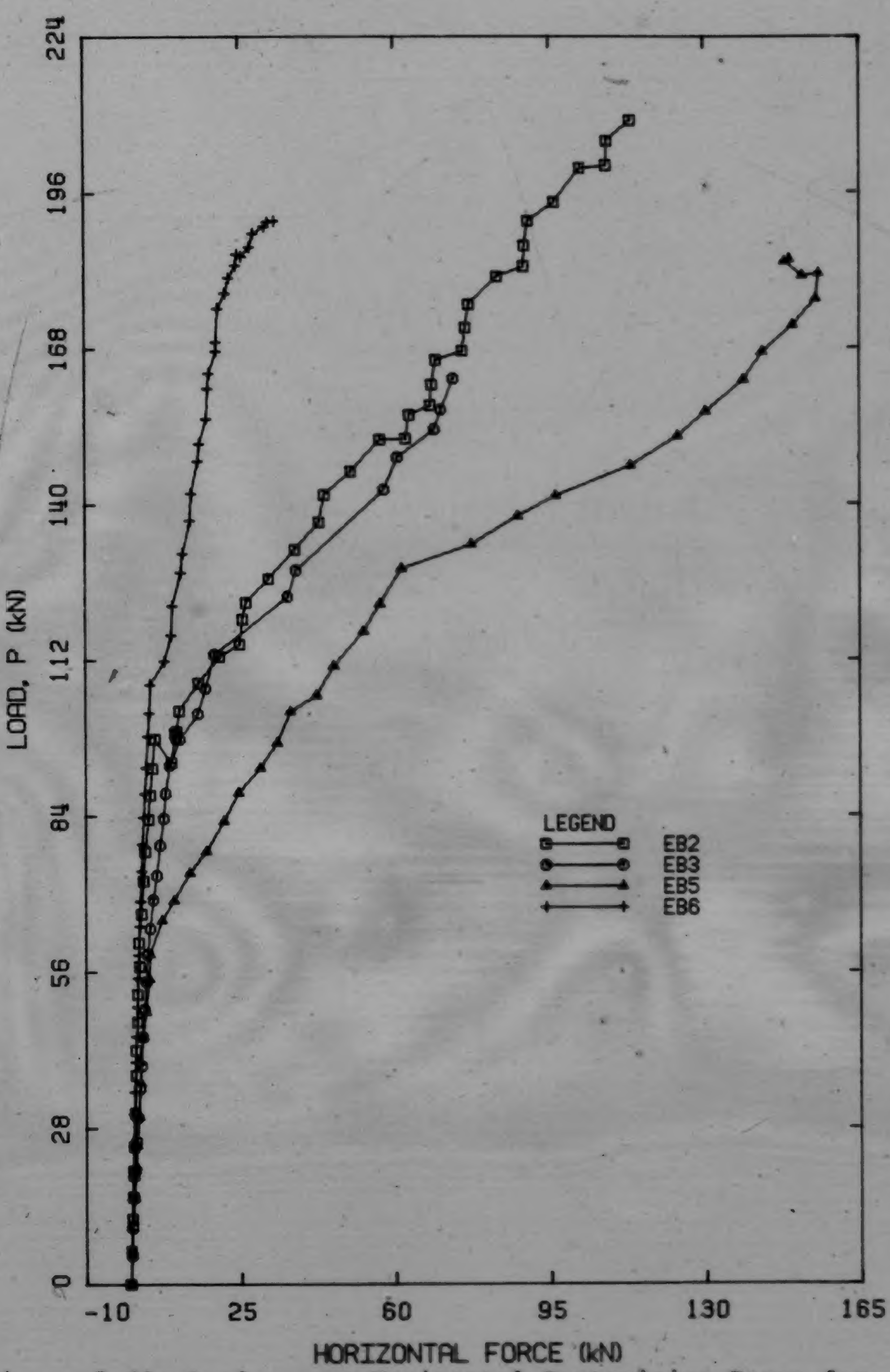

Figure 5.62a Load versus Horizontal Restraining Force for Type EB Beams

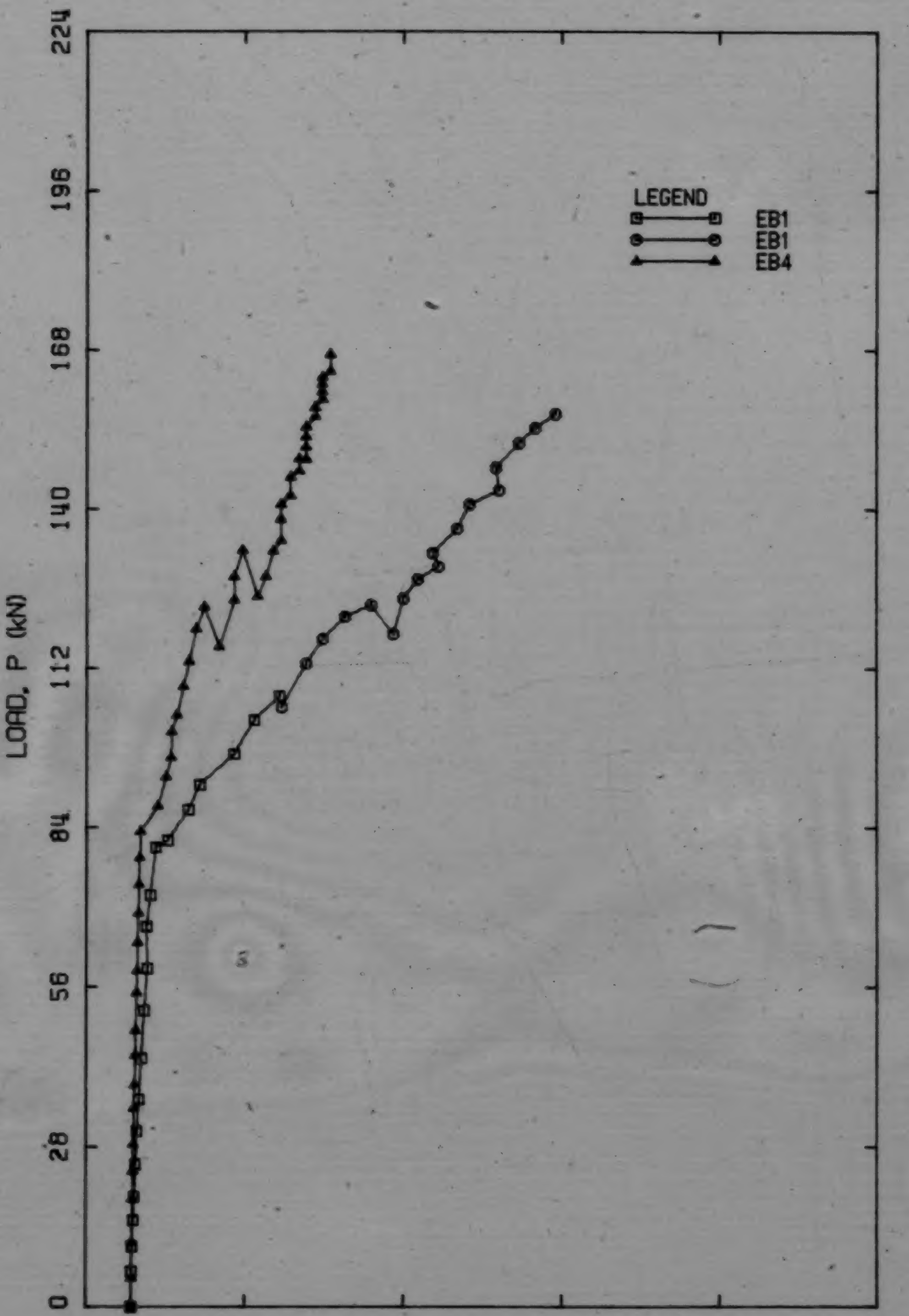

Figure 5.62b Load versus Horizontal Restraining Force for Type EB Beams

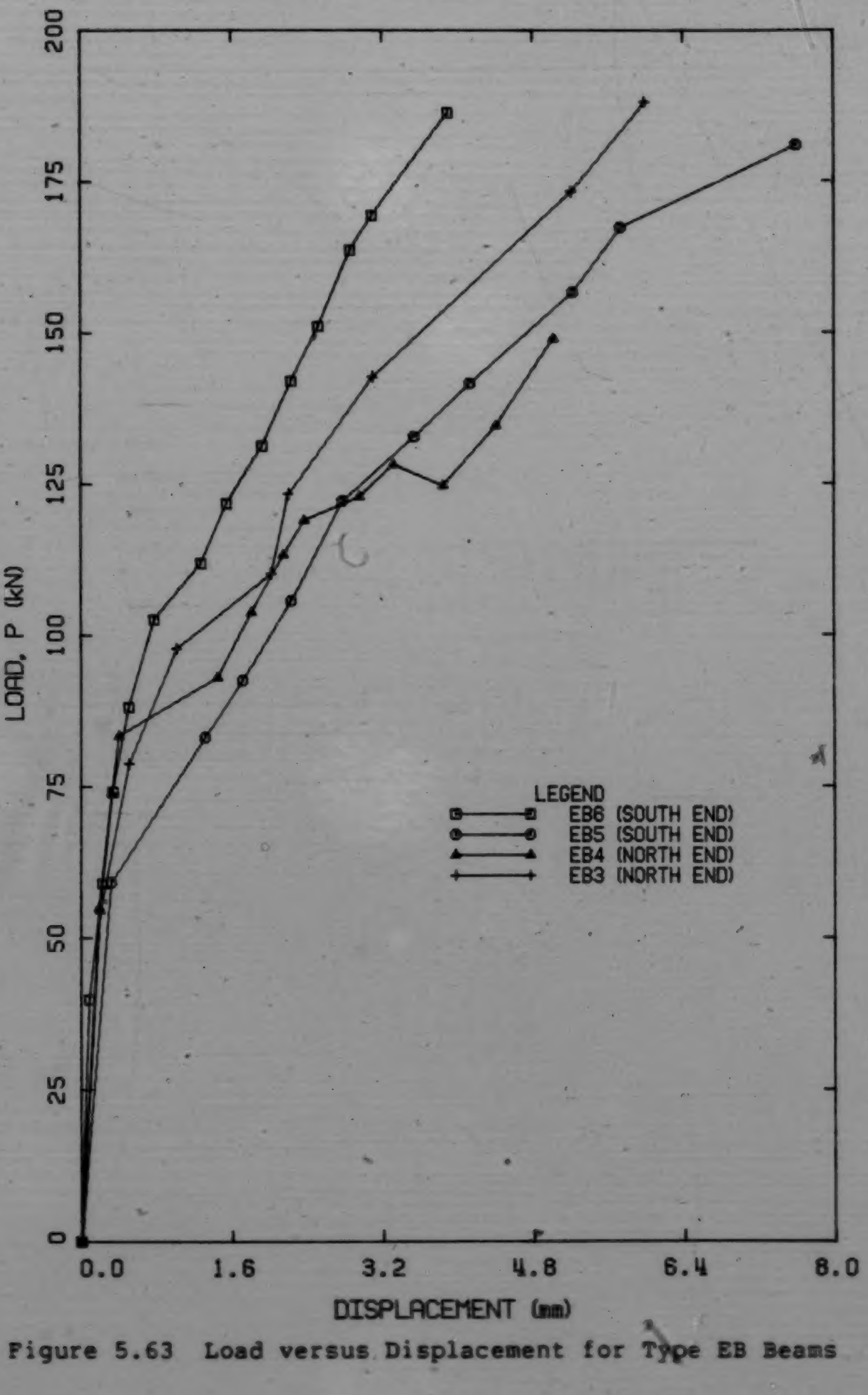

Figure 5.63 Load versus Displacement for Type EB Beams

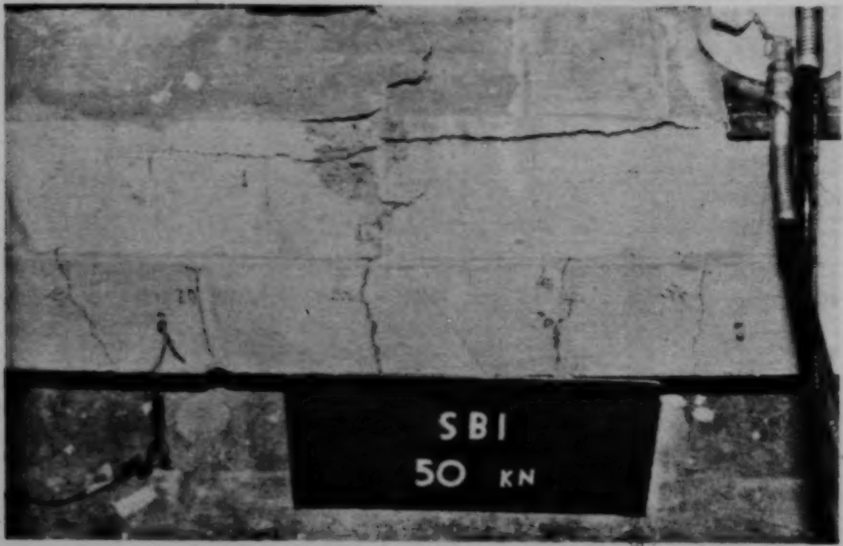

Plate 5.1 Failure of Beam SB1

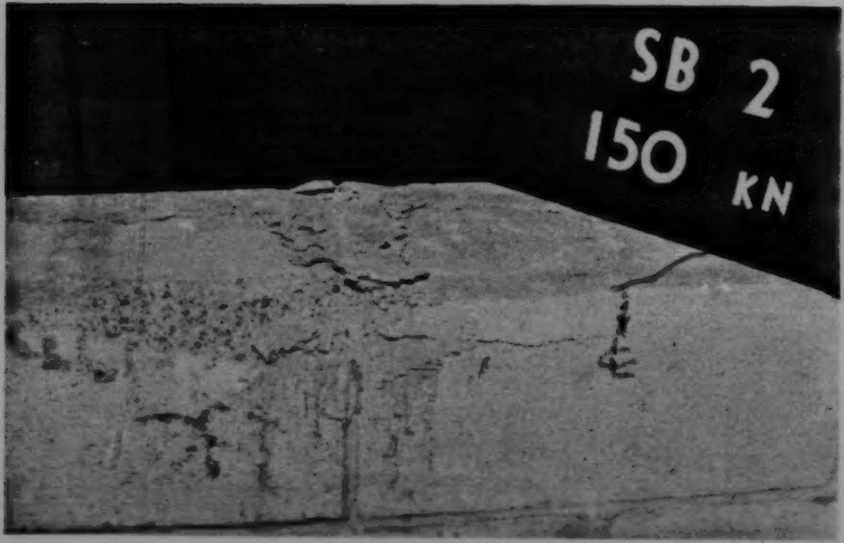

Plate 5.2 Failure of Beam SB2

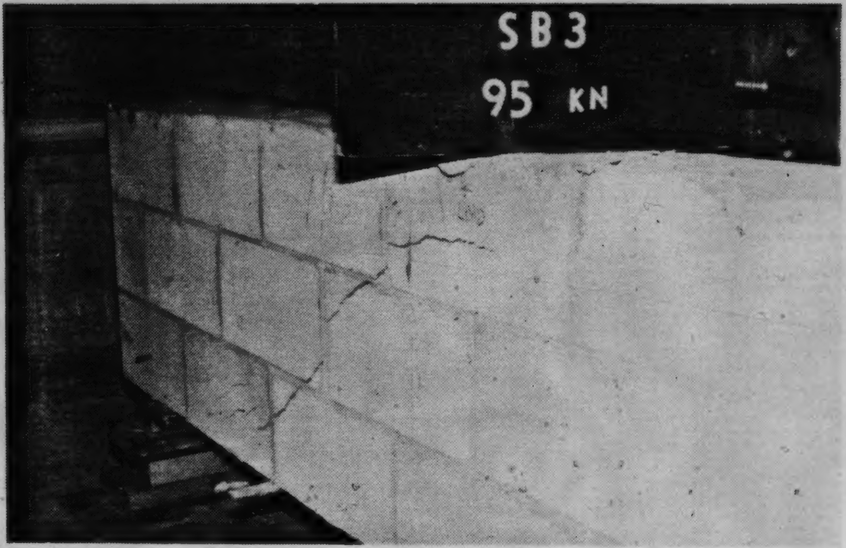

Plate 5.3 Failure of Beam SB3

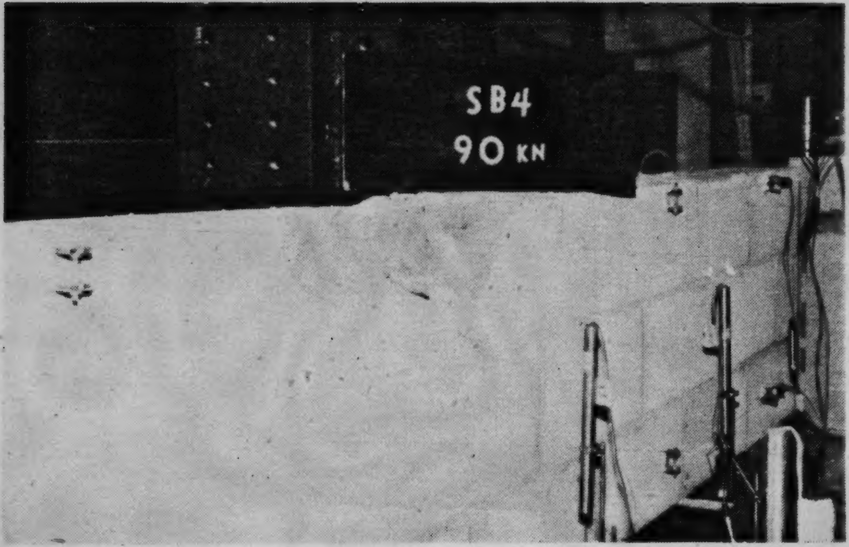

Plate 5.4 Failure of Beam SB4

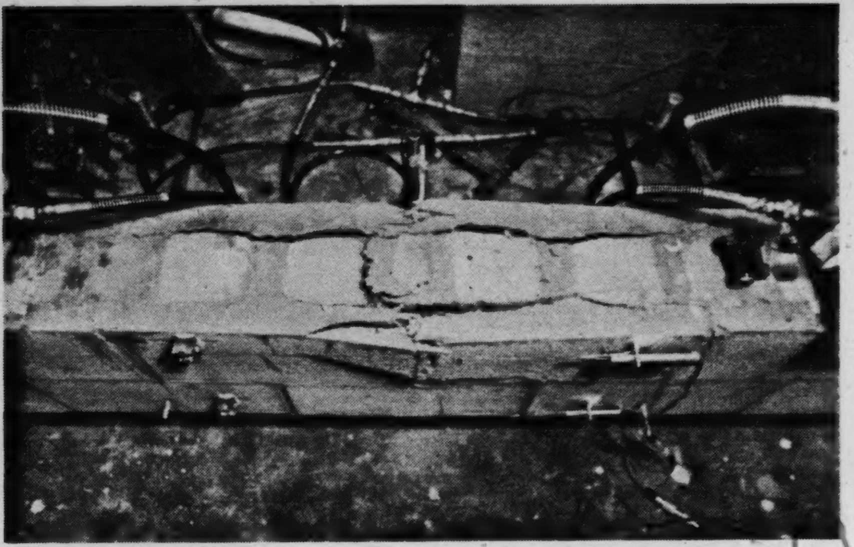

Plate 5.5 Failure of Beam RB1

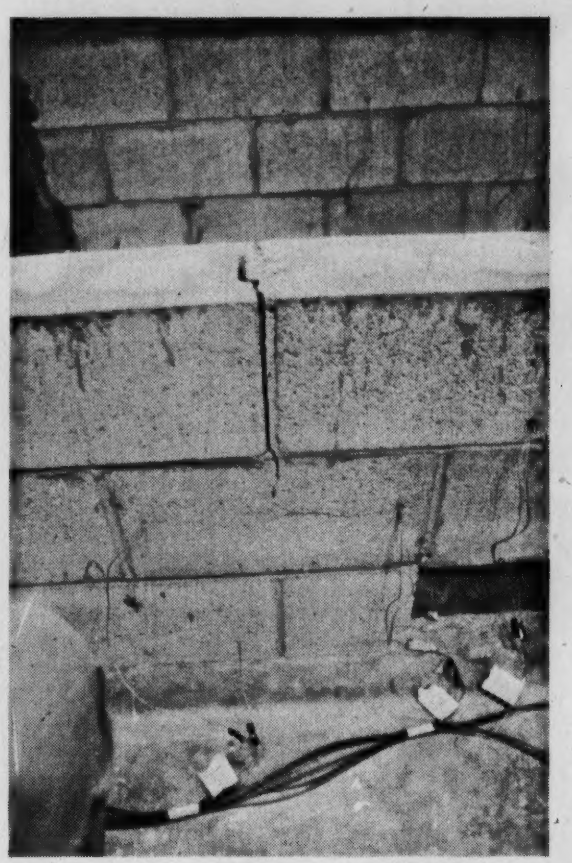

Plate 5.6 Cracks at North Support of Beam RB1

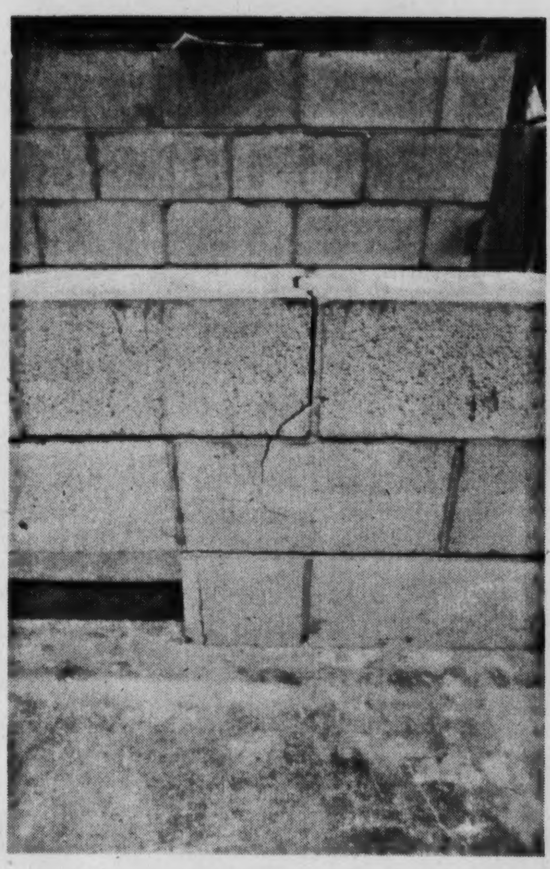

Plate 5.7 Cracks at South Support of Beam RB1

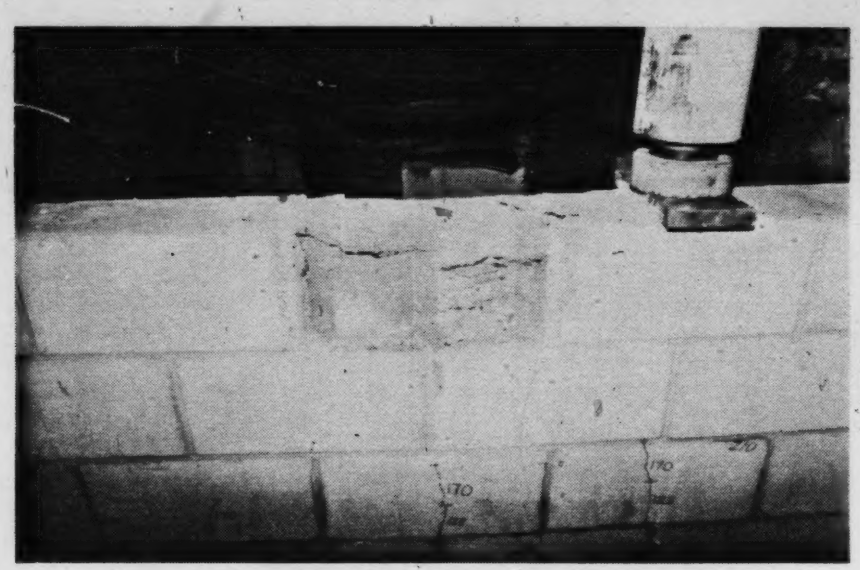

Plate 5.8 Failure of Beam RB2

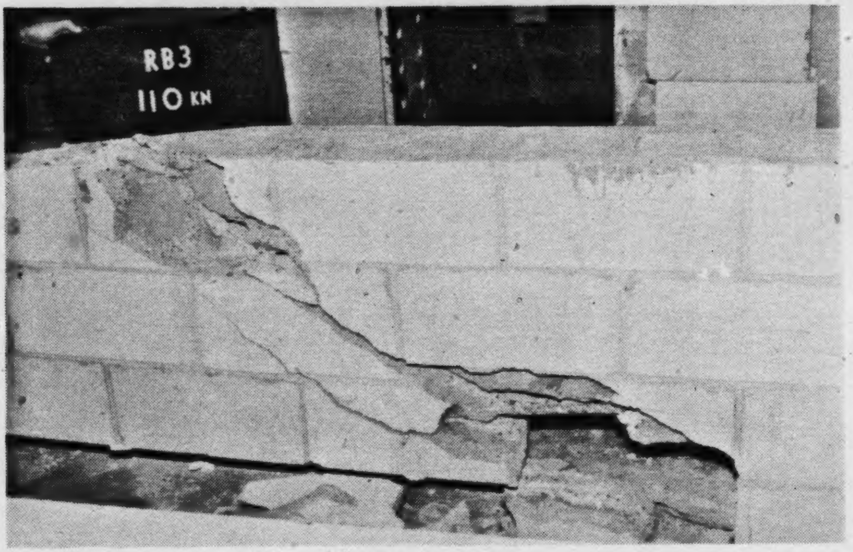

Plate 5.9 Failure of Beam RB3

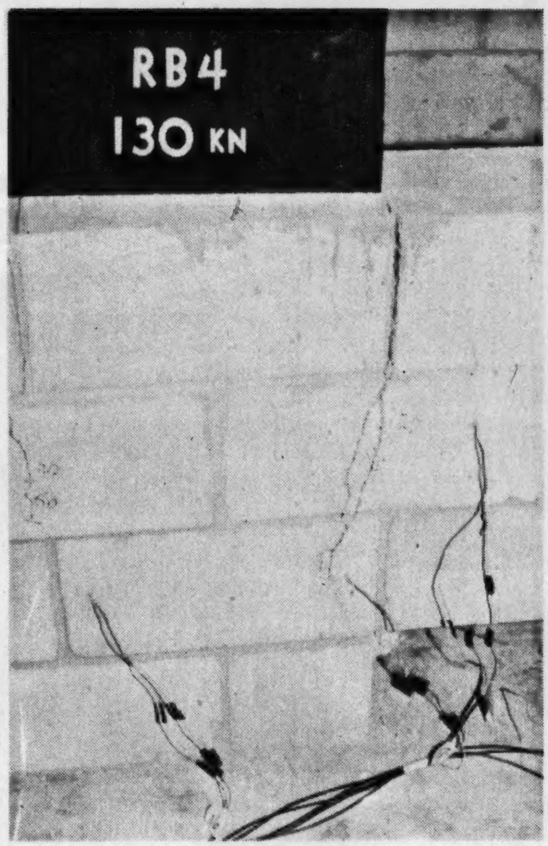

Plate 5.10 Cracks at North Support of Beam RB4

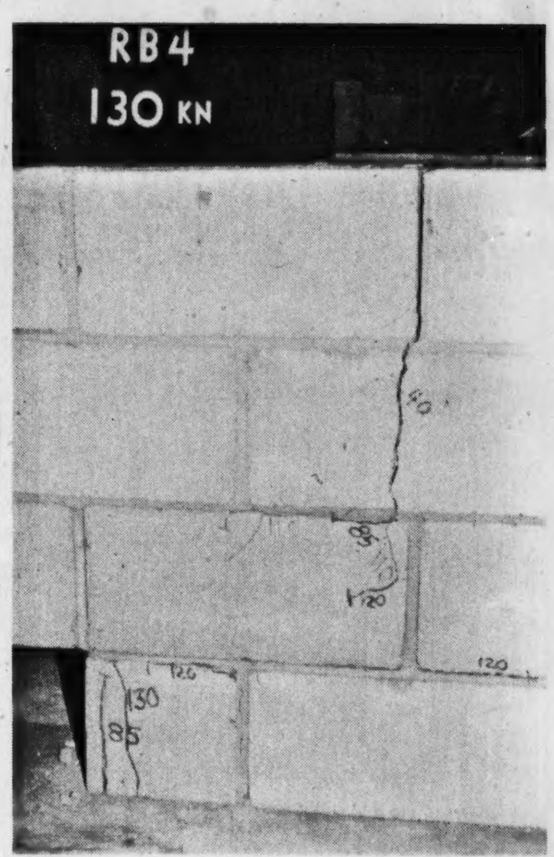
RB4
130 KN
40
85
120
120
120
130
85

Plate 5.11 Cracks at South Support of Beam RB4

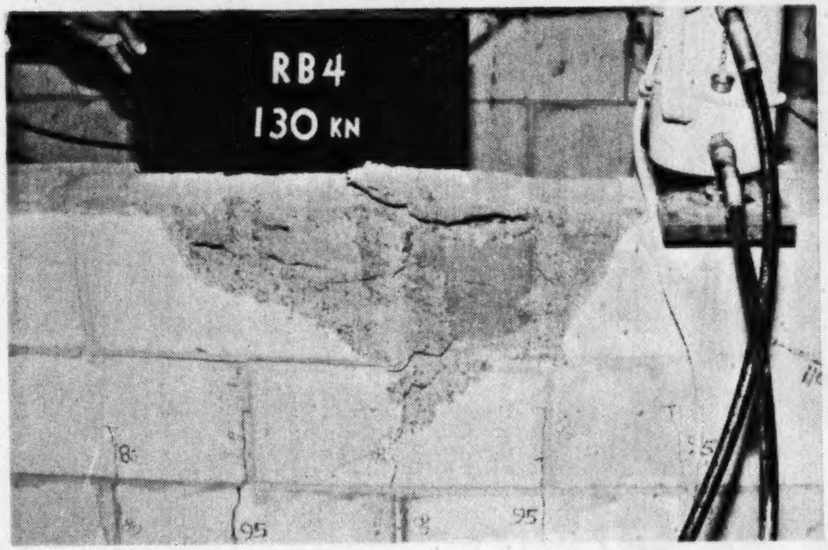
RB4
130 KN
8
95
95
95

Plate 5.12 Failure of Beam RB4

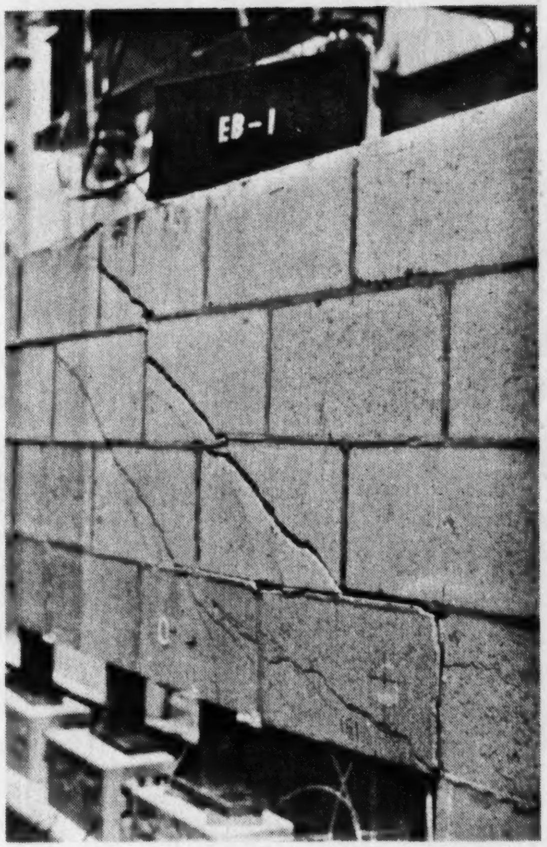

Plate 5.13 Failure of Beam EB1

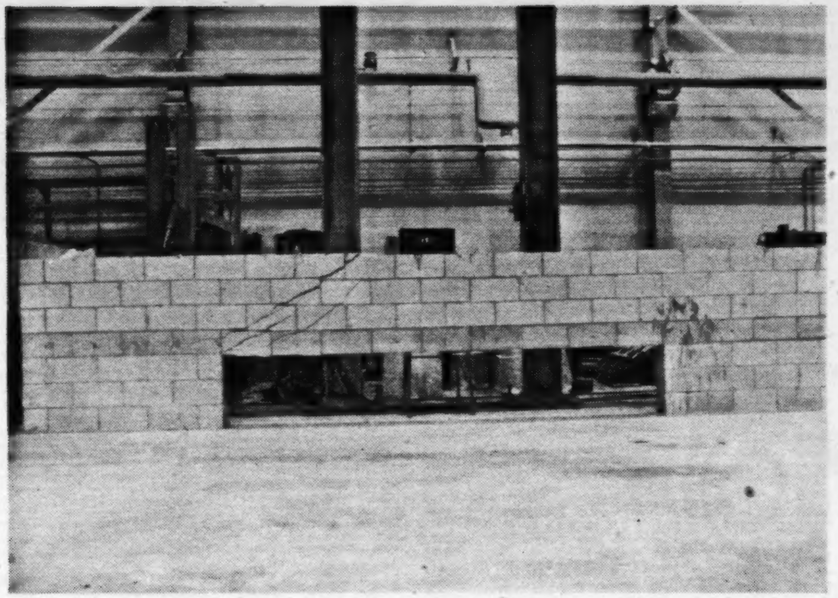

Plate 5.14 Beam EB1 after Test

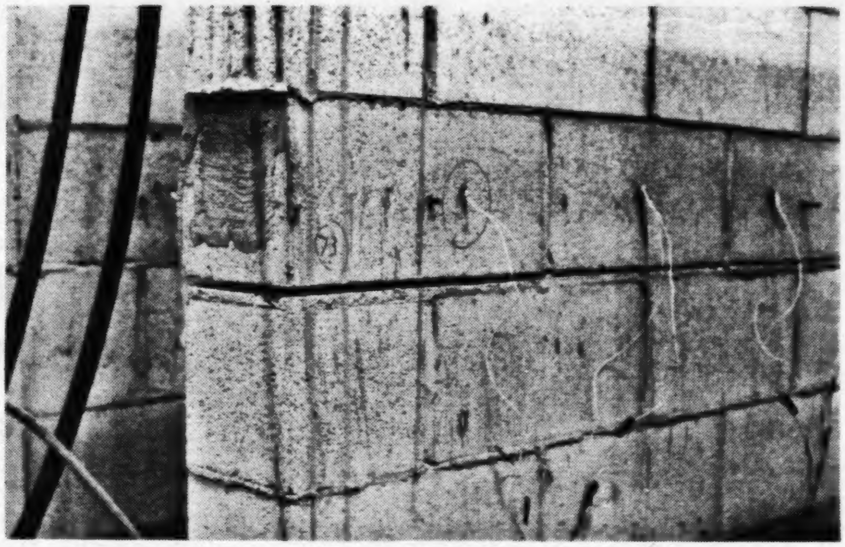

Plate 5.15 Crack at Interface of Beam EB2 and Supporting Wall

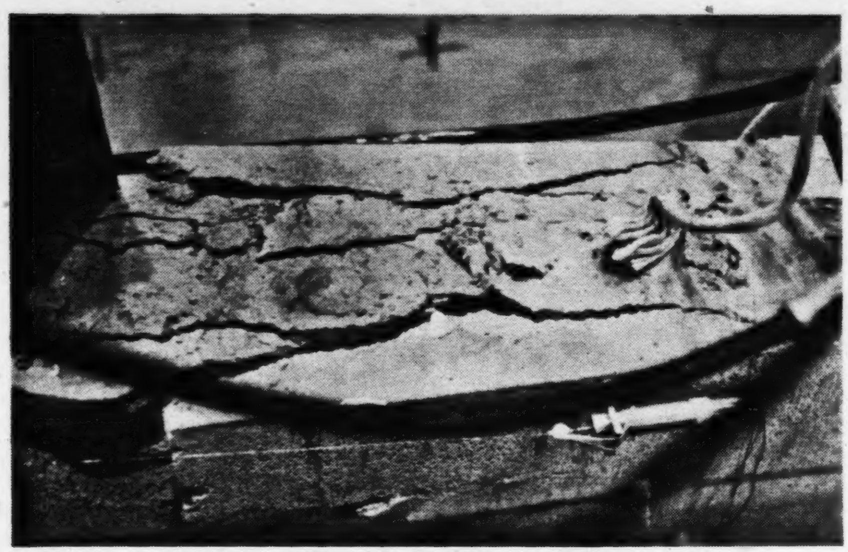

Plate 5.16 Failure of Beam EB2

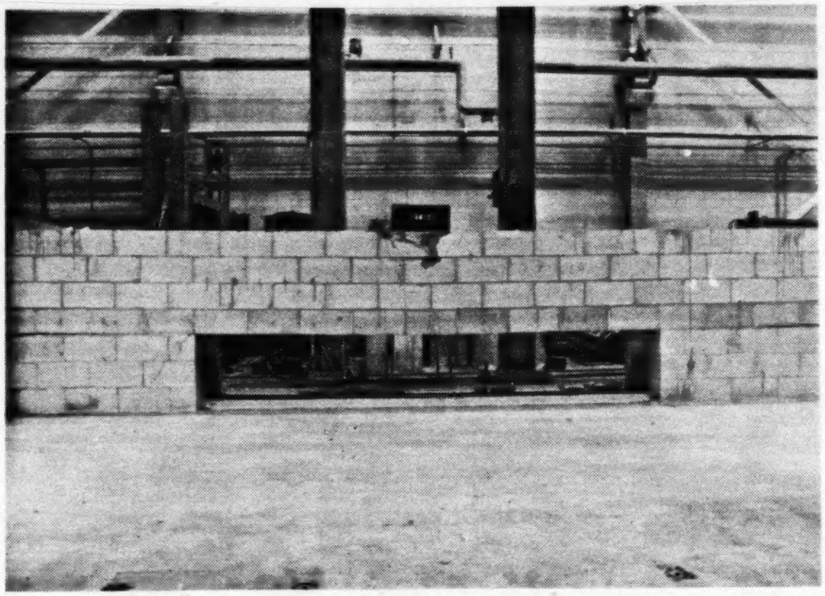

Plate 5.17 Beam EB2 after Test

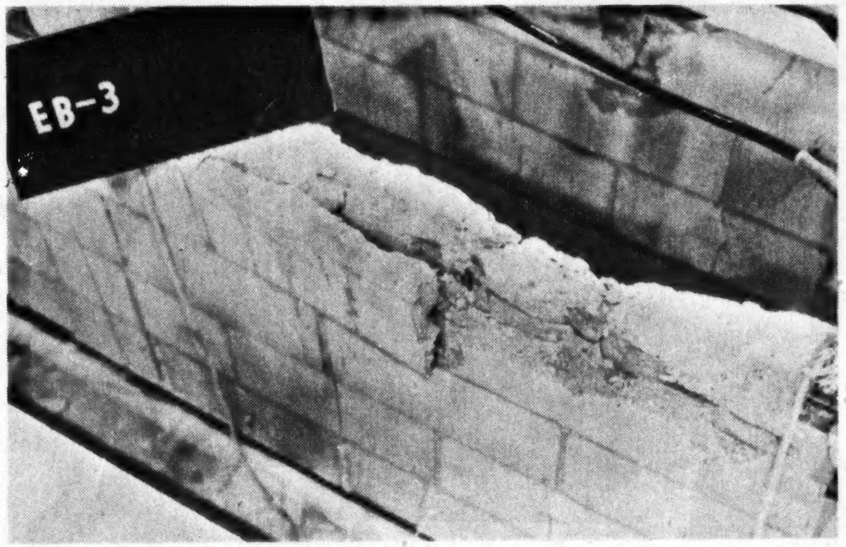

Plate 5.18 Failure of Beam EB3

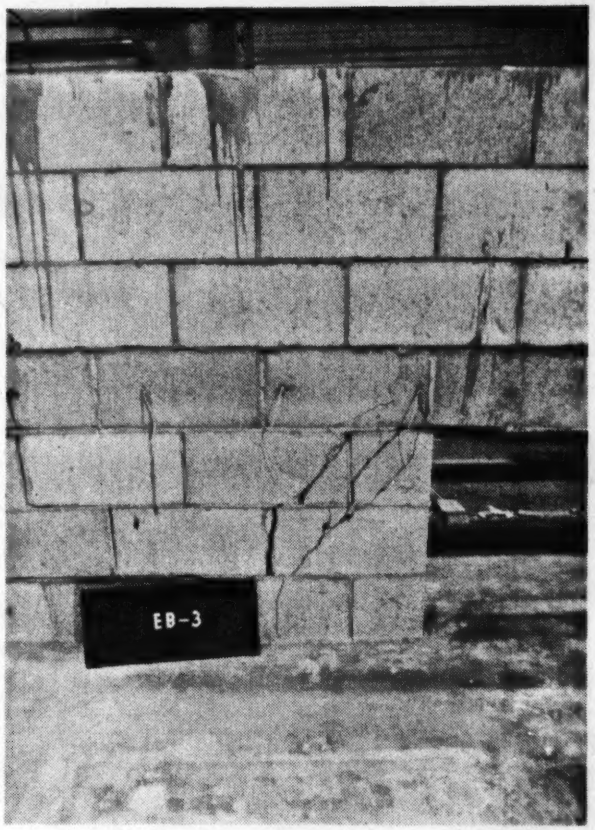

Plate 5.19 North Supporting Wall of Beam EB3 after Test

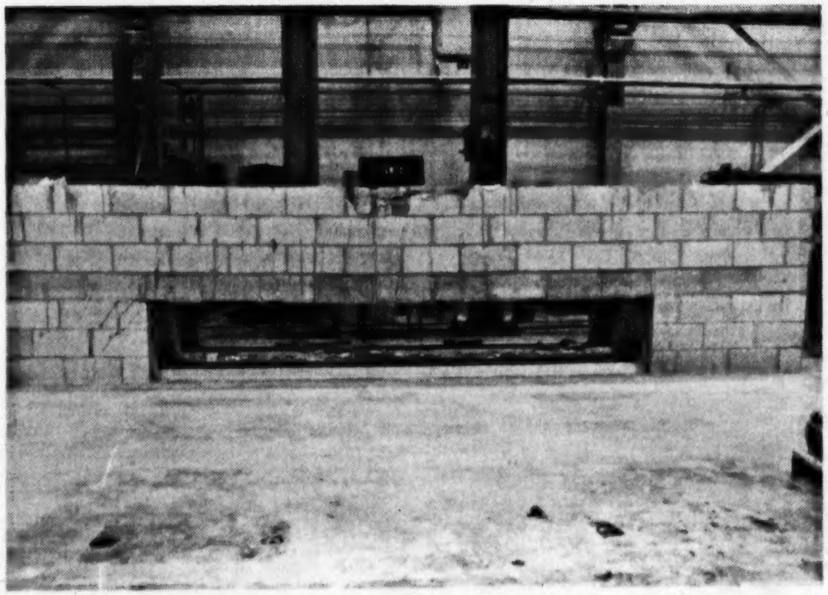

Plate 5.20 Beam EB3 after Test

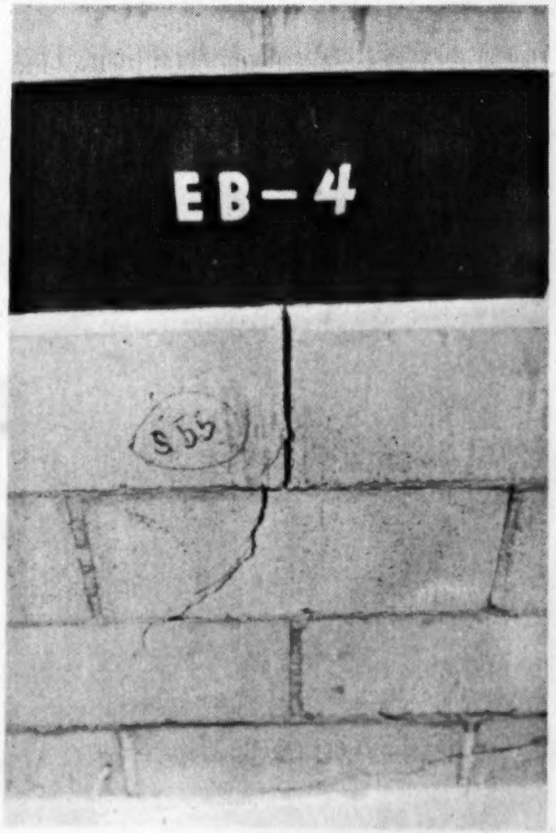

Plate 5.21 Cracks above South Support of Beam EB4

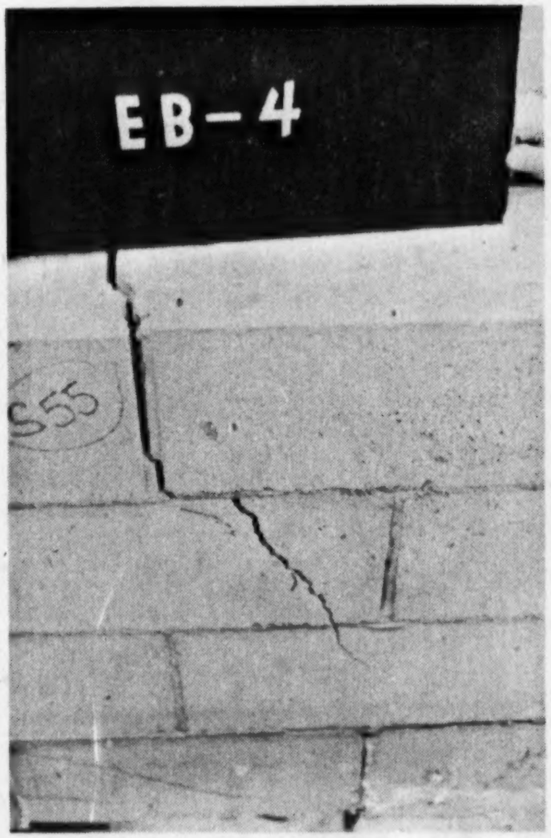

Plate 5.22 Cracks above North Support of Beam EB4

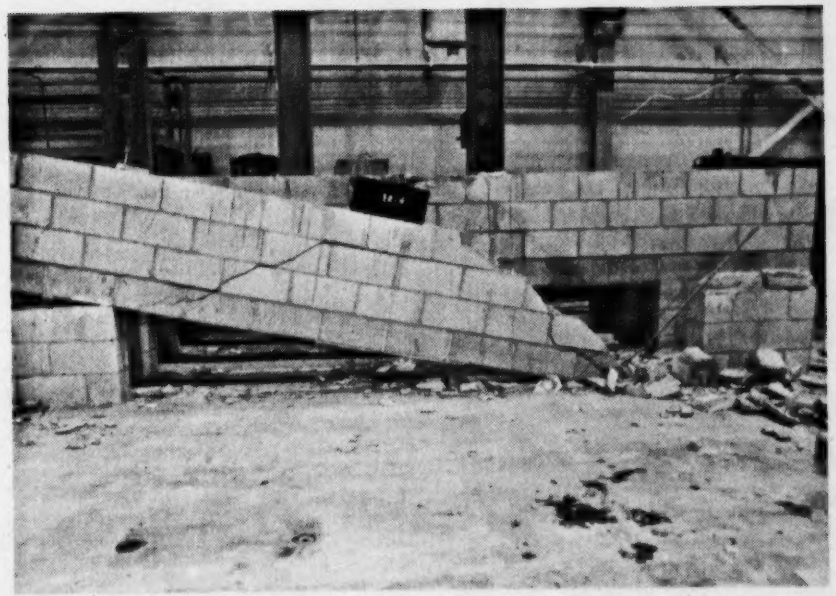

Plate 5.23 Beam EB4 after Test

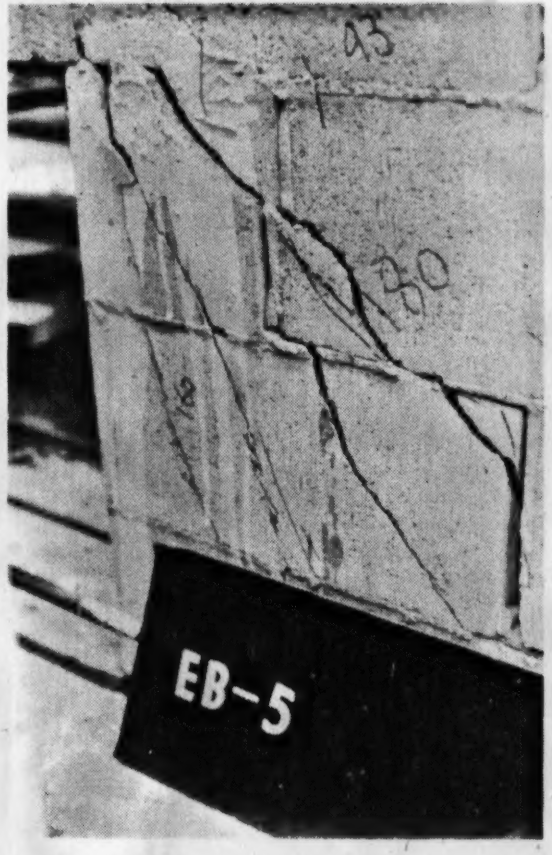

Plate 5.24 South Supporting Wall of Beam EB5 after Test

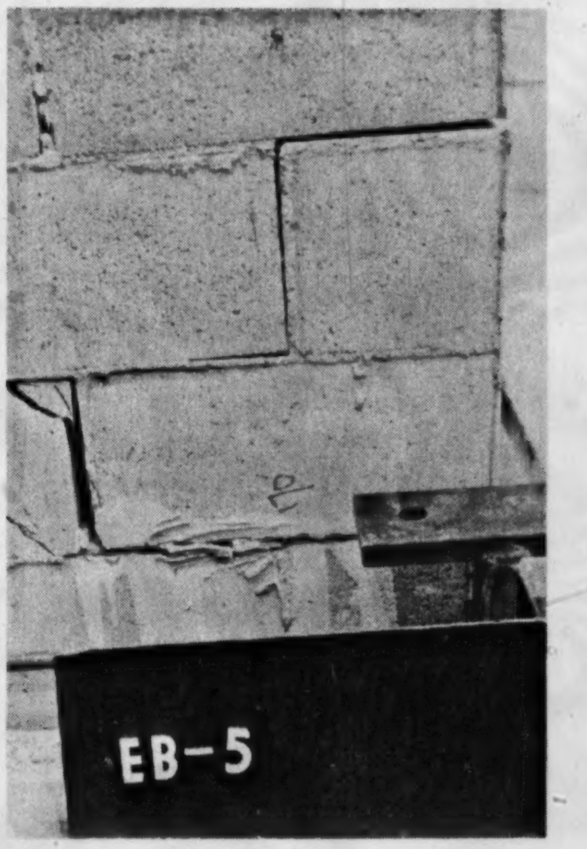

Plate 5.25 South Supporting Wall of Beam EB5 after Test

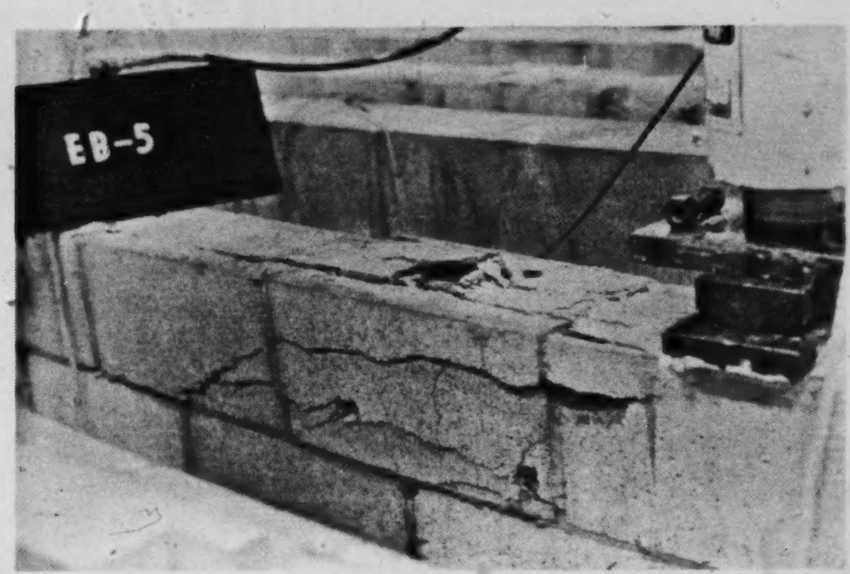

Plate 5.26 Failure of Beam EB5

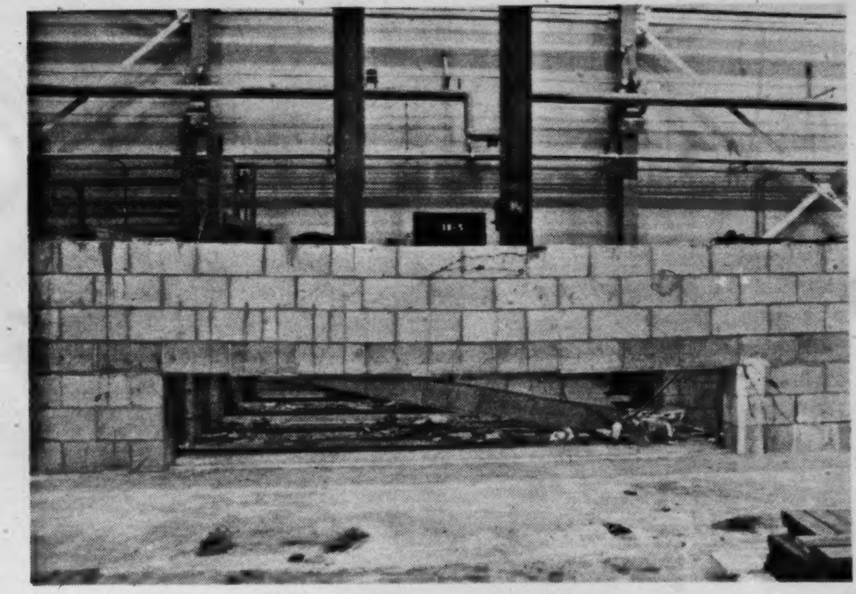

Plate 5.27 Beam EB5 after Test

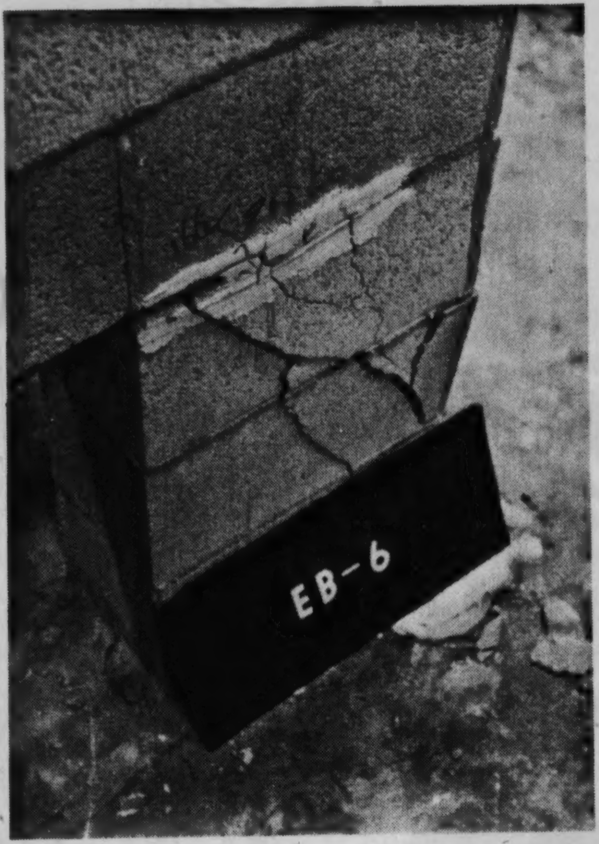

Plate 5.28 South Supporting Wall of Beam EB6 after Test

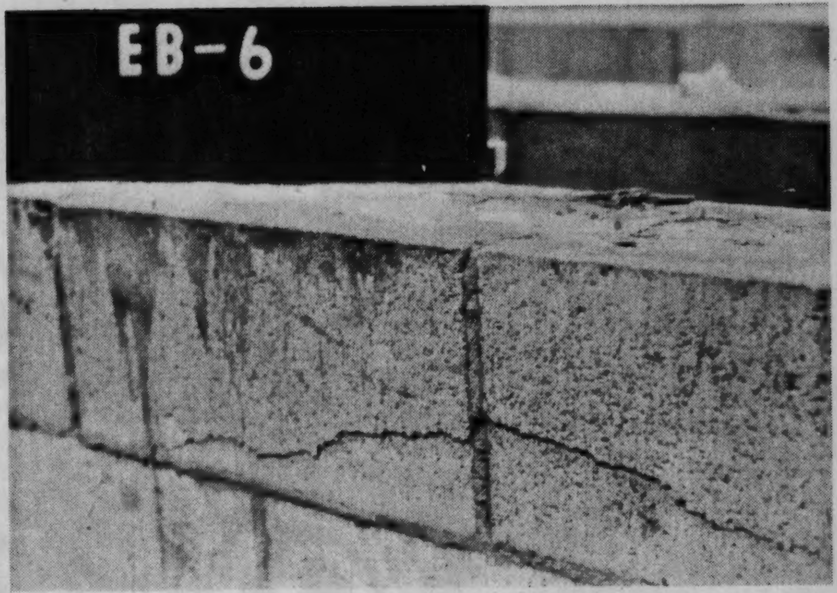

Plate 5.29 Failure of Beam EB6

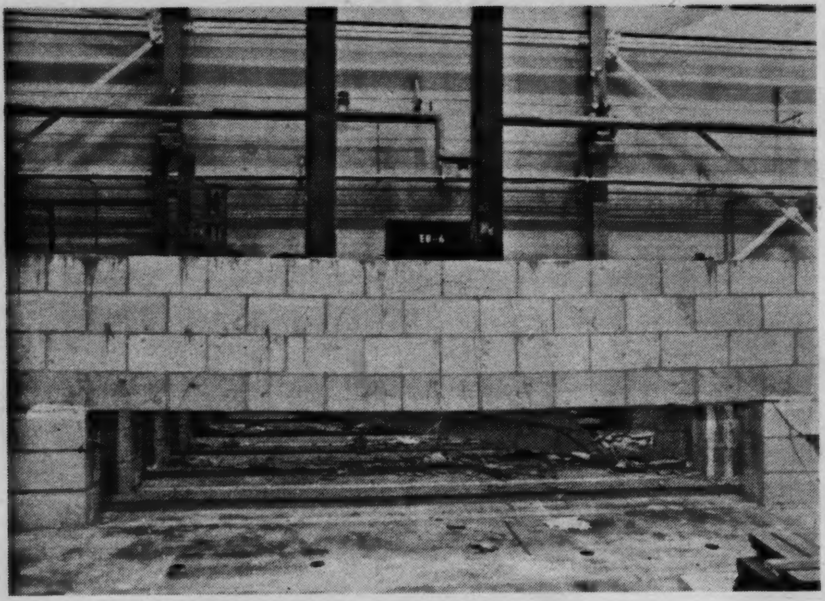

Plate 5.30 Beam EB6 after Test

6. Discussion of Beam Test Results

6.1 Introduction

In this chapter, a discussion of the test results for the unrestrained and restrained beams is presented. The first part deals with the experimental results for unrestrained beams, the second part compares the behavior of unrestrained and restrained members and the third part applies existing theories to predict the magnitude of restraining forces and the capacity of restrained beams. For the unrestrained beams, test results are interpreted and compared with calculated values based on existing theories for reinforced concrete. Analytical values are based on the two different material properties obtained from prism tests in the two different orientations, i.e., f'_{mn} and E_{mn} for load normal to the bed joints (obtained from prisms in the first and second series), and the f'_{mp} and E_{mp} for load parallel to the bed joints (obtained from prisms in the third series). Because the strength of mortar in the masonry prisms was lower than that in the beam specimens, the material properties obtained from the prism tests are not expected to be the same as those of the beams.

6.2 Failure Mode - General Remarks

The grout readily filled the voids in each concrete block from the bottom to the top of all beams. However, even though the grout was quite fluid, it is questionable if the vertical spaces between the masonry units were completely filled. Thus, for those beams built in running bond, imperfections may have been present in terms of vertical planes of weakness spaced at half block lengths. Therefore, flexural cracks initiating at the bottom of the beams would tend to propagate rapidly upward along these planes of weakness. It was actually observed that flexural cracks were spaced at approximately 200 mm (one half a block length) and extended almost up to the top course in most beams.

Shear cracks usually developed across the blocks and sloped towards the load points and the supports. However, some shear cracks ran either along the horizontal bed joints or the vertical head joints. This is probably due to the local variations in the strength of masonry and the imperfections in grouting as already mentioned.

In all beams, longitudinal cracks at the interface of the face shell and the grout at the top of the beams were usually clearly visible when the applied load was close to the maximum value. Crushing in the compressive region usually consisted of crushing of the mortar joints, followed by spalling of face shells and finally crushing of the grout. This may imply that true composite action does not exist in this region and the compressive stress may not be distributed evenly between the grout and the blocks. This may be due to the difficulty in grouting the small void between the masonry units resulting in the concentration of compressive force mainly on the two face shells.

Except for Beams EB5, EB2 and RB2, failure of beams with web reinforcement was due to tension steel yielding followed by crushing in the compressive zone. Beams EB5 and EB2 failed when the steel stress was a little less than the yield stress while Beam RB2 failed when the steel stress was much below the yield stress. Yielding of the web reinforcement was not detected in any of the beams at the strain gauge locations.

For beams with no shear reinforcement, failure was due to diagonal tension with the longitudinal steel remaining below yield except in Beam SB3. A comparison of crack patterns for Beams SB3 and RB3 indicates that the inclined cracks developed in the restrained beam at a higher load than that for the unrestrained beam. Obviously, this is due to the compressive forces acting at the end of the restrained beam. The maximum shearing stresses in these beams just before failure are tabulated in column 3 of Table 6.1.

A comparison of Beams SB4 and SB3 (Table 5.1) indicates that they have the same yield load and approximately the same maximum load. However Beam SB3 failed in a shear mode whereas Beam SB4 failed in a flexural mode. This implies that the shear capacity and the flexural capacity of this beam were close to the same value. The introduction of web reinforcement changed the failure mode but the capacity remained approximately the same. However, the behavior of the restrained counterparts was different, the capacity of Beam RB3 was only 110.3 kN while that of RB4 was 135.3 kN. The introduction of web reinforcement in this case not only changed the failure mode but also assisted in developing a higher capacity.

For Type EB beams with web reinforcement (Beams EB2, EB3, EB5 and EB6), the support walls cracked seriously at about the maximum load. Such support wall failure was not observed in other beams without web reinforcement (Beams EB1 and EB4) as the maximum vertical applied load was lower. The cracking in the support wall is likely a tension failure of the masonry due to the large vertical applied load and the high frictional force developed at the interface of the wall and the beam.

Table 6.2 tabulates the ratio of maximum loads for restrained beams to those of the unrestrained counterparts. Clearly, the ratio increases as the depth of beam increases. A ratio of 1.50 compared with 1.18 indicates the importance of web reinforcement in increasing the capacity of a restrained beam. The ratio for Type EB beams are lower than that of Beam RB2. This is expected, since the restraint provided by the short support walls is lower than that provided by the fixed abutments.

The load versus reinforcement strain relationships for Type RB beams, as shown in Figures 5.32 to 5.35, indicate that maximum compressive stresses always occur at the edge of the supports. Figures 5.36 to 5.39 for Type EB beams indicate that very small compressive strains were developed.

6.3 Cracking Moments for Simply Supported Beams

In the initial loading stages, the steel strain curves were nearly linear and the strains were quite small, as shown in Figure 5.29. The masonry in the tension zone effectively contributed in resisting the applied moment until tension failure occurred with the formation of the first flexural cracks. The load at which the first crack occurred corresponds with the load at which there is a sudden change in the slope of the steel strain curve. These cracking loads were approximately equal to 7.7 kN for Beam SB1, 18.2 kN for Beam SB4 and 30.2 kN for Beam SB2. Including the effect of beam dead weight, the total external moment at cracking was 11.4 kN.m for Beam SB1, 25.1 kN.m for Beam SB4 and 40.6 kN.m for Beam SB2.

With the use of Equation 2.2 and two values of f'_m, namely f'_{mn} and f'_{mp}, cracking moments can be estimated. The test and the computed results are shown in columns 4, 5 and 6 of Table 6.1 and also plotted in Figure 6.1. It is observed that the difference in cracking moments based on f'_{mn} and f'_{mp} increases as the beam depth increases.

Moreover, the computed values based on f'_{mp} are in better agreement with the test results. This suggests that the cracking moment for masonry beams may be obtained by means of Equation 2.2, in which the value of f'_m is taken as f'_{mp}.

6.4 Location of the Neutral Axis

Assumming the strain is linearly distributed, the location of the neutral axis can be determined from surface strains in the constant moment region. The relationship between the applied load and the position of the neutral axis above the longitudinal reinforcement is shown in Figures 6.2 to 6.4 for Type SB, RB and EB beams respectively. For all beams, the neutral axis moved rapidly upward as maximum load was approached.

Based on prism tests, the modular ratio n equals 16 for load perpendicular to the bed joints and 45 for load parallel to the bed joints. Neutral axis locations for simply supported beams based on these two values can be determined with the use of Equation 2.3 and computed values are plotted in Figure 6.2. There is fair agreement between the location obtained from measured strains and the location calculated with $n = 45$. This suggests that the modulus of elasticity, E_{mp}, obtained from prisms loaded parallel to the bed joints is an appropriate value to be used in calculations for deformations of masonry beams.

It should be noted that the location of the neutral axis based on surface strain measurements is probably higher than the true location, because the surface strain measurements are not very dependable. This is especially true of the measurement at the level of the longitudinal reinforcement, where the gauge length could include a number of flexural cracks. Moreover, the strain may not be distributed linearly.

The surface strain curves presented in Figures 5.48 to 5.61 indicate that the compressive strains at the top of the beams increased practically linearly with the applied load almost up to the failure load.

6.5 Simply Supported Masonry Beams in the Service Load Range

The behavior of a singly reinforced masonry beam is clearly illustrated by the relation between the applied load and the strain in the tension reinforcement at mid-span, as shown in Figure 5.29. As the load was increased, the steel strain increased very slowly until the flexural cracks appeared, and then the strains increased more rapidly but linearly until the beam failed.

In order to predict the steel strain at a known beam load, the straight line-no-tension theory may be used. Applying Equation 2.8 and the two moduli of elasticity, E_{mn} and E_{mp}, the steel strains can be predicted. Test results and computed values based on the two moduli values are plotted in Figures 6.5 to 6.7 for the three simply supported beams. The computed values based on E_{mp} are in very good agreement with test results. The disagreement in the initial loading range is expected since the computed values are based on the assumption that masonry cannot withstand tensile stress.

From a comparison of the test results and the computed values, we can conclude that:

1. A linear stress-strain relationship can be used to predict the reinforcement strain in a masonry beam at a known service load.
2. The modulus of elasticity to be used in calculation of service load and deflection of masonry beams is the modulus determined from prism tests in which load is applied parallel to the bed joints.

6.6 Ultimate Strength of Simply Supported Beams

For all the simply supported beams containing shear reinforcement, the maximum capacity was reached when crushing of the masonry occurred after the tension reinforcement yielded. Thus the flexural strength of the section was reached when the strain in the extreme compression fiber reached its ultimate strain.

In order to predict the ultimate capacity of masonry beams, an approach similar to that used in reinforced concrete appears appropriate. Using Equation 2.12, resisting moments were computed based on the two compressive strengths, f'_{mn} and f'_{mp}. Values of the observed maximum bending moments and the calculated maximum resisting moments are tabulated in Table 6.1 (columns 7, 8 and 9).

A comparison of the test and computed moments indicate that the capacity of masonry beams can be reasonably predicted using Whitney's rectangular stress block if the prism strength normal to the bed joints, f'_{mn}, is used. However, one would expect that the capacity would be best predicted by the prism strength parallel to the bed joints, f'_{mp}. This discrepancy may be due to the fact that the strength of the mortar in the prisms was significantly lower than that in the beams.

Since crushing of the masonry always initiated at the mortar head joints partly due to the imperfection as already discussed in Section 6.2, it seems that the strength of mortar is an important parameter in the stress-strain behavior in the compression region. Further investigation into the flexural strength of concrete masonry is required to establish if the stress distribution used in reinforced concrete is suitable for the prediction of the ultimate strength of masonry beams.

6.7 Deflection of Simply Supported Beams

In the initial loading stage, a masonry beam is uncracked and the moment of inertia or the flexural rigidity is large resulting in a very small deflections. After the formation of flexural cracks, the rigidity of the beam decreases and the rate of deflection increases. The experimental load-deflection curves indicate that after the formation of initial flexural cracks, the behavior is practically linear.

For Beam SB3 (beam without web reinforcement), the load deflection ralationship is similar to that for Beam SB4 (beam with web reinforcement) up to about 75 kN, as shown in Figure 6.8. Beyond that load, the deflection curve of Beam SB3 changes suddenly, with the curve become concave upward probably due to the opening and widening of the diagonal shear cracks.

Due to the lack of experimental data and the complex interaction of the constituents, prediction of deflections of masonry beams is difficult. In this study, deflections at working loads are compared with computed values based on the approach used in reinforced concrete.

For third point loading, the immediate centerline deflection (Δ) caused by service loads can be calculated using the equation

$$\Delta = \frac{23PL^3}{648EI} \qquad (6.1)$$

where

EI = flexural rigidity

The moment of inertia, I, depends on the extent of cracking at the load level considered. Based on the cracking moments observed in the tests and the effective moment of inertia based on Equation 2.13, deflections were computed for the two different modulus values, E_{mn} and E_{mp}. The computed and measured deflections are presented in Figures 6.9 to 6.11. Deflections based on E_{mp} are in closer agreement with measured values than those based on E_{mn}. For working loads, the computed deflections based on E_{mp} are conservative.

Equation 2.13 for the determination of effective moment of inertia was developed for reinforced concrete based on uniformly distributed loading. Since the cracking of masonry beams is different than that of reinforced concrete beams, the use of Equation 2.13 may be questioned. Moreover, the moment of inertia along the beam is actually varying and approaches the uncracked moment of inertia at both supports. Deflections based on an I value calculated by means of Equation 2.13 are not expected to be in good agreement and would overestimate the observed values. Further study of the effective moment of inertia of masonry beams is needed.

With $E = E_{mp}$, the calculated load-deflection curves based on uncracked and cracked moment of inertia, together with the experimental curves are plotted in Figures 6.12 to 6.14. It is observed that the experimental curves are roughly bounded by the two calculated curves.

6.8 Effect of End Restraint on the Load-Deflection Relationship for Masonry Beams

A comparison of the centerline deflections presented in Table 5.2 indicates that the unrestrained beams (Type SB beams) were more ductile and attained larger deflections at ultimate load than their restrained counterparts. Figure 6.15 shows the load-deflection relationships for Type SB and Type RB beams. The simply supported beams exhibited an almost linear relation between applied load and midspan deflection, as is typical of under-reinforced concrete beams. After the tension reinforcement yielded, the applied load remained almost constant while the deflection increased significantly. Final collapse occurred when the applied load was slightly higher than the yield load. The behavior of the restrained beams was quite different from that of the unrestrained beams. In the initial stage of loading, although the relation is quite linear, the curves are much steeper than those for the Type SB beams. Clearly, this is due to the presence of horizontal restraining forces. For Beam RB2, the load-deflection relation is approximately linear up to a load close to the maximum. However, at slightly above 50% of the maximum load, the load-deflection relations for Beams RB4 and RB1 change suddenly and slope almost parallel to those for their simply supported counterparts. The difference between the load carrying capacities for the restrained and simply supported beams increases with increasing beam depth.

Figure 6.16 shows the load-deflection relationships for Type SB, RB and EB beam specimens having a depth of four courses. The curves for Type EB beams (beams supported on walls) fall above that for Beam SB2 and below that for Beam RB2. The behavior of Type EB beams can be roughly separated into two ranges. When the applied load is below 100 kN, the behavior of the Type EB beams is very similar to that of Beam RB2. When the load is above 100 kN, the behavior of the Type EB beams becomes very similar to that of Beam SB2. This probably indicates that the restraints provided by the supporting walls had reached a maximum when the beam load was about 100 kN.

6.9 Effect of End Restraints on the Load-Tension Reinforcement Strain Relationships

Figure 6.17 shows the load and midspan tension reinforcement strain relationships for Type RB and Type SB beams. For Type SB beams, masonry below the neutral axis acted in tension until the formation of the first flexural cracks, thus the initial portion of the curves are relatively steep. At higher loads, the tension force in the beam is mainly provided by the tension reinforcement and the behavior can be represented by straight lines passing through the origin. The maximum load is reached after the tension reinforcement has yielded. The behavior of the Type RB beams is different, in that the initial portion of the curves is much steeper, and the abrupt change in the slope occurs at a much larger load, indicating that the formation of the flexural cracks was delayed by the horizontal restraining force. Moreover, the behavior tends to be more rounded than bilinear as compared to the unrestrained beams. After the formation of flexural cracks, the behavior of Type RB beams is very different from that of Type SB beams. Although the load-strain relationships are still approximately linear, with the slope for Beam RB4 parallel to that for Beam SB4, the slope for Beam RB1 is less steep while that for Beam RB2 is much steeper than their simply supported counterparts. This probably indicates that the restraining force in Beam RB4 is fairly constant while that in Beam RB1 is continuously decreasing and that in Beam RB2 is continuously increasing up to the maximum load.

Figure 6.18 presents the load-strain relationship for all three beam types with the same depth. The curves for Type EB beams are all bounded below by the curve for Beam SB2 and above by that for Beam RB2. Cracking loads for Type EB beams are between those for Beam RB2 and SB2. After the Type EB beams cracked, their load-strain behavior is approximately linear with a slope equal to about the average of that for Beams RB2 and SB2.

6.10 Effect of Shear Reinforcement

In concrete block masonry beams, shear reinforcement is inserted in the voids of the concrete block units. Since the distance between the centres of the voids is 200 mm, the spacing of the stirrups has to be a multiple of 200 mm.

In the present study, single-leg stirrups with a cross-sectional area of 100 mm^2 were located in every void in both shear spans. Test results indicate that this shear reinforcement arrangement was sufficient to prevent diagonal tension failure. Beams failed in a flexural mode, but hairline shear cracks were evident in most of the beams at the conclusion of the tests.

Test results for Beam SB3 indicate that, for a beam without shear reinforcement, it was possible to stress the longitudinal steel to its yield point prior to diagonal tension failure when the amount of tension reinforcement was 0.64%.

As can be observed from Figures 5.40 to 5.47, practically no strain was recorded in the stirrups except in that stirrup located closest to the load point. This stirrup exhibited a sudden increase in strain at a particular load level, probably indicating that diagonal tension cracks propogated across the section where the stirrup was located.

The following discussion relates to strains in the stirrups closest to the load points. Load-strain curves for Type RB and Type SB beams are shown in Figure 6.19. The abrupt change in the strain readings for Type RB beams occurred at a much higher load level than that for their simply supported counterparts and the difference increased as the number of courses (depth of beam) increased. Almost no strain was recorded in stirrups in Beam RB2 while the stirrup strain in Beam SB2 almost reached yield at maximum load. This indicates that the formation of diagonal tension cracks is delayed by the horizontal restraining force.

Figure 6.20 shows the load-strain relationships for the Type SB, RB and EB beams with a depth of 4 courses. This figure indicates that the behavior of the shear reinforcement is affected by the amount of restraining force present. The strain curves for Type EB beams fall between that for Beam RB2 which had the highest restraint and that for Beam SB2 which had the lowest restraint. This indicates that some restraining force did occur for the beams resting on walls.

In order to show the difference between the shear stress in the beam and the stress in a stirrup at the same section, values of shear stress, based on V/bd and values of the stress in the stirrup, as determined by Equation 2.16 were calculated for each beam and are shown in Figures 6.21 to 6.27. Clearly, the difference between the actual stress in the beam (v) and the stress in the stirrups (v_s) is very large for Type RB and EB beams. However, the difference is much less for Beam SB4 and for Beam SB2 in which the difference is practically equal to zero near maximum load.

However, the computed stirrup stresses are obtained from the strains measured at mid-depth of the beam, whereas diagonal tension cracks may not cross the stirrup at that same position. Although the stirrup stress cannot be determined at the diagonal tension cracks, the calculated stirrup stresses are a lower bound.

6.11 Ultimate Capacity of Restrained Masonry Beams

Section 2.4 described the use of a three-hinged arch model for analyzing conditions in a restrained beam. In order to apply the model it is necessary to approximate the stress at the failure points and the depth of bearing. Since the prism strength normal to the bed joints, f'_{mn}, provides a satisfactory basis for predicting the ultimate capacity of the simply supported beams, it is also used to establish a value for the stress at the failure points in a restrained beam. The depth of thrust is assumed equal to 20% of the depth of the beam. On the basis of these assumptions, the failure moment based on arching action can be computed. The computed moments with and without considering the deflections are giving in columns 5 and 6 of Table 6.3. The close agreement between test and computed results especially for Type RB beams suggests that three-hinged arch action based on suitable assumptions can be used to predict with reasonable accuracy the ultimate capacity of restrained beams. Deflection has a very slight effect on the computed failure load and can be neglected in the computations.

6.12 End Restraint

The present study is not primarily concerned with determining the magnitude and location of restraining forces. However, based on the data obtained from the tests and with the use of Equations 2.24 and 2.27, the magnitude of the restraining forces can be estimated.

In order to apply Equations 2.24 and 2.27, the location of the longitudinal force must be known. However, this location cannot be directly determined from the data obtained from the tests. If we assume that the compressive stress at the support varies linearly below the centroid, as shown in Figure 6.28(a), the resultant force acts at approximately 32 mm above the steel for Beam RB2 and at approximately 35 mm below the steel for Beam RB1. However, crack patterns and reinforcement strains at the edge of the support indicate that cracks extended down to the level of steel long before maximum load was reached. Thus the section above the steel would not resist any compressive stress and it is possible that the compressive stress was only distributed from the bottom of beam to the level of steel, as shown in Figure 6.28(b). Therefore, the location of the axial force is assumed to be at two-thirds of the distance from the level of steel to the bottom of beam for

Type RB beams. For Type EB beams, the restraining force is assumed to act at the bottom of the beam since it is the only location where restraining force actually exists.

With the above assumptions, the restraining force at ultimate load for all the beams can be computed by using Equation 2.27, with $a = 0.85c$. Values of computed restraining force and total compressive force at mid-span for each beam are tabulated in columns 7 and 8 of Table 6.3. The computed values shown in Table 6.3 indicate that the values of the total thrust used in Equation 2.18 (column 4 in Table 6.3) and the total compressive force determined by Equation 2.27 (column 8 in Table 6.3) are in fair agreemnet.

Using Equation 2.24, the restraining force for each specimen was computed at various load values. These computed restraining forces and the total compressive forces at mid-span are presented in Figures 6.29 to 6.31 for Type RB beams. The computed restraining forces for Type EB beams are plotted in Figure 6.32. This figure indicates that the magnitude of the restraint increases with increasing support wall length.

The calculated restraining forces for all Type EB beams are higher than the measured horizontal forces. This is to be expected since the measured forces did not include the frictional forces at the interface of the wall and the beam.

Table 6.1 Measured and Predicted Values

Beam	Failure Load (kN)	Shear Strength (N/mm²)	Cracking Moment			Failure Moment		
			Measured (kN.m)	Cal.* (kN.m)	Cal.** (kN.m)	Measured (kN.m)	Cal.* (kN.m)	Cal.** (kN.m)
1	2	3	4	5	6	7	8	9
SB1	50.9		11.4	10.5	13.2	61.1	45.6	60.6
SB2	153.0		40.6	44.5	54.7	183.6	145.7	160.7
SB4	90.3		25.1	25.2	30.7	108.4	95.7	110.7
SB3	93.2	1.00				111.8		
RB3	110.3	1.19				132.4		
EB1	156.8	1.20				188.2		
EB4	167.3	1.28				200.8		

* Using $f'_m = f'_{mp} = 7.1$ MPa
** Using $f'_m = f'_{mn} = 16.4$ MPa

Table 6.2 Ratio of Maximum Loads

Beam/Beam	Ultimate Load Ratio
RB1/SB1	63.4/50.9 = 1.25
RB2/SB2	241.1/153.0 = 1.58
RB3/SB3	110.3/93.2 = 1.18
RB4/SB4	135.3/90.3 = 1.50
EB2/SB2	208.9/153.0 = 1.37
EB3/SB2	196.0/153.0 = 1.28
EB5/SB2	183.9/153.0 = 1.20
EB6/SB2	191.0/153.0 = 1.25

Table 6.3 Measured and Predicted Values

Beam	Failure Load (kN)	Failure Moment (kN.m)	Predicted Values				
			$H=f'_{mn}bt$ (kN)	$H(h-t-\Delta)$ (kN.m)	$H(h-t)$ (kN.m)	F (kN)	C (kN)
1	2	3	4	5	6	7	8
RB1	63.4	76.1	243	69	76	85	334
RB2	241.1	289.3	493	305	312	281	495
RB4	135.3	162.4	368	166	174	158	408
EB2	208.9	250.7	413	256	261	154	402
EB3	196.3	235.6	"	"	"	115	375
EB5	183.9	220.7	"	255	"	94	343
EB6	191.0	229.2	"	254	"	93	353

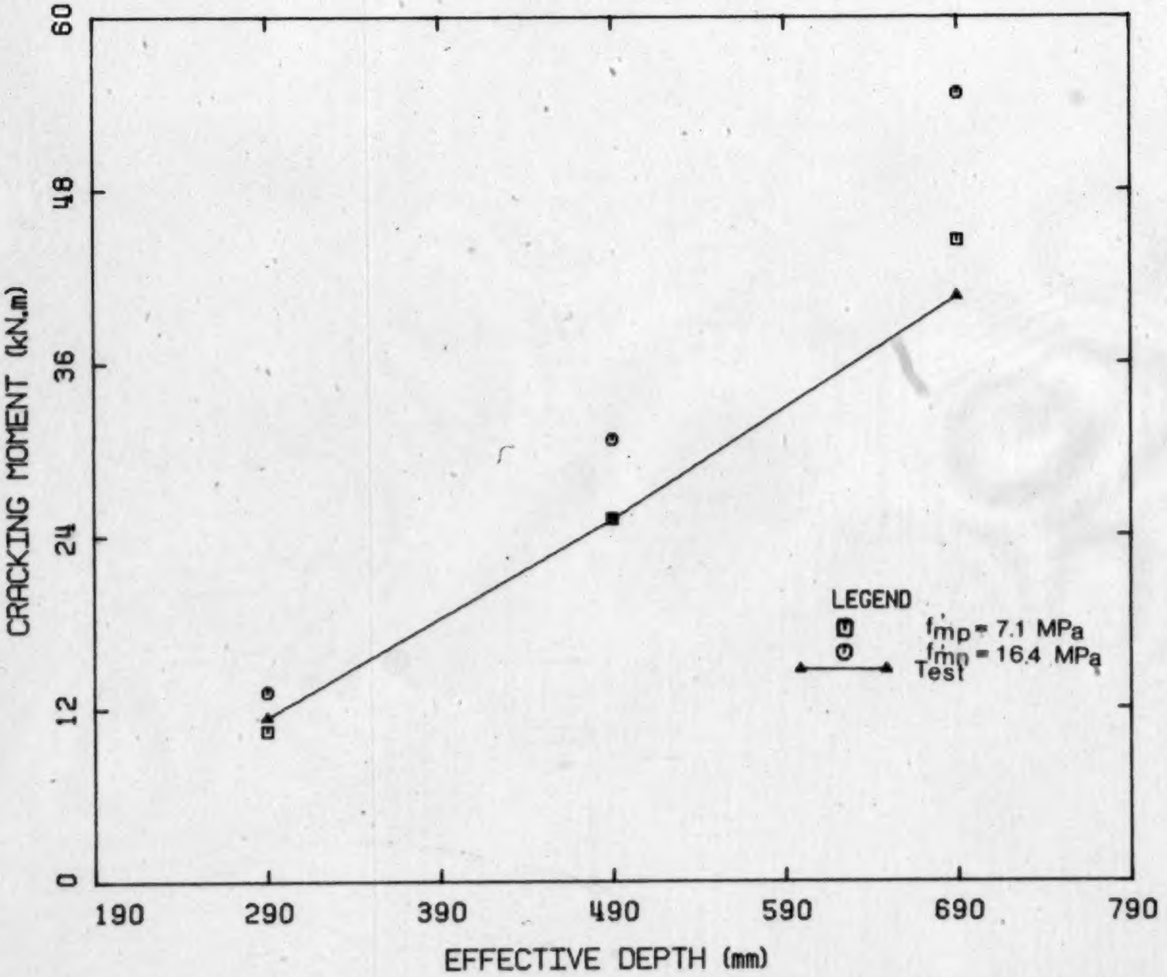

Figure 6.1 Cracking Moment versus Effective Depth of Simply Supported Beams

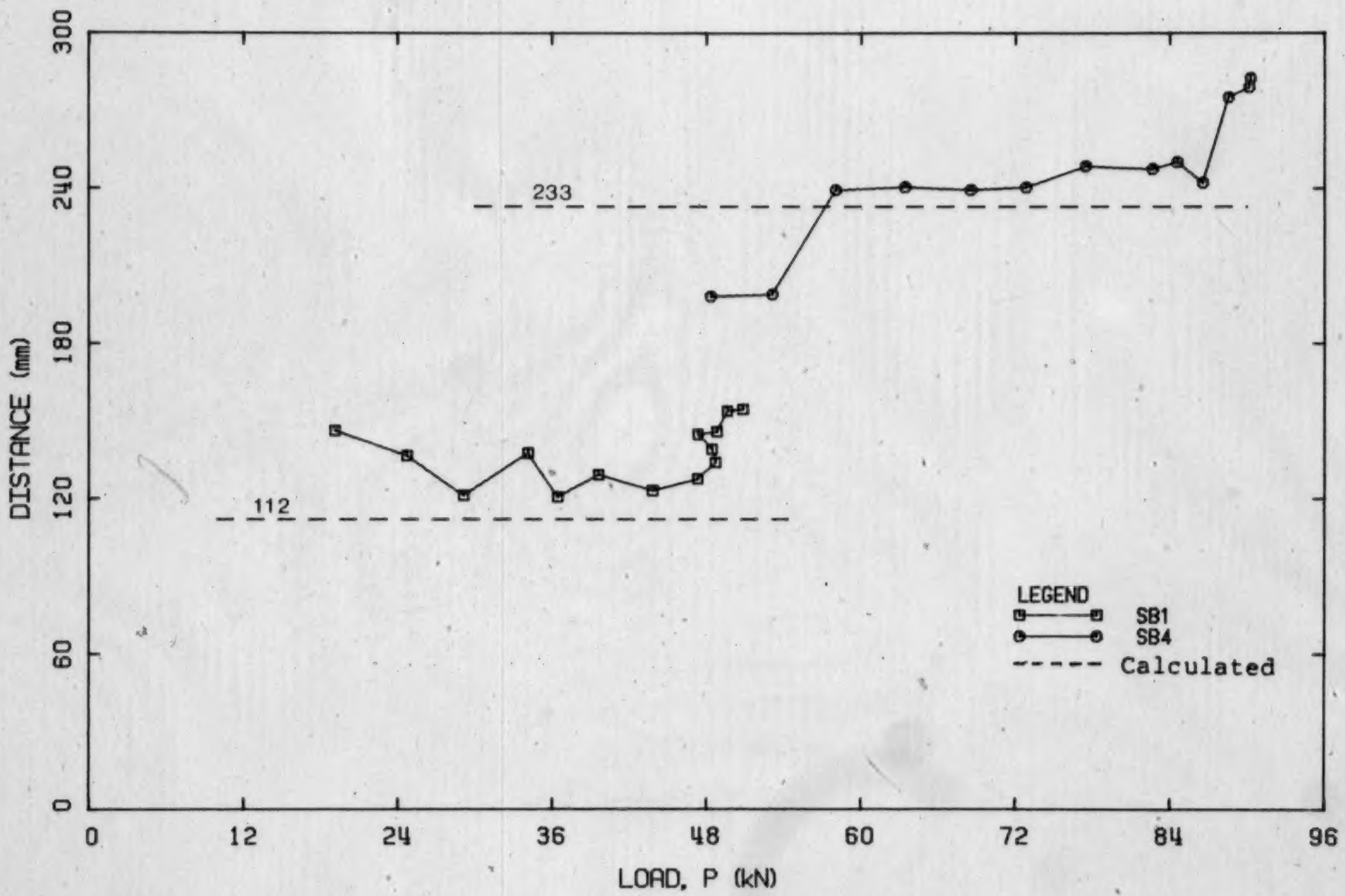

Figure 6.2 Neutral Axis Position in Type SB Beams

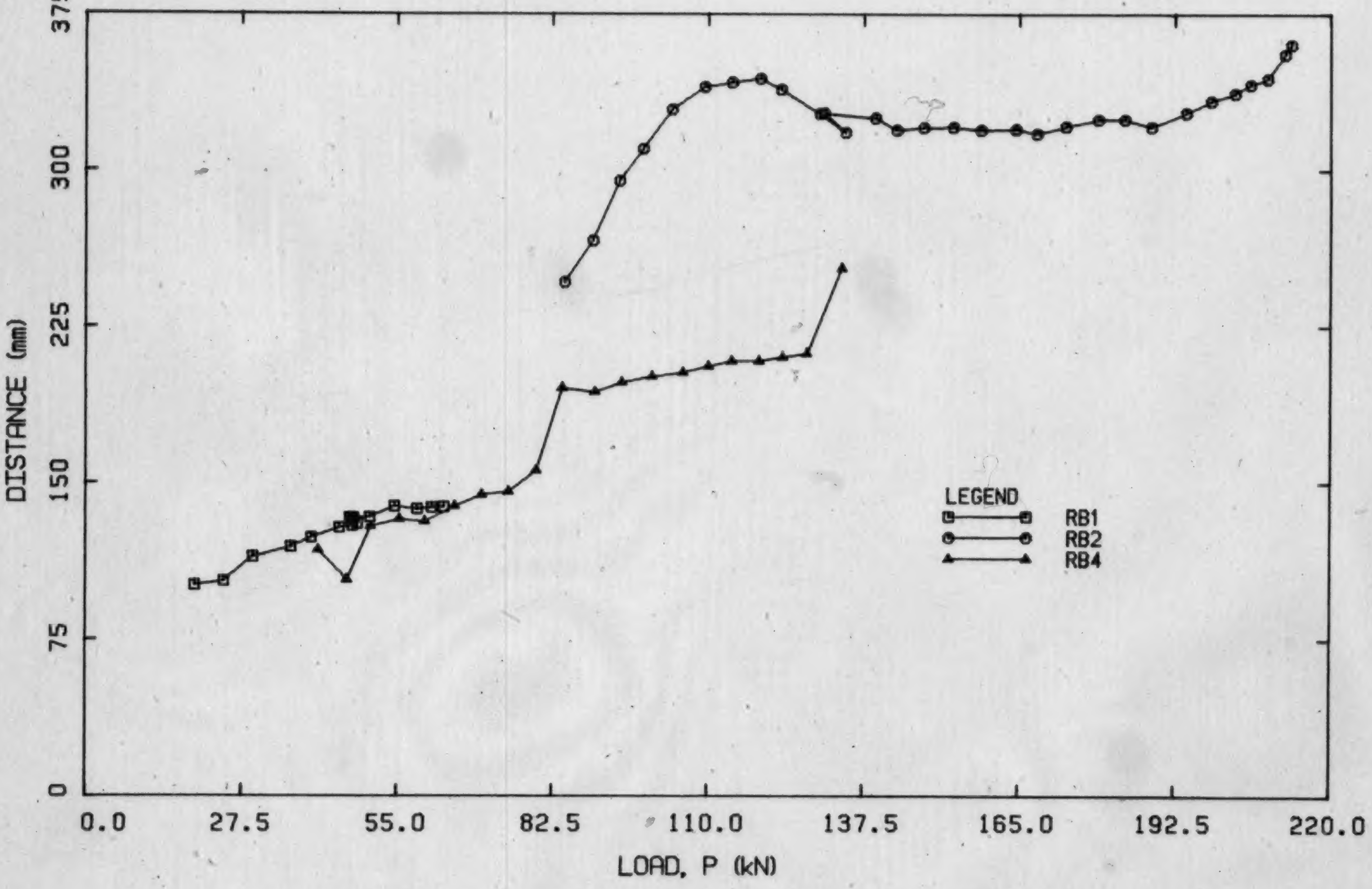

Figure 6.3 Neutral Axis Position in Type RB Beams

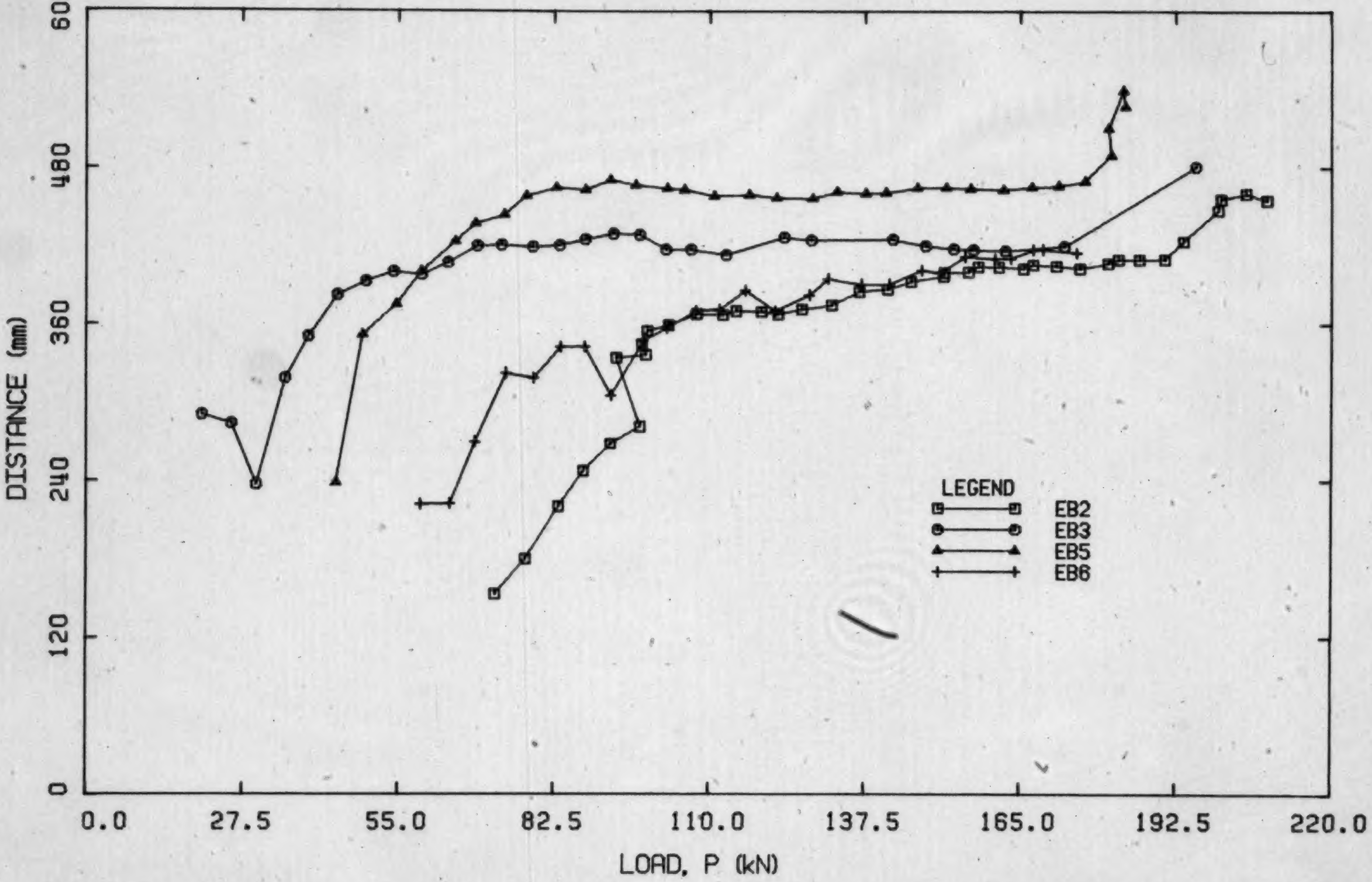

Figure 6.4 Neutral Axis Position in Type EB Beams

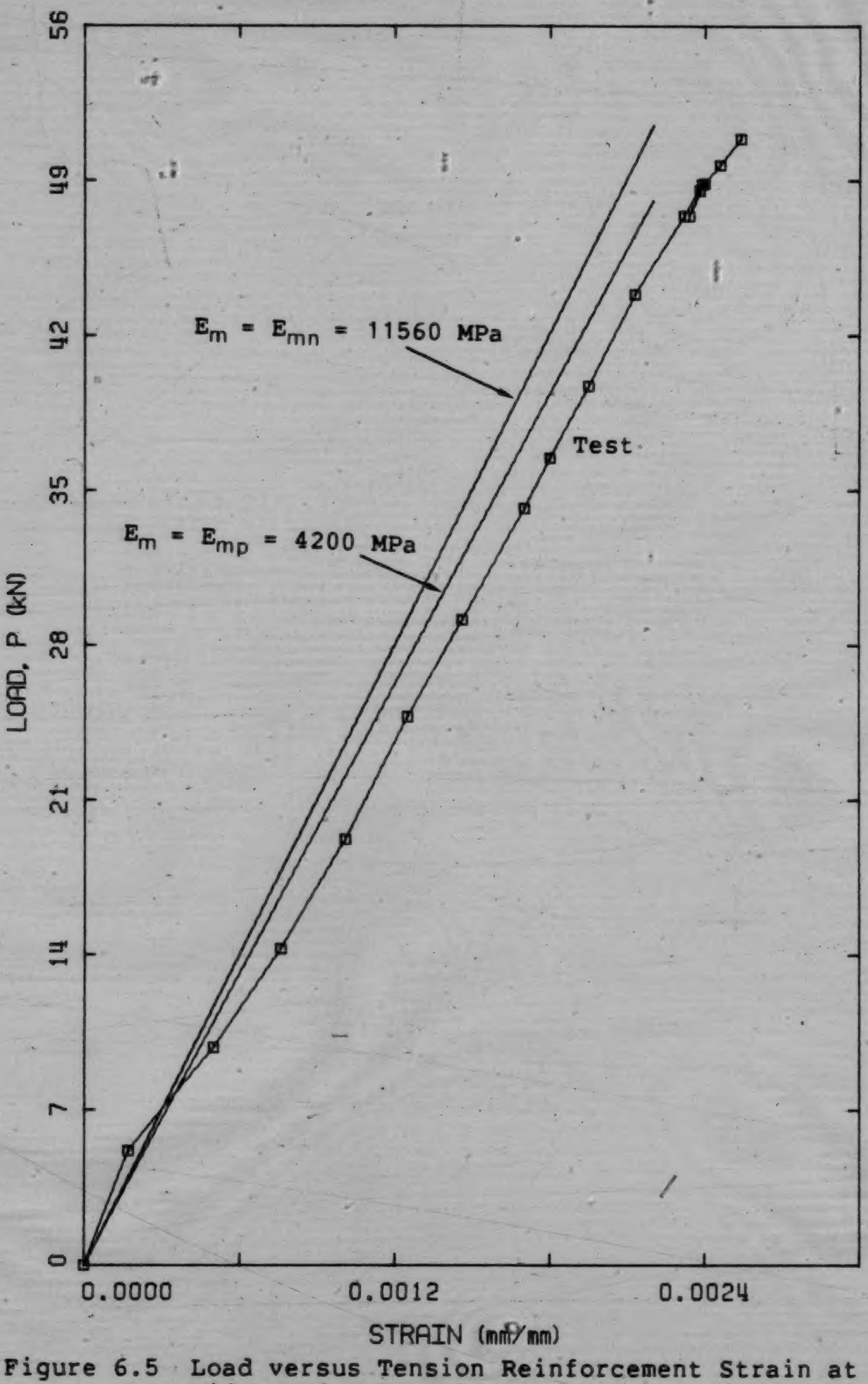

Figure 6.5 Load versus Tension Reinforcement Strain at Midspan for Beam SB1

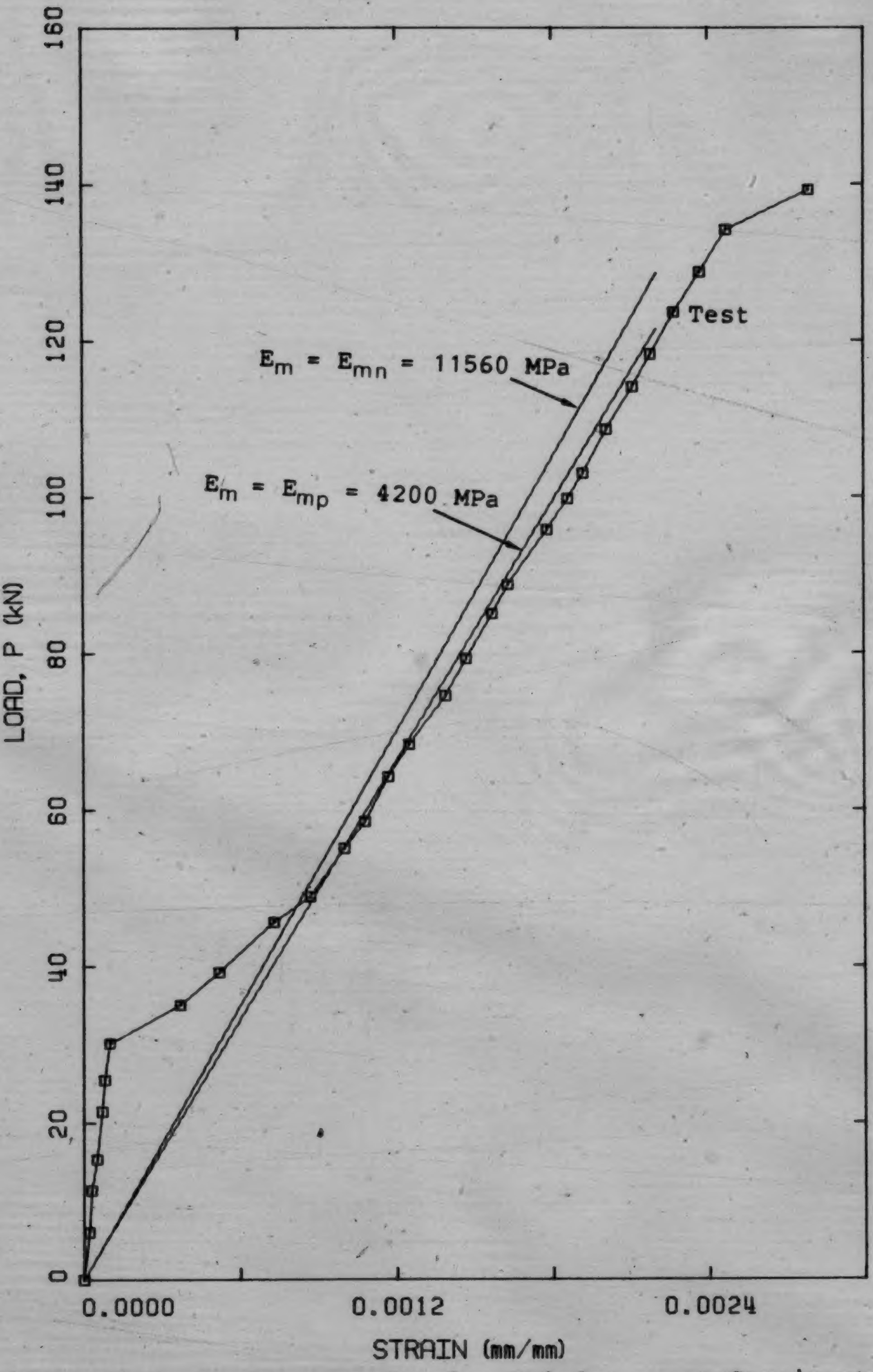

Figure 6.6 Load versus Tension Reinforcement Strain at Midspan for Beam SB2

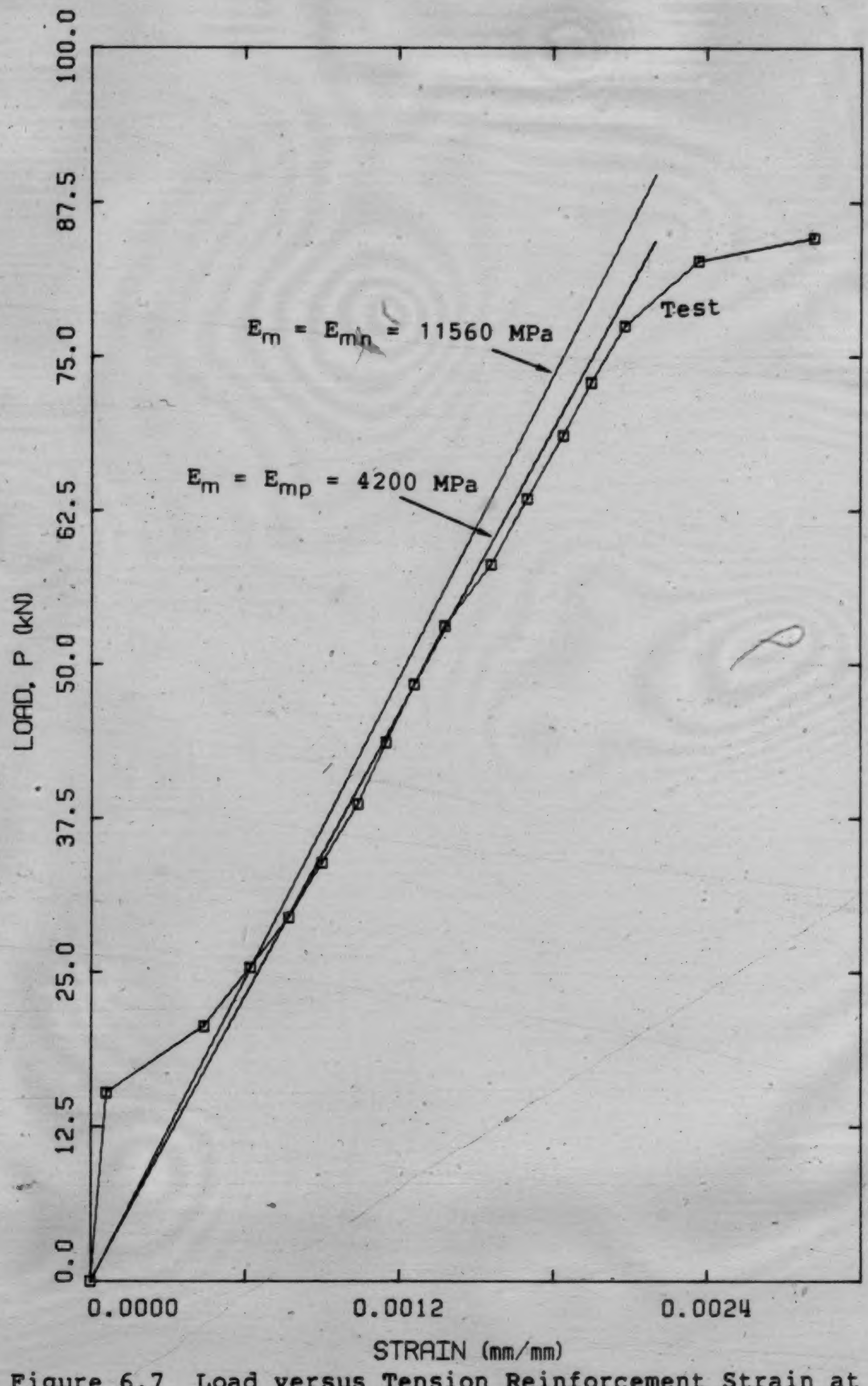

Figure 6.7 Load versus Tension Reinforcement Strain at Midspan for Beam SB4

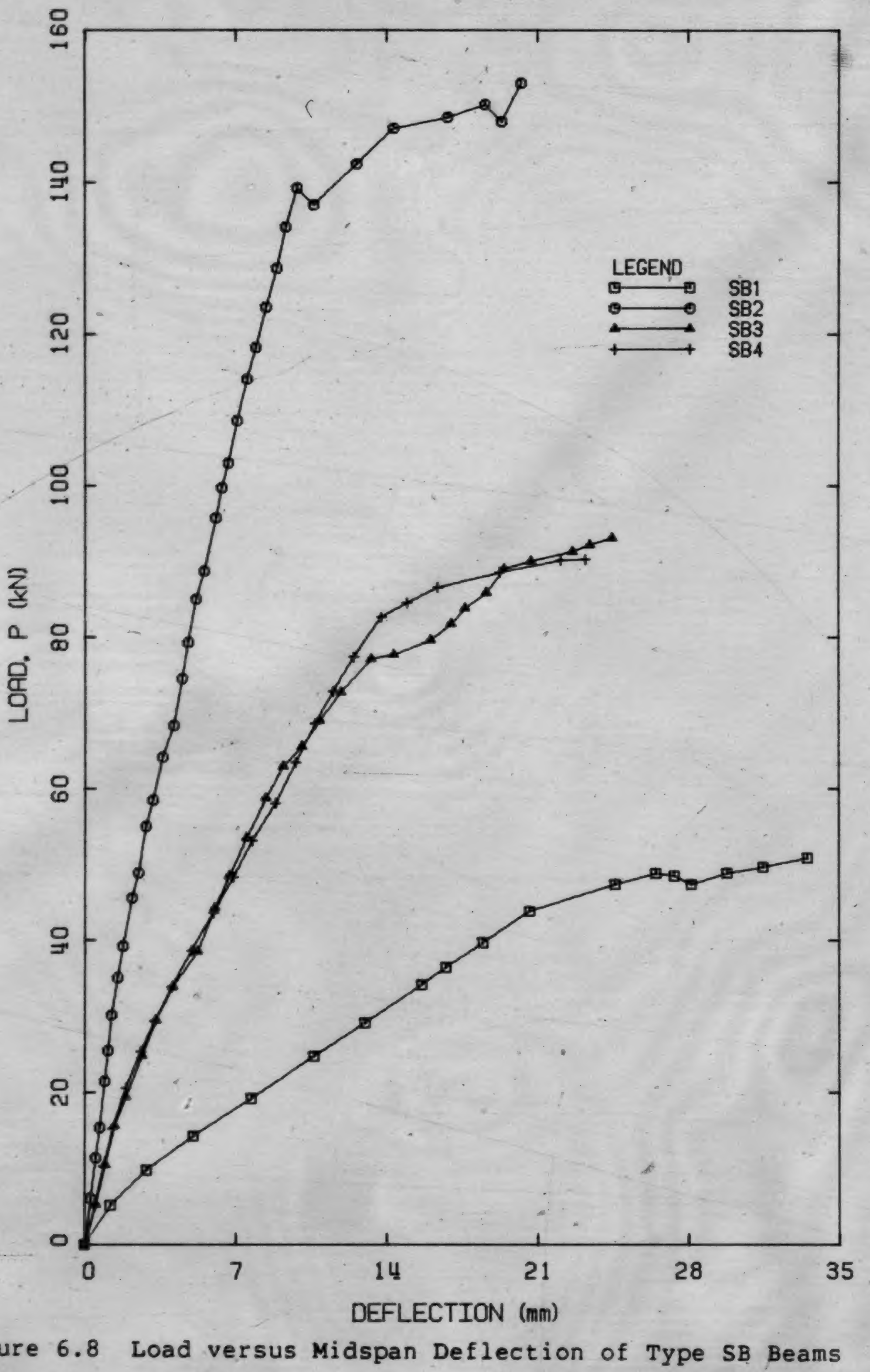

Figure 6.8 Load versus Midspan Deflection of Type SB Beams

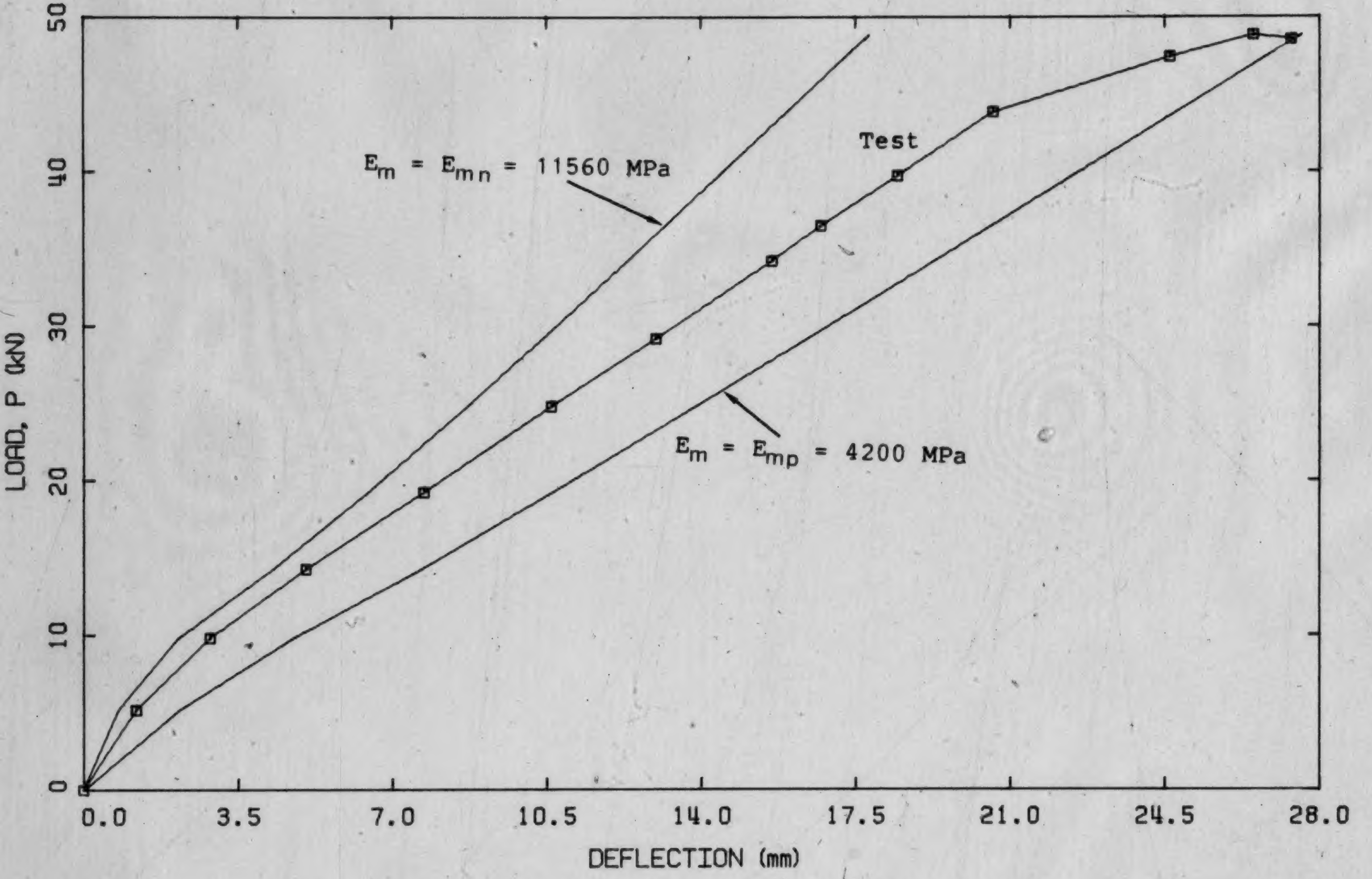

Figure 6.9 Load versus Deflection for Beam SB1

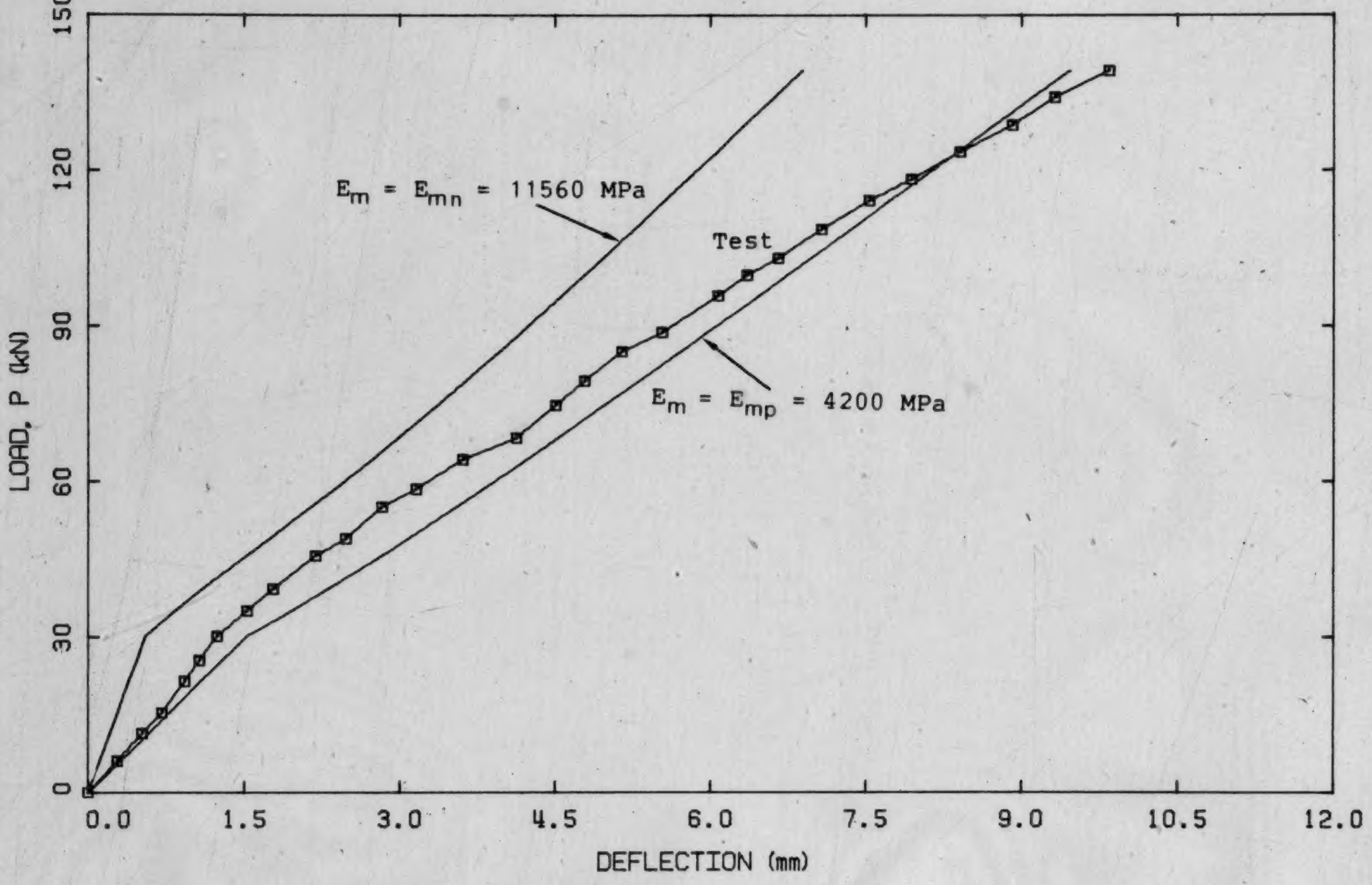

Figure 6.10 Load versus Deflection for Beam SB2

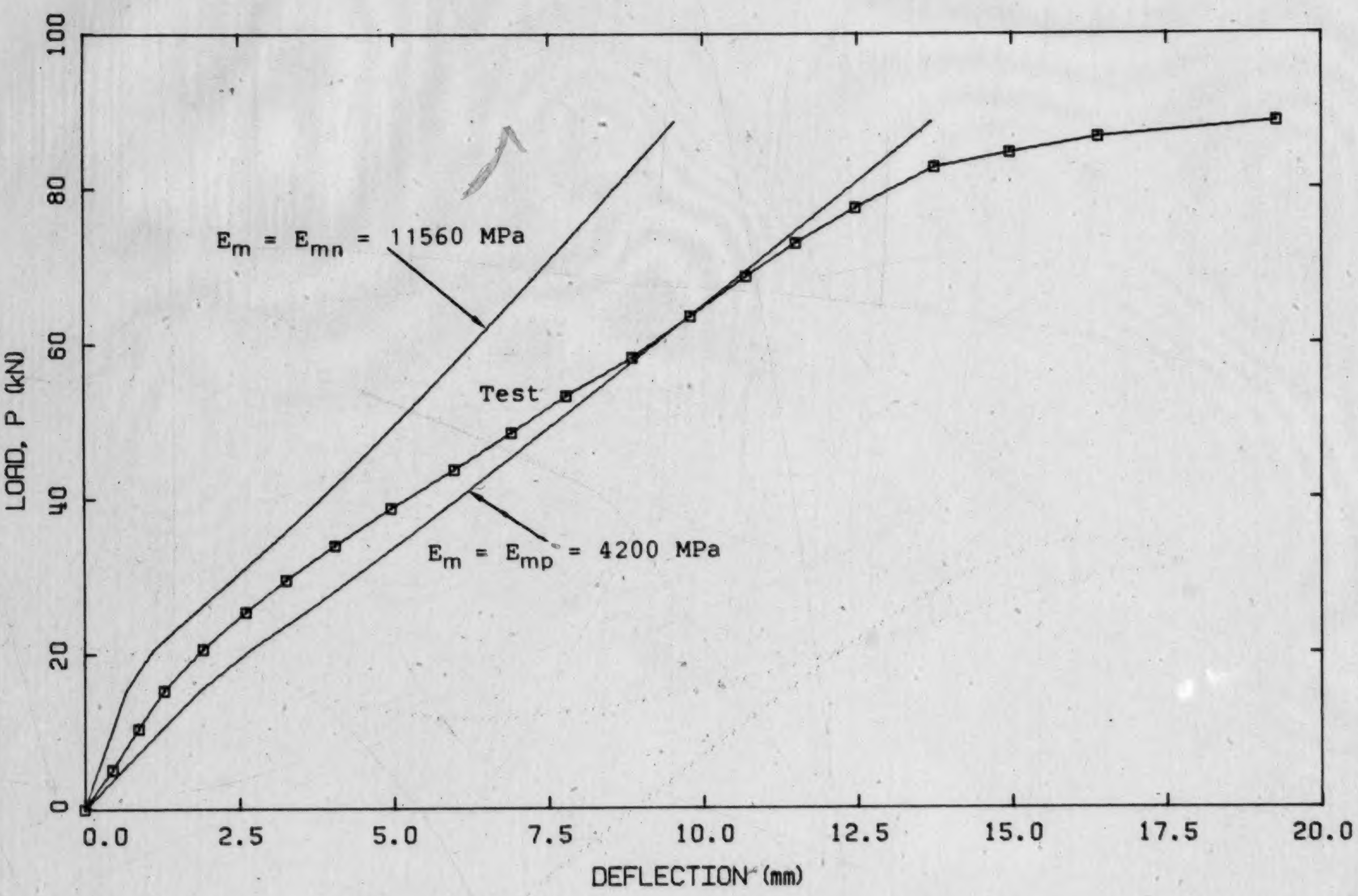

Figure 6.11 Load versus Deflection for Beam SB4

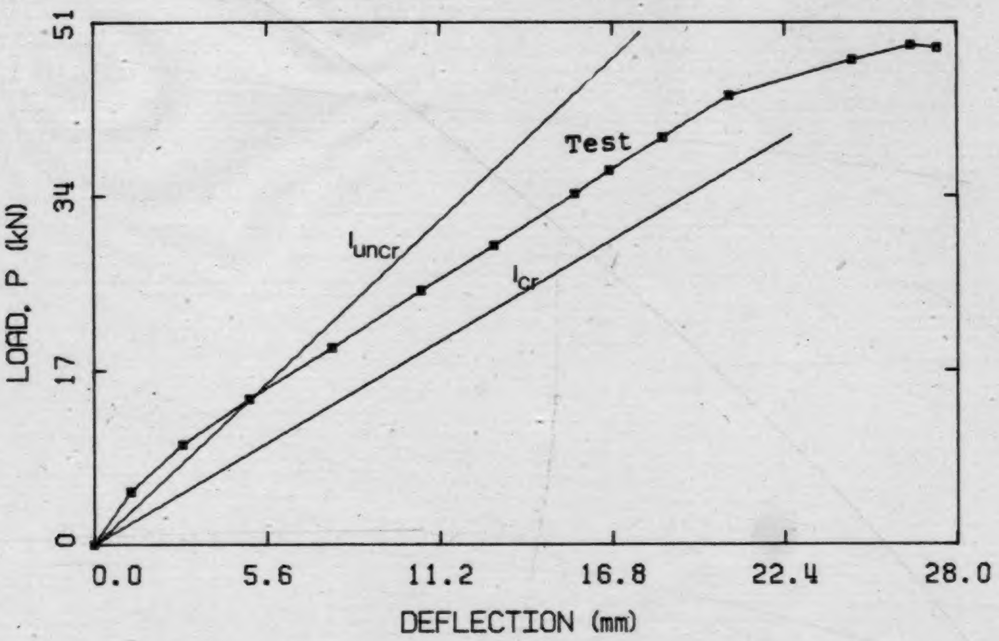

Figure 6.12 Load versus Deflection for Beam SB1

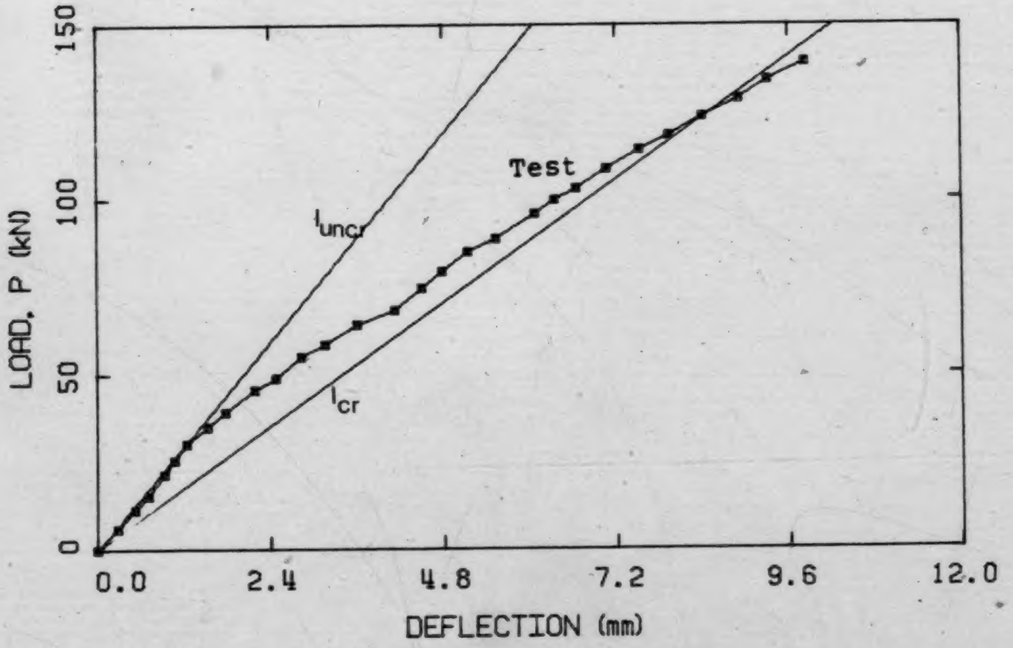

Figure 6.13 Load versus Deflection for Beam SB2

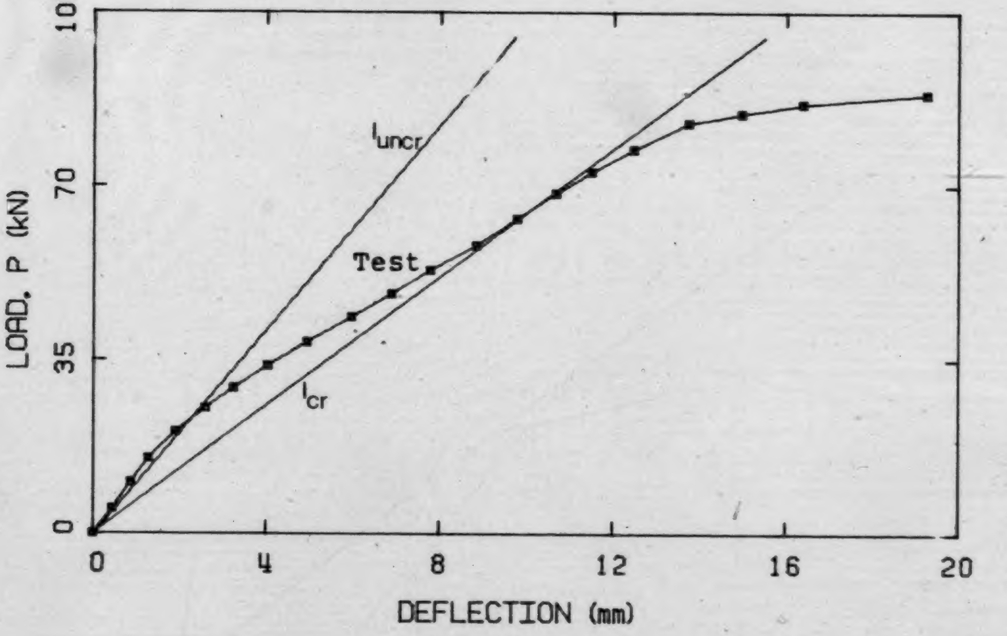

Figure 6.14 Load versus Deflection for Beam SB4

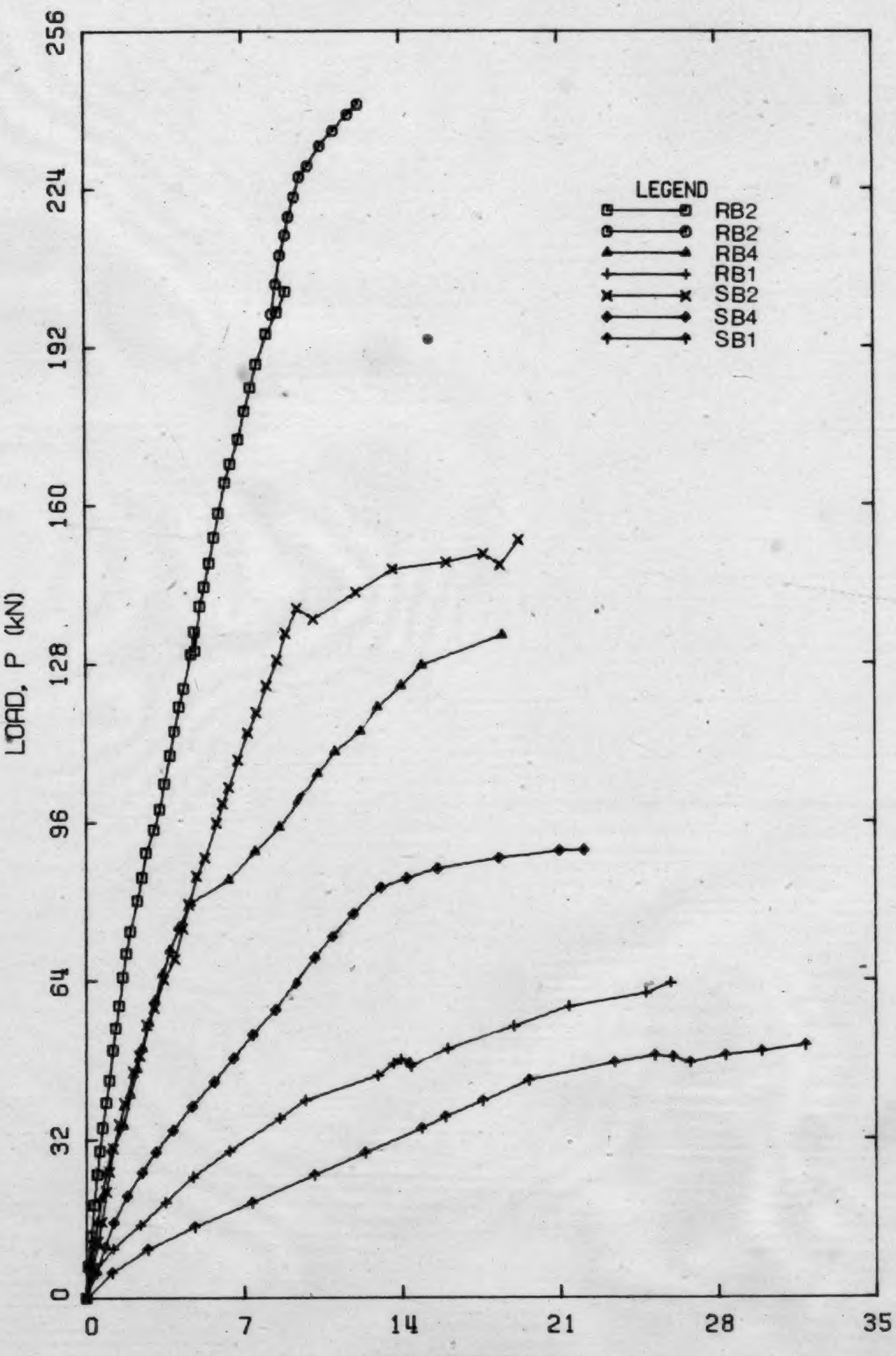

Figure 6.15 Load versus Deflection for Type SB and RB Beams

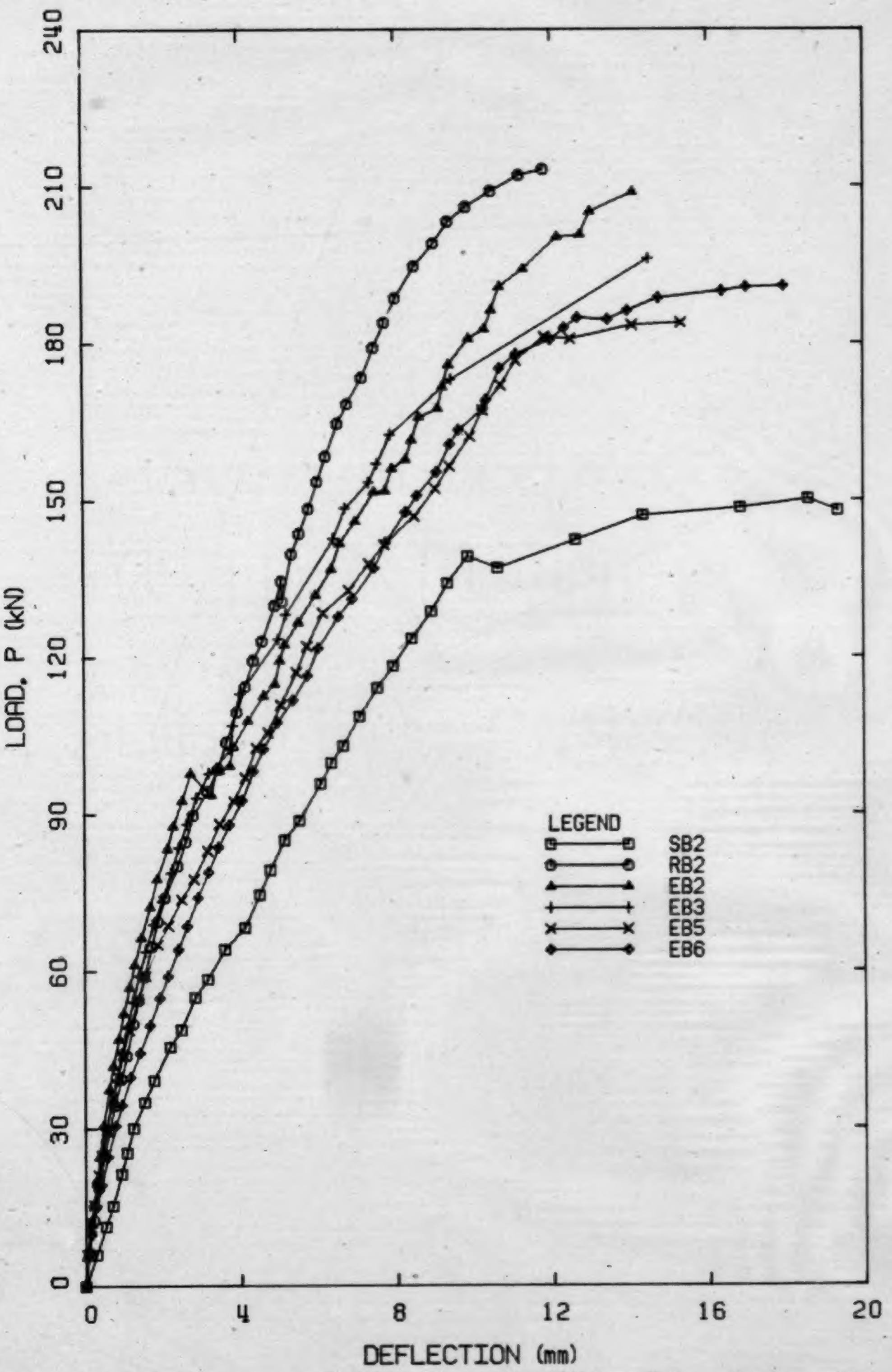

Figure 6.16 Load versus Deflection for SB2, RB2 and Type EB Beams

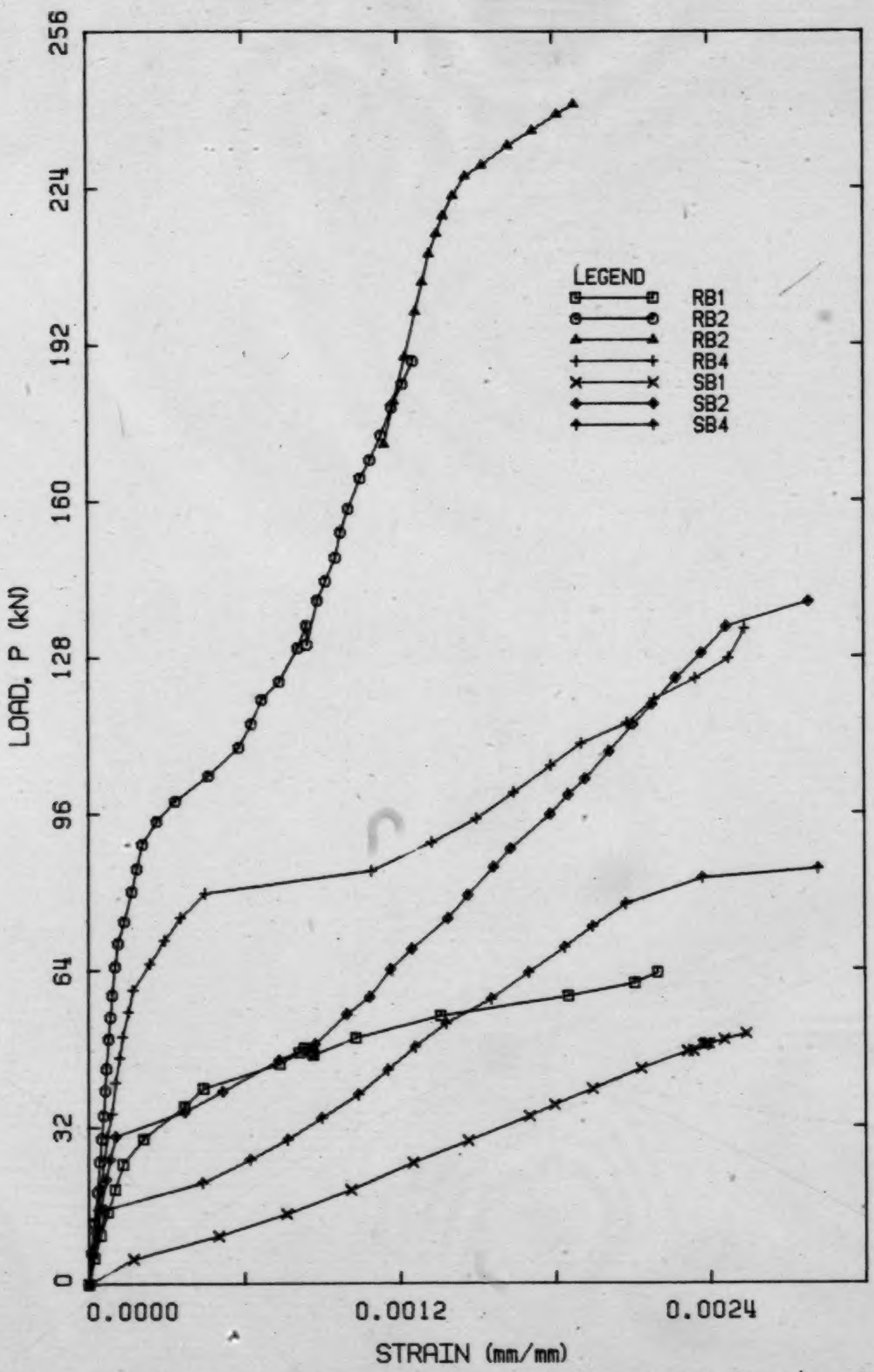

Figure 6.17 Load versus Tension Reinforcement Strain at Midspan for Type SB and RB Beams

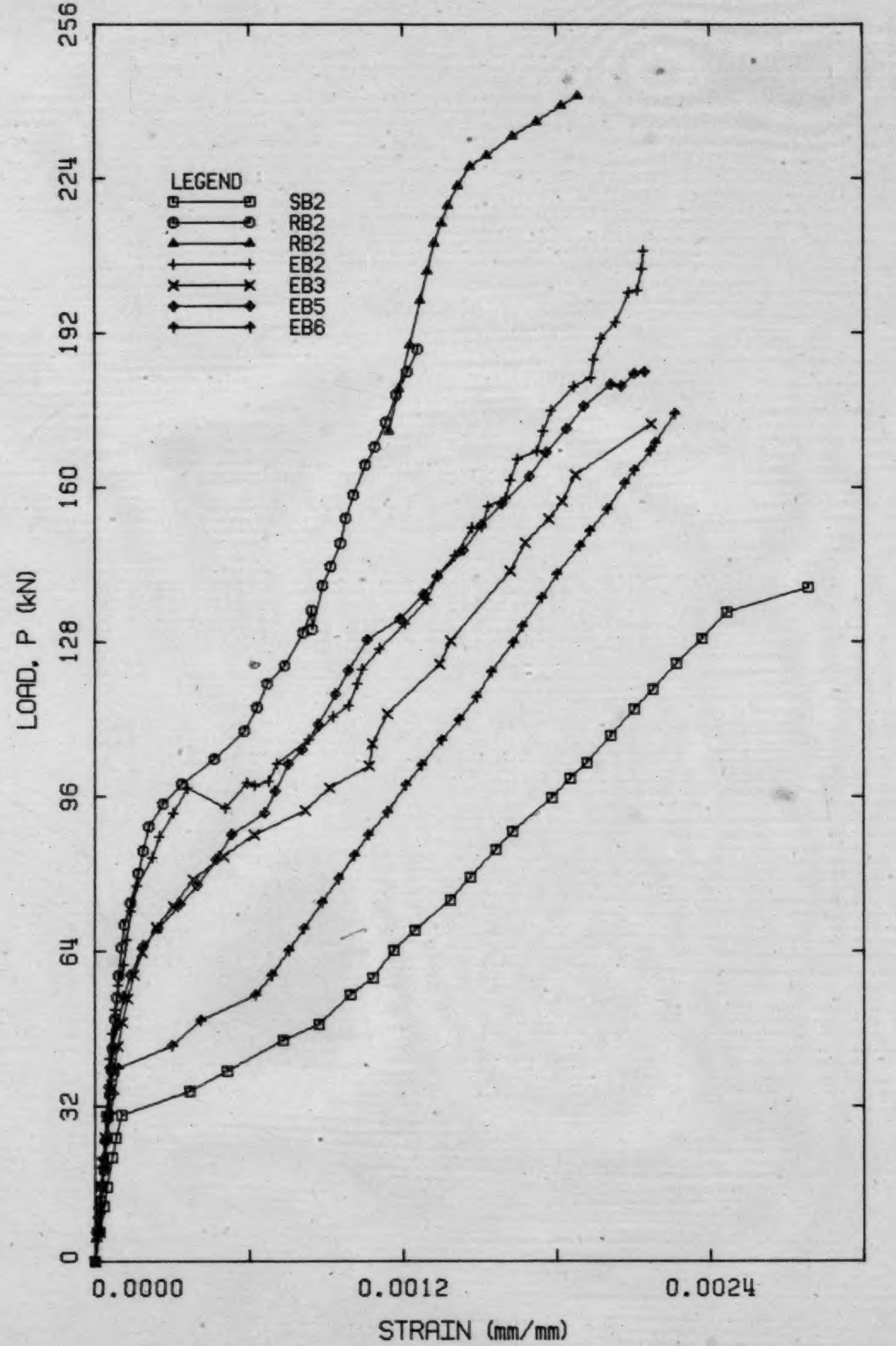

Figure 6.18 Load versus Tension Reinforcement Strain at Midspan for SB2, RB2 and Type EB Beams

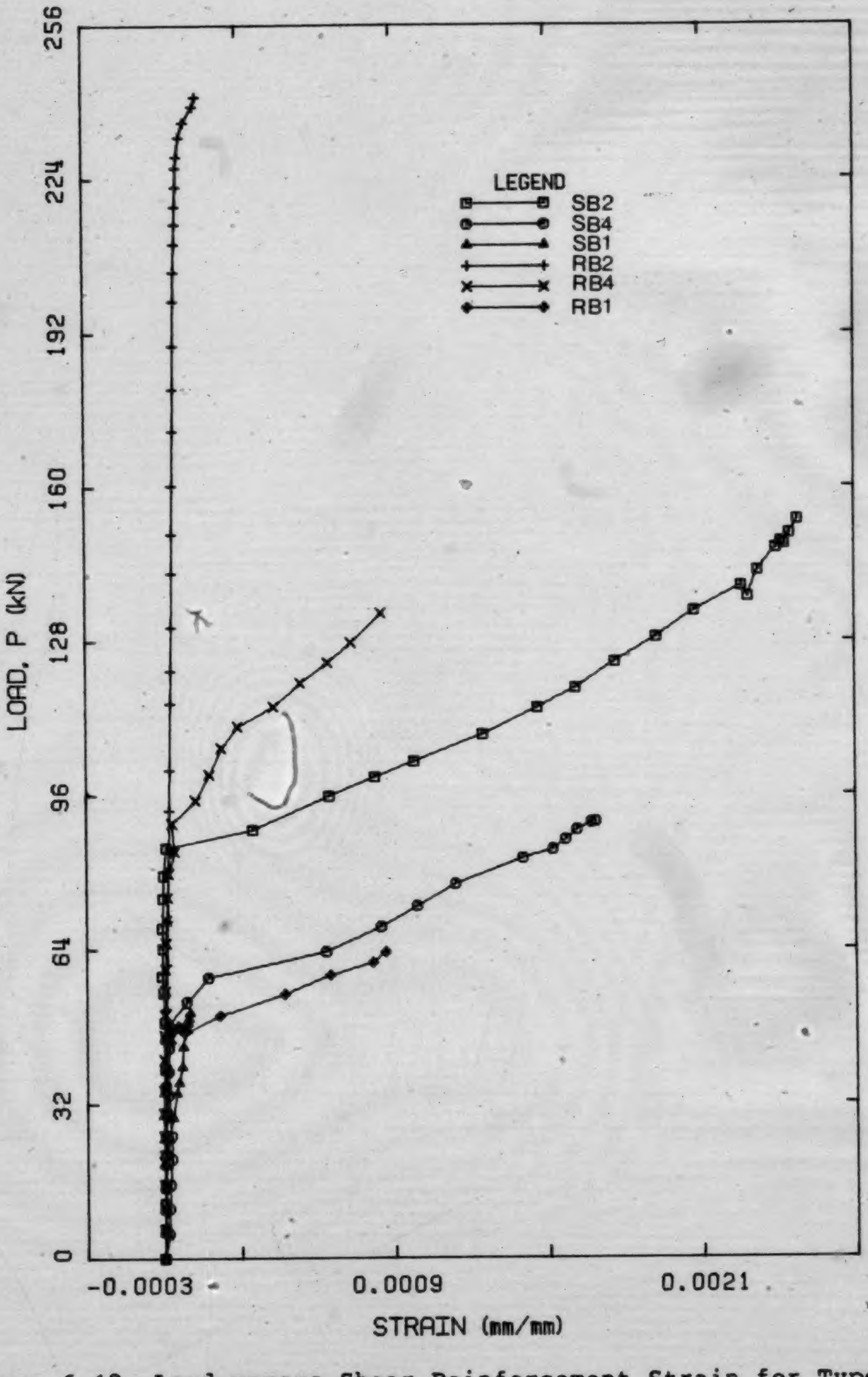

Figure 6.19 Load versus Shear Reinforcement Strain for Type SB and RB Beams

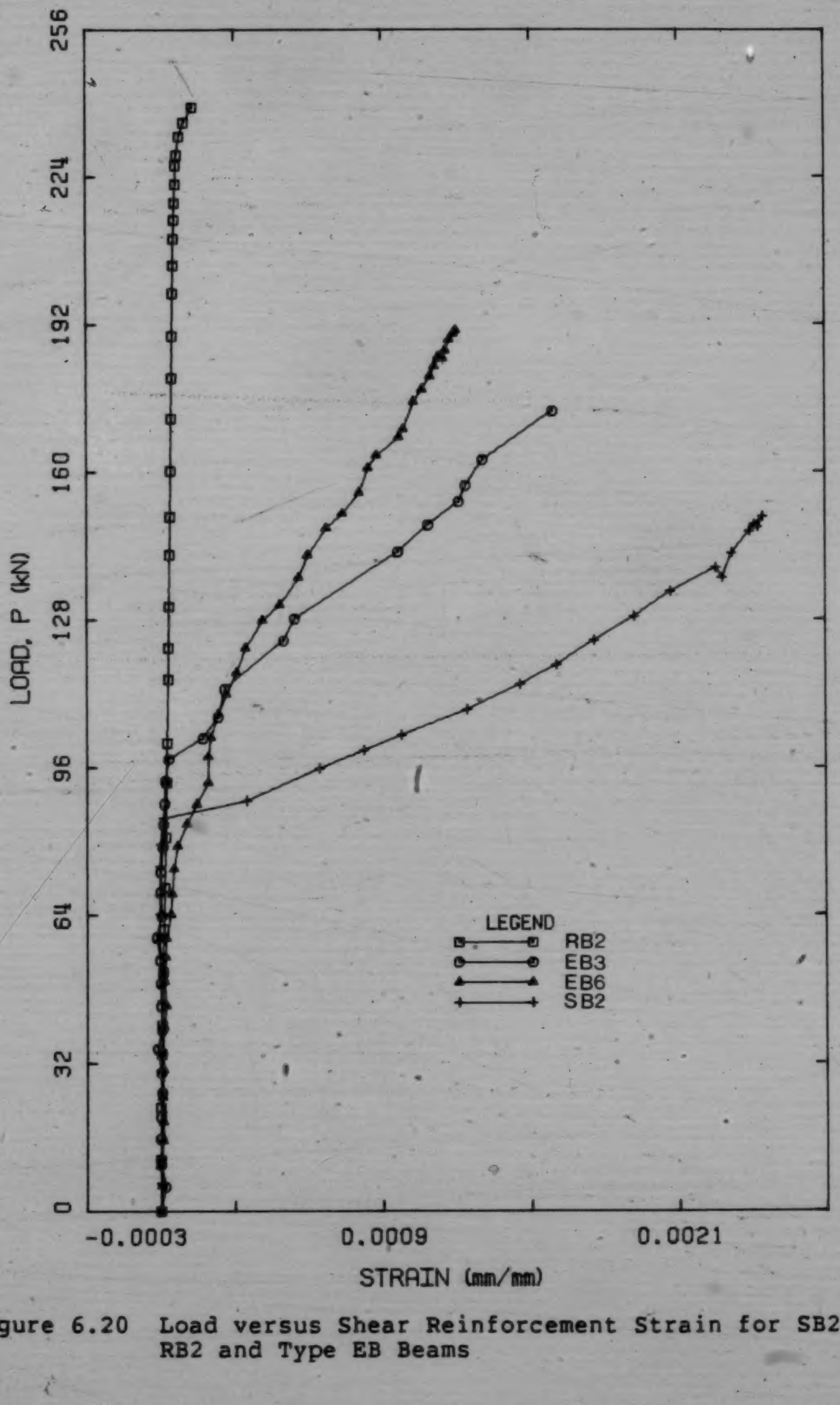

Figure 6.20 Load versus Shear Reinforcement Strain for SB2, RB2 and Type EB Beams

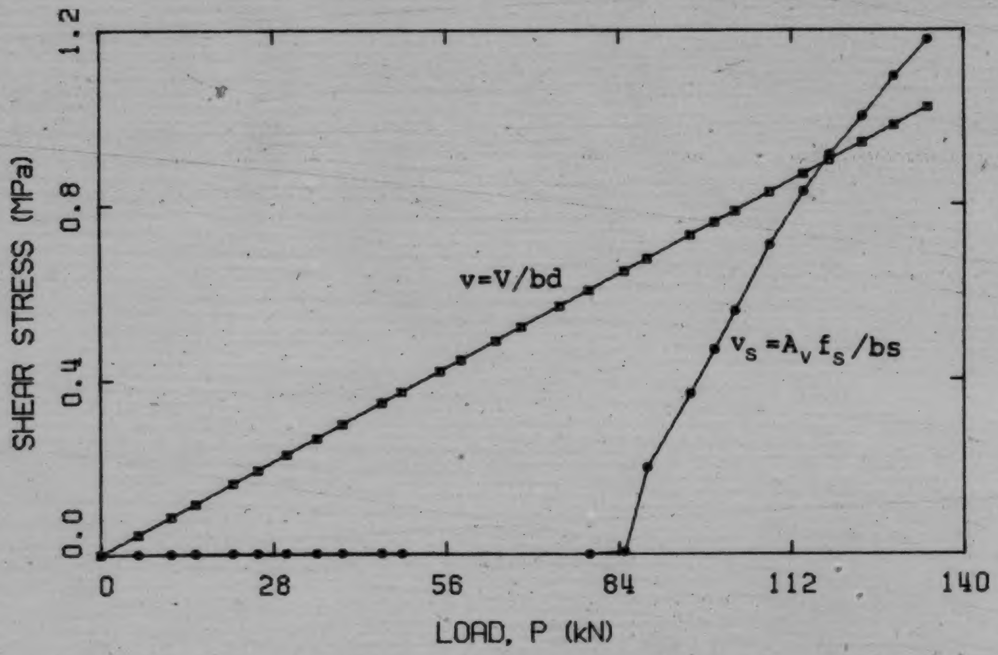

Figure 6.21 Shear Stress versus Load for Beam SB2

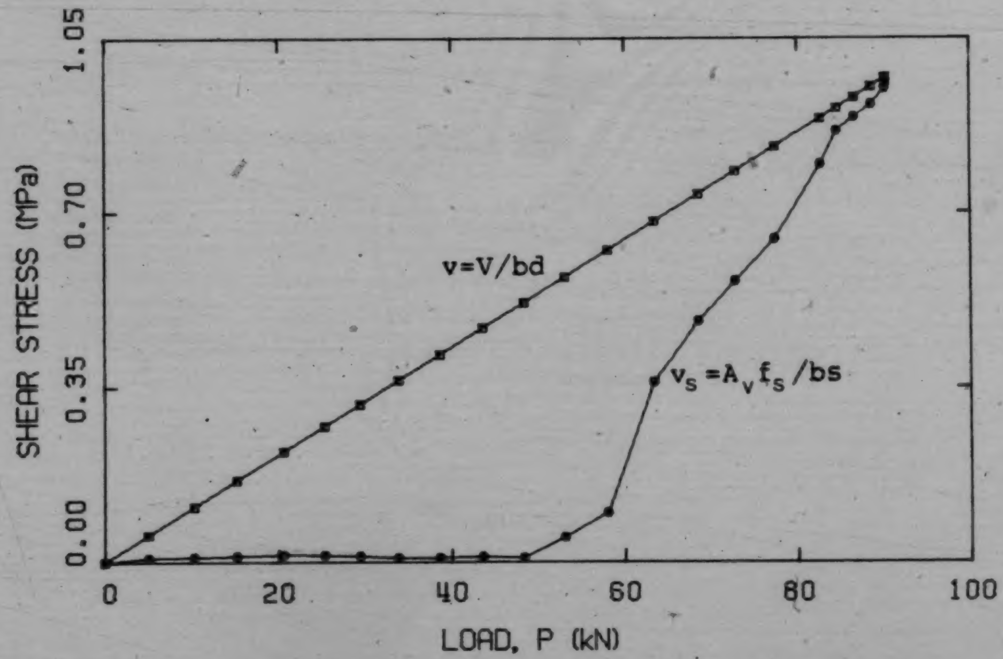

Figure 6.22 Shear Stress versus Load for Beam SB4

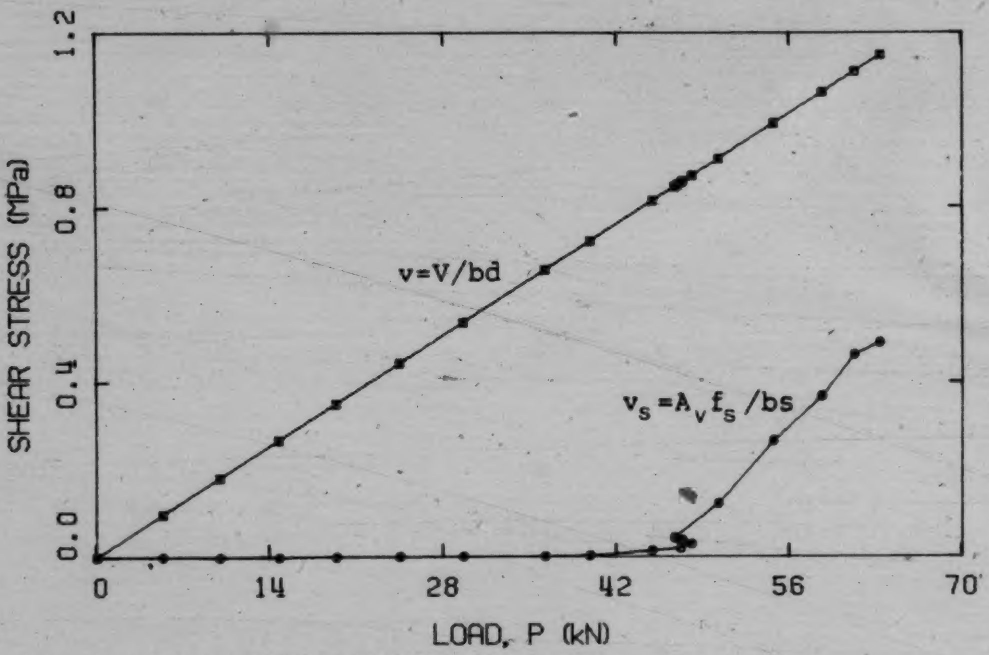

Figure 6.23 Shear Stress versus Load for Beam RB1

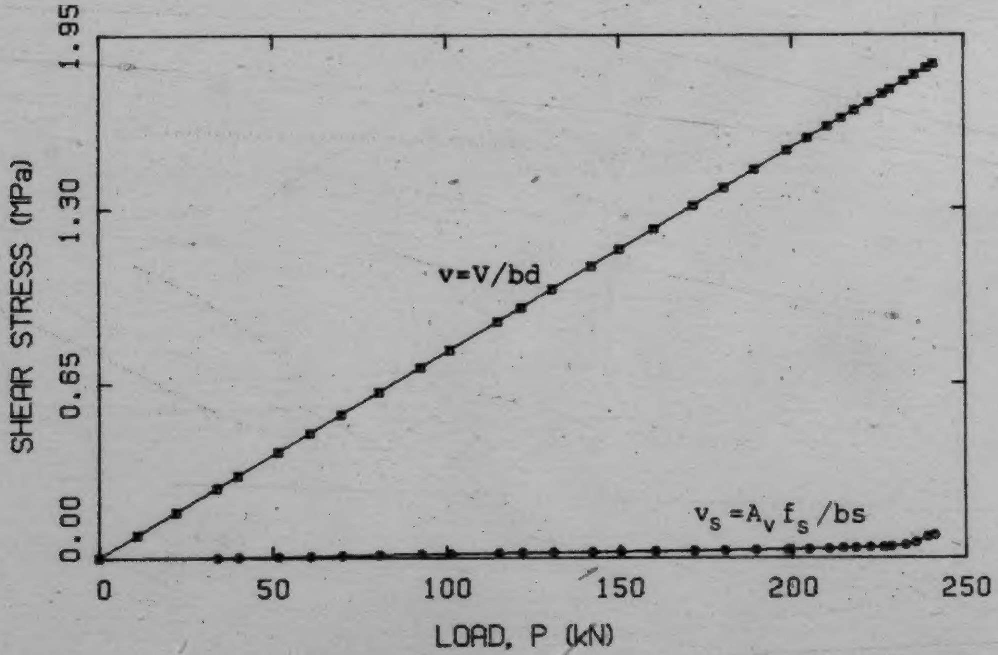

Figure 6.24 Shear Stress versus Load for Beam RB2

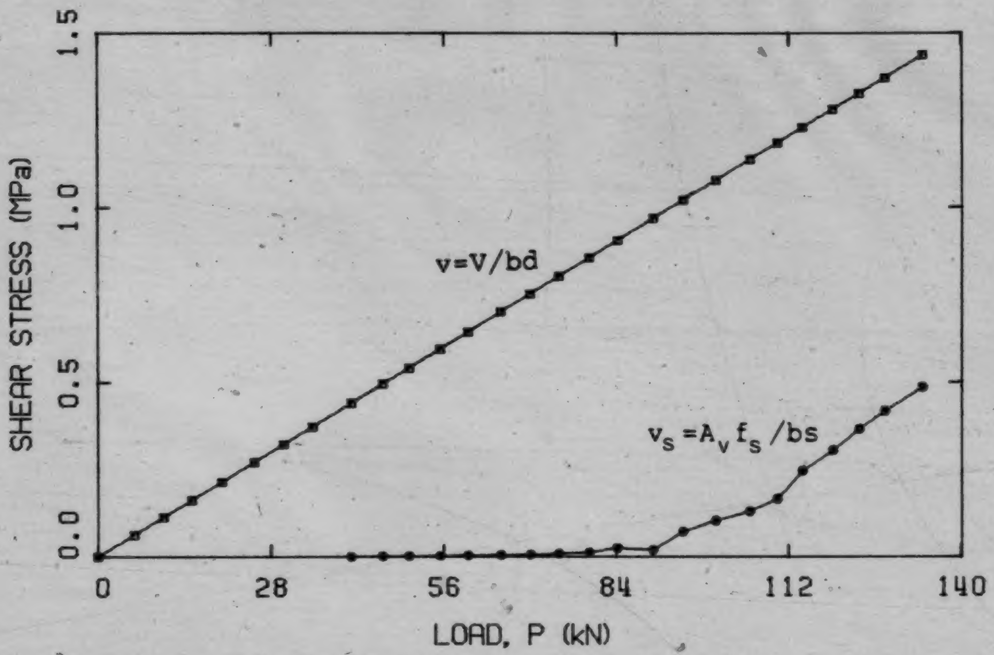

Figure 6.25 Shear Stress versus Load for Beam RB4

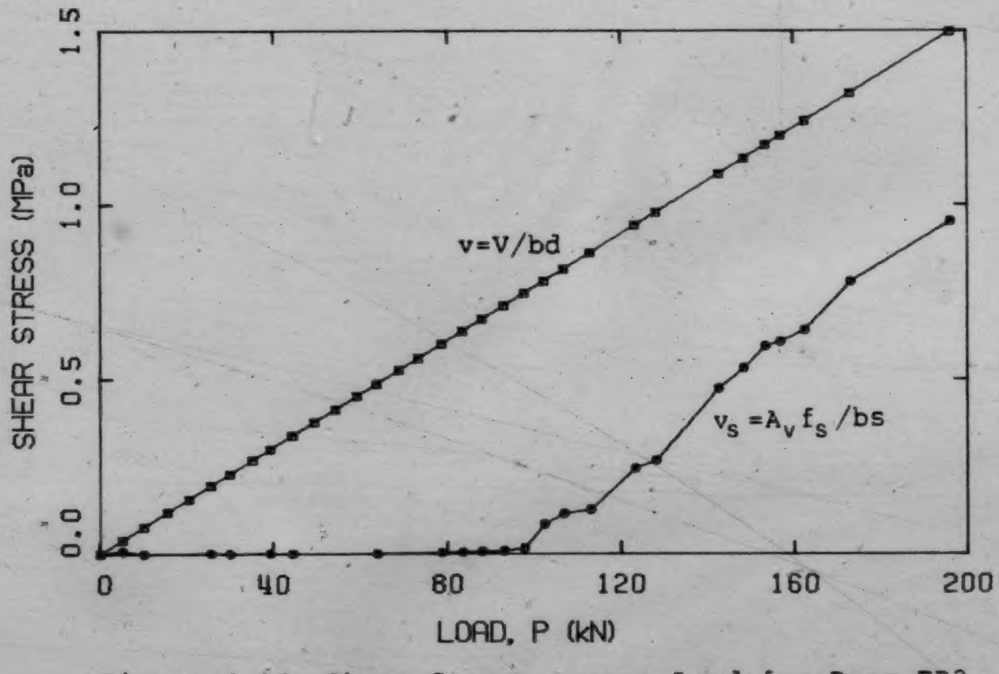

Figure 6.26 Shear Stress versus Load for Beam EB3

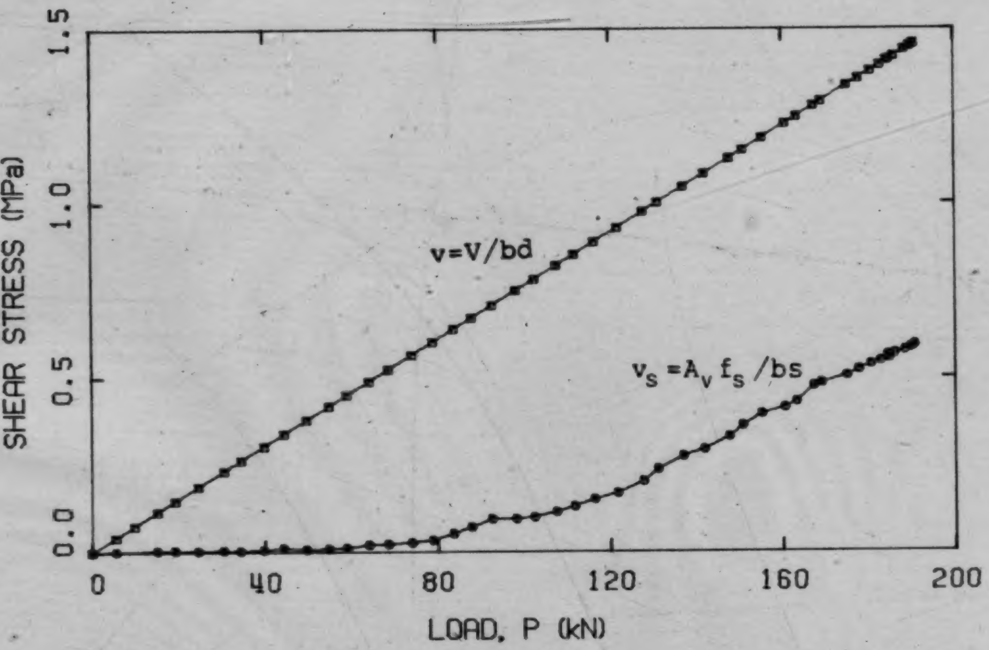

Figure 6.27 Shear Stress versus Load for Beam EB6

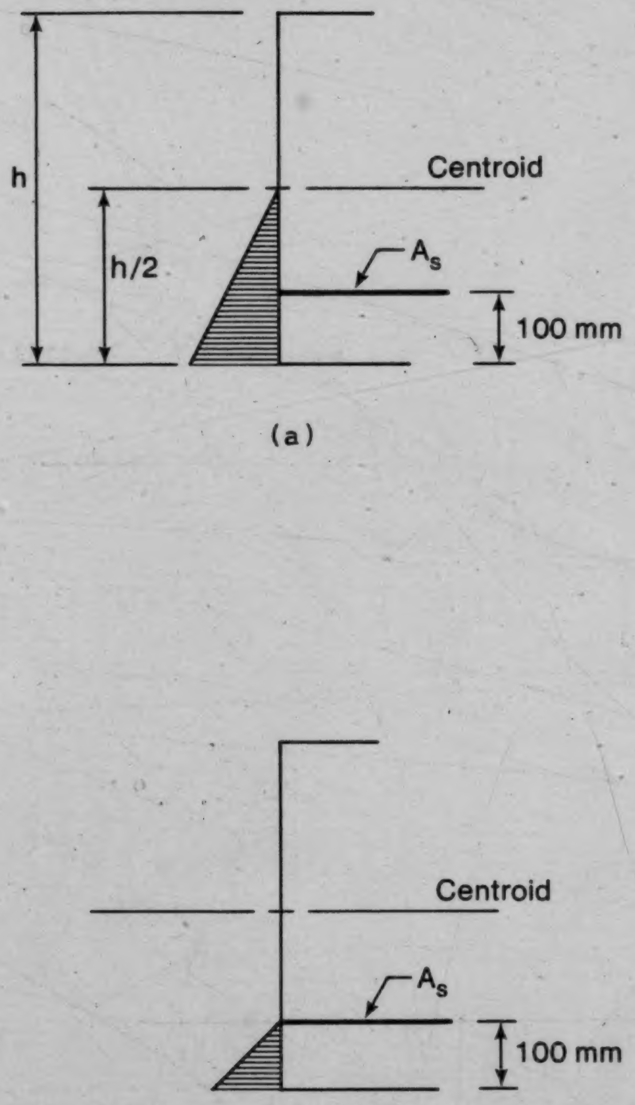
h
h/2
Centroid
A_s
100 mm
(a)
Centroid
A_s
100 mm
(b)

Figure 6.28 Stress Distribution at End of Beam

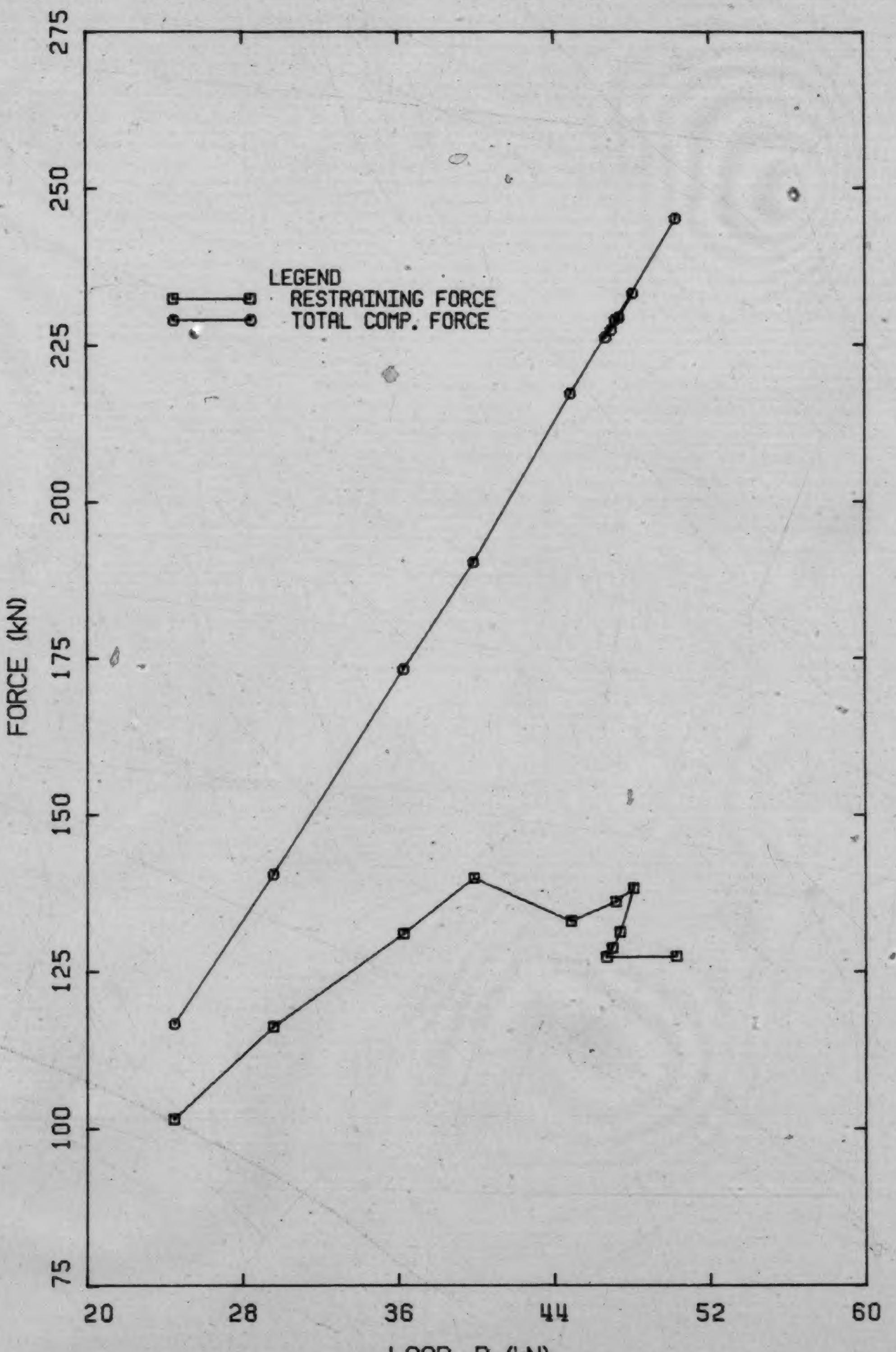

Figure 6.29 Restraining Force versus Load and Compressive Force versus Load for Beam RB1

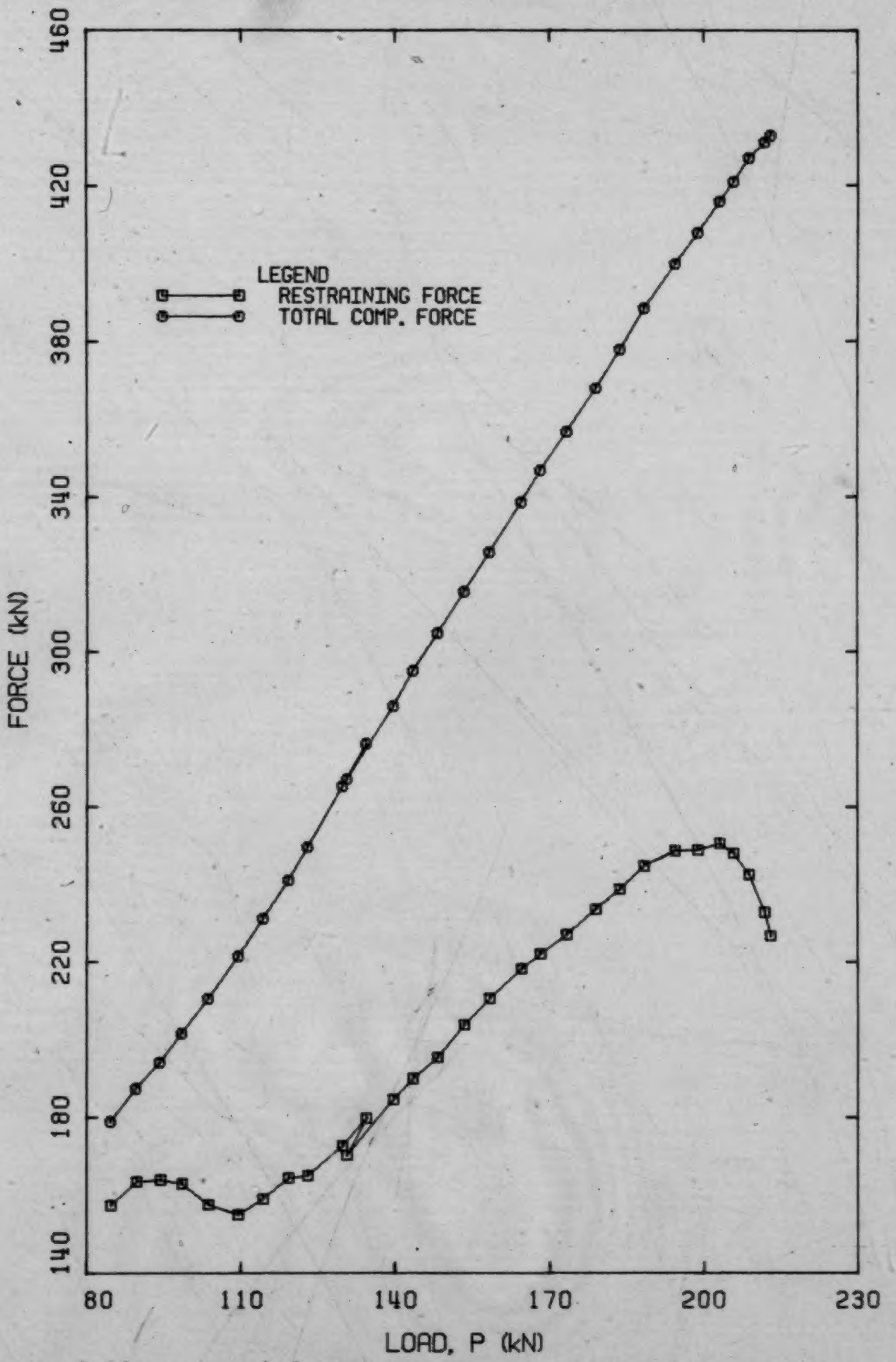

Figure 6.30 Restraining Force versus Load and Compressive Force versus Load for Beam RB2

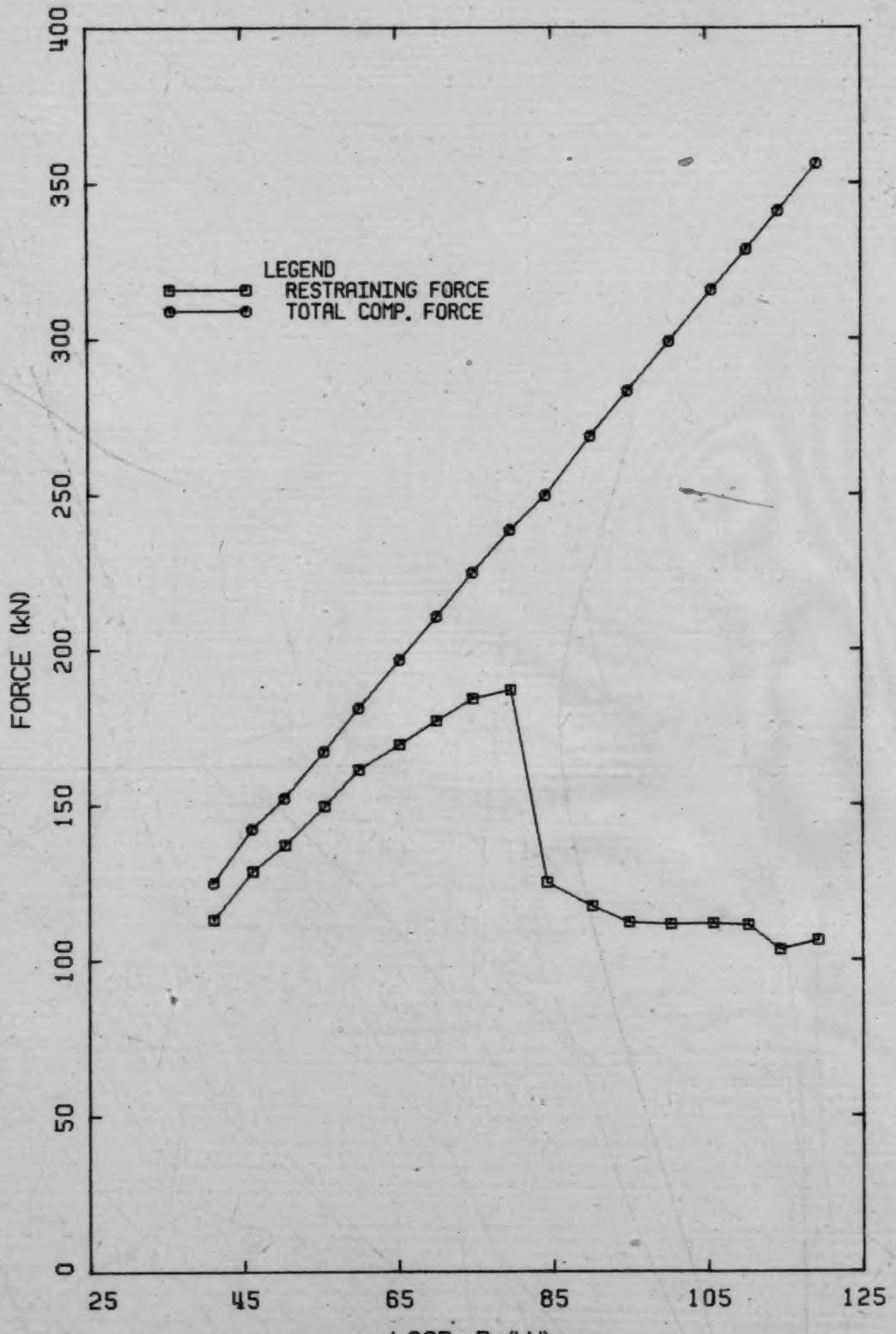

Figure 6.31 Restraining Force versus Load and Compressive Force versus Load for Beam RB4

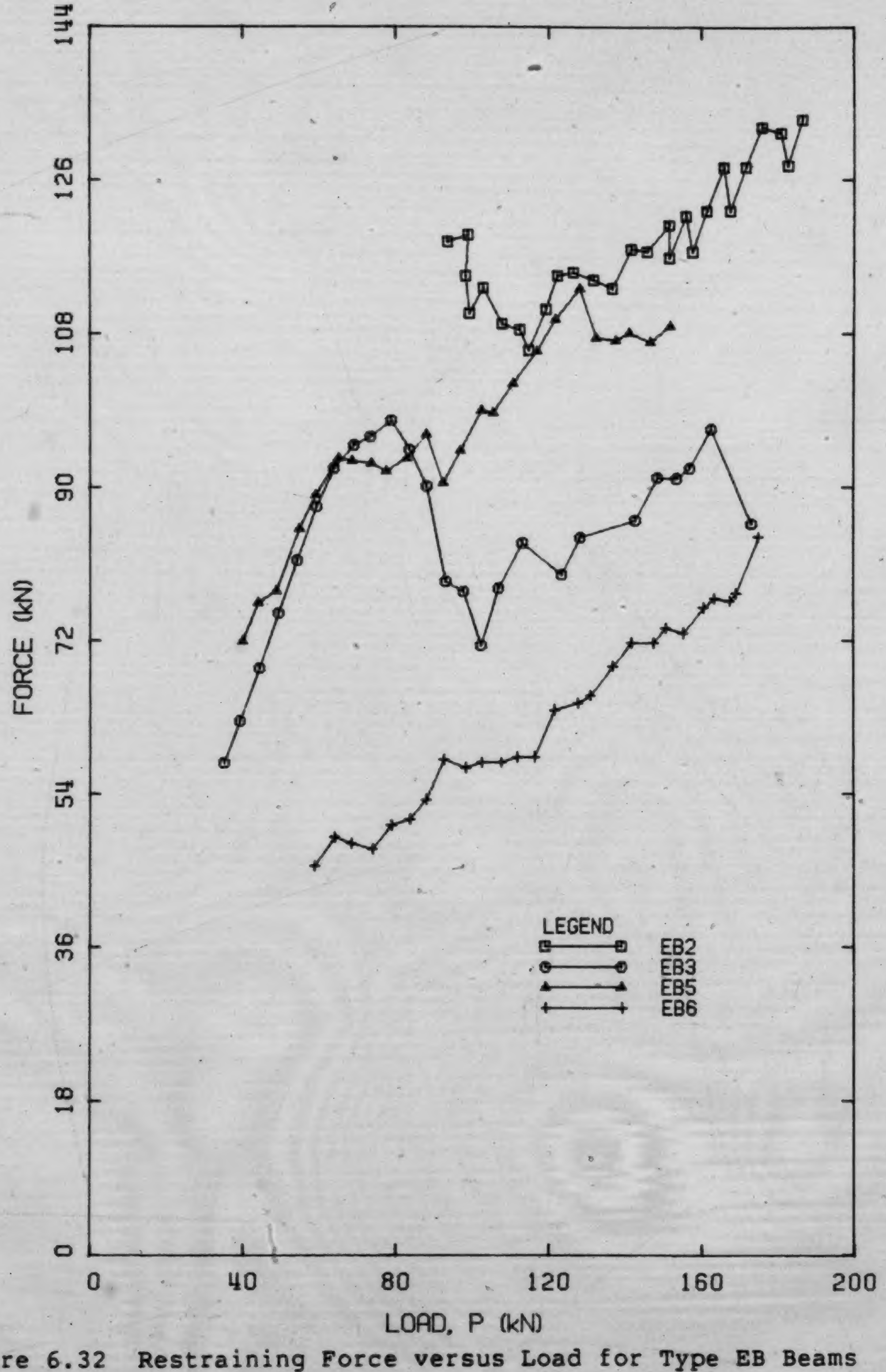

Figure 6.32 Restraining Force versus Load for Type EB Beams

7. Summary and Conclusions

7.1 Summary

This investigation was undertaken to examine the behavior of restrained and unrestrained reinforced concrete masonry beams. The experimental phase of the study consisted of compressive tests of grouted masonry prisms in two different orientations, and tests of fourteen full scale beam specimens with three different support conditions. The purposes of the tests were: 1) to establish the difference in strength, modulus of elasticity and failure mode for prisms loaded parallel and perpendicular to the bed joints; 2) to study the effectiveness of reinforcement in masonry beams; 3) to study the effects of end restraints on the failure mode and strength of masonry beams. Test results obtained from the beam specimens included failure loads, vertical deflections and strains in the reinforcement. Test results for unrestrained beams were analysed using the present reinforced concrete approach. Approximate procedures using idealized behavior were proposed for determining the amount of restraining force and the ultimate strength of restrained beams.

7.2 Observations and Conclusions

Based on the test results obtained in this investigation, the following conclusions are presented.

1. The values of compressive strength and modulus of elasticity of masonry prisms loaded parallel to the bed joints are approximately one half of the values obtained for prisms loaded normal to the bed joints.
2. Failure of masonry prisms loaded parallel to the bed joints initiates by crushing of the head mortar joints, indicating that the strength of mortar is an important parameter in the strength of the masonry under this service orientation.
3. Suitably detailed web reinforcement in a masonry beam prevents diagonal tension failure prior to yielding of the longitudinal reinforcement.
4. The presence of end restraints increases the capacity of masonry beams.
5. The amount of restraint created by short lengths of supporting wall is not as large as the restraint created by fixed end abutments.
6. For a given span length, the capacity of restrained beams increases with increased beam depth.
7. Generally, the failure load of a beam containing web reinforcement is higher than that of a similar beam without web reinforcement, with the former failing in a flexural mode and the latter failing in a shear mode.
8. Cracks in masonry beams usually propagate along mortar

joints.

9. Crushing in the compressive region of a masonry beam is initiated by crushing of the head mortar joints, thus the mortar compressive strength has a significant effect on the flexural strength.
10. The load-deflection behavior of simply supported beams in the service load range is linear.
11. Cracking moment, deflection and ultimate capacity of masonry beams can be satisfactorily predicted by analysis similar to that employed for reinforced concrete.
12. Analysis based on a three-hinged arch model provides reasonable predictions of ultimate loads for restrained masonry beams.

Bibliography

1. Withey, M. O. "Tests on Brick Masonry Beams." Proceedings, American Society for Testing Materials, Vol. 33, 1933, pp. 651-665.

2. Hansen, J. H. "Developments in Reinforced Brick Masonry." American Society of Civil Engineers, Transactions, Vol. 99, 1934, pp. 748-768.

3. Thomas, F. G., and Simms, L. G. "The Strength of Some Reinforced Brick Masonry Beams in Bending and in Shear." The Structural Engineer, Vol. XVII, July, 1939, pp. 330-349.

4. Johnson, F. B., and Thompson, J. N. "Correlation of Tests of Masonry Assemblages with Strength Characteristics of Reinforced Masonry Beams." International Conference on Masonry Structural Systems, University of Texas, Austin, 1967.

5. Sahlin, S. "Structural Masonry." Prentice-Hall, Inc., N. J., 1971.

6. Suter, G. T., and Hendry, A. W. "Shear Strength of Reinforced Brickwork Beams." The Structural Engineer, Vol. 53, No.6, June, 1975, pp. 249-253.

7. Suter, G. T., and Keller, H. "Shear Strength of Reinforced Masonry Beams and Canadian Code Implications." Proceeding of the First Canadian Masonry Symposium, Calgary, June, 1976.

8. Suter, G. T., and Keller, H. "Shear Strength of Grouted Reinforced Masonry Beams." Proceedings of the Fourth International Brick Masonry Conference, Brugge, Belgium, April, 1976.

9. Suter, G. T., and Keller, H. "Reinforced Brickwork Lintel Shear Study Utilizing Small Scale Bricks." Proceedings of the North American Masonry Conference, University of Colorado, August, 1978.

10. Rathbone, A. J. "The Behavior of Single-Course Reinforced Concrete Blockwork Beams." Second Canadian Masonry Symposium, Carleton University, Ottawa, Ontario, June, 1980.

11. British Standards Institution, CP110:Part 1:1972,The Structural Use of Concrete, Part 1. Design, Materials and Workmanship, London.

12. Suter, G. T., and Keller, H. "Carleton University Concrete Masonry Beam Tests: Shear." Department of Civil Engineering, Carleton University, Ottawa, February, 1980.

13. Kani, G. N. J. "How Safe are Our Large Reinforced Concrete Beams?" ACI Journal, Vol. 64, March, 1967, pp. 128-141.

14. McDowell, E. L., McKee, K. E., and Sevin, E. "Arching Action Theory of Masonry Walls." Journal of the Structural Division, Proceedings of the American Society of Civil Engineers, Vol. 82, March, 1956, paper 915.

15. Cohen, E. and Laing, E. Discussion of above paper, Proc. A.S.C.E., Paper 1067, ST5, 1956.

16. Baker, L. R. "Precracking Behavior of Laterally Loaded Brickwork Panels with In-Plane Restraints." Proceedings of the British Ceramic Society, Stroke-on-Trent, No. 27, Dec., 1978, pp. 129-145.

17. Hatzinikolas, M., Longworth, J., and Warwaruk, J. "Effects of Restraints on the Behavior of Concrete Masonry Beams." Alberta Masonry Institute, 1980.

18. ACI 318-77. "Building Code Requirements for Reinforced Concrete." American Concrete Institute, Detroit, Michigan, 1977.

19. CSA Standard S304-1977. "Masonry Design and Construction for Buildings." Canadian Standards Association, Rexdale, Ontario, Canada, May, 1977.

20. Branson, D. E. "Instantaneous and Time-Dependent Deflections on Simple and Continuous Reinforced Concrete Beams." HPR Report No. 7, Part 1, Alabama Highway Department, Bureau of Public Roads, Aug., 1965, pp. 1-78.

21. Hodgkinson, H. R., Haseltine, B. A., West, H. W. H. "Preliminary Tests on the Effect of Arching in Laterally Loaded Walls." T.N. 250, The British Ceramic Research Association, Stoke-on-Trent, 1976.

22. Gurfinkel, G., and Siess, C. P. "Longitudinal Restrained Reinforced Concrete Beams." Journal of the Structural Division, Proceedings of the American Society of Civil Engineers, Vol. 94, March, 1968, pp. 709-735.

23. Gustaferro, A. H., and Salse, E. A. B. "Structural Capacity of Concrete Beams During Fires as Affected by Restraint and Continuity." Proceedings 5th CIB Congress, Paris, France, 1971.

24. CSA Standard A179M-1976. "Mortar and Grout for Unit Masonry." Canadian Standards Association, Rexdale, Ontario, Canada, 1976.

25. Ridinger, W., Noland, J. L., and Feng, C. C. "On the Effect of Interface Condition and Capping Configuration on the Results of Hollow Clay Masonry Unit Compression Tests." Second Canadian Masonry Symposium, Carleton University, Ottawa, Ontario, June, 1980.

26. Maurenbrecher, A. H. P. "Effect of Test Procedures on Compressive Strength of Masonry Prisms." Second Canadian Masonry Symposium, Carleton University, Ottawa, Ontario, June, 1980.

27. Richart, F. E., Woodworth, P. M., and Moorman, R. B. "Strength and Stability of Concrete Masonry Walls." Engineering Experiment Station Bulletin No. 251, University of Illinois, Urbana, July, 1932.

28. Holm, T. A. "Structural Properties of Block Concrete." Proceedings of the North American Masonry Conference, University of Colorado, August, 1978.

29. Maurenbrecher, A. H. P. "Use of the Prism Test to Determine Compressive Strength of Masonry." Proceedings of the North American Masonry Conference, University of Colorado, August, 1978.

30. Hegemier, G. A., Krishnamoorthy, G., Nunn, R. O., and Moorthy, T. V. "Prism Tests for the Compressive Strength of Concrete Masonry." Proceedings of the North American Masonry Conference, University of Colorado, August, 1978.

31. Boult, B. F. "Concrete Masonry Prism Testing." Journal of the American Concrete Institute, Proceedings, Vol. 76, April, 1979, pp. 513-535.

32. Drysdale, R. G., and Hamid, A. A. "Behavior of Concrete Block Masonry under Axial Compression." ACI Journal, Vol. 76, June, 1979, pp. 707-721.

33. CSA-S304-M78 Standard. "Masonry Design and Construction for Buildings." Canadian Standards Association, Rexdale, Ontario, Canada, 1978.

34. Drysdale, R. G., Hamid, A. A., Heidebrecht, A. C. "Effect of Grouting on the Strength Characteristics of Concrete Block Masonry." Proceedings of the North American Masonry Conference, University of Colorado, August, 1978.

35. Sturgeon, G. R., Longworth, J., and Warwaruk, J. "An Investigation of Reinforced Concrete Block Masonry Columns." M.Sc. Thesis, University of Alberta, Edmonton, 1980.

Appendix A

Crack Patterns

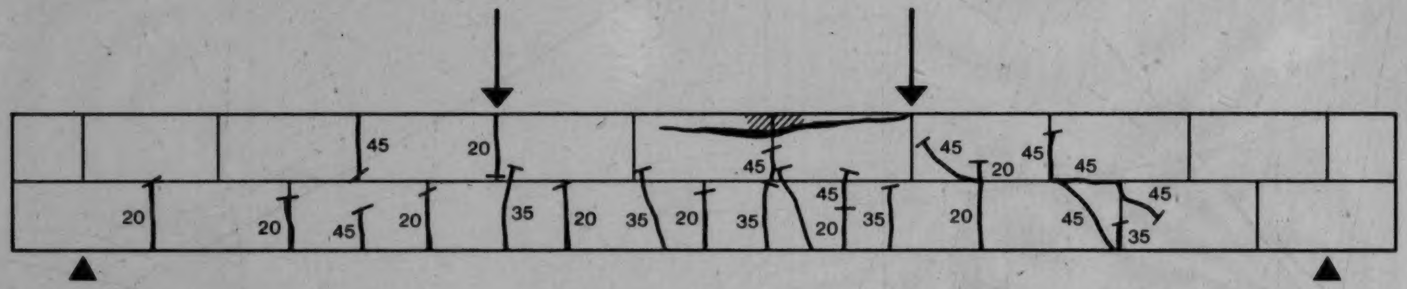
20
20
45
20
45
20
35
20
35
20
45
35
20
45
35
45
20
20
45
45
45
45
45
35

Figure A.1 Beam SB1

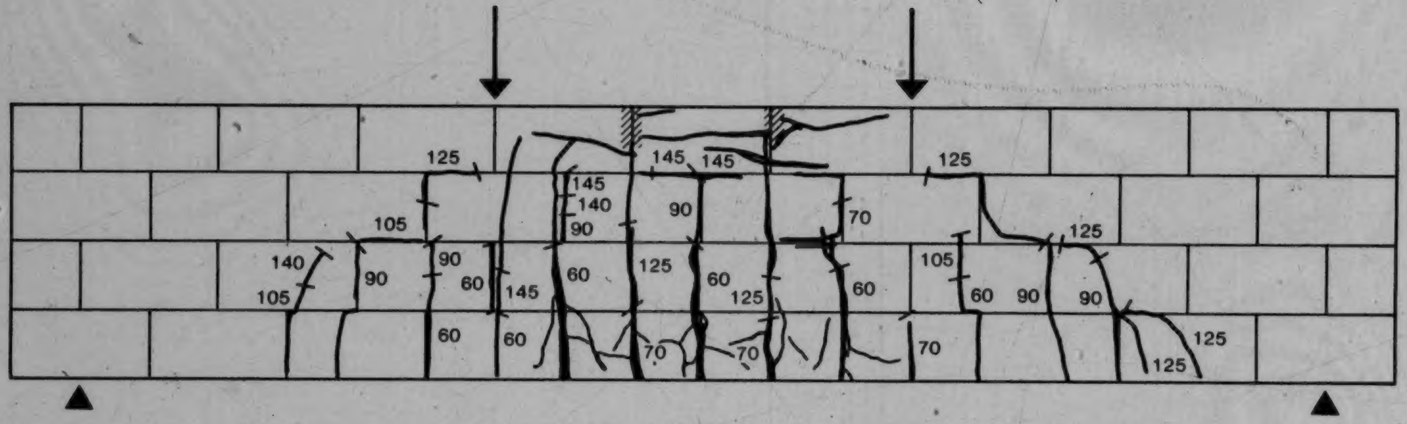
125
145
145
125
105
145
140
90
90
70
125
140
105
90
90
60
145
60
125
60
125
60
105
60
90
90
60
60
70
70
70
125
125

Figure A.2 Beam SB2

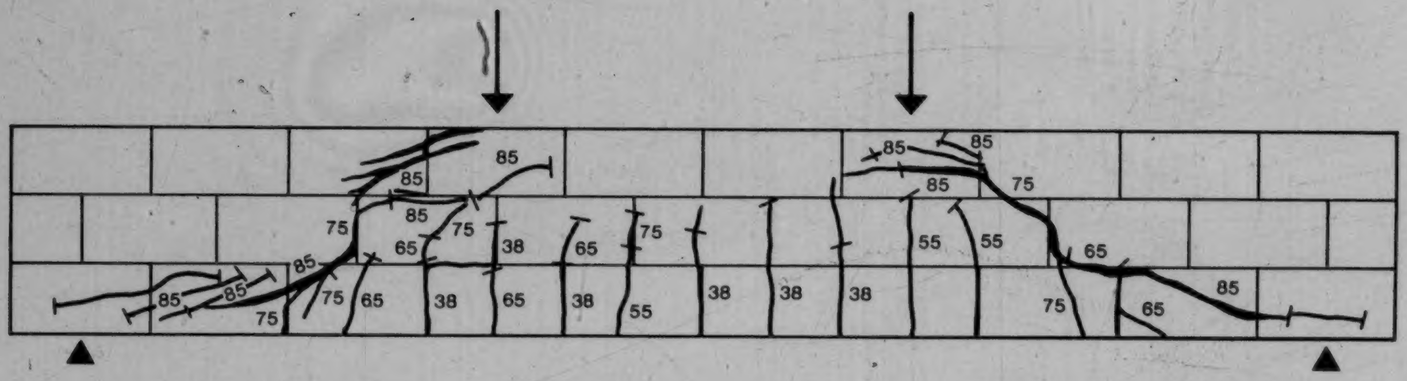
85
85
85
85
75
85
85
65
75
75
75
65
38
65
38
65
38
75
55
38
38
38
85
85
85
75
55
55
65
75
65
85

Figure A.3 Beam SB3

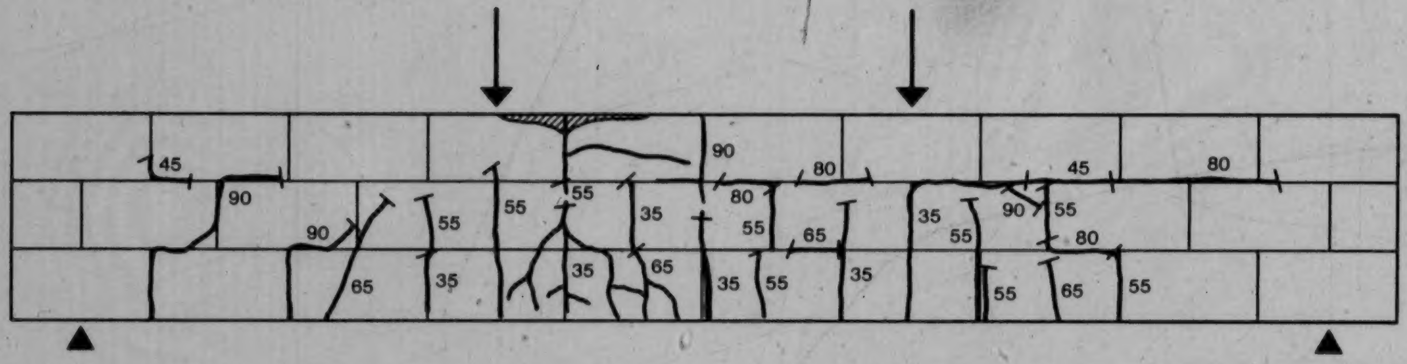
45
90
90
65
55
35
55
55
35
35
65
90
80
55
35
80
65
35
35
55
55
90
55
45
80
55
65
80
55

Figure A.4 Beam SB4

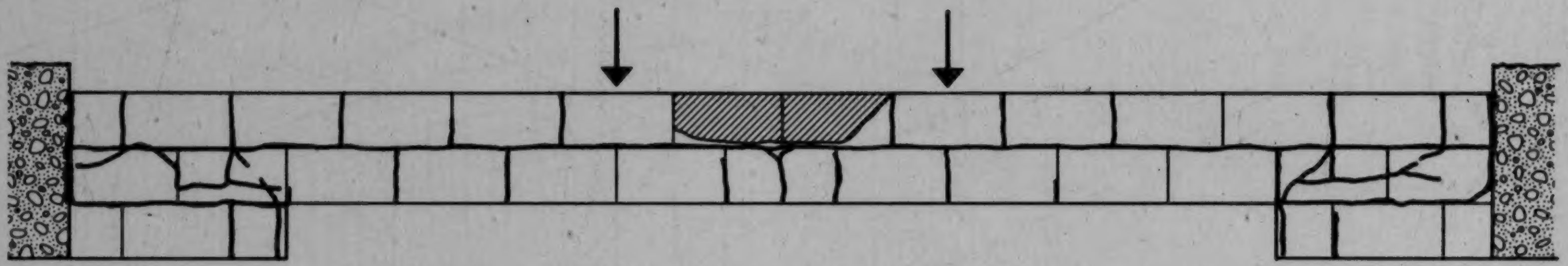

Figure A.5 Beam RB1

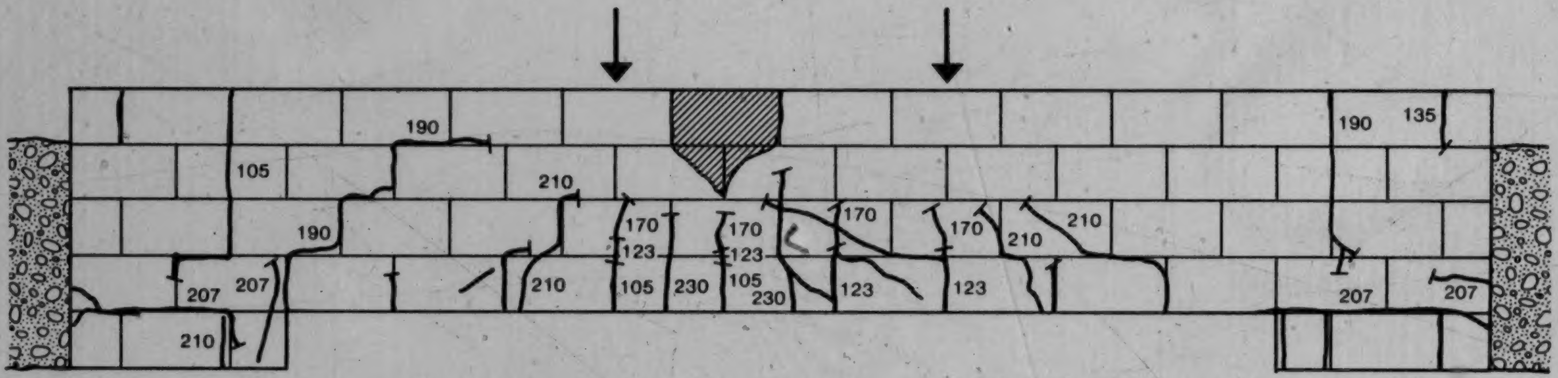
190
190
135
105
210
190
170
123
170
123
170
170
210
210
207
207
210
105
230
105
230
123
123
207
207
210

Figure A.6 Beam RB2

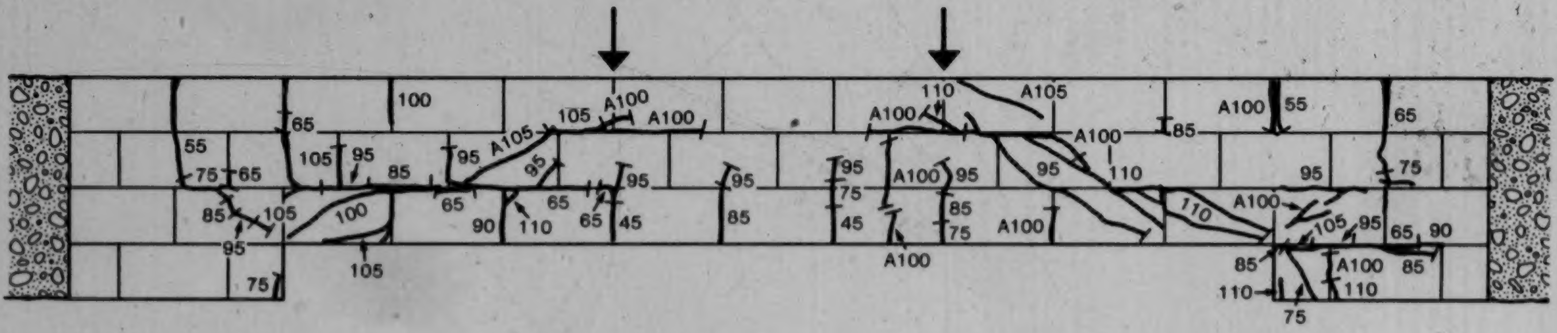
100
65
55
75
65
105
95
85
95
85
105
100
95
75
105
A105
95
105
A100
A100
65
90
110
65
65
45
95
95
85
95
75
45
A100
110
A100
A100
95
85
75
A105
A100
95
110
85
A100
A100
55
110
A100
95
105
95
65
90
85
A100
110
85
110
75
65
75
95

Figure A.7 Beam RB3

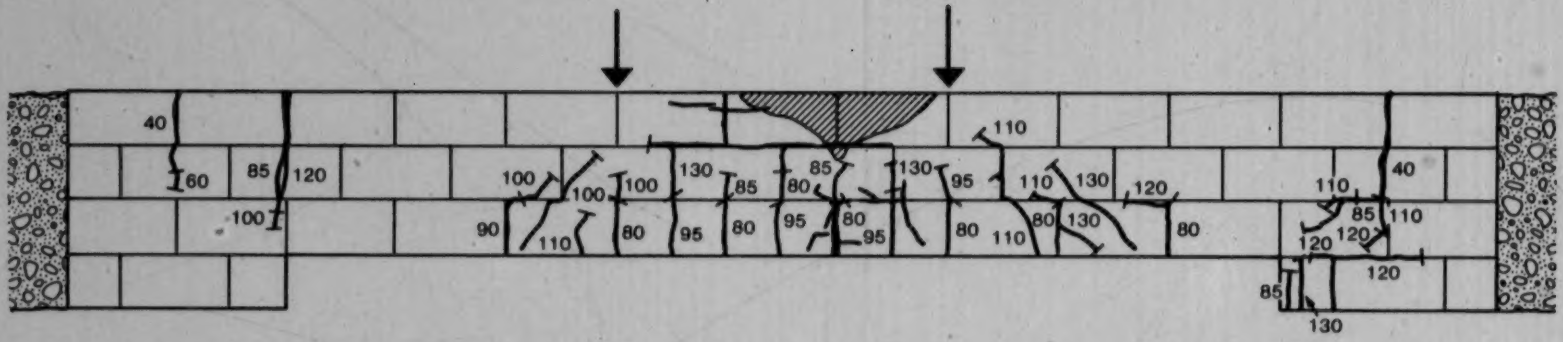
40
60
85
120
100
100
100
90
110
100
80
130
95
85
80
85
80
95
80
95
130
95
80
110
110
130
80
130
110
120
80
110
40
85
110
120
120
120
85
130

Figure A.8 Beam RB4

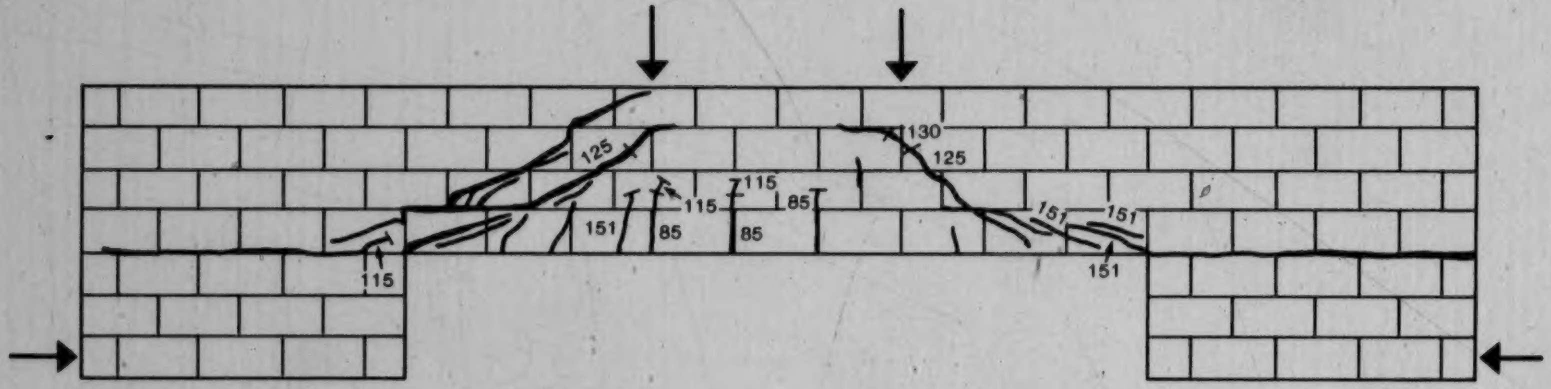
125
130
125
115
115
85
85
85
151
151
151
151
115

Figure A.9 Beam EB1

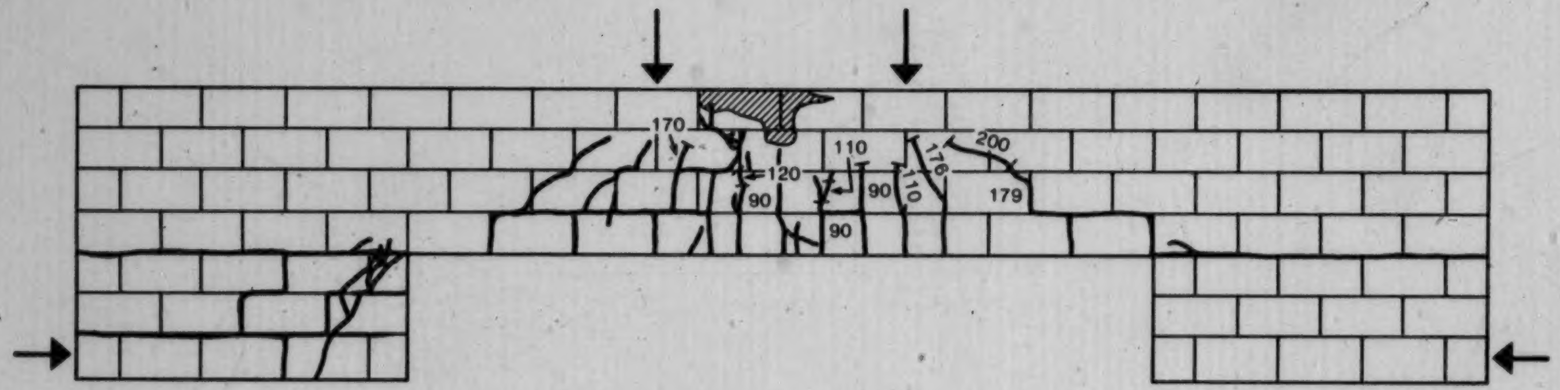
170
110
200
176
120
90
90
110
179
90

Figure A.10 Beam EB2

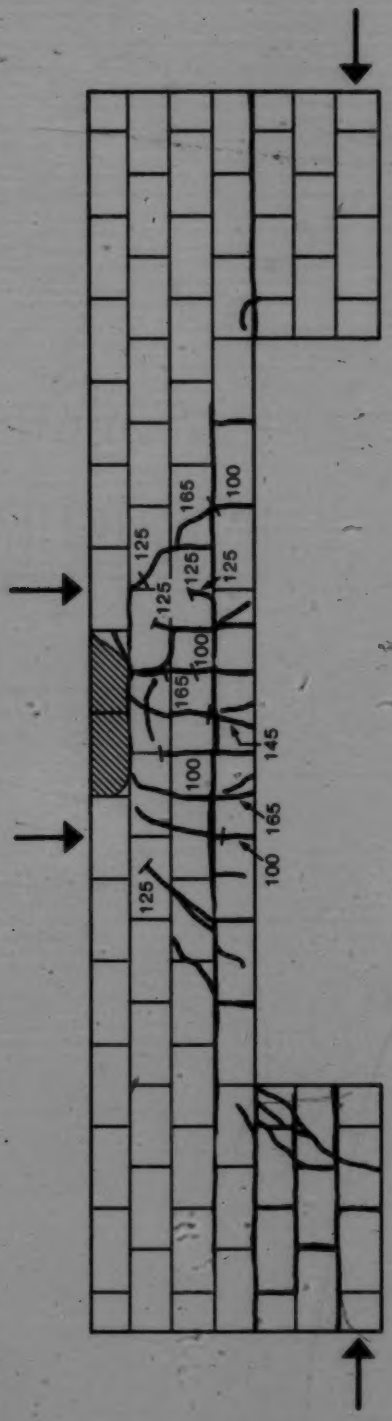
125
125
125
165
100
125
125
100
165
100
145
165
100
125

Figure A.11 Beam EB3

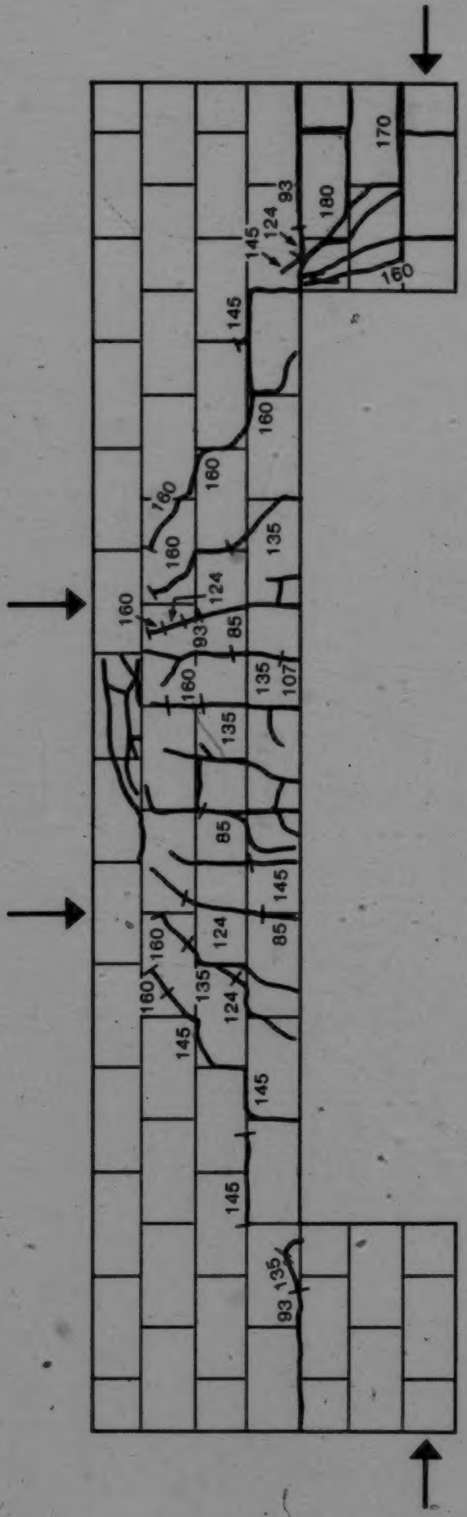
170
180
93
124
145
160
145
160
160
160
135
160
124
160
93
85
135
107
160
135
85
145
85
124
160
160
135
124
145
145
145
93
135

Figure A.12 Beam EB5

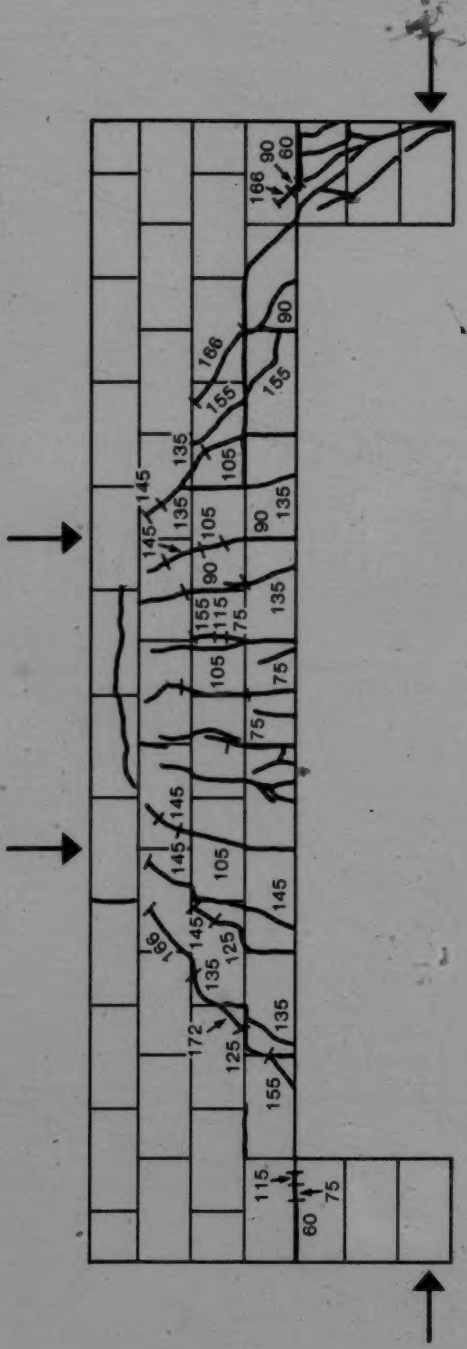
90
60
166
90
166
155
155
135
105
145
135
145
105
90
135
90
155
115
75
135
105
75
75
145
145
105
145
168
145
125
135
172
125
135
155
115
75
60

Figure A.13 Beam EB6